# Novel Supramolecular Design Strategies for Electronic and Chiroptical Functions

A Thesis Submitted for the Degree of

*Doctor of Philosophy*

**By**

**Bhawani Narayan**

**UNDER THE SUPERVISION OF**

**Prof. SUBI J. GEORGE**

**New Chemistry Unit**

**Jawaharlal Nehru Centre for Advanced Scientific Research**

**(A Deemed University)**

**Bangalore-560064 (INDIA)**

**JUNE 2015**

*Dedicated to my Teachers*

# DECLARATION

I hereby declare that the matter embodied in the thesis entitled '**Novel Supramolecular Design Strategies for Electronic and Chiroptical Functions'** is the result of investigations carried out by me at the New Chemistry Unit, Jawaharlal Nehru Centre for Advanced Scientific Research, Bangalore, India under the supervision of Prof. Subi J. George and that it has not been submitted elsewhere for any degree or diploma.

In keeping with the general practice in reporting scientific observations, due acknowledgement has been made whenever the work described is based on the findings of other investigators. Any omission that might have occurred by oversight or error of judgment is regretted.

June 2015 Bhawani Narayan

**Jawaharlal Nehru Centre for Advanced Scientific Research**

Prof. Subi J. George
New Chemistry Unit
Jawaharlal Nehru Centre for Advanced Scientific Research (JNCASR)
Bangalore-560064, India
Phone : +91 80 2208 2964
Fax: + 91 80 22082627
E-mail: george@jncasr.ac.in

Date: 18.06.2015
June, 2015

---

# CERTIFICATE

I hereby certify that the work described in this thesis titled '**Novel Supramolecular Design Strategies for Electronic and Chiroptical Functions**' has been carried out by Ms. Bhawani Narayan at the New Chemistry Unit, Jawaharlal Nehru Centre for Advanced Scientific Research, Bangalore, India under my supervision and it has not been submitted elsewhere for the award of any degree or diploma.

Prof. Subi J. George

(Research Supervisor)

# ACKNOWLEDGEMENTS

*Firstly, I would like to thank my research supervisor Prof. Subi J. George for his constant guidance and support throughout the course of my research. I am very grateful to him for suggesting many interesting projects and encouraging me towards new explorations. He has helped me out to solve many problems rationally and showed me the right way to do research. Personally, he has helped me to become a stronger and better human being.*

*I would also like to thank the Chairman of New Chemistry Unit, Prof. C. N. R. Rao, F.R.S., for being a source of constant inspiration. I am also thankful to him for providing necessary facilities to carry out this work.*

*I would like to acknowledge all my collaborators: Prof. K. S. Narayan, Dr. Satyaprasad Senanayak, Mr. Rishav Harsh from JNCASR, Prof S. Balasubramanian and Mr. Karteek Bejagam from JNCASR, Prof. Sandeep Kumar and Mr. K. Swamynathan from RRI, Dr. Girish Lakhwani, Prof. Stefan Meskers (TU/e, Netherlands) for carrying out various measurements and showing lot of enthusiasm in the collaborative projects.*

*I would like to acknowledge my course work instructors: Prof. Subi J. George, Dr. Shridhar Rajaram, Dr. Jayanta Haldar from JNCASR and Prof. P. Balram and Prof. Siddharth Sharma (IISC).*

*I am also thankful to all my teachers who have encouraged me in all aspects of life.*

*I express my sincere thanks to my lab mates Dr. K. Venkata Rao, Dr. Mohit Kumar, Ankit Jain, Chidambar Kulkarni, Krishnendu Jalani, Ananya Mishra and Suman Kuila for many fruitful discussions and maintaining a cheerful and harmonious atmosphere in the lab.*

*I am grateful to all the trainees who have worked on short term projects: Pooja, Mounika, Saurav, Salim, Thennila and Srishti.*

*I am thankful to the following people for timely assistance in various measurements: Dr. Ranjani V., (lifetime); Prof. G. U. Kulkarni (Veeco Lab); Dr.S. Basavaraja (AFM); Mrs. Usha (TEM); Mrs. Selvi (FESEM); Mrs. Suma (Confocal microscopy); Mr. Anil (XRD); Mr. Mahesh (SEM and NMR);Mr. Vasu (IR, TGA, DSC); Piyush, Amrit, Sonu (DLS); Mr. Sivakumar (HRMS).*

*I am privileged to have wonderful friends from JNCASR, RRI and IISC who have been with me in all the ups and downs of life and made life a pleasant journey.*

*I thank all the academic, technical, library and complab staff at JNCASR.*

*I am thankful to UGC-Fellowship, DST and JNCASR for funding.*

*Finally I thank my family members for their encouragement, support and love.*

# Preface

This thesis presents the design, synthesis and self-assembly properties of novel molecules for electronic and chiroptical finctions.

The thesis is majorly divided into six Chapters.

**Chapter 1** presents an overview of various design strategies employed in self-assembly of organic π-conjugated molecules and draws an analogy to the functions derived thereof. In this chapter, $C_3$-symmetric design, amphiphilic design and bischromophoric design strategies have been discussed.

**Chapter 2** deals with chirality driven self-sorting as a strategy for gaining control over the organization of donor and acceptor molecules. This chapter presents a detailed study of self-sorting phenomenon in enantiomerically pure bischromophoric naphthalene diimide derivatives. This strong chiral bias in the assemblies arises due to a strong enantiopure *trans*-cyclohexanediamide core employed in the molecular design. This behaviour has been further utilized in creating mixed and orthogonal arrangement of donor-acceptor stacks by employing bischromophoric 1,5 dialkoxynaphthalene as the donor.

**Chapter 3** deals with amphiphilic design strategy for creating highly ordered assemblies with high association constants, thereby improving the mobility of the self-assembled chromophore on a device structure. In this regard, we have studied both *p*-type and *n*-type chromophores and found the electronic properties superior to any other design of these chromophores studied so far. This chapter is further divided into two parts.

**Chapter 3.1.** deals with the impact of amphiphilic design strategy on oligo (*p*-phenylenevinylene) chromophore. Detailed spectroscopic and microscopic investigations confirmed the presence of two self-assembled states, tubes and sheets. The tubes were found to be the kinetic aggregates which could be transformed to the sheets (thermodynamic) on annealing. Mobilities as high as $0.01 cm^2/V^{-1}s^{-1}$ were obtained for the sheets which is comparable to OPV in the vapour deposited and crystalline states and the one among the highest values for self-assembled chromophores studied on a device structure.

**Chapter 3.2.** describes the impact of amphiphilic design on naphthalene diimide chromophore (*n*-type) and again proves the superiority of this design strategy for electronic functions.

**Chapter 4** presents detailed investigations of self-assembled and bulk state properties of $C_3$-symmetric Naphthalene diimides. $C_3$- symmetric 1,3,5 Benzenetricarboxamide (BTA) core has been employed to create strong hydrogen bonded assemblies. A subtle change of spacer connecting the BTA core to the naphthalene diimide chromophore gives rise to distinct self-assembled and bulk properties. While the molecule with a flexible ethylenediamine spacer is liquid crystalline and has hexagonal packing, the molecule with a rigid benzene spacer packs in a lamellar fashion.

**Chapter 5** deals with chiroptical amplification of circularly polarized luminescence (CPL). We have created helical supramolecular emissive assemblies by designing $C_3$-symmetric cyanostilbenes, where we have exploited cyanostilbene as an aggregation induced enhanced emission (AIEE) chromophore. Chiral side chains have been incorporated in the molecular design to give rise to helical assemblies. The chiral $C_3$-symmetric cyanostilbene was found to be CPL active, and remarkable amplification of CPL was obtained by co-assembly of chial and achiral molecules.

**Chapter 6** presents the results of Bischromophoric cyanostilbenes, which have been synthesized by employing enantiomerically pure *trans*-cyclohexanediamide core. These molecules have been designed for chiral, enantiomeric, luminescent assemblies and are potential candidates for CPL.

# TABLE OF CONTENTS

# Chapter-2

***Autoresolution of Segregated and Mixed p-n Stacks via Homochiral Supramolecular Polymerization in Solution***



# Chapter-3

**Amphiphilic Design Strategy For Improved Electronic Functions**

**Chapter 3.1.** ***Self-Assembly of p-type oligo(p-phenylenevinylene) Amphiphiles: Free Standing, Ordered Sheets with Enhanced Mobility***

## Chapter-4

## Chapter-5

***Chiroptical Amplification of Circularly Polarized Luminescence***

## Chapter-6

***Bischromophoric Cyanostilbenes: Luminescent, Enantiomeric Assemblies***

# Chapter-1

# Introduction

# Chapter-1

# Introduction

## Design Strategies for Functional Self-Assembled Chromophores


### *Abstract*

*This Chapter aims at highlighting the various design strategies for self-assembled π-conjugated systems dealt with in the thesis entitled 'Novel Supramolecular Design Strategies for Electronic and Chiroptical Functions.' Three main design strategies have been used throughout the thesis, namely, the amphiphilic design strategy, $C_3$-symmetric 1,3,5 benzenetricarboxamide based multichromophoric design strategy and the trans-1,2-cyclohexanediamide based bischromophoric design strategy. The amphiphilic design renders stability to the self-assembled chromophores by synergistic π-π and hydrophobic interactions, and improves the ordering of the self-assembled π-conjugated systems. This ordering tremendously improves the electronic properties of the assemblies. The $C_3$-symmetric design strategy based on 1,3,5 Benzenetricarboxamide (BTA) core reinforces the assemblies by multiple H-bonding and provides directional self-assembly. The trans-1,2-cyclohexanediamide based bischromophoric design strategy, on the other hand, is mainly employed for chiroptical functionality. These moieties have a strong chiral preference and thereby possess the ability of homochiral recognition. This design has been employed to create assemblies for both chiroptical and electronic functionality through chirality driven formation of mixed and orthogonal donor-acceptor stacks.*


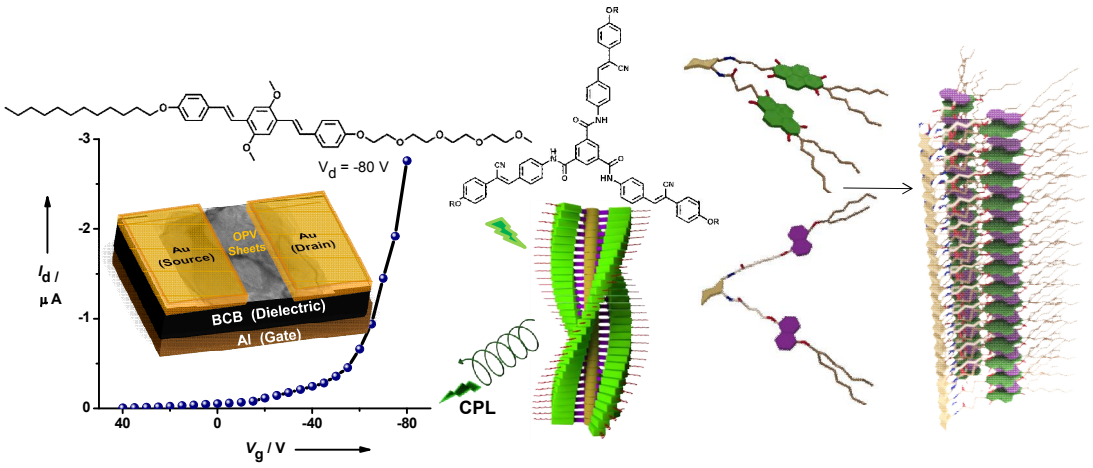

## 1.1. Self-Assembled π-Conjugated Molecules for Various Applications

π-conjugated chromophores are well-sought out candidates for various electronic, biological and material applications.[1] Self-assembly is a strategy of ordering these chromophores by which their efficiency of performance is enhanced. Not only the chemical structure of the chromophore backbone, but the supramolecular ordering also plays a decisive role in judging the performance of these units.[2] Self-assembled chromophores find applications in electronics[3] as the active layer of Field-Effect Transistors (FETs), in Light Emitting Diodes (LEDs) due to their ease of conducting electrons/holes through the π-conjugated backbone. Liquid crystalline molecules obtained from macroscopic ordering of chromophores have become integral components of Liquid Crystal Displays (LCDs). Another interesting property of self-assembles chromophores is their fluorescence. Fluorescent gels obtained from self-assembled chromophores have been well-exploited in light harvesting and in creating white light emitting materials.[4] Fluorescent chromophores have also been used to understand chiroptical phenomenon such as Circularly Polarized Luminescence (CPL) [5] and employed in security tags, 3-D displays and as bioprobes. Water compatible self-assembled molecules have found versatile applications in the field of medicine as drug-carriers, mitochondrial markers and as Magnetic Resonance Imaging (MRI) contrast agents. There are a plethora of applications resulting from self-assembled materials which have developed in a very short span of time. Detailed discussion of all these functions is beyond the scope of this Chapter. Various design strategies have been sought for in the past, to increase the interchromophoric organization. We have described the importance and scope of three main design strategies which are of relevance in this thesis, namely, the amphiphilic design strategy, $C_3$-symmetric 1,3,5 benzenetricarboxamide based multichromophoric design strategy and the *trans*-1,2-cyclohexanediamide based bischromophoric design strategy. Further sections would describe these in detail.

## 1.2. Amphiphilic Design Strategy

Amphiphiles are a special class of molecules, consisting of hydrophobic and hydrophilic domains, making them compatible with both polar and non-polar solvents. Various studies on amphiphilic designs in the past have focussed on the formation of

variety of nanostructures resulting from the self-assembly of amphiphilic molecules, and the various solubility and energy minimization parameters governing their formation.[7] Amphiphilic design strategy has been elegantly employed on π-conjugated organic chromophoric backbones, to improve their semiconducting behaviour.[8] Organic semiconductors are an interesting topic of research as they provide opportunities to create cost-effective, flexible and easily functionalizable electronic devices. In this regard, the chemical structure along with the supramolecular ordering play an equally decisive role in determining the efficiency of the device. Although the vacuum deposited and the crystalline counterparts have shown excellent charge-transport properties, the charge carrier behaviour of solution-processed, self-assembled chromophores has remained low.[9] Controlling the morphologies at the nanometer-scale in solution- processable polymers during its fabrication via spin-coating is challenging due to their structural defects.[10] In this regard, the self-assembly of π-conjugated oligomers, with well-defined chemical structure, in solution using supramolecular design principles, has attracted immense attention as it allows enhanced structural control over the organization and functional properties.[11] However, the electroactive devices fabricated from these oligomeric counterparts have shown poor mobilities, probably due to the solubilizing side chains employed in the molecular design that disrupts the extended π-π stacking in the assemblies, creating disorder. In this regard, an amphiphilic design for self-assembly of chromophores can be of particular interest.[12] Furthermore, it has been demonstrated by various research groups that amphiphilic designs on π-conjugated core can give rise to less dynamic self-assemblies with high association constants, due to synergistic interplay of π-π stacking and hydrophobic effects.[13] Thus, a combination of amphiphilic design with the electroactive chromophore can be highly potent in giving rise to highly anisotropic assemblies with stronger π-π interactions and hence resulting in better electronic mobilities. In this section, we highlight the self-assembly of various π-conjugated amphiphiles that have been synthesized for opto-electronic applications, and have shown excellent charge-transport properties by virtue of an amphiphilic design.

## 1.2.1. Amphiphilic Design Strategy on *p*-type Organic Semiconductors

### 1.2.1.1. Oligo(*p*-phenylenevinylene) Amphiphiles

Oligo(*p*-phenylenevinylene)s, commonly abbreviated as OPVs have been a topic of interest in organic electronics, primarily because of their polymeric counterparts, poly (*p*-phenylenevinylene)s or PPVs, which have shown excellent electronic properties in photovoltaic and electroluminescent devices (Figure 1.1.a).[14] Various elegant design strategies have been experimented on the OPV backbone to improve their electronic properties. One of them is the amphiphilic design strategy, which was first demonstrated by Wong and co-workers.[15]

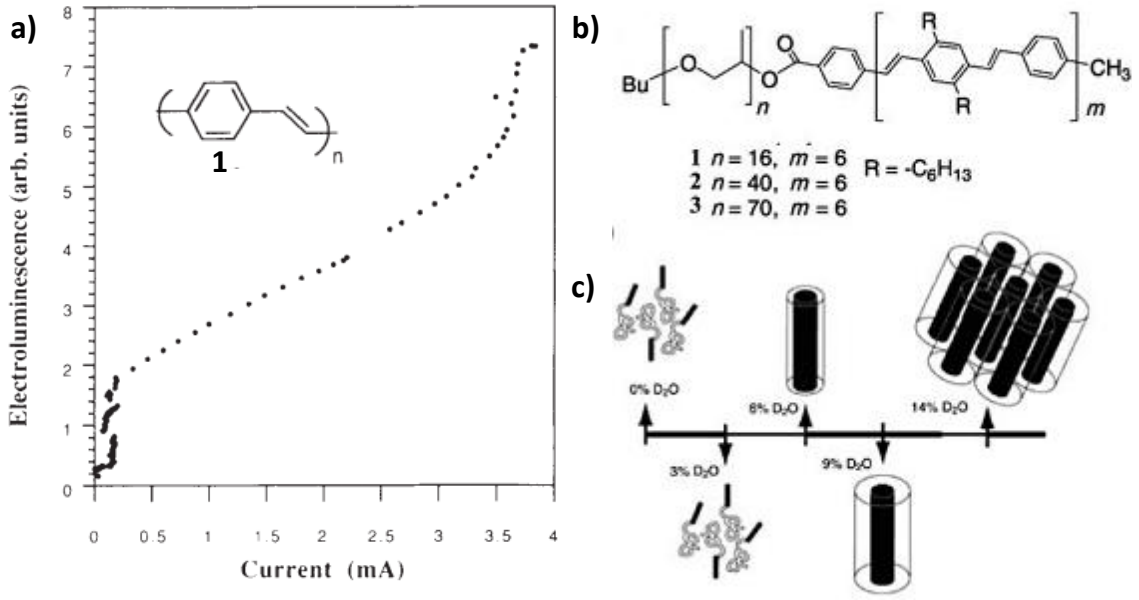


*Figure 1.1. Various studies of PPVs and block copolymers of OPVs: a) Integrated light output plotted against current in electroluminescent devices fabricated from PPV as the electroactive layer; inset: structural representation of PPV; b) Molecular structure of OPV block copolymers; c) Schematic representation of the self-assembly of copolymer **3** in solution into hexagonally packed micells (Figures a reproduced with permissions from references 14, b and c from 16, respectively).*

However, their work was focussed on improving the solubility of the bolaamphiphilic species, so that third order non-linear behaviour could be studied at higher concentrations. Wang *et al*. in the year 2004 studied the self-assembly of OPV

amphiphiles that had a rod-coil structure (Figure 1.1.b) and self-assembled to form cylindrical micells in solution (Figure 1.1.c)[16] These morphologies have been probed by Small Angle Neutron Scattering (SANS) and observed to develop from dimers to hexagonally packed micelles.

Stupp and co-workers have synthesized a series of amphiphilic OPVs with varying lengths of the hydrophilic moiety and have found them to be thermotropic and lyotropic liquid crystalline materials (Figure 1.2).[17] Detailed self-assembly studies have been carried out in polar solvents and these OPV derivatives have been found to form luminescent gels. However, hole-transport properties of OPV amphiphiles are hitherto unknown. In this Thesis (Chapter 3.1), we present detailed studies of highly ordered sheets formed by the self-assembly of OPV amphiphiles.[18] The self-assembly studies have been carried out in varying compositions of THF-water. Solvent and temperature dependent phase transitions from scrolled tubes to 2-D sheets have been carefully characterized, and fabricated on a device structure. The hole mobilities obtained by fabricating the self-assembled sheets of OPV amphiphiles on Field Effect Transistors were found to be $8x10^{-3}cm^2V^{-1}s^{-1}$, which is comparable to OPVs in crystalline and vacuum deposited states and the highest value obtained for other *p*-type amphiphiles on a device structure.[19]

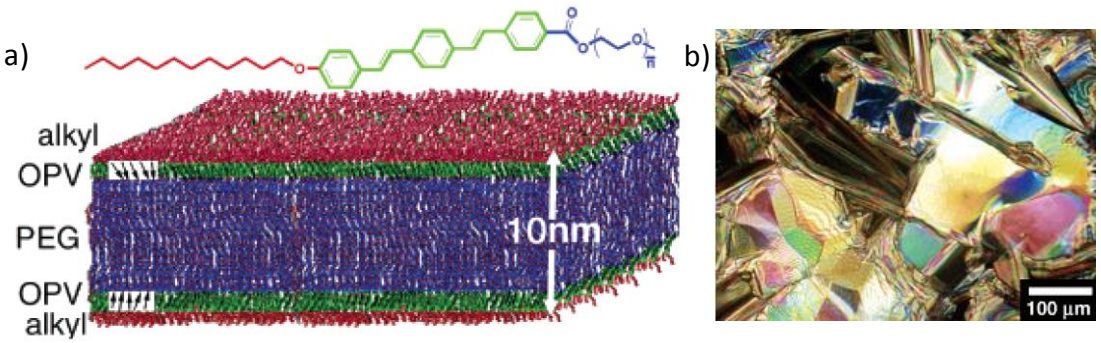


*Figure 1.2. Self-assembly and liquid crystallinity in OPV amphiphiles studied by Stupp and co-workers: a) Molecular representation along with schematic representation of formation of bilayers in OPV self-assemblies; b) mosaic birefringence texture in liquid crystalline OPV amphiphile as observed between cross polarizers (Figures a and b reproduced with permissions from reference 17).*

### 1.2.1.2. Hexa-peri-Hexabenzocoronene (HBC) Amphiphiles

Hexa-peri-Hexabenzocoronenes (HBCs) are yet another interesting class of electroactive chromophores, known for their huge planar core with extended π-conjugation, which equips them with a tendency to form highly organized assemblies. The self-assembly behaviour of HBCs in the liquid crystalline state along with the electronic properties has been studied in detail by Müllen and co-workers.[20] On the other hand, Aida and co-workers have focussed on the self-assembly of HBCs and obtained interesting 1-D structures, suitable for device purposes.[21] An amphiphilic design on the HBC core (Figure 1.3.a) has yielded semiconducting graphitic nanotubes, by strong aromatic interactions between the HBC cores and hydrophobic effects leading to bilayer formation and interdigitation of alkyl chains, forming the inner and outer walls of the nanotube. The resultant nanotubes retain the electroactive nature of constituent chromophores as exhibited from their redox active nature. A single nanotube exhibits resistivity of 2.5 MΩ at 285 K after treatment with $NOBF_4$, which acts as an oxidising agent. Interestingly, the resulting nanotubes from **5** appear to be aligned along the fibre long axis (Figure 1.3.b).[22] The ease of solution processability is evident from the fact that the microscopic fibres can be lifted with a glass hook (Figure 1.3.c). As a result, these processed nanofibers exhibit high anisotropic conductivity upon iodine doping.

In yet another interesting application of an amphiphilic design, Aida and co-workers have constructed photoconductive coaxial nanotubes with efficient exciton migration along the HBC stacks.[23] Trinitrofluorene/$C_{60}$, which are electron deficient moieties, were cleverly functionalized at the hydrophilic end to result in D-A dyads (Figure 1.3.d). The hydrophilic tetraethyleneglycol chain acted as a spacer between the donor and acceptor and prevented ground state charge-transfer interactions from taking place. These D-A dyads self-assemble in polar solvents resulting in co-axial nanotubes, in which the acceptor forms the inner and outer lamellae and the donor constitutes the core of the nanotube. Flash photolysis Time Resolved Microwave Conductivity (FP-TRMC) measurements done on these nanotubes revealed high charge carrier mobilities (~ 3 $cm^2V^{-1}s^{-1}$) on a single nanotube (Figure 1.3.e).

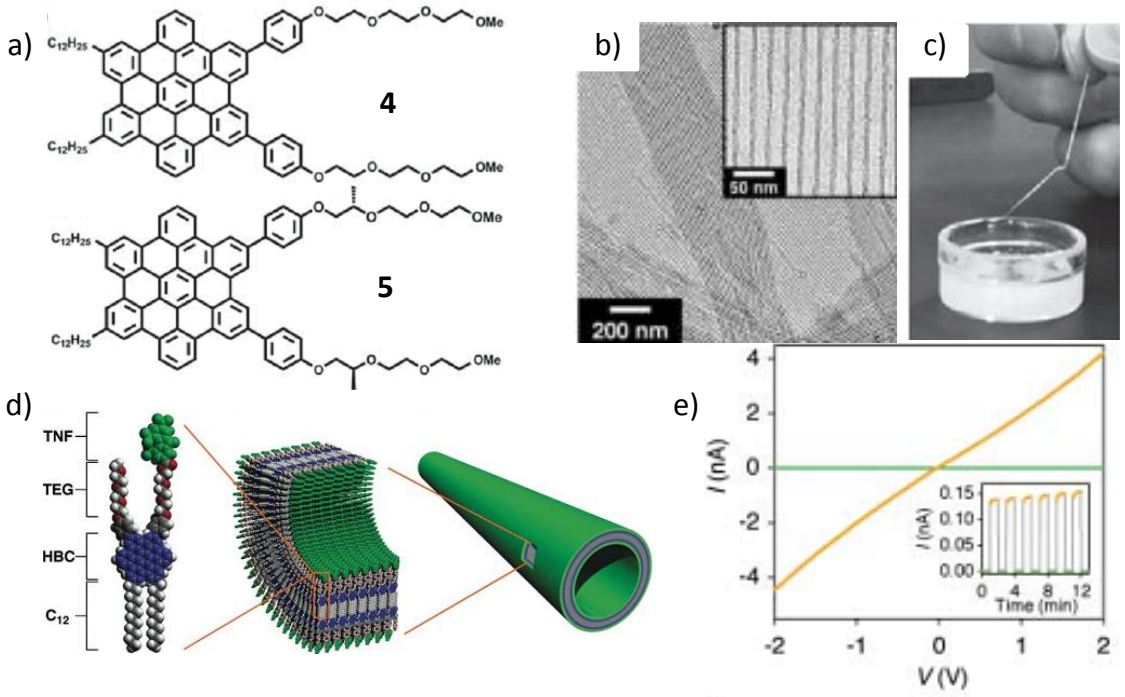


*Figure 1.3. Amphiphilic HBCs studied by Aida and co-workers: a) Molecular structures of the achiral (**4**) and chiral (**5**) HBC amphiphiles; b) TEM image of nanotubes formed by HBC amphiphile with $C_{13}H_{27}$ as the hydrophobic side chain at different magnifications; c) A macroscopic fiber consisting of bundled nanotubes of **5** processed by using a glass hook; d) Schematic representation of D-A dyad in an amphiphilic design and its hierarchical self-assembly to give coaxial nanotubes; d) I-V plot at 25 °C of a cast film of the nanotubes of the coaxial nanotube with (orange) and without (green) photoirradiation (l = 300 to 650 nm). (Inset: Change in electric current at 25° C of a cast film of the nanotubes in response to turning on (orange) and off (green) photoirradiation) (Figure b reproduced with permission from reference 21b, c from reference 22, d and e from 23 respectively).*

## 1.2.2. Amphiphilic Design Strategy on *n*-Type Organic Semiconductors

### 1.2.2.1. Perylene Bisimide Amphiphiles

Perylene Bisimides (PBIs), or perylene diimides (PDIs), are well-known *n*-type organic semiconductors.[24] These chromophores are of particular interest due to their wide spectral overlap with the solar spectrum, high photostability, and considerable π-

interactions that result in better electronic coupling and facilitate nanostructure formation. They are attractive candidates in organic solar cells and are promising replacement for fullerenes in organic photovoltaics.[25] Various attempts have been made to improve the solubility and supramolecular ordering of PBI chromophores simultaneously by non-covalent strategies. Würthner and co-workers have extensively probed into PBI self-assemblies in water and organic solvents by using non-covalent strategies like H-bonding and solvophobic interactions, and found the association constant of PBIs to be very high in aqueous medium ($K>10^8$ $M^{-1}$).[26] Therefore, aqueous self-assembly of PBI dyes is expected to have high interchromophoric ordering, which would reflect in enhanced electronic properties.

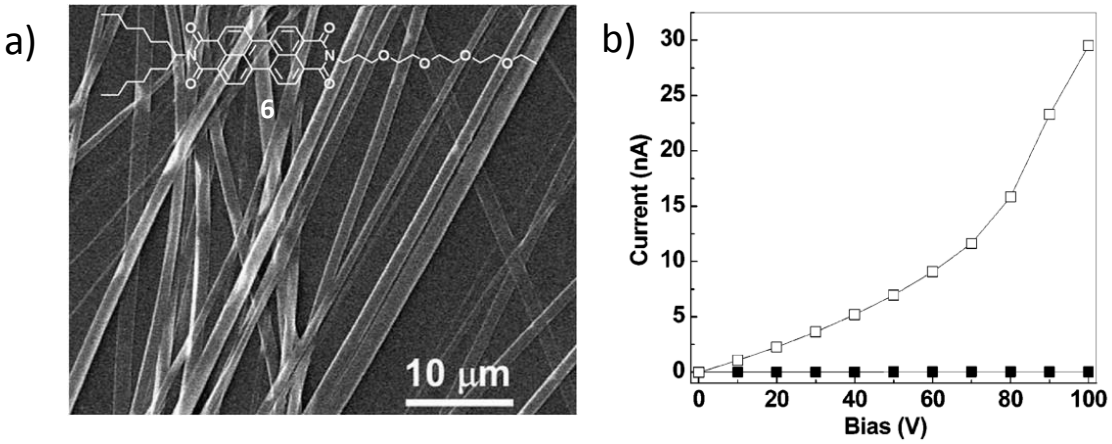


*Figure 1.4. a) Molecular structures of amphiphilic PBI 6; b) I–V curves measured on a nanobelt of **6** in air (open rectangle) and in saturated hydrazine vapour (closed rectangle) (Figures reproduced with permissions from reference 29).*

The first PBI amphiphile was reported by Chang and co-workers,[27] in which the PBI core was bay substituted with cationic groups, to impart water solubility. They achieved lyotropic liquid crystalline phases by the self-assembly of these molecules at appropriate concentrations, with dichroic ratios comparable to commercial polarizers. On the other hand, Zang and co-workers have studied the uncharged amphiphilic counterparts of PBI and were successful in generating long nanobelts by the self-assembly of these molecules in methanol-water compositions.[28]. Milimeter long nanobelts were achieved by the self-assembly of **6** in ethanol-water compositions (Figure 1.4.a).[29] These nanobelts were fabricated on a two-probe device structure as

the electroactive layer, and an increased current by three orders of magnitude were found for pristine single nanobelts on exposure to hydrazine vapours, due to the formation of radical anions (Figure 1.4.b).

Rybtchinski and co-workers have studied a series of PBI amphiphiles.[30] Self-assembled networks of PBIs with polyethylene glycol (PEG) chain were found to be useful as filtration membranes for nanoparticles, reiterating the reinforcement brought about by amphiphilicity.[31] Few other PBI amphiphiles were found to self-assemble into 2-D crystalline materials with exciton diffusion lengths of 120 nm.

Interestingly, PBIs have also been functionalized with peptides to result in functional materials. L-tyrosine functionalized PBI amphiphiles demonstrated by Banerjee and co-workers have been found to self-assemble in aqueous media by H-bonding and π-stacking interactions and have been found to be responsive to pH changes.[32] These molecules form luminescent hydrogels at high concentrations and exhibit photo-switchable conductivity with high on/off ratios when irradiated by white light. In another interesting example, Li and co-workers have been able to tune the self-assembled structures of L-lysine functionalized PBIs from fibres to sheets to nanotubes by changing the acetone-water ratios during the process of self-assembly.[33] Electronic measurements on these nanostructures showed respective conductivities of $10^{-3}$, $10^{-2,}$ and $10^{-6}$ S $cm^{-1}$ for fibers, sheets and nanotubes, respectively.

#### 1.2.2.2. Naphthalene Diimide Amphiphiles

*n*-type rylene diimides,[34] particularly perylene bisimides have been sought for as a replacement for the inorganic counterparts as the active layer in organic electronics as exemplified in the previous section. However, functionalized perylene bismides, being highly hydrophobic molecules, face solubility problems. The smaller counterparts, naphthalene diimides are attractive in the aspects of easy functionalization and high solubility.[35] Core and bay substituted naphthalene diimide self-assemblies have been studied in solvents ranging from Methylcyclohexane to aqueous systems. Various nanostructures have been constructed from the self-assembly of naphthalene diimides, such as tubes, tapes, ribbons and helices.[36] However, NDI aromatic cores are small and to create ordered assemblies, the interactions need to be reinforced. Parquette

and co-workers have utilized peptidic self-assembly (Figure 1.5.a),[37] which has strong hydrogen bonds to create less dynamic assemblies with high association constants. Matile and co-workers have also employed NDIs to create synthetic ion channels,[38] and reinforced the NDI arrays by H-bonding interactions from the bay substituted groups (Figure 1.5.b).

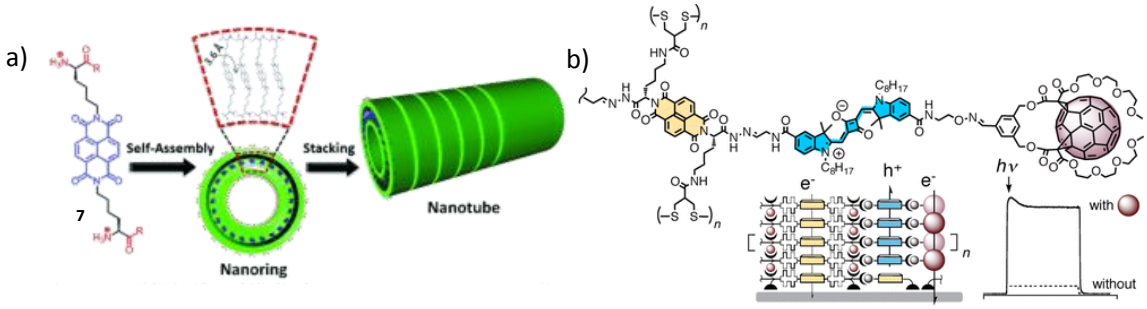


*Figure 1.5. Self-assembly of NDIs strengthened with assisted H-bonds: a) NDI-peptidic bolaamphiphiles that form rigid nanotubes upon self-assembly (The blue sections of **6** undergo hydrophobic π–π stacking interactions, and the red sections electrostatic interactions; b) Schematic of synthetic ion channels created by arrays of self-assembled NDI by Matile and co-workers; inset of Figure b shows a schematic representation of photocurrent generated with and without fullerene (Figures a reproduced with permission from reference 37a and b reproduced with permissions from reference 38).*

Hierarchial self-assemblies of NDI amphiphiles have been demonstrated to form ordered nanostructures and exhibit interesting properties such as reversible vapochromism and aggregate to aggregate transformation,[39] but their electronic properties in the amphiphilic design have not been investigated so far. In an attempt to prove the role of an amphiphillic design to improve the molecular ordering, reflecting in their enhanced electronic properties, we have studied **NDI-Amph** on a device structure (Chapter 3.2.). **NDI-Amph** self-assembles to form aligned nanofibers which are several micrometers long in THF/water compositions and has strong π-stacking and hydrophobic interactions. Top contact bottom gate transistor structures constructed from drop-casted solutions of **NDI-Amph** as the electroactive layer show *n*-type behaviour with electron mobility as high as $8.5\times10^{-3}cm^2V^{-1}s^{-1}$ and with an average mobility of $7.9\times10^{-3}cm^2V^{-1}s^{-1}$. Detailed investigations into the self-assembly characteristics and device fabrication have been discussed in Chapter 3.2.

## 1.2.3. Miscellaneous Amphiphiles

Besides employing amphiphilic designs on well-accepted *p*-type and *n*-type chromophores, this design strategy has also been adopted on various other chromophores. A very recent example is the 'butterfly shaped amphiphile' studied by Pei and co-workers (Figure 1.6.a, b).[40] This amphiphile has a benzodithiophene structure flanked by hydrophilic triethyleneglycol and hydrophobic dodecyl chains. The self-assembly of this molecule in chloroform-methanol mixtures have resulted in the formation of free-standing crystalline sheets which show excellent mobilities on an FET structure. High hole mobilities of 0.02 $cm^2V^{-1}s^{-1}$ was obtained by fabricating the self-assembled sheets as the active layer.

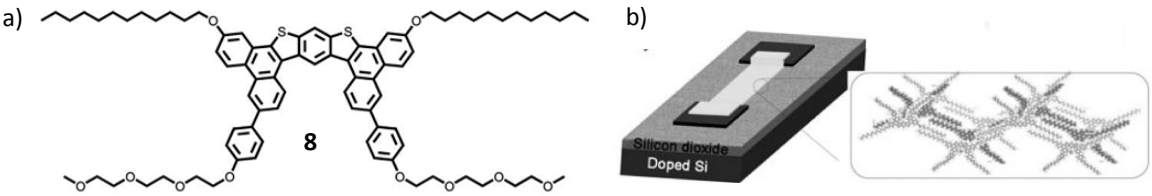


*Figure 1.6. a) Molecular structure of butterfly shaped amphiphile (**8**); b) Schematic of FET device made with self-assembled sheets obtained from **8** as the electroactive layer, inset shows the enlarged view of the molecular organization in the sheets vector. (Figures a, b reproduced with permission from reference 40).*

Another interesting investigation by Katjani and co-workers on amphiphilic dibenzo [a,c] phenazine[41] showed that these thermotropic liquid crystalline molecules arrange in head to head fashion instead of head to tail, which is the energy minimized conformation. The governing factor is the microphase separation between polar ethylene glycol chains and nonpolar alkyl chains, which forces these molecules to align in head to head fashion, resulting in the alignment of frustrated dipoles into 2-D lattice structures. Interestingly, the non-amphiphilic model compounds, which do not possess a dipole moment, do not organize into 2-D lattices. These observations highlight the amphiphilic design as well as the dipolar chromophore responsible for a super-lattice LC structure. FP-TRMC studies performed on these assemblies showed high degree of anisotropy for both the amphiphilic and the lipophilic model compounds, the latter being four times higher.

Jeong and co-workers have demonstrated the macroscopic orientation of amphiphilic tetrathiafulvalene (TTF) derivative using a similar concept.[42]

## 1.3. $C_3$- Symmetric 1,3,5-Benzenetricarboxamide Based Design Strategies

The previous section on amphiphilic design strategy clearly highlights the purpose of employing an amphiphilic design to increase ordering of chromophores in the self-assembled state by synergistic hydrophobic and π-stacking interactions. Yet another method to create strong self-assemblies is by using directional, multiple hydrogen bonds (Figure 1.7.c). The 1,3,5 benzenetricarboxamide (BTA) based $C_3$-symmetric design strategy is known to give rise to assemblies having triple hydrogen bonding, by virtue of the trisamide moieties of the BTA core.[43] The $C_3$-symmetric BTA core consists of a central benzene ring with three amide moieties. Based on the position of the nitrogen and carbonyl groups, the BTA can be 'C-centred' or 'N-centred' (Figure 1.7.a, b). If all the three substituents on the core are identical, it possesses $C_3$-plane of symmetry and can be called '$C_3$-symmetric'. However, the core can be desymmetrized by functionalizing with different groups.

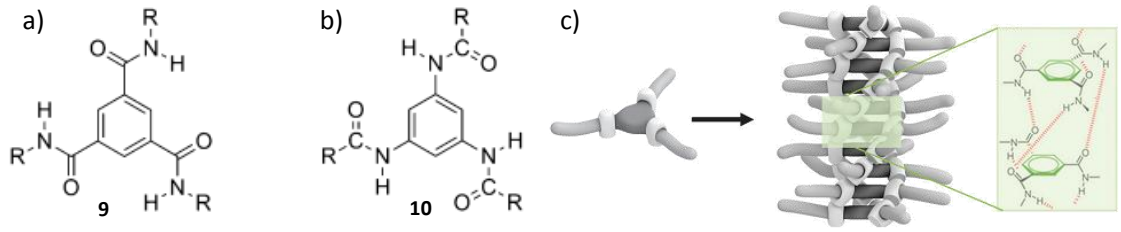


*Figure 1.7. General structural formula for a) C-centered BTAs and b) N-centered BTAs; c) Schematic representation of self-assembly of BTAs with intermolecular H-bonds (Figure c reproduced with permissions from reference 43).*

The BTA core was first synthesized by Curtius in the year 1915 and has since then gained importance in various disciplines of science.[44] The simplest BTA derivatives are the alkyl substituted ones, which are synthetically facile and at the same time intriguing in their properties. BTAs can form crystals or liquid crystalline phases depending on the length and nature of the alkyl chain (branched/unbranched). The

liquid crystalline properties of alkyl substituted BTAs were illustrated as early as early as 1980s and have been revisited by Schmidt and co-workers [58] recently (Figure 1.8.b). Ferroelectric properties have been obtained in columnar assemblies of liquid crystalline alkyl substituted BTAs by Sijbesma and co-workers.[45] These are seen to possess a macrodipole by the alignment of trisamide microdipoles pointing in one direction (Figure 1.8.e). Remnant polarization observed in organic thin films of these BTAs can be useful in diodes and non-volatile memory devices. Alkyl substituted BTAs have further found applications in strengthening polymeric assemblies (Figure 1.8.a).[46] Another application of BTAs is its application as a nucleating and clarifying agent for the bulk polymer isotactic polypropylene (iPP), which has been successfully commercialized.[47]

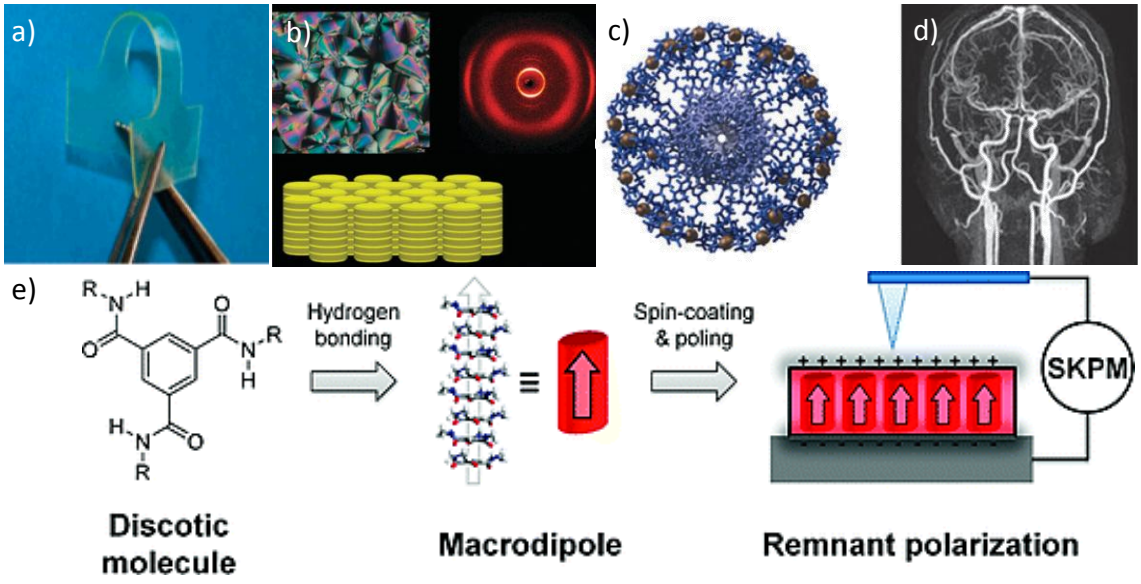


*Figure 1.8. Alkyl substituted BTAs in material applications: a) Supramolecular elastic material obtained by using BTA as a crosslinker in a polymer backbone; b) Schematic representation of hexagonal columnar mesophases formed by BTA derivatives (inset shows birefringent focal conical textures and diffraction gratings); c) Schematic representation of self-assembled BTA for application as MRI contrast agent; d) diagram of a section of brain obtained from a MRI scan; e) ferroelectric material formed by ordering of BTA, creation of a macrodipole and its subsequent application in ferroelectric device.(Figures a reproduced with permissions from reference, 46, b-d from reference 43 and e from reference 45a respectively).*

Apart from applications in materials, BTAs have also been used in the field of biology and medicine. Gd (III)–DTPA based BTAs have been successfully used as MRI contrast agents (Figure 1.8.c, d).[48] Both in vitro and in vivo experiments on these derivatives with sizes in the 6 nm range showed excellent contrast-enhanced magnetic resonance imaging (MRI). These were highly stable and had low clearance rates making them potential candidates for further developments in molecular imaging.

Synthetic ease and sensitivity of the spectroscopic signatures to various conformational and dynamic changes enable alkyl substituted BTA self-assemblies to be used as model systems for mechanistic and chiral amplification studies.[49] Detailed self-assembly studies of BTAs in non-polar solvents by Meijer and co-workers have led to the development of two main models of self-assemblies (Figure 1.9.a).[50] The co-operative or the nucleation-elongation model assumes the self-assembly to take place in two steps, the formation of a critical nucleus followed by the elongation/ growth, analogous to chain-growth polymerization in conventional polymers (Figure 1.9.b). The cooperative mechanism of self-assembly assumes size dependent association constants. The isodesmic model on the other hand, assumes a stepwise growth and assumes an equal association constant for each step, similar to step-growth polymerization in conventional polymers.

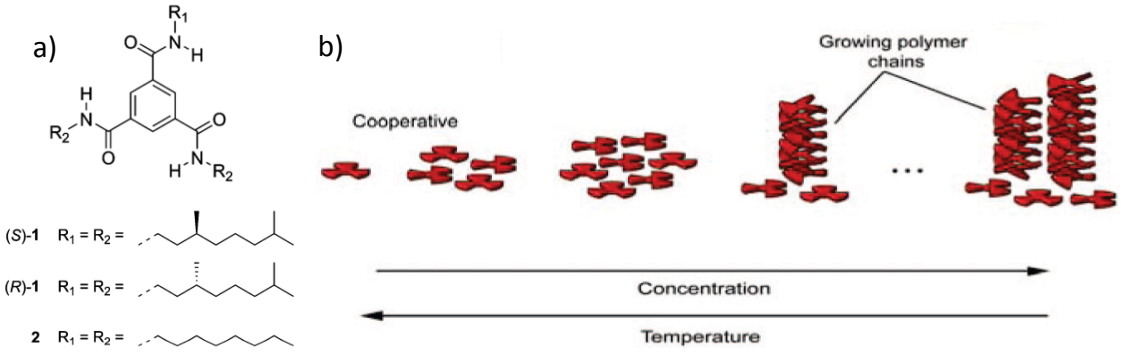


*Figure 1.9. a) Various achiral and chiral BTA derivatives investigated by Meijer and co-workers that have led to the development of chiral amplification phenomenon; b) schematic representation of cooperative mechanism of self-assembly generally observed for BTAs as a function of concentration and temperature. (Figure b reproduced with permissions from reference 2b).*

These mechanisms can be elucidated by monitoring the spectroscopic changes either by varying the concentration or by varying the temperature. Temperature dependent studies are more reliable as the number of data points generated are much more than in concentration dependent studies and can be fitted well to the proposed models of self-assembly.

Temperature dependent UV-vis and Circular Dichroism (CD) measurements of chiral and achiral self-assemblies of alkyl substituted BTAs have shown a highly cooperative mechanism of self-assembly with high cooperativity parameters.[51] Extensive studies on chiral and achiral self-assemblies of BTAs have thrown light on chiral amplification processes. These phenomena are popularly called 'Sergeants and soldiers' and 'Majority rules' respectively. A quantitative estimate of the parameters like 'helix reversal penalty' and 'mismatch penalty' were obtained through theoretical insights. [52] These calculations predict the feasibility of copolymerization. Furthermore, they also investigated the behaviour of these non-linear effects with temperature and concentration.

## 1.3.1. Multichromophoric BTA Based Systems

1,3,5 Benzenetricarboxamides have been successfully appended with chromophores to study the synergistic effects of triple helical hydrogen bonding in synergy with π-stacking interactions. These have further resulted in unique materials arising from the property of the substituent chromophore.

Elemans and co-workers have successfully synthesized $C_3$-symmetric porphyrins (Figure 1.10.a) and observed the unexpected formation of highly patterned surfaces at macroscopic scale lengths, in the order of several square micrometers by evaporation of droplets containing the self-assembled molecules (Figure 1.10.b).[53] These surfaces were cleverly used for aligning liquid crystals. They have also carried out detailed investigations of the self-assembly of the chiral analogue of this $C_3$-symmetric porphyrin trimer in different solvents and correlated this behaviour to the aggregation of the molecule at a solid−liquid interface.[54] Recently, other derivatives of $C_3$-symmetric porphyrins were reported by the same group and chiral amplification studies by copolymerization of the chiral and achiral analogues were reported.[55]

Interestingly, the choice of solvent played a crucial role in the successful amplification of chirality in co-assembled stacks.

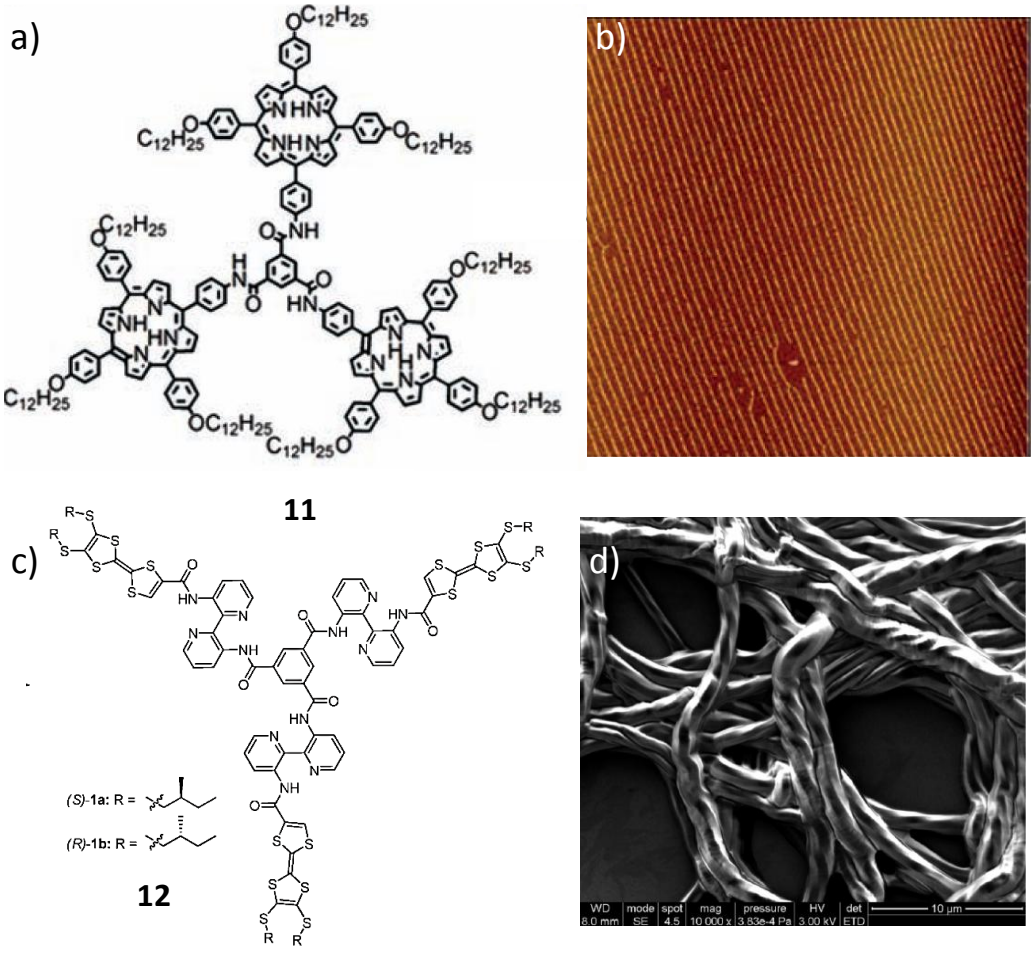


*Figure 1.10. Few multichromophoric $C_3$-symmetric BTAs and their hierarchial structures: a) $C_3$-symmetric porphyrin **11**; b) macroscopic surface patterns obtained on a gold substrate by surface evaporation of a droplet containing the chromophore; c) $C_3$-symmetric TTF **12**; d) FE- SEM image showing macroscopic chirality in the self-assembled structure (Figures a, b reproduced with permissions from reference 53 and c, d from reference 56a).*

Amabilino and co-workers have carried out insightful studies on $C_3$-symmetric BTA based tetrathiafulvalenes (TTF) (Figure 1.10.c).[56] They have demonstrated the expression of chirality in enantiomeric non-amphiphilic $C_3$-symmetric TTFs at both nanoscopic and meseoscopic level as proved by the bundles of twisted fibers seen by microscopic techniques (Figure 1.10.d). In another consecutive report of the same

molecule, they have found the helical self-assembled fibers to be largely influenced by the substrate used.[57]

Various $C_3$-symmetric azobenzene based derivatives reported by Schmidt and co-workers show remarkably stable light-induced orientation in initially amorphous thin-film architectures, which can serve as stable holographic volume gratings.[58] Investigations into the origin of this behaviour revealed the efficient formation of stable, ordered domains in which the three azobenzene groups orient perpendicular to the polarization of the inscribing light beam. Another report on BTA based azobenzene derivatives by Lee and co-workers have shown stimuli responsive self-assemblies that can morphologically transform from fibers to spheres and vice versa by changing the solvent conditions.[59]

Few other interesting $C_3$-symmetric multichromophoric derivatives based on oligo(*p*-phenylenevinylene)[60] and oligo(*p*-phenylene ethylene)[61] derivatives have focussed on the effects of hydrogen-bonding and chiral amplification in these assemblies. Most of these assemblies were found to be cooperative and were attributed to the directional H-bonds. Recent studies on amphiphilic OPE based tricarboxamides have shown an isodesmic mechanism of self-assembly due to the lack of highly directional H-bonds.[62] Sudholter and co-workers have studied the properties of $C_3$-symmetric triphenylenes and found them to be thermotropic liquid crystalline materials.[63]

We have functionalized *n*-type naphthalene diimides on the $C_3$-symmetric BTA core[64] and synthesized two $C_3$-NDI derivatives with a difference in the nature of the spacer connecting the core to the naphthalene diimides. Interestingly, we have found striking differences in the bulk state and self-assembled characteristics with a subtle variation of the spacer. While the molecule with the flexible alkyl spacer is liquid crystalline and forms a hexagonal columnar phase, the molecule with a rigid benzene spacer does not show phase transitions. On the other hand, supramolecular chirality is expressed in the self-assembled state of $C_3$-NDI with the rigid spacer while the alkyl spacer is found to be inefficient in translating the molecular chirality into supramolecular level. These observations are discussed in detail in Chapter 4 of this thesis.

Another $C_3$-symmetric design strategy has been exemplified in Chapter 5 entitled 'Chiroptical Amplification of Circularly Polarized Luminescence'. In this Chapter, we have attached cyanostilbenes to the BTA core. The choice of the chromophore was based on its Aggregation Induced Enhanced Emission (AIEE) property,[65] which when clubbed with chirality would lead to chiral luminescent assemblies. These assemblies were CPL active and employed in the amplification of chirality in the excited state by co-assembly with the achiral monomers.

## 1.4. Diaminocyclohexane Based Bischromophoric Design Strategy

*Trans*-1,2-diaminocyclohexane has been versatilily employed by organic chemists for the formation of Low Molecular Weight Gelators (LMWG) and for synthesizing chiral catalysts for enantioselective separations. It has been interestingly substituted with chromophores to create bischromophoric compounds that have been used to understand excitonic coupling, and also for various functional applications in electronics and chirality. This design strategy has been elaborated in this section. For the sake of convenience, we have divided this section into two parts that discuss the applications of these molecules as gelators and functional bischromophoric molecules.

### 1.4.1. Diaminocyclohexane Based Gelators

Hanabusa and co-workers carried out pioneering studies on alkyl substituted *trans*-1,2-(diamido)cyclohexanes and found them to be Low molecular mass gelators (Figure 1.11.a).[66] These compounds were found to gel in a variety of solvents ranging from non-polar hexane to polar protic solvents like ethanol and methanol, polar aprotic solvents like acetonitrile, DMF and DMSO and aromatic solvents like benzene and toluene. Since then, these compounds have gained importance due to their excellent gelation capability towards a wide range of organic solvents. These assemblies were characterized by FT-IR spectroscopy which gave evidence for the existence of intermolecular H- bonds, by virtue of the bisamides (Figure 1.11.c). Furthermore, CD spectroscopy experiments of loose gels unambiguously proved the existence of chiral aggregates as there was negligible contribution due to Linear Dichroism (LD) and the CD spectra disappeared at high temperatures, clearly suggesting that the CD spectra do not result from chiral conformation of the molecule (Figure 1.11.b). They have also

observed helical superstructures in the form of long fibers when a TEM imaging was done on a gel sample, suggesting the macroscopic expression of chirality. Interestingly, the cis isomer was not capable of forming gels suggesting the role of equatorial amide bonds in the gelation process, which was further supported by molecular modelling studies. The racemate consisting of equimolar mixture of both (*1S,2S*) and (*1R,2R*)-*trans*-1,2- cyclohexane diamides formed unstable gels, which converted into co-crystals, indicating that these enantiomers do not co-assemble well. Furthermore their investigations have suggested that a critical alkyl chain length of six carbons or more were needed to form stable gels.

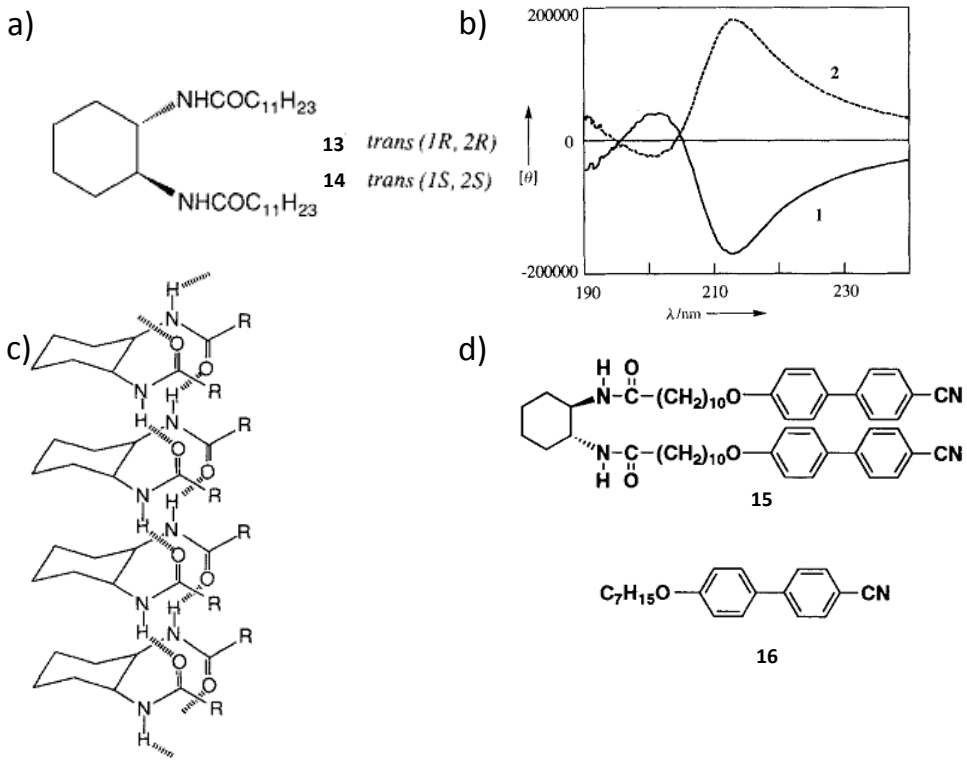


*Figure 1.11. Trans-1,2-cyclohexanediamine based gelators studied by Hanabusa and co-workers: a) molecular structures; b) CD spectra of a loose gel; c) H-bonded network proposed by molecular modelling; d) Structures of molecules for formation of liquid crystalline gelators (**15** and **16**) (Figures a-c reproduced with permissions from reference 66 and d from 68, respectively).*

In a further report by the same group, the formation of thermoreversible, liquid crystalline gels were observed by attaching a cyano-biphenyl mesogenic moiety to the enantiopure *trans* -(*1R,2R*)-cyclohexanediamide moiety.[67] This molecule has no

mesomorphic behaviour. However, on mixing **15** and **16** (anisotropic solvent), a nematic liquid crystalline state was characterized for these gels (Figure 1.11.d).

Feringa and co-workers have explored chiral recognition in azobenzene substituted *trans*-diaminocyclohexane diamides.[68] Co-assembly studies were performed between the gelator azobenzene derivative and an alkyl substituted guest molecule with an identical diaminocyclohexane framework. Strong chiral recognition interactions were seen between identical enantiomers.

## 1.4.2. Bischromophoric Functional Molecules

Various chromophores have been attached to enantiopure *trans*-1,2-cyclohexane diamines resulting in bischromophoric systems for conceptual understanding of excitonic coupling and for electronic and chiroptical purposes.

The bischromophoric system designed by Berova and co-workers in the year 1997 by functionalizing trans cyclohexanol with fluorophores, such as 2-naphthoate or 6-methoxy-2-naphthoate,[69] connected by an ester linker was aimed at increasing the sensitivity of excitonic coupling by fluorescence detected circular dichroism (FDCD), as this method is based on direct measurement of emitted radiation against a zero background. The selective occurrence of CD and fluorescence active signals in this method gave further impetus to the work. Model compounds synthesized from *trans*-cyclohexane derivatives proved useful in understanding the principles of FDCD technique. The extent of fluorescence polarization was also correlated with FDCD in a subsequent work by the same group.[70]

Kawai and co-workers have developed a series of bischromophoric compounds based on perylene bisimides to obtain chiroptical functionalities (Figure 1.12.b).[71] These molecules were majorly based on binaphthyls and *trans*-1,2-diaminocyclohexane. The perylene chromophore was functionalized to the chiral core by imidation reaction and was separated from the core by 1 and 2-carbon spacers.[72] Efficient excitonic coupling was found in the fluorescent assemblies of these molecules which also turned out to be CPL active. CD and CPL signatures in various solvents were demonstrated through spectroscopic investigations (Figure 1.12.b).

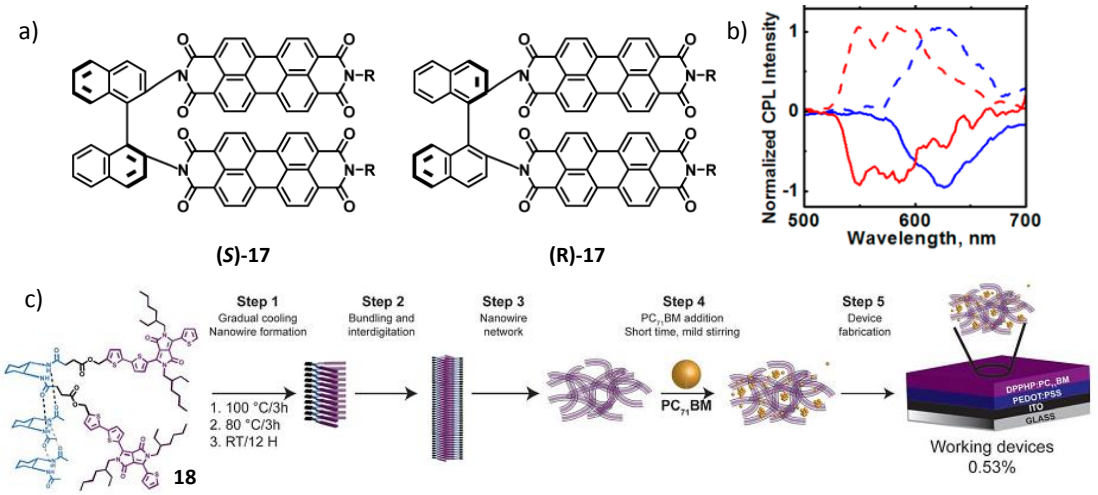


*Figure 1.12. Few functional bischromophoric molecules reported in literature: a) Bischromophoric perylene bisimides reported by Kawai and co-workers; b) CPL activity of (**S**)-**17** and (**R**)-**17** in chloroform at a concentration of $1\times10^{-3}$ M (red lines) and $3\times10^{-3}$ M (blue lines); (c) Bischromophoric thiophene **18** designed by Stupp and co-workers and steps towards the fabrication of the molecule as the donor counterpart in organic solar cell (Figures a, b reproduced with permissions from reference 71b and c from reference 74).*

Bischromophoric thiophenes have been developed by Stupp and co-workers (Figure 1.12.c).[73] These formed grooved nanowires upon self-assembly in toluene and were then spin casted along with PCBM to produce a percolating network of self-assembled nanowires and fullerene acceptors to form organic bulk heterojunctions. The device efficiencies were enhanced by 23% as the hairpin structures of these bischromophoric molecules interact well with the fullerenes in receptor-ligand type configurations at the heterojunction of the two domains. These molecules were also fabricated in solar cells with $C_{71}$ donor by improved fabrication techniques that showed 54% efficiency improvement.[74]

We have employed a bischromophoric design strategy to facilitate the creation of mixed and orthogonal *p-n* stacks in solution (Chapter 2.1). Homochiral polymerization of bischromophoric Naphthalene diimides (NDIs) has been characterized extensively by spectroscopic and mechanistic investigations. A step ahead, we have constructed

donor-acceptor stacks, with bischromophoric 1,5 dialkoxynaphthalenes (DAN) and achieved a chirality control over donor-acceptor organization. Mixed and orthogonal stacks were observed when the donor and acceptors identical and opposite chiralities respectively. This concept has also been extended to three component system, consisting of the bischromophoric donor and enantiomeric acceptors, where the wrong enantiomeric acceptor autoresolves to give segregated stacks. Such an unprecedented chirality control on donor-acceptor organization paves way for creation of controlled *p-n* junctions which are of interest in electronic applications.

## 1.5. Conclusions and Outlook

We have thus presented a detailed account of a series of design strategies which are of relevance in the present thesis. Various molecules, synthetic ease and applications have been explained in each subsection. All these strategies aim at increased π-conjugated chromophoric ordering. While the amphiphilic design uses synergistic hydrophobic and π-stacking interactions, the latter two use multiple hydrogen-bonding interactions to reinforce the assembly. The first two design strategies are mainly employed for extracting electronic functions while the bischromophoric strategy is meant for chiroptical function.

In the present thesis, we have employed the amphiphilic design strategy to improve the interchromophoric interactions in the self-assembled state and studied the effect of the supramolecular ordering on electronic properties on Field Effect Transistors (FETs). Improved mobilities were obtained by fabricating the amphiphilic self-assemblies as the electroactive layer. We have generalized the strategy by studying *p*-type oligo(*p*-phenylenevinylene) amphiphiles and a *n*-type naphthalene diimide amphiphile (Chapter 3.1. and 3.2., respectively).

The $C_3$-symmetric design strategy has been utilized to obtain reinforced H-bonded assemblies in the case of $C_3$-symmetric NDIs (Chapter 4). A case study of two $C_3$-symmetric NDIs has been presented where subtle change in the nature of the spacer brings about significant differences in the bulk and self-assembled characteristics. Chapter 5 exploits the cooperative behaviour of BTAs and describes the chiroptical amplification of CPL. Novel $C_3$-cyanostilbenes have been synthesized which form CPL

active chiral, luminescent assemblies. Co-assembly of the chiral and achiral $C_3$-cyanostilbenes results in significant amplification of CPL.

The Bischromophoric design strategy based on *trans*-1,2-bis(amido)cyclohexane has been employed for two purposes. The first is employed for chiral self-sorting of Bischromophoric donors and acceptors (Chapter 2). Control over the organization of *p-n* stacks has been achieved by employing this chiral core in the molecular design. While the donors and acceptors of same chirality result in the formation of alternate stacks by homochiral polymerization, the enantiomeric donors and acceptors form orthogonal stacks. We have also successfully demonstrated the autoresolution of the wrong enantiomeric assembly from a tricomponent mixture consisting of enantiomeric acceptors and a bischromophoric donor. We have also employed this design strategy for creating enantiomeric, luminescent assemblies in the case of bischromophoric cyanostilbenes (Chapter 6).

## 1.6. References

[1] a) T. Aida, E. W. Meijer, S. I. Stupp, *Science* **2012**, *335*, 813.

[2] a) F. Würthner, *Angew. Chem. Int. Ed.* **2001**, *40*, 1037; b) F. J. M. Hoeben, P. Jonkheijm, E. W. Meijer, A. P. H. J. Schenning, *Chem. Rev*. **2009**, *109*, 5687; c) A. P. H. J. Schenning, E. W. Meijer, *Chem. Commun*. **2005**, 3245; d) A. C. Grimsdale, K. Müllen, *Angew. Chem. Int. Ed.* **2005**, *44*, 5592.

[3] a) D. Braun, *Mater. Today* **2002**, *5*, 32; b) R. H. Friend, R. W. Gymer, A. B. Holmes, J. H. Burroughes, R. N. Marks, C. Taliani , D. D. C. Bradley, D. A. dos Santos, J.-L. Brédas, M. Löglund, W. R. Salaneck, *Nature* **1999**, *397*, 121.

[4] a) A. Ajayaghosh, V. K. Praveen; *Acc. Chem. Res*. **2007**, *40*, 644; b) S. S. Babu, V. K. Praveen, A. Ajayaghosh, *Chem. Rev.* **2014**, *114*, 1973; c) K. V. Rao, K. K. R. Datta, M. Eswaramoorthy, S. J. George, *Chem. Eur. J.* **2012**, *18*, 2184.

[5] a) J. P. Riehl, F. S**.** Richardson, *Chem. Rev*. **1986**, *86*, 1; b) E. G. Moore, A. P. S. Samuel, K. N. Raymond, *Acc. Chem. Res*. **2009**, *42*, 542; c) K. Watanabe, K. Suda, K. Akagi, *J. Mater. Chem. C* **2013**, *1*, 2797.

[6] a) T. Shimizu , M. Masuda, H. Minamikawa, *Chem. Soc. Rev*. **2005**, *105*, 1401; b) N. Kimizuka, Self-Assembled Nanomaterials I, ed. T. Shimizu, Springer, Berlin-Heidelberg , **2008**, *219*, 1.

[7] N. Koch, Supramolecular Materials for Opto-Electronics, Royal Society of Chemistry, **2014**.

[8] a) A. O. Patil , A. J. Heeger, F. Wudl, *Chem. Rev*., **1988**, *88*, 183; b) A. Kraft, A. C. Grimsdale, A. B. Holmes, *Angew. Chem . Int. Ed.* **1998**, *37*, 402.

[9] a) A. Saeki, Y. Koizumi, T. Aida, S. Seki, *Acc. Chem. Res.* **2012**, *45*, 1193; b) M. Hasegawa, M. Iyoda, *Chem. Soc. Rev*. **2010**, *39*, 2420; c) T. Lei, J. Pei, *J. Mater. Chem*. **2012**, *22*, 785.

[10] J. Roncali, *Chem. Rev.* **1992**, *92*, 711.

[11] a) R. E. Martin, F. Diederich, *Angew. Chem. Int. Ed.* **1999**, *38*, 1350; b) J. M. Tour, *Chem. Rev.* **1996**, *96*, 537; c) *Electronic Materials: The Oligomer Approach* (Eds.: K. Müllen, G.Wegner), WILEY-VCH, Weinheim, **1997**.

[12] a) Y. Yamamoto, T. Fukushima, Y. Suna, N. Ishii, A. Saeki, S. Seki, S. Tagawa, M. Taniguchi, T. Kawai, T. Aida, *Science* **2006**, *314*, 1661; b) H. J. Kim, T. Kim, M. Lee, *Acc. Chem. Res*. **2011**, *44*, 72; c) C. Wang, Z. Wang, X. Zhang, *Acc. Chem. Res.* **2012**, *45*, 608–618; d) K. V. Rao, K. Jayaramulu, T. K. Maji, S. J. George, *Angew. Chem. Int. Ed.* **2010**, *49*, 4218.

[13] a) F. J. M. Hoeben, I. O. Shklyarevskiy, M. J. Pouderoijen, H. Engelkamp, A. P. H. J. Schenning, P. C. M. Christianen, J. C. Maan, E.W. Meijer, *Angew. Chem. Int. Ed.* **2006**, *45*, 1232; b) X. Zhang, Z. Chen, F. Würthner, *J. Am. Chem. Soc*. **2007**, *129*, 4886; c) K. V. Rao, S. J. George, *Org. Lett.* **2010**, *12*, 2656; d) L. C. Palmer, S. I. Stupp, *Acc. Chem. Res*. **2008**, *41*, 1674.

[14] a) J. H. Burroughes, D. D. C. Bradley, A. R. Brown, R. N. Masks, K. M. Mackay, R. H. Friend, P. L. Burns, A. B. Holmes, *Nature* **1990**, *347*, 539; b) M. Granstroöm, K. Petritsch, A. C. Arias, A. Lux, M. R. Andersson , R. H. Friend, *Nature* **1998**, *395*, 257; c) A. Kraft, A. C. Grimsdale, A. B. Holmes, *Angew. Chem. Int. Ed.* **1998**, *37*, 402.

[15] a) M. S. Wong, M. Samoc, A. Samoc, B. Luther-Daviesa, M. G. Humphrey, *J. Mater. Chem*. **1998**, *8*, 2005; b) Y. Tao, A. Donat-Bouillud, M. D'Iorio, J. Lam, T. C. Gorjanc, C. Py, M. S. Wong, Z. H. Li , *Thin Solid Films*, **2000**, *363*, 298; c) Y. Tao, A. Don at-Bouillud, M. D'Iorio, J. Lam, T. C. Gorjanc, C. Py and M. S. Wong, *Synthetic Metals*, **2000**, *111*, 417.

[16] H. Wang, W. You, P. Jiang, L. Yu, H. Hau Wang, *Chem. Eur. J.*, **2004**, *10*, 986.

[17] J. F. Hulvat, M. Sofos, K. Tajima, S. I. Stupp, *J. Am. Chem. Soc.*, **2005**, *127*, 366.

[18] B. Narayan, S. P. Senanayak, A. Jain, K. S. Narayan, S. J. George, *Adv. Funct. Mater*. **2013**, *23*, *3053*.

[19] a) C. D. Dimitrakopoulos, P. R. L. Malenfant, *Adv. Mater*. **2002**, *14*, 99; b) P. T. Herwig, K. Müllen, *Adv. Mater*. **1999**, *11*, 480; c) T. Yasuda, M. Saito, H. Nakamura, T. Tsutsui, *Appl. Phys. Lett*. **2006**, *89*, 182108.

[20] M. D. Watson, A. F. Kötter, K. Müllen, *Chem. Rev*., **2001**, *101*, 1267.

[21] a) J. P. Hill, W. Jin, A. Kosaka, T. Fukushima, H. Ichihara, T. Shimomura, K. Ito, T. Hashizume, N. Ishii, T. Aida, *Science* **2004**, *304*, 1481; b) W. Jin, Y. Yamamoto, T. Fukushima, N. Ishii, J. Kim, K. Kato, M. Takata, T. Aida, *J. Am. Chem. Soc*. **2008**, *130*, 9434.

[22] Y. Yamamoto, T. Fukushima, W. Jin, A. Kosaka, T. Hara, T. Nakamura, A. Saeki, S. Seki, S. Tagawa, T. Aida, *Adv. Mater*. **2006**, *18*, 1297.

[23] Y. Yamamoto, T. Fukushima, Y. Suna, N. Ishii, A. Saeki, S. Seki, S. Tagawa, M. Taniguchi, T. Kawai, T. Aida, *Science* **2006**, *314*, 1761.

[24] a) F. Würthner, *Chem. Commun.* **2004**, 1564; b) M. R. Wasielewski, *Acc. Chem. Res*. **2009**, *42*, 1910.

[25] a) H. Usta, A. Facchetti, T. J. Marks, *Acc. Chem. Res*. **2011**, *44*, 501; b) R. R. Reghu, H. K. Bisoyi, J. V. Grazulevicius, P. Anjukandi, V. Gaidelis, V. Jankauskas, *J. Mater. Chem*. **2011**, *21*, 7811; c) S. Rajaram, R. Shivanna, S. K. Kandappa, K. S. Narayan, *J. Phys. Chem. Lett*. **2012**, *3*, 2405.

[26] D. Görl, X. Zhang, F. Würthner, *Angew. Chem. Int. Ed.* **2012**, *51*, 6328.

[27] I. K. Iverson, S.-W. Tam-Chang, *J. Am. Chem. Soc.* **1999**, *121*, 5801.

[28] a) K. Balakrishnan, A. Datar, R. Oitker, H. Chen, J. Zuo, L. Zang, *J. Am. Chem. Soc.* **2005**, *127*, 10496.

[29] Y. Che, A. Datar, K. Balakrishnan, L. Zang, *J. Am. Chem. Soc.* **2007**, *129*, 7234.

[30] E. Krieg, B. Rybtchinski, *Chem. Eur. J.* **2011**, *17*, 9016.

[31] E. Krieg, H. Weissman, E. Shirman, E. Shimoni, B. Rybtchinski, *Nat. Nanotechnol*. **2011**, *6*, 141.

[32] a) S. Roy, D. K. Maiti, S. Panigrahi, D. Basak, A. Banerjee, *RSC Adv*. **2012**, *2*, 11053; b) D. K. Maiti, A. Banerjee, *Chem.Comm.* **2013**, *49*, 6909.

[33] Y. Sun, C. He, K. Sun, Y. Li, H. Dong, Z. Wang, Z. Li, *Langmuir* **2011**, *27*, 11364.

[34] X. Zhan, A. Facchetti, S. Barlow, T. J. Marks, M. A. Ratner, M. R. Wasielewski, S. R. Marder, *Adv. Mater*. **2011**, *23*, 268.

[35] a) L. Zang, Y. Che, J. S. Moore, *Acc. Chem. Res.* **2008**, *41*, 1596; b) S. V. Bhosale, C. H. Jani, S. J. Langford, *Chem. Soc. Rev.* **2008**, *37*, 331.

[36] H. Shao, M. Gao, S. H. Kim , C. P. Jaroniec, J. R. Parquette, *Chem. Eur. J.* **2011**, *17*, 12882.

[37] a) H. Shao, J. Seifert, N. C. Romano, M. Gao, J. J. Helmus, C. P. Jaroniec, D. A. Modarelli, J. R. Parquette, *Angew. Chem. Int. Ed.* **2010**, *49*, 7598; b) H. Shao, T. Nguyen, N. C. Romano, D. A. Modarelli, J. R. Parquette, *J. Am. Chem. Soc.* **2009**, *131*, 16374.

[38] a) P. Talukdar, G. Bollot, J. Mareda, N. Sakai, S. Matile, *J. Am. Chem. Soc*. **2005**, *127*, 6528; b) G. Sforazzini, E. Orentas, A. Bolag, N. Sakai, S. Matile, *J. Am. Chem. Soc*. **2013**, *135*, 12082.

[39] M. Kumar, S. J. George, *Chem. Eur. J.* **2011**, *17*, 11102.

[40] J. Yin, Y. Zhou, T. Lei, J. Pei, *Angew. Chem. Int. Ed*. **2011**, *50*, 6320.

[41] M.-C. Yeh, Y.-L. Su, M.-C. Tzeng, C. W. Ong, T. Kajitani, H. Enozawa, M. Takata, Y. Koizumi, A. Saeki, S. Seki, T. Fukushima, *Angew. Chem. Int. Ed.* **2012**, *51*, 1.

[42] N. Kim, L. Wang, D.-Y. Kim, S.-Ho Hwang, S.-Wei Kuo, M.-H. Lee, K.-U. Jeong, *Soft Matter* **2012**, *8*, 9183.

[43] S. Cantekin, T. F. A. de Greef, A. R. A. Palmans, *Chem Soc. Rev*. **2012**, *41*, 6125.

[44] T. Curtius, *J. Prakt. Chem.* **1915**, *91*, 39.

[45] a) C. F. C. Fitié , W. S. C. Roelofs, M. Kemerink, R. P. Sijbesma, *J. Am. Chem. Soc*. **2010**, *132*, 6892; b) C. F. C. Fitié, W. S. C. Roelofs, P. C. M. Magusin, M. Wübbenhorst, M. Kemerink, R. P. Sijbesma, *J. Phys. Chem. B* **2012**, *116*, 3928.

[46] J. Roosma, T. Mes, P. Leclère, A. R. A. Palmans, E. W. Meijer, *J. Am. Chem. Soc*. **2008**, *130*, 1120.

[47] a) F. Abraham, S. Ganzleben, D. Hanft, P. Smith, H.-W. Schmidt, *Macromol. Chem. Phys*. **2010**, *211*, 171; b) M. Blomenhofer, S. Ganzleben, D. Hanft, H.-W. Schmidt, M. Kristiansen, P. Smith, K. Stoll, D. Maeder, K. Hoffmann, *Macromolecules* **2005**, *38*, 3688.

[48] P. Besenius, J. L. M. Heynens, R. Straathof, M. M. L. Nieuwenhuizen, P. H. H. Bomans, E. Terreno, S. Aime, G. J. Strijkers, K. Nicolay, E. W. Meijer, *Contrast Media Mol. Imaging*, **2012**, *7*, 356.

[49] A. R. A. Palmans, E. W. Meijer, *Angew. Chem. Int. Ed*. **2007**, *46*, 8948.

[50] M. M. J. Smulders, M. M. L. Nieuwenhuizen, T. F. A. de Greef, P. van der Schoot, A. P. H. J. Schenning, E. W. Meijer, *Chem. Eur. J.* **2010**, *16*, 362.

[51] M. M. J. Smulders, A. P. H. J. Schenning, E. W. Meijer, *J. Am. Chem. Soc*. **2008**, *130*, 606.

[52] a) A. J. Markvoort, H. M. M. ten Eikelder, P. A. J. Hilbers, T. F. A. de Greef, E. W. Meijer, *Nat Commun.* **2011**, *2*, 509; b) M. M. J. Smulders, P. J. M. Stals, T. Mes, T. F. E. Paffen, A. P. H. J. Schenning, A. R. A. Palmans, E. W. Meijer, *J. Am. Chem. Soc*. **2010**, *132*, 620; c) M. M. J. Smulders, I. A. W. Filot, J. M. A. Leenders, P. van der Schoot, A. R. A. Palmans, A. P. H. J. Schenning, E. W. Meijer, *J. Am. Chem. Soc*. **2010**, *132*, 611.

[53] R. van Hameren, P. Schön, A. M. van Buul, J. Hoogboom, S. V. Lazarenko, J. W. Gerritsen, H. Engelkamp, P. M. Christianen, H. A. Heus, J. C. Maan, T. Rasing, S. Speller, A. E. Rowan, J. A. A. W. Elemans R. J. M. Nolte, *Science* **2006**, *314*, 1433.

[54] R. van Hameren, A. M. van Buul, M. A. Castriciano, V. Villari, N. Micali, P. Schön, S. Speller, L. Monsù Scolaro, A. E. Rowan, J. A. A. W. Elemans, R. J. M. Nolte, *Nano Lett.* **2008**, *8*, 253.

[55] N. Veling, R. van Hameren, A. M. van Buul, A. E. Rowan, R. J. M. Nolte, J. A. A. W. Elemans, *Chem. Commun.* **2012**, *48*, 4371.

[56] a) I. Danila, F. Riobe, F. Piron, J. Puigmarti-Luis, J. D. Wallis, M. Linares, H. Agren, D. Beljonne, D. B. Amabilino, N. Avarvari, *J. Am. Chem. Soc*. **2011**, *133*, 8344; b) I. Danila, F. Riobe, J. Puigmarti-Luis, A. Perez del Pino, J. D. Wallis, D. B. Amabilino, N. Avarvari, *J. Mater. Chem.*, **2009**, *19*, 4495.

[57] I. Danila, F. Pop, C. Escudero, L. N. Feldborg, J. Puigmarti-Luis, F. Riobe, N. Avarvari, D. B. Amabilino, *Chem. Commun*., **2012**, *48*, 4552.

[58] K. Kreger, P. Wolfer, H. Audorff, L. Kador, N. Stingelin-Stutzmann, P. Smith, H.-W. Schmidt, *J. Am. Chem. Soc.* **2010**, *132*, 509.

[59] S. Lee, S. Oh, J. Lee, Y. Malpani, Y.-S. Jung, B. Kang, J. Y. Lee, K. Ozasa, T. Isoshima, S. Y. Lee, M. Hara, D. Hashizume, J.-M. Kim, *Langmuir* **2013**, *29*, 5869.

[60] J. van Herrikhuyzen, P. Jonkheijm, A. P. H. J. Schenning, E. W. Meijer, *Org. Biomol. Chem.* **2006**, *4*, 1539.

[61] F. Wang, M. A. J. Gillissen, P. J. M. Stals, A. R. A. Palmans, E. W. Meijer, *Chem. Eur. J.* **2012**, *18*, 11761.

[62] J. Buendía, L. Sánchez, *Org. Lett.* **2013**, *15*, 5746

[63] I. Paraschiv, M. Giesbers, B. van Lagen, F. C. Grozema, R. D. Abellon, L. D. A. Siebbeles, A. T. M. Marcelis, H. Zuilhof, E. J. R. Sudhölter, *Chem. Mater.* **2006**, *18*, 968.

[64] B. Narayan, C. Kulkarni, S. J. George, *J. Mater. Chem. C* **2013**, *1*, 626.

[65] a) J. Liu, H. Su, L. Meng, Y. Zhao, C. Deng, J. C. Y. Ng, P. Lu, M. Faisal, J. W. Y. Lam, X. Huang, H. Wu, K. Sing Wong, B. Z. Tang, *Chem. Sci*. **2012**, *3*, 2737; b) J. Mei, Y. Hong, J. W.Y. Lam, A. Qin, Y. Tang, B. Z. Tang, *Adv. Mater*. **2014**, *26*, 5429.

[66] K. Hanabusa, M. Yamada, M. Kimura, H. Shirai, *Angew. Chem. Int. Ed*. **1996**, *35*, 1949.

[67] K. Hanabusa, K. Shimura, K. Hirose, M. Kimura, H. Shirai, *Chem. Lett*. **1996**, 885.

[68] M. de Loos, J. van Esch, R. M. Kellogg, B. L. Feringa, *Angew. Chem. Int. Ed*. **2001**, *40*, 613.

[69] J.-G. Dong, A. Wada, T. Takakuwa, K. Nakanishi, N. Berova, *J. Am. Chem. Soc*. **1997**, *119*, 12024.

[70] T. Nehira, C. A. Parish, S. Jockusch, N. J. Turro, K. Nakanishi, N. Berova, *J. Am. Chem. Soc*. **1999**, *121*, 8681.

[71] a) J. Kumar, H. Tsumatori, J. Yuasa, T. Kawai, T. Nakashima, *Angew. Chem. Int. Ed.* **2015** , *54*, 5943; b) T. Kawai, K. Kawamura, H. Tsumatori, M. Ishikawa, M. Naito, M. Fujiki, T. Nakashima, *ChemPhysChem* **2007**, *8*, 1465; c) J. Kumar, T. Nakashima, H. Tsumatori, T. Kawai, *J. Phys. Chem. Lett*. **2014**, *5*, 316.

[72] a) J. Kumar, T. Nakashima, H. Tsumatori, M. Mori, M. Naito, T. Kawai, *Chem. Eur. J.* **2013** , *19*, 14090.

[73] I. D. Tevis, W.-W. Tsai, L. C. Palmer, T. Aytun, S. I. Stupp, *ACS Nano*, **2012**, *6*, 2032.

[74] A. Ruiz-Carretero, T. Aytun, C. J. Bruns, C. J. New comb, W.-Wen Tsai, S. I. Stupp, *J. Mater. Chem*. **2013**, *1*, 11674.

# Chapter-2

# Autoresolution of Segregated and Mixed p-n Stacks *via* Homochiral Supramolecular Polymerization in Solution

# Chapter-2

## Autoresolution of Segregated and Mixed p-n Stacks *via* Homochiral Supramolecular Polymerization in Solution


## *Abstract*

*'Homochiral supramolecular polymerization', driven by enantioselective recognition of monomeric units in solution, is proposed to be one of the main reasons for homochirality in nature. Understanding these processes in synthetic molecular systems is therefore, important. Although chirality driven narcisstic self-sorting has been studied in discrete molecular complexes, on surfaces, or on solid-liquid interfaces, homochiral supramolecular polymerization in solution phase is very rarely reported. A strong chiral mismatch between the enantiomers with an ability of homochiral recognition is the prime requisite for obtaining assemblies with narcisstic self-sorting. We have achieved chirality driven self-sorting in solution by employing enantiomerically pure trans-1,2-bis(amido)cyclohexane cores, as these chiral motifs have a strong chiral mismatch between the enantiomers, leading to self-sorting of enantiomeric assemblies.*

*In this Chapter, we describe our results of homochiral polymerization of Bischromophoric Naphthalene diimides (NDIs), which has been characterized extensively by spectroscopic and mechanistic investigations. A step ahead, we have constructed donor-acceptor stacks, with bischromophoric 1,5 dialkoxynaphthalenes (DAN) and achieved a chirality control over donor-acceptor organization. Mixed and orthogonal stacks were observed with donors and acceptors of identical and opposite chiralities respectively. This concept has also been extended to three component system, consisting of the bischromophoric donor and enantiomeric acceptors, where the wrong enantiomeric acceptor autoresolves to give segregated stacks. Such an unprecedented chirality control on donor-acceptor organization paves way for creation of controlled p-n junctions which are of interest in electronic applications.*


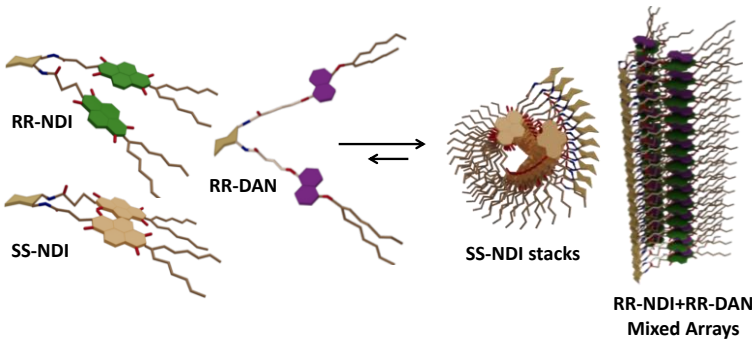


Manuscript based on this work: B. Narayan, K. Bejagam, S. Balasubramanian, S. J. George (under preparation).

## 2.1. Introduction

'Self-sorting' is the process of recognition of identical units, depending on structure or function from a pool of units.[1] Nature successfully manages self-sorting processes, in biological systems like the cell, where the units are compartmentalized according to functions, or in the genetic material, for e.g. DNA or RNA by the complementarity of base pairs.[2] These 'molecular codes' are responsible for the high degree of selectivity in various biological processes occurring in nature. Comprehensive investigations on the self-sorting in various designed complex molecular systems has revealed that these 'molecular codes' depend on size, shape, complementarity of the participating units, steric factors, etc. 'Chirality driven self-sorting' lays the foundation for a distinct branch of investigations, as these are relevant in understanding the homochirality in nature and auto-amplification processes leading to enrichment of a single enantiomer.

Homochiral supramolecular polymerization is the chirality driven narcissistic self-sorting of enantiomeric monomers during their self-assembly. This supramolecular autoresolution process in which the molecular components sort themselves to stereo-chemically pure assemblies in solution is analogous to the Louis Pasteur's resolution experiments to form conglomerate crystals.[3] Although chirality driven self-sorting has been well studied in discrete organic/co-ordination assemblies in solution,[4] on surfaces[5] and on solid-liquid interfaces,[6] chiral self-recognition of monomers during the extended supramolecular polymerization in solution is seldom reported. One of the reasons could be that majority of the dynamic supramolecular chiral systems are designed with monomers with remote chiral side chains and the absence of strong chiral mismatch and dynamic nature leads to co-assembly rather than self-sorting.[7] However, this heterochiral recognition of enantiomeric monomers in supramolecular systems gave us mechanistic insights into the various asymmetric preferences in nature like chiral amplification.[8] Another challenge in this field is the lack of experimental techniques to probe and characterize the homochiral assemblies, unlike the characterization of analogous conglomerate structures in crystals, where one can resolve the crystal structure unambiguously by X-ray crystallography. Despite these challenges, Aida and co-workers have successfully demonstrated the enantioselective

polymerization using S-shaped diketopiperazine (Figure 2.1.a)[9] and bowl-shaped macrocyclic chiral monomers[10] with strong self-recognition abilities. Moreover, the kinetic stabilities of these homochiral assemblies helped to characterize them in a unique manner by using size exclusion chromatography. Very recently, Meijer and co-workers have demonstrated co-operative homochiral selective polymerization of porphyrin (Figure 2.1.b) [11] and star-shaped monomers equipped with multiple chiral side chains at the periphery to impart them strong chiral mismatch.[12] Herein we report for the first time homochiral supramolecular polymerization of self-recognizing aromatic donor (D) and acceptor (A) monomers to construct segregated (orthogonal) and mixed (alternate) p-n stacks in solution state.

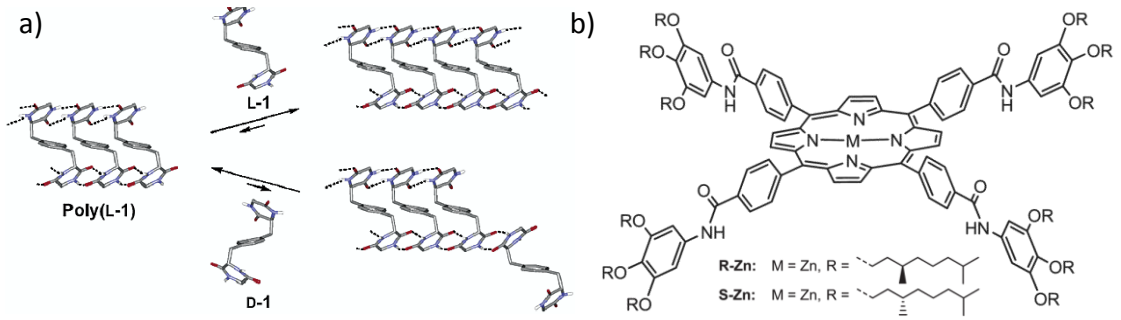


*Figure 2.1. Few examples of chirality driven narcisstic self-sorting of enantiomeric assemblies achieved in solution: a) Schematic representation of homochiral supramolecular polymerization of 'S-shaped' diketopiperazine derivatives; b) Molecular structures of Zn-Porphyrin derivatives that undergo chirality driven self-sorting, as characterized by mechanistic investigations in solution. (Figures a and b reproduced with permissions from references 9 and 11 respectively).*

Molecular level control on the organization of donor and acceptor molecules in multi-component Donor-Acceptor (D-A) nanostructures is very important for extracting desired functions.[13] Orthogonal or segregated organization of D and A molecules leads to interfacial p-n-heterojunctions conducive for efficient charge separation and hence are promising active materials for organic solar cells.[14] On the other hand, co-facial (alternate) D-A nanostructures are attractive candidates for organic ferroelectrics.[15] Various supramolecular design strategies have been employed in the past to control the nanoscale organization of D and A molecules in these nanostructures. Segregated organization has been achieved via structural mismatch of D and A molecules (Figure

2.2.a)[16] or by multiple H-bonding between D and A molecules functionalized with hetero-complementary functional groups (Figure 2.2.b).[17] An efficient amphiphilic design in which covalently connected D and A molecules are compartmentalized in the hydrophobic and hydrophilic domains have also been reported for the segregated D-A organization (Figure 2.2.c).[18] On the other hand foldameric (Figure 2.2.d)[19] and non-covalent amphiphilic designs (Figure 2.2.e)[20] have been employed for the creation of mixed stacks. However, a chirality driven self-sorting strategy has not been exploited to date, for biasing the organization of such π-complementary D and A monomers[21] in supramolecular stacks in solution.

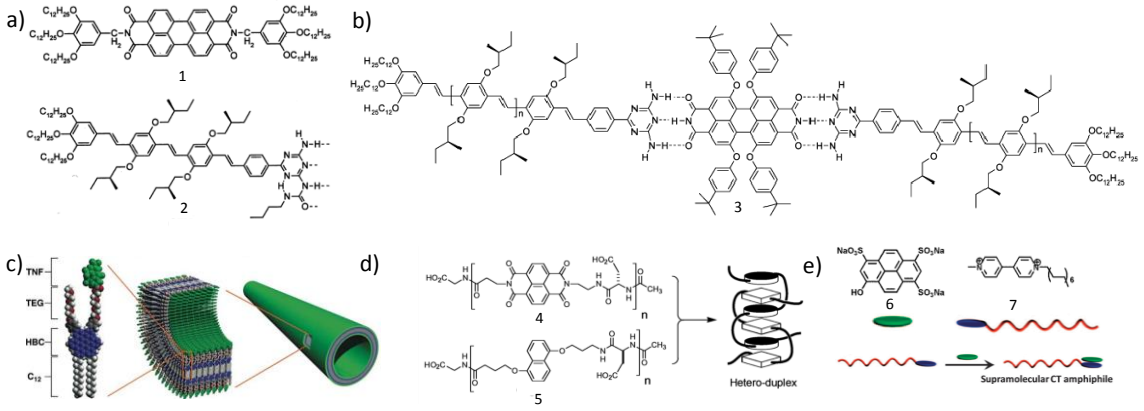


*Figure 2.2. Various design strategies employed for achieving mixed and orthogonal arrangement of donors and acceptors: a) segregated arrangement obtained by creating a structural mismatch between Perylene Bisimide (PBI) (**1**) and Oligo (p-phenylenevinylene) (OPV) (**2**) chromophores; b) orthogonal arrangement by introducing multiple complementary H-bonds between PBI and OPVs forming a segregated complex (**3**); c) amphiphilic design strategy where the donor and acceptor form coaxial nanotube, and are therefore spatially separated; d) foldameric design strategy to create mixed charge-transfer (CT) complex between **4** and **5**; e) non-covalent approach that induces the donor and acceptor to form mixed stacks by formation of a supramolecular amphiphile (Figures a, b, c, d and e reproduced with permissions from references 16d, 17, 18, 19b, 20a, respectively).*

The concept of chirality driven self-sorting introduced in this Chapter for realizing supramolecular p-n assemblies with controlled D-A organization is shown in Figure 2.3. Homochiral polymerization of enantiomerically pure monomers of donors

and acceptors with opposite chirality would result in segregated D-A stacks. On the other hand, multi-component homochiral assembly of D and A monomers with similar chirality would result in mixed D-A organization. In other words, chirality driven narcissistic self-sorting of D and A chiral monomers would result in the narcissistic (segregated) and social (mixed) stacking of π-complementary aromatic units.

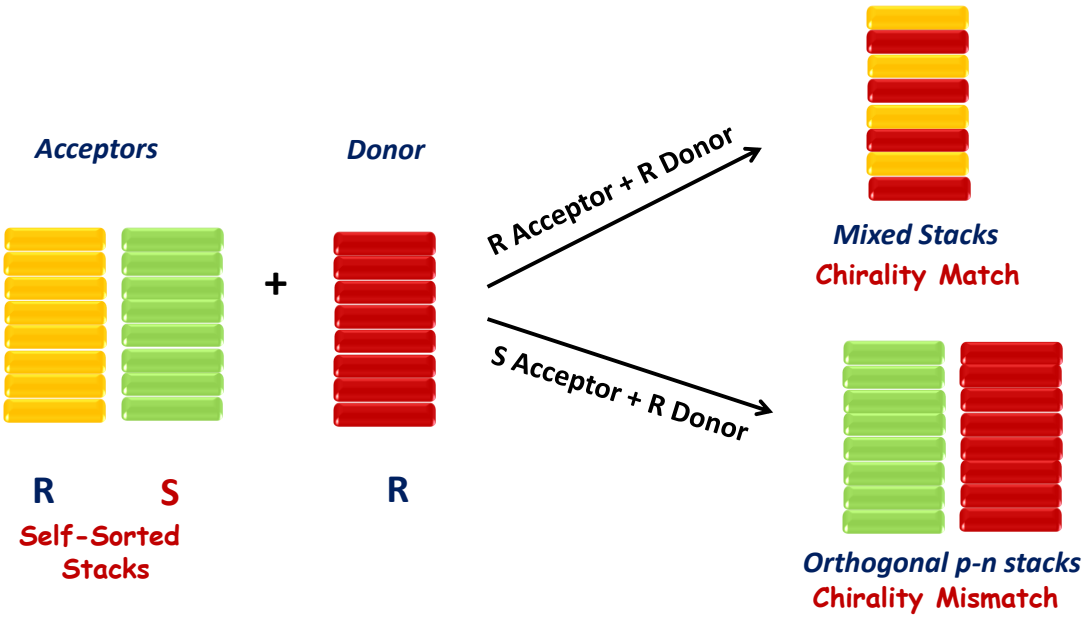


*Figure 2.3. Schematic of chirality driven homochiral polymerization of donors and acceptors leading to mixed and orthogonal stacks.*

## 2.2. Design Strategy

The prime challenge to realize the concept of chirality driven self-sorting of donor-acceptor stacks is to identify self-recognizing motifs with strong chiral mismatch between the enantiomers to functionalize the donor and acceptor chromophores. We have employed enantiomerically pure *trans*-1,2-bis(amido)cyclohexane with two stereogenic centres as the self-assembling chiral group in our molecular design. This moiety is derived from *trans*-1,2-cyclohexanediamine, which has been widely employed for the resolution of enantiomeric mixtures[22] and the corresponding rationally designed bischromophoric derivatives have been extensively used as model systems to study exciton chirality[23] and for the design of self-assembled functional materials (Figure 2.4).[24]

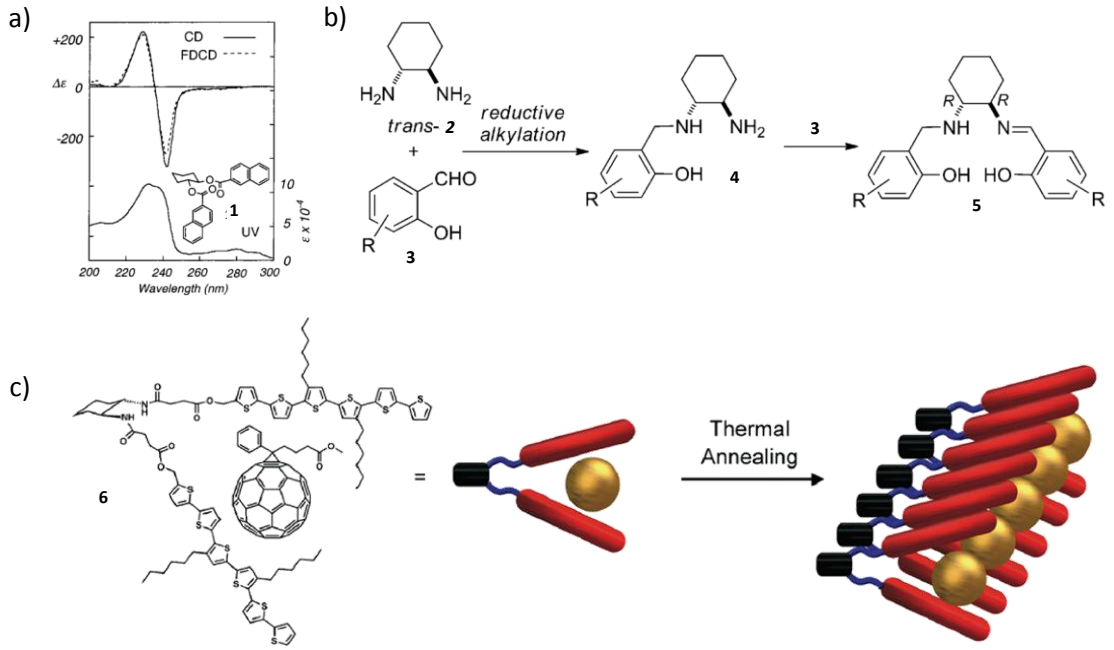


*Figure 2.4. Few examples of trans-1,2-cyclohexane derivatives used in literature for various functional purposes: a) (1R,2R)-trans-1,2-cyclohexanediol 1,2-bis-(2-naphthoate) (**1**) used as a model compound for probing the potential of fluorescence-detected circular dichroism (FDCD) to extend the scope of the exciton chirality method by Berova and coworkers; b) synthetic route to trans-diaminocyclohexane based salalen type ligands (**5**) well exploited by Berkessel and coworkers as organocatalysts for enantioselective separations; c) Bischromophoric thiophene (**6**) designed by Stupp and coworkers, that forms grooved nanowires and acts as the donor component of organic bulk heterojuctions, with fullerene as the acceptor domain (Figures a, b, and c reproduced with permissions from references 23b, 22b and 24b respectively).*

Our preference to employ *trans*-1,2-cyclohexanediamine was further motivated by an early study by Feringa and coworkers, where chiral recognition has been shown in the self-assembled aggregates of corresponding bis(ureido) derivatives.[25] Thus, the core-to-core H-bonding interactions between the bis(amido) cyclohexane moieties are expected to provide significant energy difference between homochiral and heterochiral stacking of the enantiomeric molecules during the supramolecular polymerization process.

To facilitate the investigation of the chirality driven control on the donor-acceptor organization through spectroscopic probes, we have chosen the well-studied

naphthalenedimide (NDI) and 1, 5-dialkoxy naphthalene (DAN) derivatives as donor and acceptor chromophores respectively. The molecular structures of the bischromophoric molecules, (1R,2R)-(-)-bis(amido)Naphthalene diimide (**RR-NDI**), (1S,2S)-(+)-bis(amido)Naphthalene diimide (**SS-NDI)**, (1R,2R)-(-)-bis(amido)Dialkoxynaphthalene (**RR-DAN**) and (1S,2S)-(-)-bis(amido)Dialkoxynaphthalene (**SS-DAN**) used in the present study are shown in Figure 2.5.

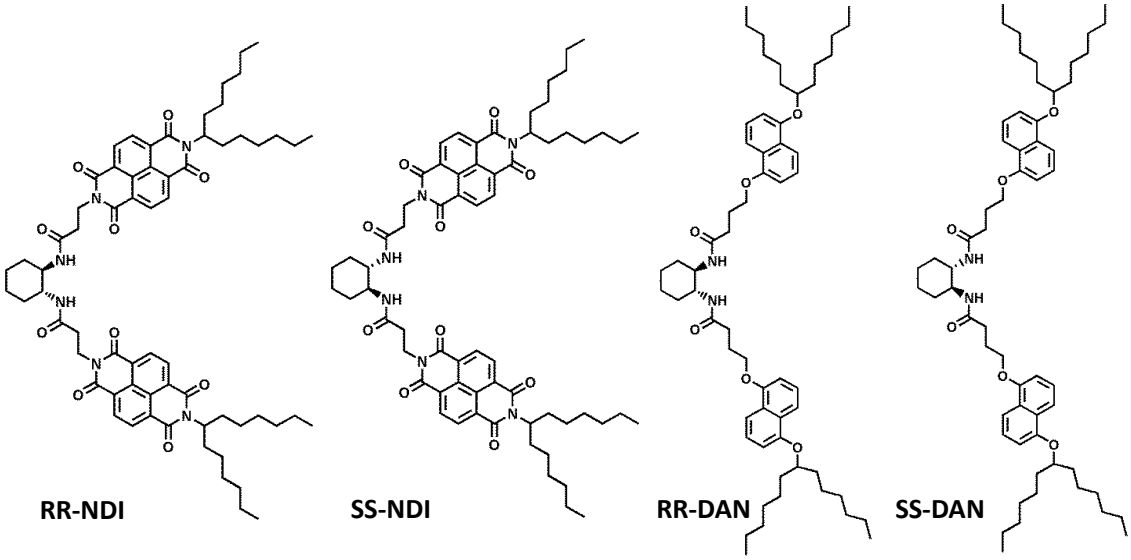


*Figure 2.5. Molecular structures of trans-cyclohexanediamide based bischromophoric donors (**RR-DAN**, **SS-DAN**) and acceptors (**RR-NDI**, **SS-NDI**).*

Bischromophoric NDI derivatives were synthesized by the imidation of alkyl substituted naphthalene monoimide monoanhydride derivative with beta-alanine functionalized *trans*-1,2-cyclohexanediamide molecules. On the other hand, the bischromophoric naphthol derivatives were synthesized by the amidation of (*1R*,2*R*)-(-)-1,2-Diaminocyclohexane and (1*S*,2*S*)-(+)-1,2-Diaminocyclohexane, respectively, with the acid functionalized naphthol derivative (Schemes 2.1.-2.3.). Swallow tail alkyl chains have been attached to both NDI and DAN derivatives to provide enough solubility to the molecules. All the derivatives were characterized completely by $^{1}H$ and $^{13}C$ NMR spectroscopy and high-resolution mass spectrometry (HRMS). (See section 2.6.2. for details).

## 2.3. Homochiral Supramolecular Polymerization of Bischromophoric Naphthalene diimides

The first step towards the realization of chirality driven orthogonal and alternate donor-acceptor arrays is to investigate whether the proposed design strategy based on self-recognizing *trans*-1,2-cyclohexanediamides is efficient in driving the homochiral supramolecular polymerization, leading to self-sorted assemblies of bischromophoric Naphthalene diimides .

### 2.3.1. Self-Assembly of Bischromophoric Naphthalene diimides

Bischromophoric NDI derivatives exist as monomers in 1,1,2,2 tetrachloroethane (TCE) solvent at room temperature and in methyl cyclohexane (MCH) solvent at high temperatures as evident from the corresponding absorption spectral features (Figure 2.6.a, b). On the other hand, absorption spectra of these NDIs in MCH at room temperature showed broadening with reversal of vibrionic band intensities at 360 nm and 380 nm, characteristic of H-type aggregation of NDIs, suggesting the assembly of these molecules (Figure 2.6.a). Hence, the supramolecular polymerization was performed in TCE/MCH solvent mixture under thermodynamic conditions by slowly cooling the solutions of NDI monomers ($2.5x10^{-5}$ M) from 368.15 K to 298.15 K with a temperature gradient of 1 K/min. Circular dichroism spectra of resulting solutions of **SS-NDI** and **RR-NDI** showed mirror image bisignated profile, typical of enantiomeric assemblies with helically organized chromophores. The bisignated CD signal in MCH showed maxima at 344 nm, 359 nm and 391 nm in the NDI region and 250 nm in the amide region, with a zero-crossing at 383 nm, close to the absorption maximum characteristic of exciton coupled NDI chromophores in a chiral environment.

Interestingly, enantiomeric NDI monomers in TCE also showed, weakly coupled mirror image CD spectra with maximum at 385 nm significantly different from that of the assemblies, thus indicating a different origin (Figure 2.6.c). Concentration dependent studies on the g-values further elucidated the difference in origin of CD signals in TCE and MCH (Figure 2.6.d). The g-values in TCE monitored at 385 nm remained constant at $-2.1x10^{-4}$ for **RR-NDI** while there was a non-linear increase in the

g-value ($4x10^{-4}$ to $1.6x10^{-3}$ on going from $10^{-5}$ M to $10^{-4}$ M) obtained at 359 nm in MCH, suggesting the intra and inter-monomeric interactions, respectively being the origin of different CD profiles.

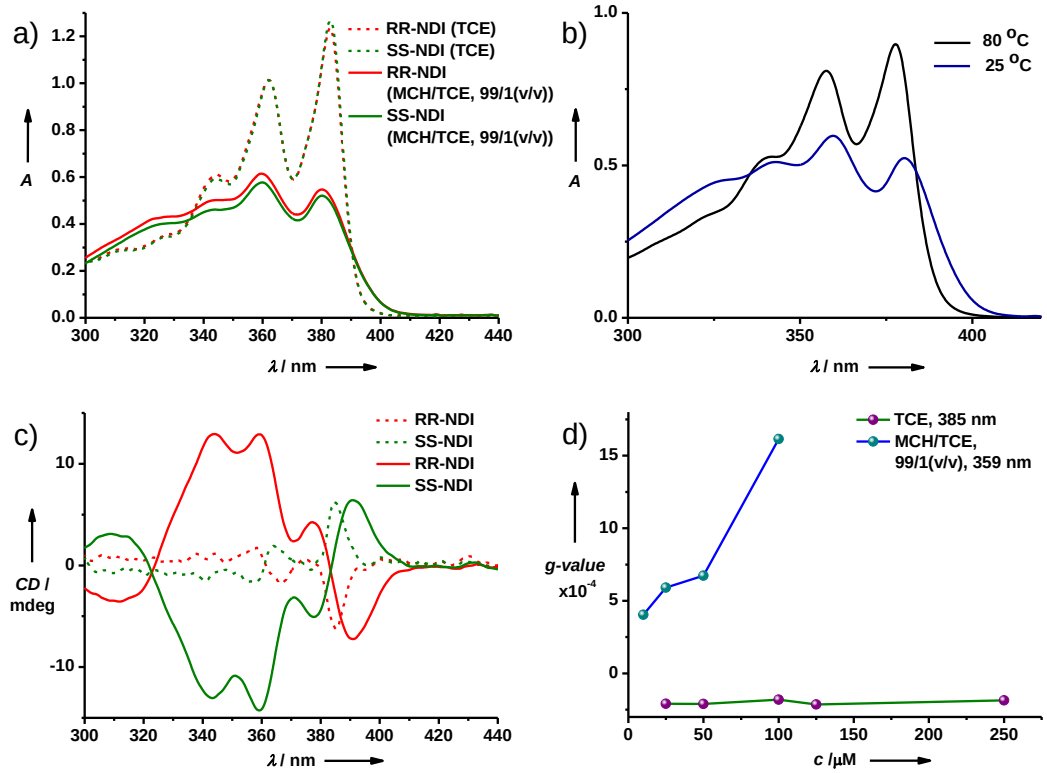


*Figure 2.6. Spectroscopic characterization of the monomeric and self-assembled states of **RR**- or **SS-NDI**: a) Absorption spectral features of monomeric (TCE) and self-assembled (MCH/TCE, 99/1, (v/v)) in dilute solutions of bischromophoric NDIs; b) temperature dependent absorption spectral changes involved in assembled to monomeric transition in **SS-NDI** due to melting of aggregates MCH/TCE, 99/1, (v/v), ($c=2.5x10^{-5}$ M); c) CD spectra of dilute solutions of Bischromophoric NDIs ($c=2.5x10^{-5}$ M) in 1,1,2,2 Tetrachloroethane (TCE) (dotted lines) and MCH/TCE, 99/1, (v/v) (solid lines) respectively; d) Plot of g-value versus concentration explaining the intramolecular and intermolecular origins of the CD signal in TCE and MCH/TCE, 99/1, (v/v) respectively.*

## 2.3.2. Mechanistic Investigations into the Self-Assembly

In order to understand the mechanism of self-assembly of bischromophoric NDIs, we have carried out temperature dependent spectroscopic measurements, while

monitoring a particular wavelength which is sensitive to the changes brought about by temperature effects.

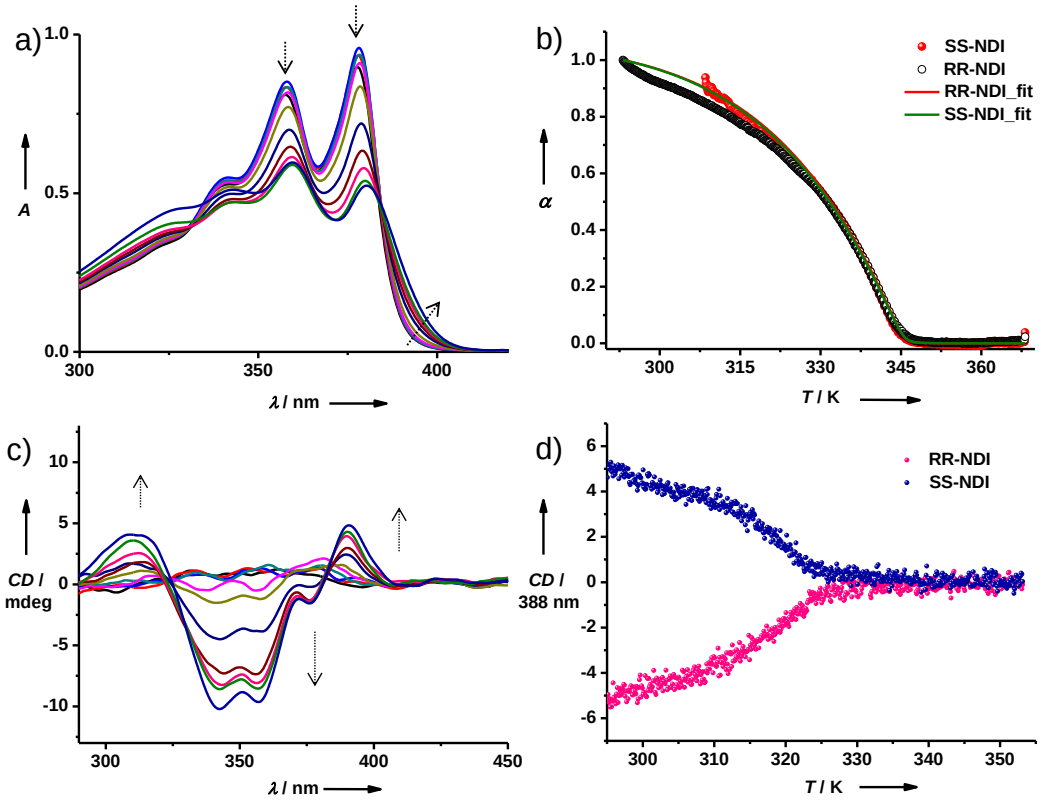


*Figure 2.7. Investigation of cooperative mechanism of self-assembly in bischromophoric NDIs through temperature dependent measurements: a) Variable temperature spectra showing a transition from monomeric to self-assembled state in* ***SS-NDI*** *($c=2.5x10^{-5}$ M); b) Plot of fraction of aggregates α versus temperature obtained by monitoring spectral changes at 399 nm in the absorption spectra on cooling $10^{-4}$ M solutions of Bischromophoric NDIs (-dT/dt=1 K/min) demonstrating cooperative mechanism of self-assembly (the scatter plots are the experimental curves and the solid lines are the cooperative fits); c) Variable Temperature CD spectra of* ***SS-NDI*** *obtained by cooling a $2.5x10^{-5}$ M solution in MCH/TCE, 99/1, (v/v) from 358.15 K to 298.15 K (-dT/dt= 1 K/min); d) Cooperative cooling curves obtained by monitoring CD at 388 nm as the solutions of Bischromophoric NDIs were cooled from 358.15 K to 298.15 K (-dT/dt= 2 K/min, $c= 2.5x10^{-5}$ M); (the arrows in Figure a and c are provided to guide the eye).*

Dilute solutions of bischromophoric NDIs were heated to high temperatures, where the assembly breaks down to monomers (typically 363.15 K) (Figure 2.7.a, c), which were then cooled back to 298.15 K, at a slow cooling rate (-dT/dt=1 K/min), to ensure thermodynamic equilibrium. The cooling curves so obtained were fitted using matlab software using a cooperative model developed by Eikelder and coworkers.[26] These measurements were done by monitoring the absorption and CD changes.

The plot of α (degree of aggregation) versus temperature obtained by monitoring the absorption changes at 399 nm during the temperature dependent polymerization of enantiomeric NDIs ($10^{-4}$ M) showed non-sigmoidal curves with a nucleation regime followed by a steep elongation regime, characteristic of co-operative supramolecular assembly (Figure 2.7.b). Fitting of these cooling curves with a temperature-dependent nucleation- elongation model yielded an elongation temperature ($T_e$), the temperature, at which propagation process sets in, of 345.35 K. As expected, probing the CD spectra also revealed mirror-image non-sigmoidal cooling curves for **SS-** and **RR-NDI**s (Figure 2.7.d).

| Concentration (M) | | $\Delta H°_e$ (kJ/mol) | $\Delta S°_e$ (kJ/mol.K) | $\Delta H°_{nuc}$ (kJ/mol) | $T_e$ (K) |
|---|---|---|---|---|---|
| $10^{-4}$ | **RR-NDI** | -45.26±0.24 | -0.055±0.001 | -29.41±0.63 | 345.16±0.06 |
| | **SS-NDI** | -45.43±0.54 | -0.055±0.002 | -27.51±0.66 | 344.91±0.08 |
| $5x10^{-5}$ | **RR-NDI** | -50.03±0.51 | -0.07±0.002 | -27.70±0.96 | 336.41±0.09 |
| | **SS-NDI** | -60.48±0.96 | -0.1±0.003 | -20.51±0.36 | 335.72±0.08 |
| $2.5x10^{-5}$ | **RR-NDI** | -56.94±1.29 | -0.09±0.004 | -16.97±0.33 | 325.04±0.11 |
| | **SS-NDI** | -58.13±0.96 | -0.09±0.002 | -18.66±0.3 | 325.67±0.08 |

*Table 2.1. Thermodynamic parameters obtained from co-operative fits of cooling curves obtained by monitoring the absorption changes at 399 nm in the UV spectra of **SS-NDI** or **RR-NDI** at different concentrations in MCH/TCE, 99/1, (v/v).*

The thermodynamic parameters obtained from the cooperative fits for both **RR-NDI** and **SS-NDI**, well correlated with each other, suggesting similar homochiral polymerization for the pure enantiomers (Table 2.1).

## 2.3.3. Chirality Driven Self-Sorting in Bischromophoric NDIs

In order to study the self-recognizing/self-discrimination behaviour of **RR-NDI**/**SS-NDI** enantiomers in self-assembled enantiomeric mixtures, temperature dependent supramolecular polymerization of bischromophoric mixtures with varying enantiomeric excess (ee) were carried out under thermodynamic conditions (MCH/TCE, 99/1, (v/v)), c = 2.5x10$^{-5}$ M) and the spectral characteristics of resulting assemblies were recorded at 298.15 K.

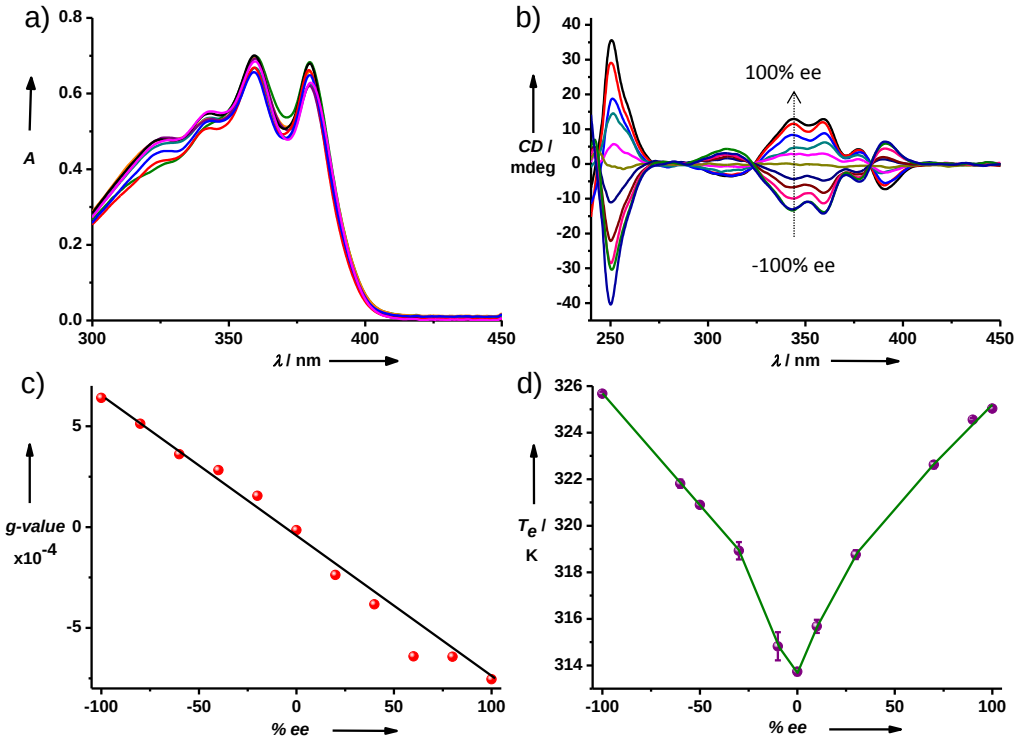


*Figure 2.8. Spectroscopic investigations of homochiral polymerization process in bischromophoric NDIs: a) Absorption spectra of thermodynamically cooled self-assembled solutions of various enantiomeric mixtures (-100% ee to 100% ee) showing negligible changes; b) respective CD spectra having a monotonic increment in the CD intensity with increasing ee; c) linear fit of g-value versus % enantiomeric excess (% ee) ruling out chiral amplification in mixed compositions; d) Plot of $T_e$ versus % ee showing a clear decrease in $T_e$ with decreasing enantiomeric excess as a proof of narcisstic self-sorting leading to supramolecular conglomerates (the $T_e$ at 0% ee is same as the $T_e$ of 100% ee of half the concentration); (c = 2.5x10$^{-5}$ M, l = 10 mm). The error bars in Figure d have been obtained from cooperative fits.*

Absorption spectra of the self-assembled solution hardly showed any change, whereas the bisignated CD spectra showed a monotonic increase in their intensity with increase in ee (Figure 2.8.a, b). This is further evident from the plot of dissymmetry factor ($g_{CD}$) against ee which showed a linear change (Figure 2.8.c). This suggests that the assemblies constructed form the equimolar mixture of **SS-NDI** and **RR-NDI** (1:1 mixture) monomers are either self-recognition driven homochiral stacks (supramolecular conglomerates) or self-discrimination driven heterochiral stacks (supramolecular racemates). Although the similarity between the absorption spectra of assemblies constructed from various enantiomeric mixtures with that of enantiomerically pure assemblies suggested the formation of homochiral stacks, it was necessary to resort to more reliable probes to ascertain this observation.

Various research groups have probed homochiral polymerization in supramolecular systems by various methods, depending on the nature of the system under investigation. Aida and co-workers have developed a unique Size Exclusion Chromatography (SEC) coupled with a CD detector to probe the self-sorting in kinetically stable assemblies. Very recently, Kawai and co-workers have used microscopic techniques to probe this self-sorting in supramolecular assemblies.[27] In case of dynamic, cooperative supramolecular systems, Meijer and co-workers have demonstrated that the elongation temperature can be an efficient probe to monitor the chirality driven self-sorting process because of its concentration dependence.[11] Considering the co-operative nature of supramolecular polymerization in our system, we have followed this method. A plot of $T_e$ of various assemblies versus corresponding ee gives a parabolic curve, with a decrease in the elongation temperature with decreasing enantiomeric excess and with the minimum $T_e$ for the equimolar mixture of monomers hinting towards the formation of supramolecular conglomerates (Figure 2.8.d). Interestingly the $T_e$ of 1:1 mixture of **RR-NDI** and **SS-NDI**, matched exactly with that of the enantiomerically pure assemblies at half the concentration, thus providing an unequivocal proof for the self-recognizing homochiral polymerization in the present system (Figure 2.9).

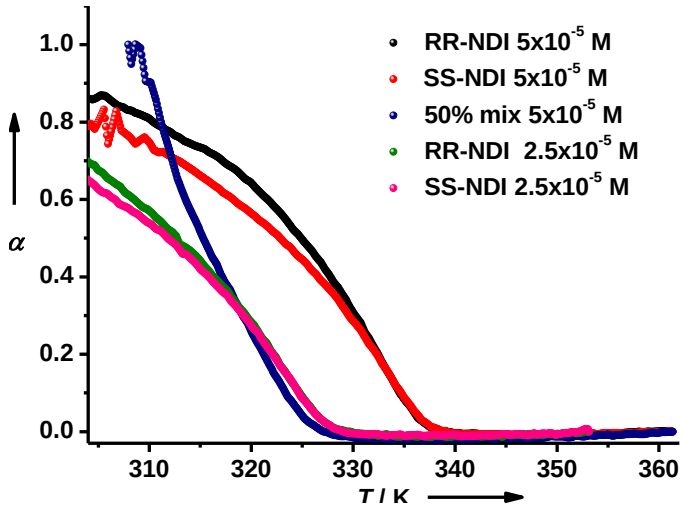


*Figure 2.9. Plot of fraction of aggregates (α) versus temperature of various concentrations of equimolar mixtures of **RR-NDI** and **SS-NDI** obtained by monitoring absorption at 399 nm (-dT/dt= 1 K/min, 358.15 K to 298.15 K) showing a clear decrease in the $T_e$ value of the 50:50 composition compared to the enantiomerically pure sample at the same concentration and the $T_e$ obtained at this composition matching with the $T_e$ of the enantiomerically pure sample at half the concentration; thus proving autoresolution process leading to the formation of supramolecular conglomerates.*

### 2.3.4. Theoretical Insights into Homochiral Recognition

A microscopic understanding of the preference for self-sorting was arrived through molecular modeling. Homo and hetero dimers, as shown in Figure 2.10.a, b were considered as basic building units of an assembly. In order to decrease the computational cost, swallow tails were truncated to methyl groups. The geometry of each dimer was optimized within a force-field approach post an initial relaxation carried out via a Molecular Dynamics (MD) simulation at 5 K. These structures were used as the input for the single point quantum calculations to determine the energies at B3LYP level of theory using Gaussian-09*. The homochiral dimer is seen to be favored over the heterochiral one by 15.1 kcal/mol. A difference in chirality leads to significant differences in molecular packing resulting in an energy penalty for a hetero dimer. The energy penalty offered by the optimized core alone (chopping off NDI) was accounted to be 5.1 kcal/mol at B3LYP/6-31g(d) level of theory (Figure 2.10.c, d).

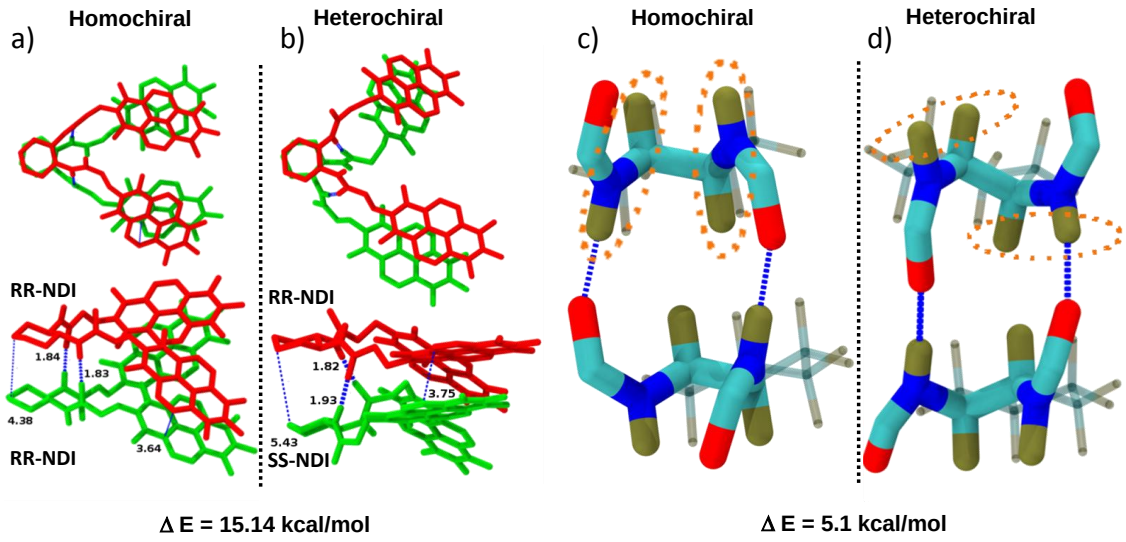


*Figure 2.10. a), b) Top (top panels) and side views of dimeric models of **RR-NDI** and **RR-NDI** (left) and **SS-NDI** and **RR-NDI** (right). Difference in energy was determined at DREIDING*//B3LYP/6-311+g(d,p) level of theory. Distances are specified in Å. Each molecule is either shown in red or green to provide clarity; c), d) Dimeric models of homochiral and heterochiral configurations of the **RR-/SS-** chiral core. In a hetero dimer, both the amide groups of either **SS-NDI** or **RR-NDI** rotate to form hydrogen bond with the other NDI molecule. As a result, two hydrogens come closer as marked in a hetero dimer. NDI molecules are not shown for clarity.*

## 2.4. Chirality Driven Mixed and Orthogonal D-A Stacks

A step ahead, we sought for the construction of orthogonal and mixed p-n assemblies via homochiral supramolecular polymerization of rationally designed donor and acceptor monomers. In this regard, we have designed *trans*-1,2-bis(amido)cyclohexane functionalized dialkoxy naphthalene (**RR-** or **SS-DAN**) derivatives as donor monomers which are well- studied donor chromophores for NDI acceptor molecules[28] Though a bischromophoric DAN derivative with an ethylene spacer would have been the ideal structural match for bischromophoric NDIs, it was synthetically challenging. Although the DAN derivatives also self-assemble in TCE/ MCH solvent mixtures, the absorption spectral changes and CD intensity are minimal upon stacking to follow the polymerization process spectroscopically. However, the weakly bisignated CD signal in TCE-MCH solvent mixture indeed showed the presence

of exciton coupled CD spectra characteristic of helically stacked DAN chromophore (Figure 2.11.b).

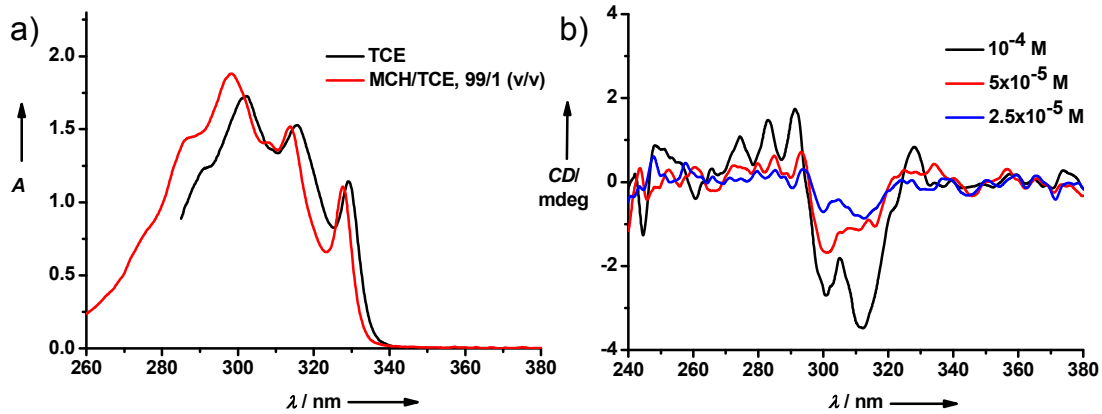


*Figure 2.11. Self-assembly of **RR-DAN**: a) Absorption spectra in TCE (molecularly dissolved) and MCH/TCE, 99/1, (v/v) (self-assembled) having very little changes on aggregation, ($c=10^{-4}$ M); b) CD spectra of various concentrations in MCH/TCE, 99/1, (v/v) showing weakly bisignated CD signal indicative of excitonically coupled chromophores.*

TEM studies further confirmed the self-assembly of these DAN derivatives. The TEM samples were prepared by drop-casting the thermodynamic sample of self-assembled **RR-DAN** (MCH/TCE, 99/1, (v/v)) on to a copper grid and staining with uranyl acetate. One dimensional nanostructures with average lengths of 500 nm and average width 100 nm (Figure 2.12.) were observed throughout the sample, suggesting self-assembly of **RR-DAN**.

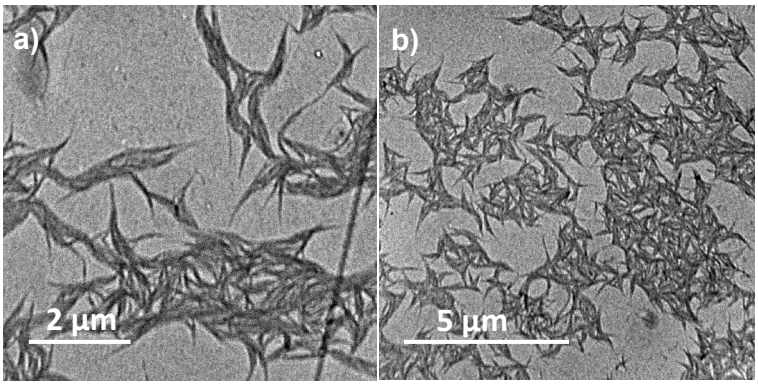


*Figure 2.12. Fibrous morphology obtained for self-assembled **RR-DAN** ($10^{-4}$ M, MCH/TCE, 99/1, (v/v)) as observed by TEM (the sample was stained with uranyl acetate).*

### 2.4.1. Spectroscopic and Morphological Characterization of D-A Organization

In order to realize the p-n assemblies, multi-component co-polymerization of enantiomeric mixtures of donor and acceptor monomers were attempted in a similar fashion as that of homo-polymerization described above (MCH/TCE, 99/1, (v/v), $c=10^{-4}$ M,-dT/dt=1K/min). Co-polymerization of donor and acceptor molecules to mixed p-n assemblies can be probed spectroscopically by the appearance of charge-transfer (CT) absorption band at higher wavelength characteristic of co-facial D-A organization. It should be noted that the strength of the present NDI-DAN CT pair is weak probably due to their structural mismatch in spacer lengths and as a result, more equivalents of acceptor DAN derivatives were required to ensure the complete CT complexation. First, we attempted the two component polymerization of enantiomeric NDI monomers, **SS-NDI** and **RR-NDI**, with increasing equivalents of **RR-DAN** and the intensity of CT band at 503 nm of resulting stacks formed under thermodynamic conditions were probed at 298.15 K and plotted against the equivalents of **RR-DAN** for both D-A pairs (Figure 2.13).

It is evident from Figures 2.13, that homochiral supramolecular co-polymerization between D and A monomer with similar chirality (**RR-NDI** and **RR-DAN**) indeed leads to alternately organized p-n stacks as evident from the appearance of strong charge-transfer (CT) band with a maximum at 503 nm, characteristic of NDI-DAN co-facial CT pairs.[29] Formation of mixed CT stacks is further evident from the deep red colour of the co-polymerized solutions (inset of Figure 2.13.a). Probing the intensity of the charge-transfer band as a function of equivalents of DAN showed a saturation with 10 equivalents of DAN monomers (Figure 2.13.b). Furthermore, the NDI region was indicative of reduced π-π interactions between the NDI cores, due to the formation of mixed stacks in the case of **RR-NDI**, while no significant changes were observed in the case of **SS-NDI**, suggesting the formation of orthogonal arrays (Figure 2.13.c, d). The CT stacks were however, achiral, as proved by the absence of a CD signal in the CT region.

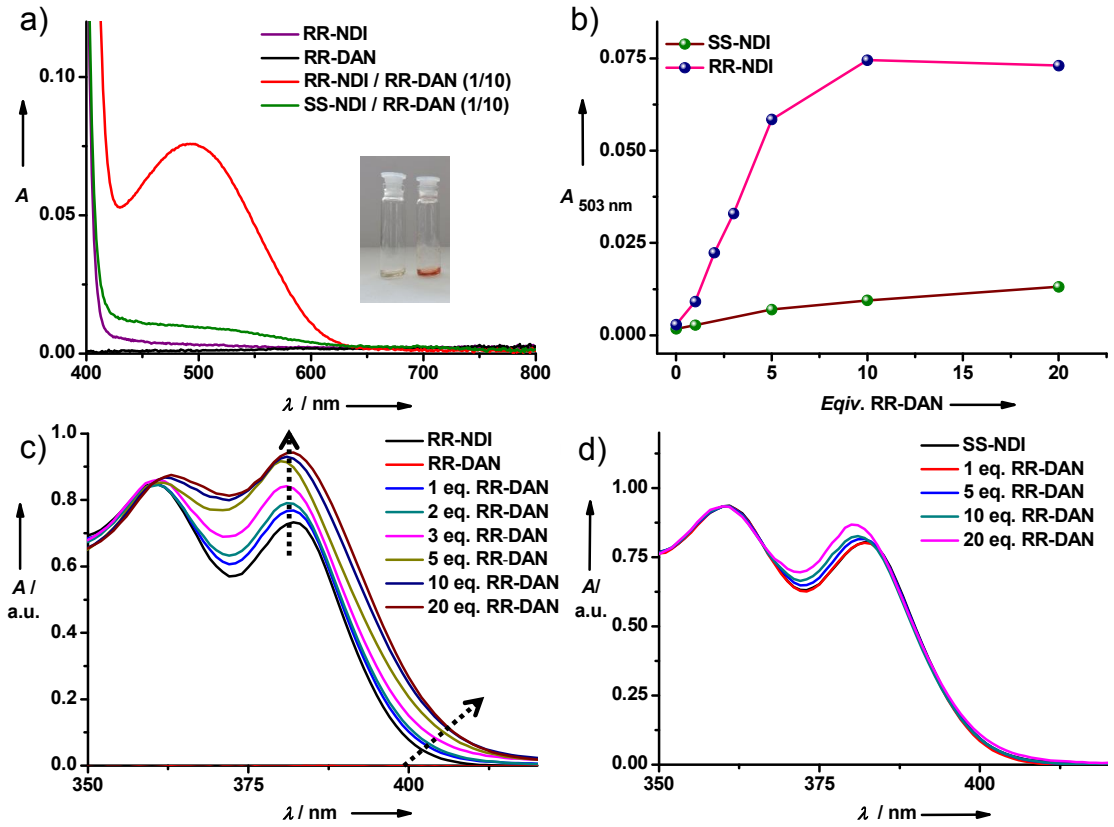


*Figure 2.13. Investigations of homochiral supramolecular polymerization of D-A monomers using CT complexation as a probe: a) Absorption spectra of co-polymerized solutions of **RR-/SS-NDI** with 10 equivalents of **RR-DAN**, demonstrating the formation of alternate and segregated D-A stacks, respectively (the inset in Figure a is the photograph of the respective co-assembled solutions, the left being a solution containing **SS-NDI** and 10 equivalents of **RR-DAN** and the one on the right being a solution containing **RR-NDI** and 10 equivalents of **RR-DAN**); b) Plot of absorption at CT band versus equivalents of **RR-DAN**, clearly distinguishing the mixed and orthogonal stack formation; c), d) absorption spectra normalized at 360 nm (NDI region) showing weakening of **RR-NDI** interchromophoric interactions on CT complexation (c) (arrows are provided to guide the eye) while **SS-NDI** does not show a remarkable change (d).*

Probing the intensity of the charge-transfer band as a function of equivalents of **RR-DAN** showed a saturation with 10 equivalents of **RR-DAN** monomers. High resolution mass spectrometry of the co-polymerized **RR-NDI/RR-DAN** (1/10, $10^{-4}$ M) showed a mass at 2055.2896 corresponding to the 1:1 complex reiterating the formation of co-facial CT pairs. Finally, TEM imaging of the same solution showed the formation

micrometre long fibrous structures (Figure 2.14). On the other hand, supramolecular polymerized solutions of D and A monomers with opposite chirality did not show significant CT absorption and the resulting solutions remained colourless even in the presence of high equivalents of **RR-DAN** monomers. These observations hint towards the formation of segregated homochiral donor and acceptor stacks by the self-recognition of enantiomeric monomers.

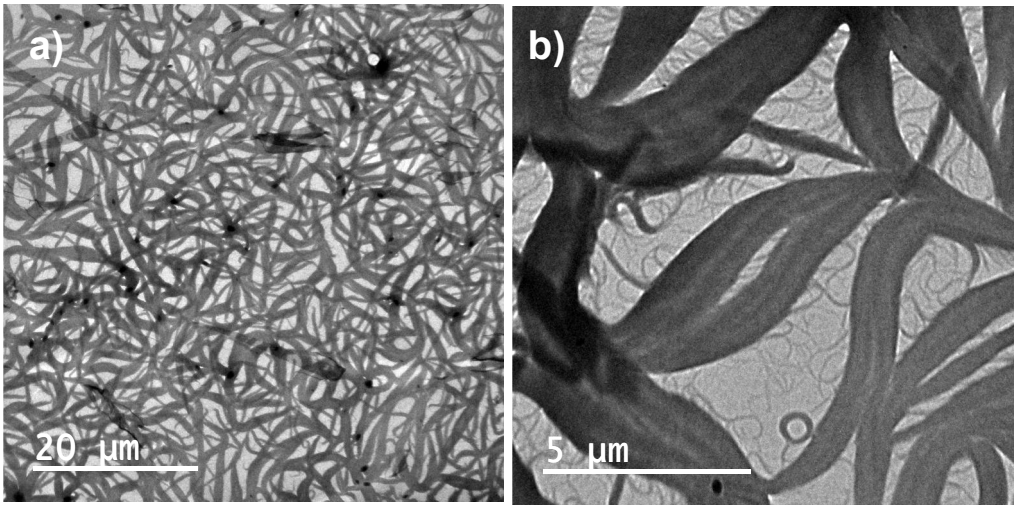


*Figure 2.14.a) and b) TEM images of $10^{-4}$ M solution of the drop casted sample of **RR-NDI** with 10 equivalents of **RR-DAN** stained with uranyl acetate showing bundles of CT fibers.*

## 2.4.2. Mechanistic Insights into D-A Co-Polymerization

It can be still argued that **RR-NDI** and **SS-DAN** with opposite chirality indeed forms mixed stacks with weak charge-transfer interactions leading to less-intense CT band rather than forming orthogonal stacks. In order to rule out the possibility of formation of mixed stacks in the case of donor and acceptor of opposite chiralities, we have turned our attention again to the mechanistic insights of temperature dependent supramolecular co-polymerization process and carried out experiments in this direction. Interestingly, the co-polymerization of mixed stacks as a function of temperature can be exclusively probed at the CT absorption maximum (503 nm), whereas segregated polymerization of free NDI monomers can be orthogonally monitored at 399 nm corresponding to the absorption of stacked NDI chromophores. The CT stacks were highly stable even at high temperatures (90 $^{o}$C); hence, the mechanism of the CT growth could be investigated only in

dilute solutions ($1.25x10^{-5}$ M). The plot of α versus temperature obtained by monitoring either 503 nm or 399 nm exhibited a sigmoidal trend, and fitted well to the isodesmic mechanism of self-assembly (Figure 2.15.a). Similarly, the isodesmic nature of the CT growth was reflected in the cooling curves obtained by monitoring either wavelength in mixed stacks, indicating the complete incorporation of **RR-NDI** monomers in the homochiral D-A stacks (Figure 2.15.b).

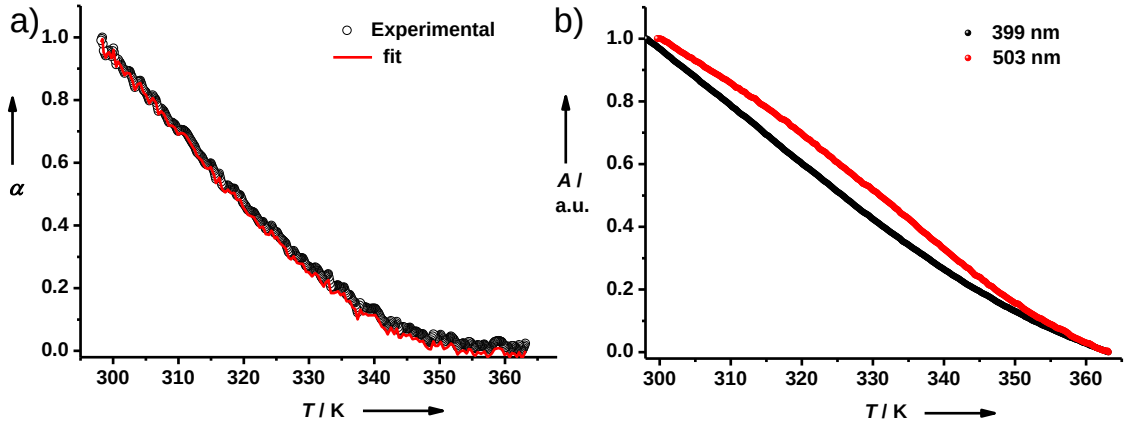


*Figure 2.15. Mechanistic investigation into the CT growth: a) Plot of fraction of aggregates α versus temperature obtained by monitoring spectral changes at 503 nm in the absorption spectra on cooling a dilute CT solution (**RR-NDI/ RR-DAN** (1/10), $c=1.25x10^{-5}$ M, -dT/dt=1 K/min) demonstrating isodesmic mechanism of self-assembly (the scatter plot is the experimental curve and the solid line is the isosdesmic fit); b) Sigmoidal profiles of cooling curves of homochiral mixed D-A obtained by monitoring the absorption changes at 399 nm/503 nm as a proof of the isodesmic nature of CT growth (**RR-NDI/ RR-DAN** (1/10), $c=10^{-4}$ M).*

On the other hand, the autoresolution of the wrong enantiomer in a D-A mixture of opposite chirality was proved unambiguously from the co-operative growth of NDI (399 nm), suggesting orthogonal segregation (Figure 2.16.a). However, probing the autoresolution process of the wrong enantiomer from an equimolar mixture of the **SS-/RR-NDI**s ($c=10^{-4}$ M) by saturating equivalents of DAN (5 eq.) was more challenging, as the broad absorption features of NDI in the mixed stacks at 399 nm have a dominating contribution in the absorption spectrum. Chirality turned out to be an effective probe to address this challenge, where the self-sorting process of the wrong enantiomer (**SS-NDI**) could be monitored by the cooperative growth of the CD signal at

364 nm similar to homochiral stacks of **SS-NDI** in the tricomponent mixture (Figure 2.16.a). The simultaneous growth of mixed CT stacks could be ascertained by the isodesmic growth at 503 nm in the tricomponent mixture. Finally, in a four component mixture consisting of equimolar concentrations of NDIs ($10^{-4}$ M) and the saturating equivalents of the donor counterparts (5 eq.), the homochiral D-A recognition and complete incorporation of NDI monomers in their respective D-A stacks was unambiguously proved by isodesmic cooling curves obtained by monitoring both 399 nm and 503 nm (Figure 2.16.c).

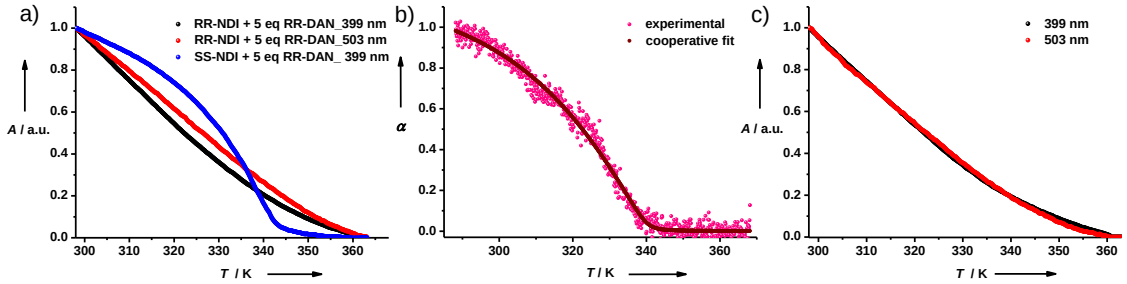


*Figure 2.16. Autoresolution of **SS-NDI** and homochiral co-polymerization of **RR-NDI** and **RR-DAN** elucidated by mechanistic investigations: a) plot of absorption changes at CT (503 nm) and NDI (399 nm) wavelengths in two component mixtures (**RR-/SS-NDI** : **RR-DAN** (5 eq.)), showing the isodesmic CT growth in mixed stacks of **RR-NDI/RR-DAN**, while a segregation process of **SS-NDI** in **SS-NDI/RR-DAN** stacks proved by a cooperative growth of **SS-NDI** monitored at 399 nm; b) autoresolution leading to formation of segregated stacks of **SS-NDI** in a tricomponent mixture consisting of equimolar mixture of bischromophoric NDIs and 5 equivalents of **RR-DAN**; c) plot of absorption changes at 399 nm and 503 nm in a four-component mixture showing isodesmic CT growth and complete incorporation of **RR-/SS-NDI** into their respective homochiral D-A stacks (the concentrations of **RR-/SS-NDI** for all the experiments were $10^{-4}$ M and 5 equivalents of **RR-DAN** were used to create D-A stacks).*

The CD spectra of the final thermodynamic state of the multicomponent mixtures were measured, to ascertain the signatures of the autoresolved enantiomer. CD spectra of the three component mixture consisting of equimolar mixtures of the bischromophoric NDIs and 5 equivalents of **RR-DAN** clearly showed the CD signal

corresponding to self-assembled stack of **SS-NDI** (Figure 2.17.a). However, the four component mixture consisting of equimolar mixtures of bischromophoric NDIs and 5 equivalents of bischromophoric DAN was CD silent, reiterating that there is complete formation of mixed stacks of opposite chiralities and proving that the CT stacks are achiral (Figure 2.17.b).

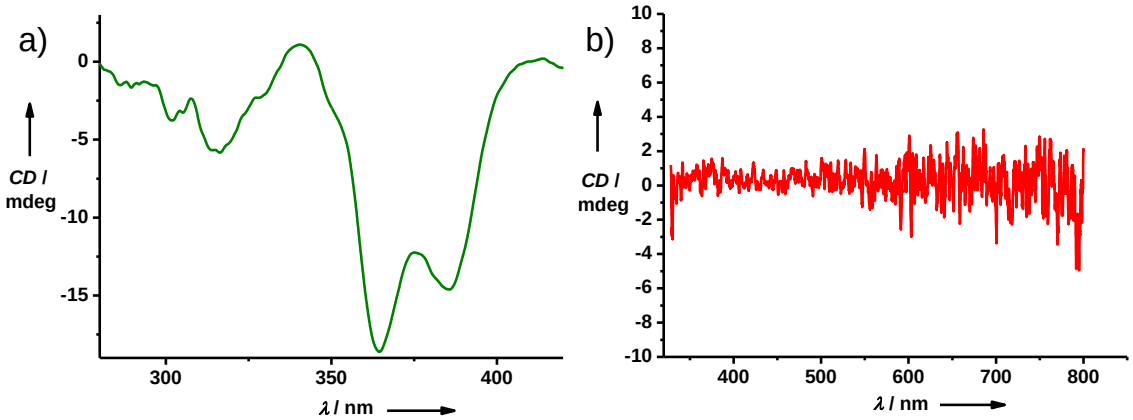


*Figure 2.17. CD spectra of the thermodynamically cooled multicomponent mixtures: a) CD spectrum of the thermodynamically cooled tricomponent mixture showing a CD signal similar to self-assembled **SS-NDI**, orthogonal segregation of the wrong enantiomer from a tricomponent mixture consisting of **RR-NDI** ($10^{-4}$ M), **SS-NDI** ($10^{-4}$ M) and **RR-DAN** ($5x10^{-4}$ M); b) CD silent spectrum of thermodynamically cooled solution of four component mixture (**RR/ SS-NDI**= $10^{-4}$ M; **RR/ SS-DAN**= $5x10^{-4}$ M) showing complete incorporation of bischromophoric NDIs and no orthogonal segregation.*

### 2.4.3. Theoretical Insights into Homochiral Recognition

As before, models for the same and opposite chiral D and A pairs were constructed. Both the structures were geometry optimized using the earlier protocol (*vide supra*) and snapshots are shown in Figure 2.18. D-A pair with opposite chiralities is less stable by 10.02 kcal/mol over the pair of same chirality, at B3LYP level of theory. As a result, the former might form segregated stacks while the latter prefer to form mixed p-n stacks. Further, TD-DFT calculations for both the pair of molecules were performed at CAM-B3LYP/6-31g(d) level to obtain the extent of charge transfer. As expected, there is not much difference in the CT between the D and A for the same and opposite chiral pairs which suggests that CT interaction is nearly the same if they

co-stack. But the formation of mixed stacks was hindered for monomers of opposite chirality, due to the high chiral mismatch penalty. Figure 2.19. shows the HOMO-LUMO diagram for the CT pair of **RR-NDI** and **RR-DAN** determined from the natural transition orbitals (NTO).

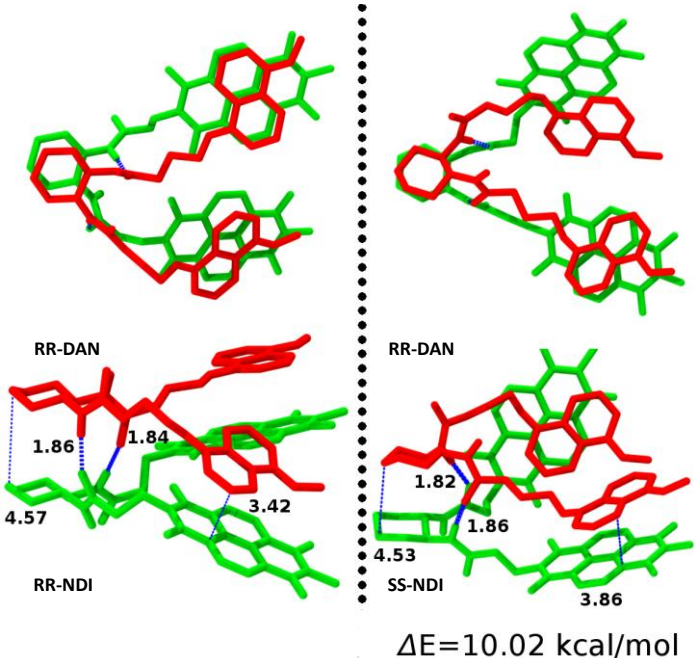


*Figure 2.18. Donor and acceptor pair of NDI and DAN molecules with same (left) and opposite (right) chirality. Energy difference was obtained at DREIDING//B3LYP/6-311+g(d,p) level of theory. Distances are specified in Å.*

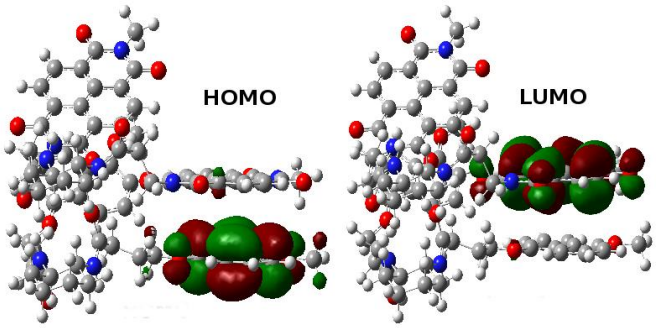


*Figure 2.19. HOMO and LUMO determined for a CT pair of **RR-NDI** and **RR-DAN** using CAM-B3LYP level of theory. HOMO lies on the DAN (donor) and LUMO lies on NDI (acceptor) suggesting the presence of charge transfer. Isosurface value of 0.02 e(Bohr)$^{-3}$ was used to plot the molecular orbitals.*

## 2.5. Conclusions

In conclusion, we have demonstrated a novel strategy based on homochiral supramolecular polymerization to obtain desired supramolecular organization of π-complementary donors and acceptors in assemblies. The chirality driven narcisstic self-sorting of the acceptors has been unambiguously proved through mechanistic insights into the cooperative segregation processes in the mixture of the acceptors, employing $T_e$ as a probe. This concept has been further realized in an unprecedented construction of mixed and orthogonal D-A stacks in solution, where the autoresolution process of the enantiomeric acceptor has been scrutinized in great detail through convincing spectroscopic and mechanistic investigations in multicomponent mixtures. These results open up a plethora of opportunities to exploit chirality for the realization of desired D-A organization and in designing electronic devices from the constructed mixed and orthogonal D-A stacks.

## 2.6. Experimental Section

### 2.6.1. General Methods

**NMR Measurements**: NMR spectra were recorded with a Bruker AVANCE 400 (400 MHz) Fourier transform NMR spectrometer with chemical shifts reported in parts per million (ppm) with respect to TMS. Splitting patterns are designated as s, singlet; d, doublet; t, triplet; m, multiplet.

**Optical Measurements**: Electronic absorption spectra were recorded on a Perkin Elmer Lambda 900 UV-Vis-NIR Spectrometer. Temperature dependent UV measurements were done in Perkin Elmer Lambda 900 UV-Vis-NIR Spectrometer equipped with a temperature controller. Circular Dichroism (CD) spectra and temperature dependent CD spectra were recorded on a Jasco J-815 spectrometer where the sensitivity, time constant and scan rate were chosen appropriately. The temperature dependent measurements were performed with a CDF-426S/15 Peltier-type temperature controller with a temperature range of 263-383 K and adjustable temperature slope.

**Transmission Electron Microscopy** (**TEM**): TEM measurements were performed on a JEOL, JEM 3010 operated at 300 kV. Samples were prepared by placing a drop of the solution on carbon coated copper grids followed by drying at room temperature. The images were recorded with an operating voltage of 300 kV. In order to get a better contrast, the samples were stained with uranyl acetate (1 wt % in water) before the measurements.

**High Resolution Mass Spectrometry** (**HRMS**): HRMS spectra were obtained on a Agilent HRMS Spectrometer (Q-TOF).

**Theoretical calculations**: All the molecules have been modelled using DREIDING force field with gasteiger charges as the partial charges. MD simulations were carried out using LAMMPS package. For initial relaxation, simulations were performed in gas-phase at 5 K in canonical ensemble (NVT). Further, these geometries were used as the input to determine the energies within quantum chemical approach using Gaussian-09 at B3LYP level of theory. Time-dependent density function theory (TD-DFT) calculations were carried out at CAM-B3LYP level of theory on the NDI-DAN CT pair to visualize the LUMO-HOMO diagram.

### 2.6.2. Synthetic Methods

The starting materials used for synthesizing various compounds were obtained from commercial suppliers. The moisture sensitive reactions were performed under an atmosphere of nitrogen. N, N Dimethylformamide (DMF), acetone and acetonitrile were dried by distillation under vacuum and dried on 3 Å molecular sieves activated at 180 $^{o}$C. Mg granules were activated with 1 M HCl to remove MgO, washed repeatedly with water and acetone and were finally kept in oven at 200 $^{o}$C. Tetrahydrofuran (THF) was distilled over Na ribbons and benzoquinone and stored. Enantiomerically pure (*1R*,2*R*)-(-)-1,2-Diaminocyclohexane and (*1S*,2*S*)-(+)-1,2-Diaminocyclohexane were obtained from Aldrich and stored at 5 $^{o}$C. Tridecan-7-amine was synthesized according to reported procedure.[29] Potassium Carbonate obtained from local suppliers was ground and dried at 180 $^{o}$C before the alkylation reactions. Analytical thin layer chromatography was carried out on Merck silica gel 60. Column chromatography was

carried out on silica gel (100-200 mesh). Size Exclusion Chromatography was performed on S-X3 and S-X1 biobeads, with chloroform as the solvent.

Proton chemical shifts are reported in ppm downfield from TMS (Tetramethylsilane) using the resonance of the deuterated solvent as internal standard. Splitting patterns are designated as s, singlet; d, doublet; bs, broad singlet; m, multiplet; t, triplet; q, quartet; dd, double doublet; ddd, double double doublet; quin, quintet and br, broad.

## 2.6.2.1. Synthetic Schemes

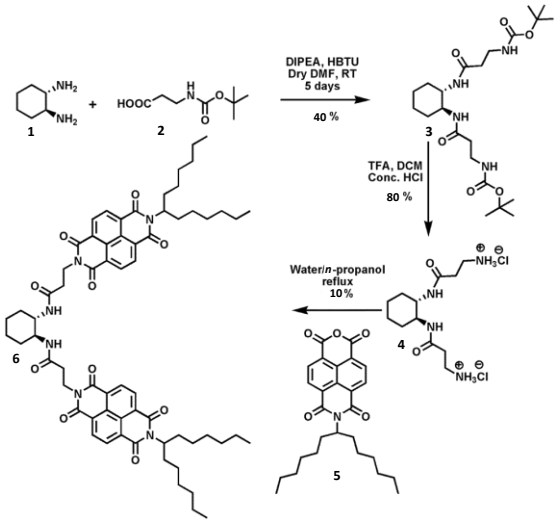


*Scheme 2.1. Synthetic route to **SS-NDI**.*

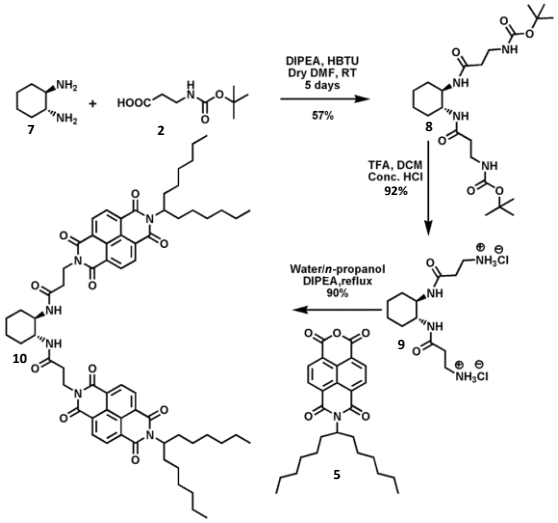


*Scheme 2.2. Synthetic route to **RR-NDI.***

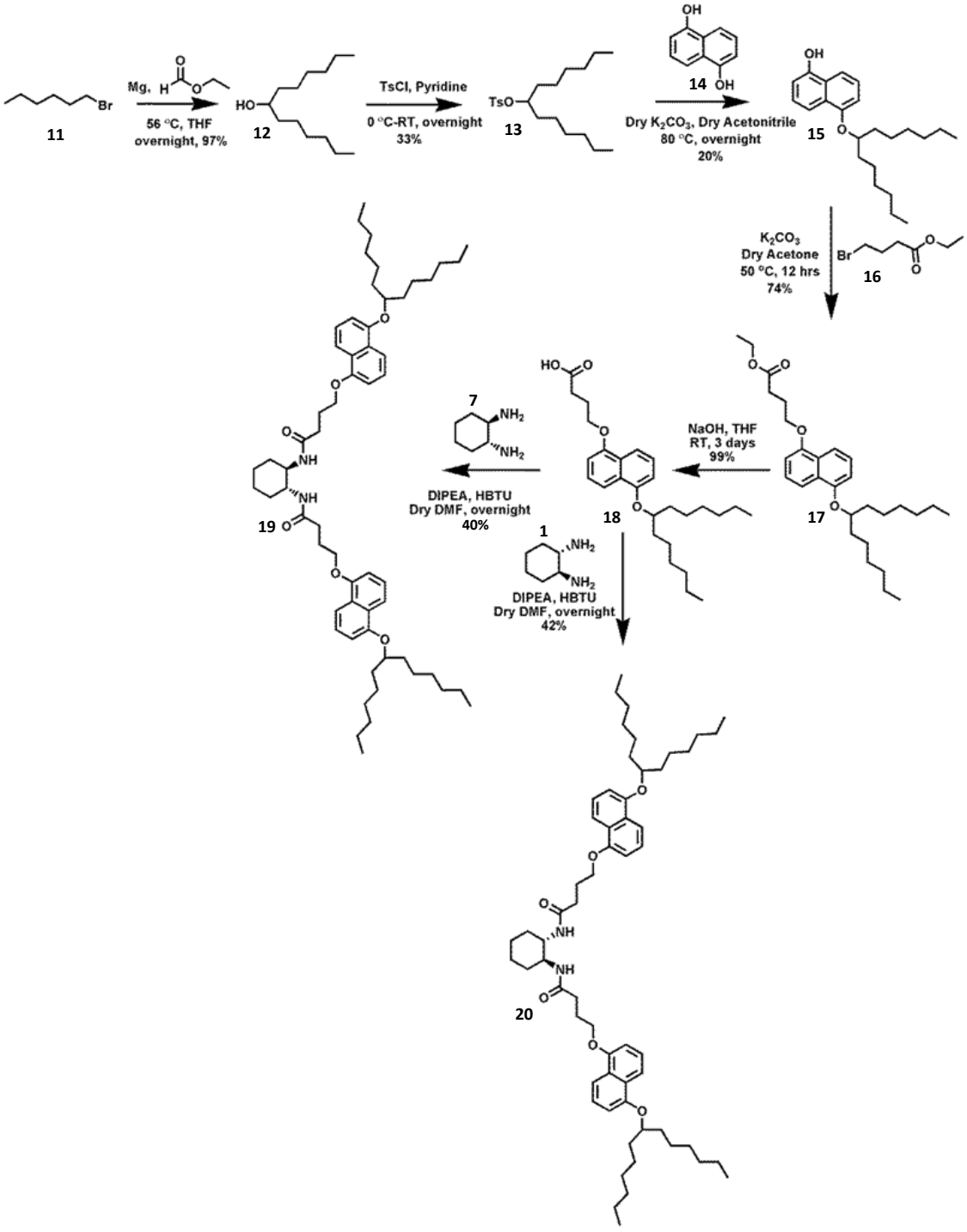


*Scheme 2.3. Synthetic steps towards **RR-DAN** and **SS-DAN**.*

## 2.6.2.2. Synthetic Procedures

**4** and **9** were synthesized according to reported procedures.[24a]

BOC protected β-alanine (**2**): Di-tert-butyldicarbonate (18.4 g, 84.3 mmol) was added drop wise to a stirred solution of β-alanine (5 g, 56.2 mmol) and NaOH (2.2 g, 54.5 mmol) in a 1:1 mixture of *t*-BuOH and water (24.5 mL each). The reaction mixture was stirred at room temperature overnight. The completion of the reaction was checked by monitoring a TLC that showed the disappearance of β-alanine. The reaction mixture was diluted with water (100 mL) and extracted with hexanes to remove excess BOC anhydride. The aqueous phase was acidified to pH 3 by adding a saturated solution of citric acid. The acidified layer was extracted with Ethyl acetate, which contained the product. The organic layer was collected, dried over $Na_2SO_4$ and concentrated to give crude N-Boc β-alanine. This was further purified by column chromatography in 10% MeOH in $CHCl_3$ to give the pure product as a transparent, viscous liquid. Yield: 63.4%; $^1$H NMR: (400 MHz, $CDCl_3$, ppm): δ= 5.04 (bs, 1H, NH); 3.4 (bs, 2H, -$CH_2$); 2.58 (bs, 2H, -$CH_2$), 1.45 (s, 9H, BOC $CH_3$); LCMS (ESI) *m/z*: calcd for $C_8H_{15}NO_4$: 189.1, found: 190.1 $[M+H]^+$.

(1S,2S)-(+)-Cyclohexanediamide (**3**) and (1R,2R)-(-)-Cyclohexanediamide (**8**) : 2-(1H-benzotriazol-1-yl)-1,1,3,3tetramethyluroium hexafluorophosphate (HBTU) (881.7 mg, 2.3 mmol), N,N-Diisopropylethylamine (DIPEA) (1.2 mL, 6.97 mmol) were taken along with **2** (265.6 mg, 2.3 mmol) in 17 mL dry DMF and stirred for 10 minutes to activate the acid. **1** (**7**) was added drop wise to this and the reaction mixture was stirred at room temperature for 5 days. The completion of the reaction was checked by a Thin Layer Chromatography (TLC) that showed the disappearance of the amine. The reaction mixture was extracted with DCM / saturated potassium carbonate repeatedly followed by extraction with water / DCM. The product comes to the organic layer which was then collected, dried on $Na_2SO_4$ and concentrated to give the pure product.

**3**: Yield: 40% $^1$H NMR: (400 MHz, $CDCl_3$, ppm): δ= 6.23 (bs, 2H), 5.24 (bs, 2H), 3.63 (bs, 2H), 3.36 (bs, 4H), 2.36 (bs, 4H), 2.0 (bs, 2H), 1.75 (bs, 2H), 1.44 (s, 9H), 1.30 (m, 4H); HRMS (ESI) *m/z*: calcd for $C_{22}H_{41}N_4O_6$: 456.2948, found: 457.3024 $[M+H]^+$.

**8**: Yield: 57% for **8**; $^1$H NMR: (400 MHz, $CDCl_3$, ppm): δ= 6.23 (bs, 2H), 5.24 (bs, 2H), 3.63 (bs, 2H), 3.36 (bs, 4H), 2.36 (bs, 4H), 2.0 (bs, 2H), 1.75 (bs, 2H), 1.44 (s,

9H), 1.30 (m, 4H); HRMS (ESI) *m/z*: calcd for $C_{22}H_{41}N_4O_6$: 456.2948, found: 457.3024 $[M+H]^+$.

BOC deprotected (1S,2S)-(+)-Cyclohexanediamide (**4**) and BOC deprotected (1R,2R)-(-)-Cyclohexanediamide (**9**): **3** (**8**) (530 mg, 1.16 mmol) was taken in a 250 mL round bottomed flask and 10 mL of Dichloromethane (DCM) was added to it. This mixture was stirred on an ice bath for 10 minutes. To this, Trifluoroacetic acid (TFA) in 10 mL DCM was added drop wise. The ice bath was removed and the reaction mixture stirred at room temperature for 48 hours. The completion of the reaction was checked by a TLC which showed complete disappearance of **3** (**8**) and appearance of a new ninhydrin active spot. TFA and DCM were completely removed under high vacuum and the reaction mixture dried in vacuum oven at 80 $^oC$ overnight. Acetone (10-12 mL) was added and the product was dissolved in it by heating and sonication. Conc. HCl (20 μL) was added to yield a dark brown precipitate. This precipitate was washed well with ethyl acetate (9 x 30 mL) till the precipitate became beige coloured. It was then collected and dried in vacuum oven at 85 $^oC$ overnight. Few impurities still remained which were removed by washing with methanol. The filtrate was concentrated and washed further with DCM to wash traces of TFA. The precipitate so obtained was characterized as the pure product.

**4**: Yield: 80%; $^1H$ NMR: (400 MHz, MeOD, ppm): δ= 3.65 (bs, 2H), 3.19 (m, 4H), 2.61 (m, 4H), 1.94 (bs, 2H), 1.77 (bs, 2H), 1.33 (m, 4H).

**9**: Yield: 92%; $^1H$ NMR: (400 MHz, MeOD, ppm): δ= 3.65 (bs, 2H), 3.19 (m, 4H), 2.61 (m, 4H), 1.94 (bs, 2H), 1.77 (bs, 2H), 1.33 (m, 4H).

Naphthalene monoimide (**5**): 1,4,5,8-Naphthalenetetracarboxylic dianhydride (3.82 g, 14.3 mmol) was taken in a 250 mL round bottomed flask, 50 ml of dry DMF was added to it and the reaction mixture was stirred under inert atmosphere while heating allowing the temperature to attain 110 $^oC$. Tridecan-7-amine (2.7 g, 13.6 mmol) in 40 mL dry DMF was introduced to this reaction mixture drop wise over a period of 45 minutes. The reaction mixture was stirred at 110 $^oC$ for 16 hrs. DMF was completely removed under high vacuum and an extraction was done with Saturated NaCl / $CHCl_3$. The organic layer was collected, dried over $Na_2SO_4$ and concentrated to obtain the crude

product. The crude mixture was washed with hexanes which dissolved the product along with the disubstituted product. The filtrate was concentrated and further purified by column chromatography (silica gel, 100-200 mesh) with a gradient elution ranging from 70% $CHCl_3$ in hexane to 5% MeOH in $CHCl_3$ followed by size exclusion chromatography (S-X3, $CHCl_3$). Yield: 43%; $^1$H NMR: (400 MHz, $CDCl_3$, ppm): δ= 8.8 (s, 4H), 5.15 (sep, 1H), 2.2 (m, 2H), 1.84 (m, 2H), 1.30-1.24 (16 H, alkyl H), 0.9 (t, 3H); $^{13}$C NMR (100 MHz, $CDCl_3$, δ): 159.1, 133.3, 128.9, 127.2, 122.8, 55.7, 55.3, 32.4, 31.8, 29.3, 27.0, 22.7, 14.2; HRMS (ESI) *m/z*: calcd for $C_{27}H_{32}NO_5$: 450.2280, found: 450.2273 $[M+H]^+$.

**SS-NDI** (**6**) and **RR-NDI** (**10**): **4** (**9**) (338 mg, 1 mmol) along with **5** (1.2 g, 2.6 mmol) was suspended in a 1:1 mixture of water/ *n*-propanol (68 mL each). The reaction mixture was sonicated for two minutes and then refluxed at 98 $^o$C for 50 hrs. Use of 2.5 equivalents of DIPEA with respect to **4** (**9**) improved the yield from 8% to 90%. The completion of the reaction was checked by monitoring a TLC that showed the disappearance of the amine and formation of the product. The reaction mixture was evaporated to dryness and purified subsequently by column chromatography (silica gel, 100-200 mesh) with eluent of polarity 2% MeOH in $CHCl_3$ and finally with size exclusion chromatography (S-X3, $CHCl_3$).

**6**: Yield: 10%; $^1$H NMR: (400 MHz, $CDCl_3$, ppm): δ= 8.73 (s, 8H), 6.38 (s, 2H), 5.15 (sep, 2H), 4.56-4.52 (m, 4H), 3.6 (bs, 2H), 2.65 (m, 4H), 2.24 (m, 4H), 2.1 (m, 2H), 1.87 (m, 4H), 1.56 (bs, 2H), 1.29-1.19 (36H, alkyl H), 0.82 (t, J=5.6 Hz, 12H); $^{13}$C NMR (100 MHz, $CDCl_3$, δ): 171.0, 163.1, 131.3, 127, 126.8, 126.3, 55.4, 53.8, 37.5, 34.8, 32.5, 32.4, 31.9, 29.3, 27.0, 24.8, 22.7, 14.2; HRMS (ESI) *m/z*: calcd for $C_{66}H_{83}N_6O_{10}$: 1119.6171, found for **6**: 1119.6173 $[M+H]^+$.

**10:** Yield: 90%; $^1$H NMR: (400 MHz, $CDCl_3$, ppm): δ= 8.73 (s, 8H), 6.38 (s, 2H), 5.15 (sep, 2H), 4.56-4.52 (m, 4H), 3.6 (bs, 2H), 2.65 (m, 4H), 2.24 (m, 4H), 2.1 (m, 2H), 1.87 (m, 4H), 1.56 (bs, 2H), 1.29-1.19 (36H, alkyl H), 0.82 (t, *J* =5.6 Hz, 12H); $^{13}$C NMR (100 MHz, $CDCl_3$, δ): 171.0, 163.1, 131.3, 127, 126.8, 126.3, 55.4, 53.8, 37.5, 34.8, 32.5, 32.4, 31.9, 29.3, 27.0, 24.8, 22.7, 14.2; HRMS (ESI) *m/z*: calcd for $C_{66}H_{83}N_6O_{10}$: 1119.6171, found for **10**: 119.6140 $[M+H]^+$.

Tridecan-7-ol (**12**): In an oven-dried 250 ml round-bottomed flask containing a magnetic pellet, a suspension of hot magnesium (3.66 g, 152.42 mmol) in dry THF (52.8 ml) was prepared under nitrogen atmosphere. A solution of 1-bromohexane (20 g, 121.94 mmol) in 28.1 ml dry THF was added drop-wise to the suspension (10 % of the solution was added beforehand followed by the rest of the addition) at 58 $^{o}$C. Ethyl formate (3.74 mL, 46 mmol mmol) in dry THF was added drop-wise to the mixture. The reaction mixture was stirred overnight at 58 $^{o}$C. Next, the reaction mixture was quenched by the addition of MeOH, followed by saturated aqueous $NH_4Cl$. The crude compound was extracted thrice with ethyl acetate. 9.06 g of the product was obtained. Yield=97 %; $^{1}$H NMR (400 MHz, $CDCl_3$, ppm): δ= 3.58 (bs, 1H); 1.64 (bs, 1H); 1.42-1.28 (alkyl H, 20H); 0.88 (s, 6H). LCMS (ESI) *m/z*: calcd for $C_{13}H_{28}O$: 200.21, found: 224 $[M+H+Na]^{+}$.

Tridecan-7-yl 4-methylbenzenesulfonate (**13**)**:** In a dry 50 ml, 2-necked round-bottomed flask containing a magnetic pellet, **12** (7 g, 35 mmol) was dissolved in anhydrous pyridine (5 ml) and kept on an ice bath. In another RB, 7.2 g (37.8 mmol) of Tosyl Chloride (TsCl) was dissolved in 12.5 ml of anhydrous pyridine. The mixture of TsCl and pyridine was then added drop-wise to the mixture containing alcohol at 0 $^{o}$C and kept stirring for 2 h. The ice bath was then removed and the reaction mixture was stirred overnight at room temperature. After the completion of the reaction, excess pyridine was quenched by the addition of 3 M HCl to the resulting crude reaction mixture. The reaction mixture was extracted twice with chloroform, washed and the combined organic layers were dried over $Na_2SO_4$. The solvent was removed under reduced pressure to afford 12.05 g of the product. Yield: 33%; $^{1}$H NMR (400 MHz, $CDCl_3$, ppm): δ= 7.78 (d, *J* = 8.4 Hz, 2H); 7.32 (d, *J* = 8.0 Hz, 2H); 4.54 (quin, *J* = 6 Hz, 1H); 2.44 (s, 3H); 1.4-1.2 (alkyl H, 20H); 0.85 (t, *J* = 6.8 Hz, 16H); LCMS (ESI) *m/z*: calcd for $C_{20}H_{34}O_3S$: 354.22, found: 262.3 $[M-91]^{+}$.

5-(tridecan-7-yloxy)naphthalen-1-ol (**15**)**:** 5.61 g (35 mmol) of **14** and 11.8 g (87 mmol) of $K_2CO_3$ were taken in a dry 3-necked 500 ml RB and suspended in 250 ml dry acetonitrile at 55 $^{o}$C under inert atmosphere. Then 11.8 g (33.3 mmol) of **13**, taken separately in a 100 ml RB, was dissolved in 10-15 ml dry MeCN and added drop-wise

to the reaction mixture. The reaction mixture was stirred at 82 $^{o}$C for 18 h. Acetonitrile was then completely evaporated and the reaction mixture was extracted with 1 N HCl and DCM. The organic layer was collected, dried over anhydrous $Na_2SO_4$ and concentrated. The crude mixture was then purified using column chromatography. The solvent used was 70-80 % $CHCl_3$ in hexane followed by 1-5 % MeOH in $CHCl_3$.. Yield= 20%; $^{1}$H NMR (400 MHz, $CDCl_3$, ppm): δ= 7.87 (d, *J* = 8.4 Hz, 1H); 7.68 (d, *J* = 8.4 Hz, 1H); 7.36 (t, *J* = 7.6 Hz, 2H); 6.83 (t, *J* = 7.6 Hz, 2H); 4.42 (quin, *J* = 5.6 Hz, 1H); 1.55 (m, 4H); 1.19 (m, 16H); 0.84 (t, *J* = 7.0 Hz, 6H). LCMS (ESI) *m/z*: calcd for $C_{23}H_{34}O_2$: 346.26, found: 347 $[M+H]^+$.

Ethyl 4-(5-(tridecan-7-yloxy)naphthalen-1-yloxy) butanoate (**17**)**:** In a 50 mL 2-necked round -bottomed flask fitted with a condenser and containing a magnetic stir bar, 1.5 g (4.38 mmol) of **15** and 7.26 g (52.6 mmol) of dry $K_2CO_3$ was dissolved in dry acetone (207 mL). A total of 4.5 g (21.9 mmol) of **16** was added slowly in small portions, and the resulting mixture was refluxed at 50 $^{o}$C for 12 h under inert atmosphere. After the completion of the reaction, acetone was evaporated. Extraction was done with 1 N HCl and DCM. The organic layer was collected, concentrated and dried. Purification of the crude product was done using column chromatography (silica gel) and size-exclusion chromatography (S-X1, $CHCl_3$) to obtain 1.48 g of the product. Yield= 74%; $^{1}$H NMR (400 MHz, $CDCl_3$, ppm): δ= 7.86 (d, *J* = 8.8 Hz, 1H); 7.78 (d, *J* = 8.4 Hz, 1H); 7.32 (t, *J* = 6 Hz, 2H); 6.82 (t, *J* = 4 Hz, 2H); 4.42 (quin, *J* = 5.6 Hz, 1H); 4.16 (t, q, 4H); 2.62 (t, 2H); 2.25 (quin, 2H); 1.55 (m, 4H); 1.19 (m, 16H); 0.88 (t, *J* = 7.0 Hz, 6H). LCMS (ESI) *m/z*: calcd for $C_{29}H_{44}O_4$: 456.32, found: 457 $[M+H]^+$.

4-(5-(tridecan-7-yloxy) naphthalen-1-yloxy) butanoic acid (**18**): 21 g (52.5 mmol) of NaOH was added to a solution of **17** (1.48 g, 3.24 mmol) in THF (148 ml). The mixture was kept for stirring 3 days. 1 M HCl was then added to the solution and extracted thrice with diethyl ether. The organic layer was then dried over anhydrous $Na_2SO_4$ .The solvent was then removed under reduced pressure to obtain quantitative yield of the product. $^{1}$H NMR (400 MHz, $CD_3CN$, ppm): δ= 7.79 (d, *J* =8.8 Hz, 1H); 7.76 (d, *J* = 8.4 Hz, 1H); 7.35 (t, *J* = 4.8 Hz, 2H); 6.92 (t, *J* = 5.6 Hz, 2H); 4.51 (quin, *J* = 5.6 Hz, 1H); 4.17 (t, 4H); 2.56 (t, 2H); 2.14 (quin, 2H); 1.55 (m, 4H); 1.19 (m, 16H); 0.88 (t, *J* = 7.0 Hz, 6H); $^{13}$C NMR (100 MHz, $CDCl_3$, δ): 179.2, 154.4, 154.3, 127.7, 127.0,

125.4, 124.9, 115.0, 113.6, 106.7, 105.3, 78.2, 66.9, 33.9, 31.9, 30.9, 29.6, 25.6, 25.4, 24.8, 22.7, 14.3; LCMS (ESI) *m/z*: calcd for $C_{27}H_{40}O_4$: 428.29, found: 429 $[M+H]^+$.

**RR-DAN** (**19**) and **SS-DAN** (**20**): In a 25 ml 2-necked RB, 500 mg (1.17 mmol) of **18** was taken in 2 ml of dry DMF. 389.28 mg (1.02 mmol) of HBTU was then added to the solution to activate the acid, followed by the addition of 243.81 (1.4 mmol) of *N*,*N*-Diisopropylethylamine (DIPEA). 53.28 mg (0.47 mmol) of **7** (**1**) was dissolved in dry DMF in a separate RB and then injected into the solution. The reaction mixture was kept stirring at room temperature overnight. It was then extracted with $K_2CO_3$ and DCM mixture followed by brine and DCM mixture. Organic layer was then collected in another RB, dried over $Na_2SO_4$, concentrated and dried over rotary evaporator. The resulting crude product was then purified using column chromatography (silica gel) to obtain a sticky solid which was then washed with hexanes to obtain white flaky powder.

**19**: Yield: 40%; $^1$H NMR (400 MHz, $CDCl_3$, ppm): δ= 7.84 (d, *J* =8.8 Hz, 2H); 7.76 (d, *J* = 8.4 Hz, 2H); 7.32 (t, *J* = 8 Hz, 4H); 6.81 (t, *J* = 7.6 Hz, 2H); 6.73 (t, *J* = 7.6 Hz, 2H); 5.91 (d, 2H); 4.42 (quin, *J* = 5.6 Hz, 2H); 4.02 (t, 4H); 3.59 (t, 2H); 2.34 (q, 2H); 2.24 (quin, 4H); 2.18 (q, 2H); 1.55 (m, 8H); 1.19 (m, 32H); 0.88 (t, *J* = 7.0 Hz, 12H); $^{13}$C NMR (100 MHz, $CDCl_3$, δ): 173.2, 154.4, 154.3, 127.7, 127.0, 125.4, 125.0, 114.8, 113.7, 106.7, 105.4,78.2, 67.3, 53.8, 34.0, 33.5, 32.4, 31.9, 29.6, 25.6, 25.4, 24.8, 22.7, 14.3; HRMS (ESI) *m/z*: calcd for $C_{60}H_{90}N_2O_6$: 934.68, found: 935.7568 $[M+H]^+$.

**20:** Yield: 42%; $^1$H NMR (400 MHz, $CDCl_3$, ppm): δ= 7.84 (d, *J* =8.8 Hz, 2H); 7.76 (d, *J* = 8.4 Hz, 2H); 7.32 (t, *J* = 8 Hz, 4H); 6.81 (t, *J* = 7.6 Hz, 2H); 6.73 (t, *J* = 7.6 Hz, 2H); 5.91 (d, 2H); 4.42 (quin, *J* = 5.6 Hz, 2H); 4.02 (t, 4H); 3.59 (t, 2H); 2.34 (q, 2H); 2.24 (quin, 4H); 2.18 (q, 2H); 1.55 (m, 8H); 1.19 (m, 32H); 0.88 (t, *J* = 7.0 Hz, 12H); $^{13}$C NMR (100 MHz, $CDCl_3$, δ): 173.2, 154.4, 154.3, 127.7, 127.0, 125.4, 125.0, 114.8, 113.7, 106.7, 105.4,78.2, 67.3, 53.8, 34.0, 33.5, 32.4, 31.9, 29.6, 25.6, 25.4, 24.8, 22.7, 14.3; HRMS (ESI) *m/z*: calcd for $C_{60}H_{90}N_2O_6$: 934.6877, found: 935.6843 $[M+H]^+$.

## 2.7. References


[1] a) M. M. Safont-Sempere, G. Fernández, F. Würthner, *Chem. Rev*. **2011**, *111*, 5784; b) J. M. Lehn, *Science* **2002**, *295*, 2400; d) L. Issacs, *Acc. Chem. Res*. **2014**, *47*, 2052; c) A. Saghatelian, Y. Yokobayashi, K. Soltani, M. R. Ghadiri, *Nature* **2001**, *409*, 797; d) M. Lal Saha, M. Schmittel, *Org. Biomol. Chem*. **2012**, *10*, 4651.

[2] a) B. Alberts, A. Johnson, J. Lewis, M. Raff, K. Roberts, P. Walter, *Molecular Biology of the Cell*, 4th ed.; Garland Science: New York, **2002**; b) K.-E. Jaeger, T. Eggert, *Curr*. *Opin. Biotechnol*. **2004**, *15*, 305; c) J. D. Watson, F. H. C. Crick, *Nature* **1953**, *171*, 737.

[3] a) L.Pérez-García, D. B. Amabilino, *Chem. Soc. Rev*. **2002**, *31* , 342; b) L. Pérez-García, D. B. Amabilino, *Chem. Soc. Rev*. **2007**, *36*, 941; c) L. Pasteur, *Ann. Chim. Phys*. **1848**, *24*, 442.

[4] a) L. J. Prins, J. Huskens, F. de Jong, P. Timmerman, D. N. Reinhoudt, *Nature* **1999**, *398*, 498; b) A. Wu, A. Chakraborty, J. C. Fettinger, R. A. Flowers, L. Isaacs, *Angew. Chem. Int. Ed*. **2002**, *41*, 4028; c) S. Ghosh, A. X. Wu, J. C. Fettinger, P. Y. Zavalij, L. Isaacs, *J. Org. Chem*. **2008**, *73*, 5915; d) H.-J. Kim, D. Moon, M. S. Lah, J-I. Hong, *Angew. Chem. Int. Ed*. **2002**, *41*, 3174; e) M. A. Masood, E. J. Enemark, T. D. P. Stack, *Angew. Chem. Int. Ed*. **1998**, *37*, 928; f) X. Shi, J. C. Fettinger, J. T. Davis, *J. Am. Chem. Soc*. **2001**, *123*, 6738.

[5] a) A. Wilson, G. Gasparini, S. Matile, *Chem. Soc. Rev*. **2014**, *43*, 1948; b) N-T. Lin, A. V. Jentzsch, L. Guénée, J.-M. Neudörfl, S. Aziz, A. Berkessel, E. Orentas, N. Sakai, S. Matile, *Chem. Sci*. **2012**, *3*, 1121; c) E. Orentas, N. Sakai, S. Matile, *Chirality* **2013**, *25*, 107.

[6] a) S. Haq, N. Liu, V. Humblot, A. P. J. Jansen, R. Raval, *Nat. Chem*. **2009**, *1*, 409; b) M. Böhringer, W.-D. Schneider, R. Berndt, *Surf. Rev. Lett*. **2000**, *7*, 661, and references therein.

[7] a) A. R. A. Palmans, E. W. Meijer, *Angew. Chem. Int. Ed*. **2007**, *46*, 8948; b) I. Danila, F. Riobe, F. Piron, J. P.-Luis, J. D. Wallis, M. Linares, H. Ågren, D. Beljonne, D. B. Amabilino, N. Avarvari, *J. Am. Chem. Soc*. **2011**, *133*, 8344; c) N.

Tomimasu, A. Kanaya, Y. Takashima, H. Yamaguchi, A. Harada, *J. Am. Chem. Soc*. **2009**, *131*, 12339; d) C. Roche, H.-J. Sun, M. E. Prendergast, P. Leowanawat, B. E. Partridge, P. A. Heiney, F. Araoka, R. Graf, H. W. Spiess, X. Zeng, G. Ungar, V. Percec, *J. Am. Chem. Soc*. **2014**, *136*, 7169.

[8] a) M. M. J. Smulders, I. A. W. Filot, J. M. A. Leenders, P. van der Schoot, A. R. A. Palmans, A. P. H. J. Schenning, E. W. Meijer, *J. Am. Chem. Soc*. **2010**, *132*, 611; b) M. M. J. Smulders, P. J. M. Stals, T. Mes, T. F. E. Paffen, A. P. H. J. Schenning, A. R. A. Palmans, E. W. Meijer, *J. Am. Chem. Soc*. **2010**, *132*, 620.

[9] Y. Ishida, T. Aida, *J. Am. Chem. Soc*. **2002**, *124*, 14017.

[10] K. Sato, Y. Itoh, T. Aida, *Chem. Sci.* **2014**, *5*, 136.

[11] F. Helmich, M. M. J. Smulders, C. C. Lee, A. P. H. J. Schenning, E. W. Meijer, *J. Am. Chem. Soc*. **2011**, *133*, 12238.

[12] M. Wolffs, J. van Velthoven, X. Lou, R. A. A. Bovee, M. Pouderoijen, J. L. J. van Dongen, A. P. H. J. Schenning, E. W. Meijer, *Chem. Eur. J*. **2012**, *18*, 15057.

[13] M. Kumar, K. V. Rao, S. J. George, *Phys. Chem. Chem. Phys*. **2014**, *16*, 1300.

[14] a) R. Bhosale, J. Misek, N. Sakai, S. Matile, *Chem. Soc. Rev*. **2010**, *39*, 138; b) A. Das, S. Ghosh, *Angew. Chem. Int. Ed*. **2014**, *53*, 2038.

[15] a) A. S. Tayi, A. Kaeser, M. Matsumoto, T. Aida, S. I. Stupp, *Nat. Chem*. **2015**, *7*, 281; b) A. S. Tayi, A. K. Shveyd, A. C.-H. Sue, J. M. Szarko, B. S. Rolczynski, D. Cao, T. J. Kennedy, A. Sarjeant, C. L. Stern, W. F. Paxton, W. Wu, S. K. Dey, A. C. Fahrenbach, J. R. Guest, H. Mohseni, L. X. Chen, K. L. Wang, J. F. Stoddart, S. I. Stupp, *Nature* **2012**, *488*, 485; c) Horiuchi , Y. Tokura, *Nat. Mater*. **2008**, *7*, 357.

[16] a) K. Sugiyasu, S-i Kawano, N. Fujita, S. Shinkai, *Chem. Mater*. **2008**, *20*, 2863; b) S. Prasanthkumar, S. Ghosh, V. C. Nair, A. Saeki, S. Seki, A. Ajayaghosh, *Angew. Chem. Int . Ed*. **2015**, *54*, 946; c) A. Das, M. R. Molla, B. Maity, D. Koley, S. Ghosh, *Chem. Eur. J.* **2012**, *18*, 9849; d) J. van Herrikhuyzen, A. Syamakumari, A. P. H. J. Schenning, E. W. Meijer, *J. Am. Chem. Soc.* **2004**, *126*, 10021.

[17] F. Würthner, Z. Chen, F. J. M. Hoeben, P. Osswald, C.-C. You, P. Jonkheijm, J. V. Herrikhuyzen, A. P. H. J. Schenning, P. P. A. M. van der Schoot, E. W. Meijer, E. H. A. Beckers, S. C. J. Meskers, R. A. J. Janssen, *J. Am. Chem. Soc.* **2004**, *126*, 10611.

[18] Y. Yamamoto, T. Fukushima, Y. Suna, N. Ishii, A. Saeki, S. Seki, S. Tagawa, M. Taniguchi, T. Kawai, T. Aida, *Science* **2006**, *314*, 1761.

[19] a) R. S. Lokey, B. L. Iverson, *Nature* **1995**, *375*, 303; b) G. J. Gabriel, B. L. Iverson, *J. Am. Chem. Soc*. **2002**, *124*, 15174.

[20] a) C. Wang, S. Yin, S. Chen, H. Xu, Z. Wang, X. Zhang, *Angew. Chem. Int. Ed*. **2008**, *47*, 9049; b) C. Wang, Y. Guo, Y. Wang, H. Xu, R. Wang, X. Zhang, *Angew. Chem. Int. Ed*. **2009**, *48*, 8962.

[21] E. Orentas, M. Lista, N.-T. Lin, N. Sakai, S. Matile, *Nat. Chem*. **2012**, *4*, 746.

[22] a) D. E. Fuerst, E. N. Jacobsen, *J. Am. Chem. Soc*. **2005**, *127*, 8964; b) A. Berkessel, T. Günther, Q. Wang, J-M. Neudörfl, *Angew. Chem. Int. Ed*. **2013**, *52*, 8467; c) A. Berkessel, M. Brandenburg, E. Leitterstorf, J. Frey, J. Lex, M. Schä fer, *Adv. Synth. Catal*. **2007**, *349*, 2385; d) M. Kaik, J. Gajewy, J. Grajewski, J. Gawronski, *Chirality* **2008**, *20*, 301.

[23] a) J.-G. Dong, A. Wada, T. Takakuwa, K. Nakanishi, N. Berova, *J. Am. Chem. Soc*. **1997**, *119*, 12024; b) T. Nehira, C. A. Parish, S. Jockusch, N. J. Turro, K. Nakanishi, N. Berova, *J. Am. Chem. Soc*. **1999**, *121*, 8681; c) S. Boiadjiev, D. A. Lightner, *Chirality* **2005**, *17*, 316.

[24] a) J. Kumar, T. Nakashima, H. Tsumatori, M. Mori, M. Naito, T. Kawai, *Chem. Eur. J.* **2013** , *19*, 14090; b) I. D. Tevis, W.-W. Tsai, L. C. Palmer, T. Aytun, S. I. Stupp, *ACS Nano* **2012**, *6*, 2032.

[25] a) J. van Esch, S. De Feyter, R. M. Kellogg, F. De Schryver, B. L. Feringa, *Chem. Eur. J.* **1997**, *8*, 1238; b) M. de Loos, J. van Esch, R. M. Kellogg, B. L. Feringa, *Angew. Chem. Int. Ed*. **2001**, *40*, 613; c) K. Hanabusa, K. Shimura, K. Hirose, M. Kimura, H. Shirai, *Chem. Lett*. **1996**, 885.

[26] H. M. M. ten Eikelder, A. J. Markvoort, T. F. A. de Greef, P. A. J. Hilbers, *J. Phys. Chem. B* **2012**, *116*, 5291.

[27] J. Kumar, H. Tsumatori, J. Yuasa, T. Kawai, T. Nakashima, *Angew. Chem. Int. Ed.* **2015**, *54*, 5943.

[28] a) H. Y. A-Yeung, P. Pengo, G. D. Pantos , S. Otto, J. K. M. Sanders, *Chem. Commun*. **2009**, 419, b) P. Talukdar, G. Bollot, J. Mareda, N. Sakai, S. Matile, *J. Am. Chem. Soc*. **2005**, *127*, 6528.

[29] S. Miao, Y. Zhu, Q. Bao, H. Li, N. Li, S. Ji, Q. Xu, J. Lu, L. Wang, *J. Phys. Chem. C* **2014**, *118*, 2154.

# Chapter-3

## Amphiphilic Design Strategy for Improved Electronic Functions

***3.1. Self-Assembly of p-type Oligo(p-phenylenevinylene) Amphiphiles: Free Standing, Ordered Sheets with Enhanced Mobility***

***3.2. Self-Assembly of n-type Naphthalene Diimide Amphiphiles: Aligned Fibers with High Mobility***

# Chapter-3.1.

## Self-Assembly of *p*-type Oligo(*p*-phenylenevinylene) Amphiphiles: Free Standing, Ordered Sheets with Enhanced Mobility


### *Abstract*

*Oligo(p-phenylenevinylenes) (OPVs) with amphiphilic design are synthesized and studies on their self-assembly characteristics are being presented. Careful spectroscopic and microscopic investigations point at two morphologically different states of assemblies, with one being two dimensional sheets and the other as nanotubes, with the appearance of scrolled sheets. Morphological and photo-physical studies reveal a unique aggregate to aggregate transition between rolled tubes and two dimensional sheets, which is outlined as a more thermodynamic aggregate. Chiroptical probing into the self-assembled states has proved that the thermodynamic aggregate (2-D sheet) is better ordered and consists of chromophores that are better excitonically coupled. The mobilities of these aggregates are also studied for a field effect transistor device and as expected, sheets supersede rolled tubes by a couple of orders. More interestingly, the mobility values obtained for the well-ordered chromophores in sheets is three orders higher than any other self-assembled OPV previously reported. It is hypothesized that the better π- interactions enforced by the amphiphilic design and the resultant supramolecular organization is a prime factor for such a remarkable rise in mobilities.*


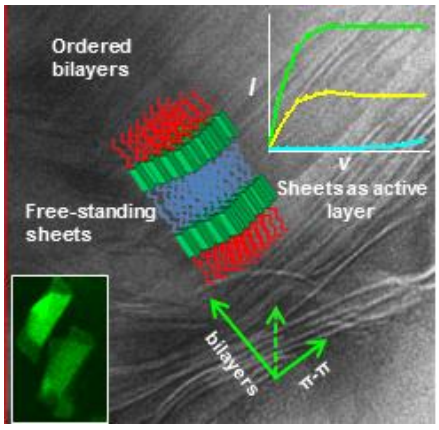


Manuscript based on this work: B. Narayan, S. P. Senanayak, A. Jain, K. S. Narayan, S. J. George, *Adv. Funct. Mater*. **2013**, *23*, 3053-3060.

## 3.1.1. Introduction

Supramolecular ordering of π-conjugated molecules plays a vital role in the performance of organic opto-electronic devices.[1] Controlling the morphologies at the nanoscale in solution processable polymers during its fabrication *via* spin-coating is challenging due to their structural defects.[2] In this respect, the self-assembly of π-conjugated oligomers, with well-defined chemical structure,[3] in solution using supramolecular design principles,[4] has attracted immense attention as it allows enhanced structural control over the organization and functional properties. However, the electro active devices fabricated from self-assembled π-conjugated oligomers have often showed poor performance[5] compared to highly organized assemblies of less processable counterparts, in the crystal and vacuum deposited thin film states.[6] One of the reasons for low efficiencies in supramolecular chromophoric systems could be the molecular design with solubilizing side chains, which hamper the molecular order and disrupt the extended π-π stacking in the assemblies. In this regard, an amphiphilic design for self-assembly of chromophores can be of particular interest.[7] Moreover, it has been shown that hydrophobic interactions between the amphiphilic systems can give rise to less dynamic assemblies with high association constants.[8] Hence, we envisage that an amphiphilic design combined with the electroactive chromophore can give rise to highly ordered assemblies with stronger π-π interactions and hence better mobilities.

Oligo(*p*-phenylenevinylene)s (OPVs) have been the subject of intense research in the field of organic electronics[3,9] as their polymeric counter-parts (PPVs) have served as the electroactive material for various applications in the past, such as in light emitting diodes.[10] A variety of supramolecular nano-architectures have been constructed, by the self-assembly of OPV donor molecules in solution,[11] however the hole transport properties of these assemblies are much lower compared[12] to other self-assembled electro-active counterparts.[5a,13] On the other hand, significantly high mobilities have been achieved for less processable OPV counterparts, when they were vacuum deposited as thin film states.[6c] (Figure 3.1.1.) Hence we have selected OPV backbone as a model system to study the effect of amphiphilic substitution and subsequent molecular ordering on the electronic properties of self-assembled chromophoric systems.

a)

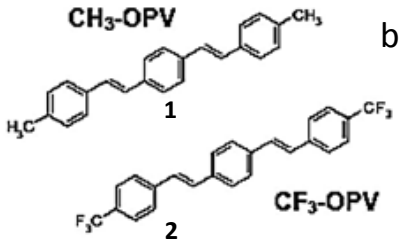


b)

| Compound | Carrier type | Mobility ($cm^2 V^{-1} s^{-1}$) | Threshold voltage (V) | On/off current ratio |
|---|---|---|---|---|
| $CH_3$-OPV | Hole | 0.13 | −33 | $5.8 \times 10^5$ |
| $CF_3$-OPV | Electron | 0.013 | 45 | $4.2 \times 10^4$ |

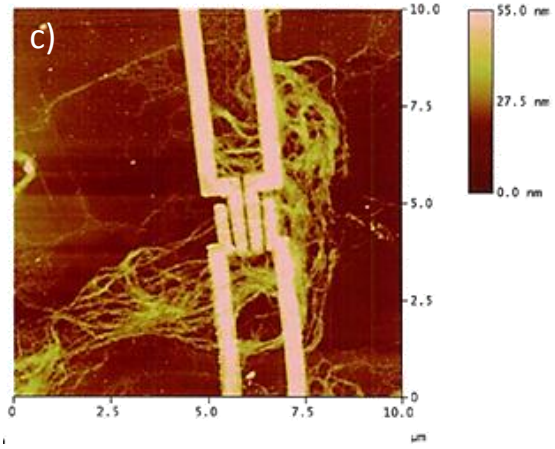


d)

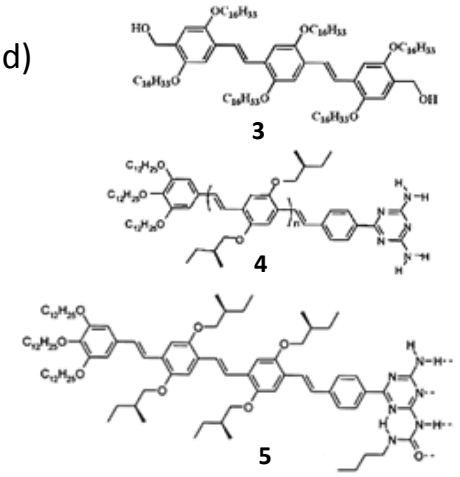


*Figure 3.1.1. Electrical properties of few OPVs reported in literature: a) Chemical structures of methyl (**1**) and triflouoromethyl (**2**) substituted OPVs and b) their hole and electron mobilities respectively measured in the vacuum deposited states listed in tabular form; c) AFM image of a device constructed from a drop-casted self-assembled solution of OPV that forms molecular wires across $Au_{60}Pd_{40}$ electrodes with low currents (in the order of $10^{-15}$/nm); d) Molecular structures of various alkyl substituted OPVs (**3**-**5**) whose mobilities were measured in the device configuration as shown in c). (Figures a, b reproduced with permissions from reference 6c and c, d reproduced with permissions from reference 12b respectively).*

In this chapter, we report the two-dimensional (2-D) self-organization of amphiphilic Oligo(*p*-phenylenevinylene)s, which form free-standing sheets[14] with highly ordered bilayers and hence, enhanced mobility. Although, OPV amphiphilic assemblies have been achieved in solution and liquid crystalline phases (Figure 3.1.2.a-c),[15] they have not yet been investigated for their electronic performances. In addition, this is the first report of 2-D organization of OPVs into sheets by a solution-state self-assembly. We further show an unprecedented, solvent dependent phase transition of these 2-D sheets to scrolled nanotubes. Chiroptical probing of the self-assembled sheets

further provided insights into the molecular organization and revealed a highly cooperative and reversible temperature dependent phase transition to less ordered assemblies. More importantly, the OPV sheets showed mobilities up to $0.8\times10^{-2}$ $cm^2V^{-1}s^{-1}$, which is many orders of magnitude greater than the reported values for the self-assemblies of OPVs and few other well-studied chromophores on a device structure.[5a,12] Recently, Pei and co-workers have shown that an amphiphilic design for chromophores can indeed result in high mobility self-assembled films (Figure 3.1.2.d-f).[14b] The mobility magnitude obtained in our system is only about an order of magnitude lower than the values obtained for vacuum-deposited OPV films[6c] and comparable to the recently reported amphiphilic chromophoric self-assembly, reiterating the importance of an amphiphilic design.[14b]

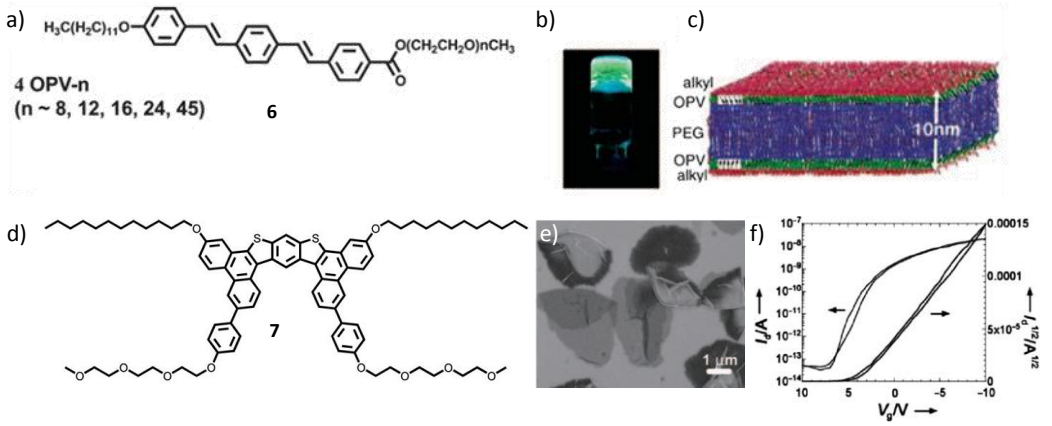


*Figure 3.1.2. Few p-type amphiphilic molecules reported in literature: a) OPV amphiphile (**6**) as reported by Stupp and coworkers; b) and c) OPV amphiphile (n = 24) derived hydrogel irradiated under 365 nm UV light and the schematic representation of its bilayer packing respectively; d) molecular structure of a butterfly shaped amphiphile consisting of a benzodithiophene core (**7**); e) free standing crystalline sheets formed by the self-assembly of **7** as seen by SEM; f) transconductance curves obtained from a device constructed by employing these sheets as the electroactive layer (Figures a-c and d-f reproduced with permissions from references 15 and 14b respectively).*

## 3.1.2. Design Strategy

The OPV amphiphiles used in this study have a rod-coil structure, with the conjugated backbone forming the rigid part and the hydrophilic tetraethyleneglycol

(TEG) chain and hydrophobic dodecyl (for **OPV-ach**) or (*S*)-citronellyl (for (***S***)-**OPV-ch**) on the opposite sides constituting the coil. The molecular structures of OPV amphiphiles are shown in Figure 3.1.3. The OPV amphiphiles were synthesized through a statistical Wittig–Horner reaction of the diphosphonates with dodecyl/ (*S*)-citronellyl substituted and tetraethylene glycol substituted aldehydes. The unsymmetrically substituted product thus obtained was purified through column chromatography on silica gel and size exclusion chromatography and have been fully characterized by nuclear magnetic resonance (NMR) spectroscopy, matrix-assisted laser desorption/ionization time-of-flight (MALDI-TOF) and high resolution mass spectrometry (HRMS). Chiral (*S*)-citronellyl side chain has been incorporated in the molecular design of (***S***)-**OPV-ch** to enable chiroptical probing into the self-assembled states.

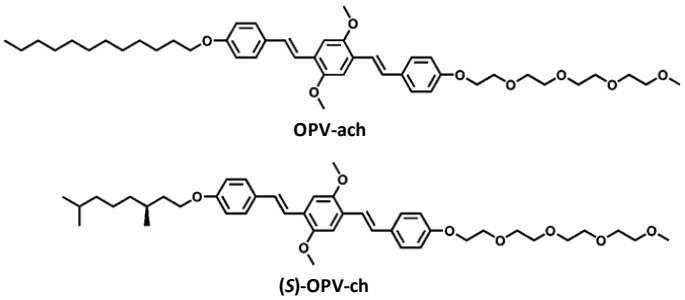


*Figure 3.1.3. Molecular structures of OPV amphiphiles under study.*

## 3.1.3. Self-Assembly of OPV Amphiphiles

The self-assembly studies of OPV amphiphiles, **OPV-ach** and (***S***)-**OPV-ch** was carried out in various compositions of THF-water solvent mixtures. Detailed investigations into the interchromophoric interactions in the self-assembled state have been carried out by various spectroscopic, chiroptical, microscopic and light-scattering techniques. The details of these investigations have been presented in this section.

### 3.1.3.1. Microscopic Investigations into the Self-Assembled States

Microscopic investigations of self-assembled OPV amphiphiles were done through Atomic force microscopy (AFM), Field Effect Scanning Electron Microscopy

(FE-SEM), Transmission Electron Microscopy (TEM) and Confocal Microscopy. TEM along with X-ray diffraction (XRD) of the self-assembled films gave insights into the molecular packing in the self-assembled structures.

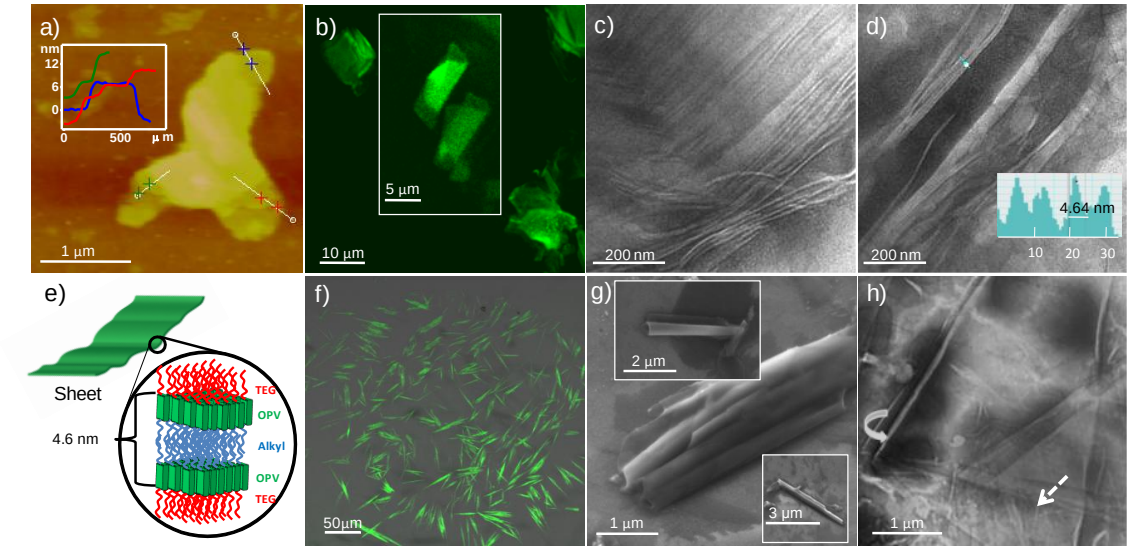


*Figure 3.1.4. Morphology of the self-assembled OPVs from various THF/water solvent mixtures: a-d) show the microscopic images of the* ***OPV-ach*** *sheets in 2.5% THF in water. a) Tapping mode AFM of a partially folded sheet. Inset shows the height profile across the folding edges, as marked by corresponding colored lines in the Figure, showing typical bilayer distances. The bilayers are clearly evident from the step profiles in height analyses; b) Confocal Microscopy images ($\lambda_{exc}$= 458 nm) showing free-standing green fluorescent sheets in solution; c) TEM image of the sheets viewed along their edges showing the bilayer arrangement; d) TEM image of a partially folded, multi-layered sheet along with the electron density profile of the layers (inset, marked as white bar in the image); e) Schematic representation of the molecular organization in the sheets; f) Confocal ($\lambda_{exc}$ = 458 nm) and g) FE-SEM images of the* ***OPV-ach*** *rolled nanotubes in 20% THF in water; h) TEM image of* ***(S)-OPV-ch*** *showing stacked sheets scrolling at the edges formed in 2.5% THF in water (dotted lines and arrows are inserted to guide the eye).*

Atomic force microscopy (AFM) studies of **OPV-ach** (2.5% THF in water) revealed the presence of large sheets of 5–50 µm width, suggesting a two-dimensional self-assembly (Figure 3.1.4.). Height profile analysis on tapping mode AFM images

clearly showed the presence of multiple layers of sheets. Single layer sheets with height close to the amphiphilic bilayer distance were also obtained through height profile investigations of tapping mode AFM images (Figure 3.1.4.a). Confocal microscopy studies showed the presence of large, free-floating sheets in solution. Bright green fluorescent sheets were observed when a solution of **OPV-ach**, sealed between glass slides was imaged at an excitation of 458 nm (Figure 3.1.4.b). The free standing nature of the sheets were evident from the presence of wrinkled and folded sheets in the confocal images, indicating that the 2-D self-assembly indeed occurred in the solution and not due to any de-wetting process on the substrates. Transmission electron microscopy (TEM) studies revealed details into the structural organization of the bilayers in the OPV sheets (Figure 3.1.4.c, d). The TEM images showed stacked sheets oriented on the surface of the copper grid, along with stacked sheets standing upright on the copper grid. Imaging of the standing edges of the sheets, which were stained with uranyl acetate on a carbon coated copper grid, clearly showed highly ordered molecular arrangement along their sliding edges (Figure 3.1.4.c). This is further evident from the TEM image in Figure 3.1.4.d, which provides a cross sectional view of partially folded multi-layer sheets. The measured periodic distance between stacked sheets from the TEM electron density profile is 4.6 nm, which matches with the OPV bilayer distance, in which the hydrophobic dodecyl chains are completely interdigitated and tilted (Figure 3.1.4.e). This indicates that the edges of the sheets consist of bilayers with the OPV backbones vertically oriented and the π- stacking direction along the plane of the sheets as reported in literature.[14b] X-ray diffraction (XRD) studies were performed on the self-assembled sheets and tubes to understand the molecular organization. The samples were prepared by drop-casting the respective self-assembled solution on glass substrates. XRD performed on these sheets exhibited a d-spacing of 4.4 nm that may be attributed to the tilted, inter-digitated bilayer distance and also show higher order reflections characteristic of the lamellar organization (Figure 3.1.5.a). On the other hand, the XRD pattern of the self-assembled tubes had a profile different from that of sheets, and consisted of multiple peaks, indicative of a less symmetrical structure (Figure 3.1.5.b).

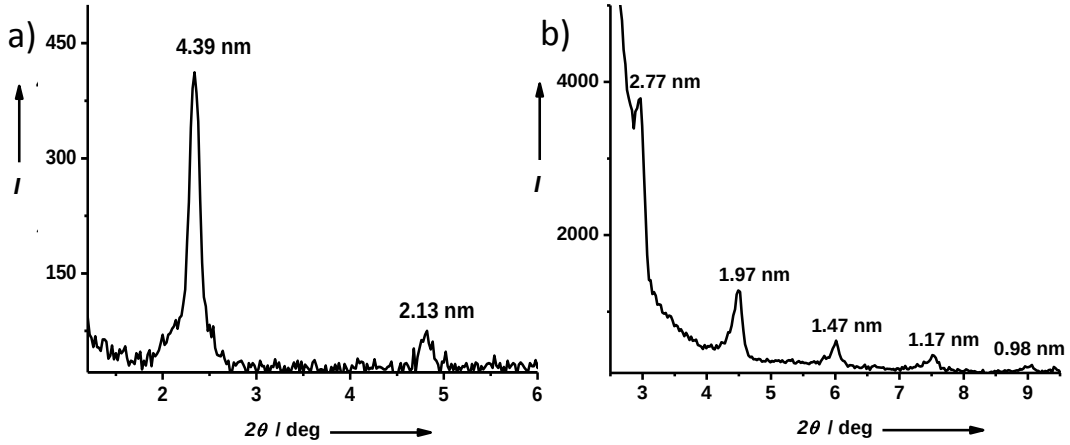


*Figure 3.1.5. X-ray diffraction profile of a)* ***OPV-ach*** *sheets (THF/water, 2.5/97.5(v/v)) with a low angle peak corresponding to bilayer distance (4.39 nm) and its diffraction (2.13 nm), indicative of lamellar packing; b) XRD profile of* ***OPV-ach*** *nanotubes (THF/water, 20/80, (v/v)) with features different from the nanosheets, consisting of many peaks indicating less symmetrical structure.*

Remarkably, the planar sheets of **OPV-ach** roll-up into 1D nanotubular structures at high percentages of THF (Figure 3.1.4.f, g). Confocal images ($\lambda_{exc}$= 458 nm) of **OPV-ach** in 20% THF-water solvent mixture, sealed between glass slides revealed the formation of 1-D structures (Figure 3.1.4.f). FE-SEM images of drop-casted solutions of OPV-ach in 20% THF-water solvent mixture revealed the tube-like structures several micrometers long, with an average diameter of 300 nm. Careful analyses of the FE-SEM images showed that these nanotubes are indeed formed by the scrolling of the 2D sheets, which was seen at higher compositions of water (Figure 3.1.4.g, insets). TEM of the tubular bundles stained with uranyl acetate revealed randomly oriented bilayers, which could be due to the irregular folding of multiple sheets. The less molecular ordering in the nanotubes was evident from the thin film XRD which revealed multiple peaks whereas XRD of sheets had only two peaks, suggesting more symmetry and higher ordering between the chromophores (Figure 3.1.5.b). Self-assembled organic nanotubes of amphiphilic molecules are generally formed through the coiling of twisted 1D nanotapes[16] or by the rolling-up (scrolling) of 2D nanosheets.[17]Although there are many examples in literature for coiled nanotubes, rolled-up nanotubes are seldom reported. It has been predicted and experimentally shown that self-assembled 2D sheets exhibit a high-temperature rolled-

up tubular phase.[18] Here, we observe that, this rolled-up tubular phase can also be attained by varying the solvent compositions. It is noteworthy that (***S***)-**OPV-ch** also exhibits two types of assemblies with different morphologies and optical properties in water-THF solvent mixtures, similar to its achiral analogue (Figure 3.1.4.h).

### 3.1.3.2. Dynamic Light Scattering Investigations

Dynamic light scattering studies (DLS) were carried out on the self-assembled solutions of **OPV-ach** and (***S***)-**OPV-ch** amphiphiles in THF-water mixtures, and unambiguously ascertained the fact that not only these assemblies are formed in solution but they are also dependent on the solvent compositions. In 2.5% THF-water solvent mixtures, **OPV-ach** exhibited large polydisperse aggregates with average hydrodynamic radii of 1000 nm (Figure 3.1.6.b), consistent with the dimensions of the 2-D sheets, obtained through microscopic techniques. However, relatively higher THF compositions (THF/water, 20/80, (v/v)) resulted in the solution state formation of nanostructures with reduced average hydrodynamic diameter of 122 nm, with much narrower distribution, reiterating the formation of tubular objects from the rolling of sheets. In this report, nanosheet assemblies would be further referred to as State A and the nanotube assembled state as State B, for simplicity. Similarly, DLS studies of (***S***)-**OPV-ch** , showed aggregates of 1000 and 120 nm, corresponding to the State A (2.5% THF) and State B (10% THF), respectively (Figure 3.1.6.a).

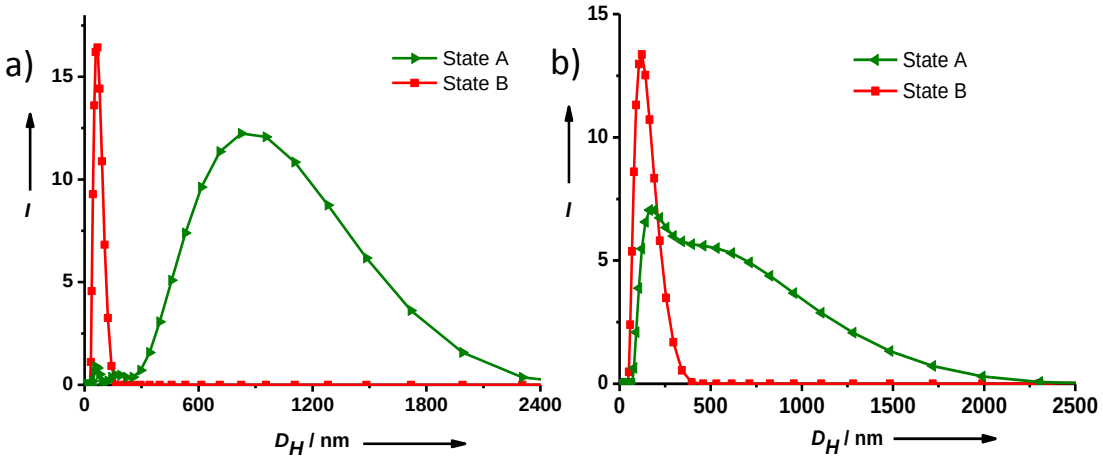


*Figure 3.1.6. Aggregate size differences in State A and State B, monitored by Dynamic Light Scattering (DLS) in a) (**S**)-**OPV-ch** and b) **OPV-ach**.*

### 3.1.3.3. Spectroscopic Probing of Self-Assembled OPV Amphiphiles in Solution

Detailed optical studies on the two self-assembled states of amphiphilic OPV were carried out through UV-Vis, fluorescence and Circular Dichroism (CD) spectroscopic techniques. These studies corroborated well with the microscopic investigations and gave insights into the distinct spectroscopic signatures for the two self-assembled states, suggesting different intermolecular interactions between OPV chromophores,[11] resulting in distinct organization of the amphiphiles.

Absorption features of **OPV-ach** nanosheets were markedly different from the tubes. While the nanosheets had a vibrionic shoulder band at 440 nm, in accord with literature reports for OPV self-assemblies with intermolecular excitonic interactions,[11] the absorption spectrum of the tubular structures did not have the vibrionic shoulder but was broadened compared to the monomeric absorption spectrum in THF. Red shifted emission bands were observed in the fluorescence spectra with maxima at 503 nm and 540 nm in the nanosheets compared to the monomer emission at 441 nm and 465 nm (Figure 3.1.7.a and b). Notably, though the vibrionic shoulder was missing in the absorption spectra of the nanotubes, the self-assembly of this state was clearly marked by its red-shifted emission bands at 491 nm and 525 nm.

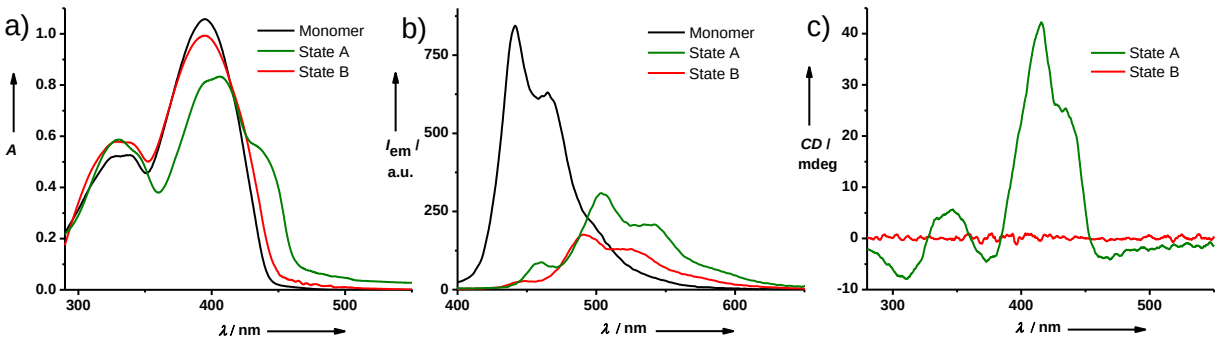


*Figure 3.1.7. Characterization of the monomer, State A and State B phases in OPV amphiphiles: a) absorption and b) emission spectra of* ***OPV-ach*** *($c = 2.5\times10^{-5}$ M, $\lambda_{exc}$= 380 nm, l = 10 mm); c) CD spectra of the two states in* ***(S)-OPV-ch*** *($c = 5\times10^{-5}$ M).*

These optical changes suggest the formation of J-aggregates of the OPV chromophores,[11c,d] which was further confirmed by excitation spectra and time-resolved fluorescence studies (Figure 3.1.8.). Excitation spectra collected at 550 nm

emission wavelength for State A showed the vibrionic shoulder at 440 nm similar to the self-assembled absorption spectrum. Time resolved fluorescence measurements clearly indicate that the lifetime of the aggregate in 2.5% THF in water ($\tau_1$ = 1.92 ns (84.3%), $\tau_2$ = 3.8 ns (15.7%) is higher than the monomer (1.53 ns), hence indicating a J- type aggregate. These measurements along with the front-face emission measurements clearly rule out the other possibilities of self-absorption and energy transfer for the fluorescence quenching of monomer. We have further studied the self-assembly of (***S***)-**OPV-ch**, bearing a chiral side chain, to obtain a detailed understanding of the packing of chromophores in the two different kinds of assemblies, using chiroptical properties as a probe. Absorption and emission studies of (***S***)-**OPV-ch** showed similar changes as that of its achiral analogue for both states. Remarkably, circular dichroism (CD) studies performed on State B showed that these assemblies are CD silent, while State A is marked by the appearance of a bisignated CD signal with the positive maximum at 415 nm and the negative maximum at 375 nm characteristic of excitonically coupled OPV chromophores (Figure 3.1.7.c).

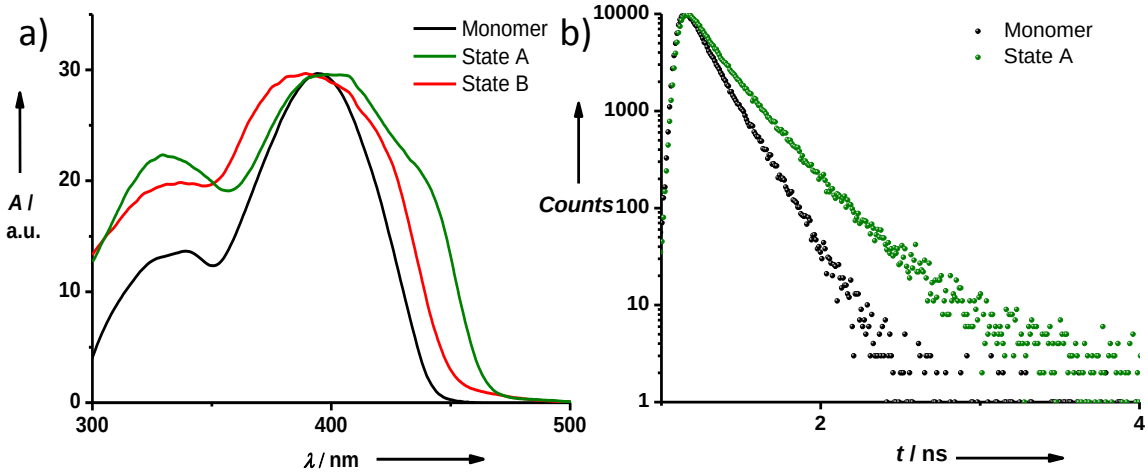


*Figure 3.1.8. Proof of formation of J-aggregates: a) Normalized excitation spectra of State A ($\lambda_{collected}$ = 550 nm), State B ($\lambda_{collected}$ = 530 nm) and monomer absorption spectra of* ***OPV-ach*** *(c = $10^{-5}$ M); b) Fluorescence lifetime decay profiles ($\lambda_{exc}$ = 405 nm) of monomer and State A (c = $2.5\times10^{-5}$ M) of* ***OPV-ach*** *monitored at 465 nm and 543 nm respectively.*

### 3.1.3.4. Phase Transitions in the Self-Assembled State

Detailed spectroscopic and chiroptical probing revealed phase transitions in OPV amphiphillic assemblies, where annealing effects were found to improve the chromophoric ordering in the assemblies, which were followed in detail through profile changes in the UV-Vis, CD and fluorescence spectra. The phase transitions were also accompanied by aggregate size changes as observed through dynamic light scattering studies.

Temperature dependent chiroptical studies of (***S***)**-OPV-ch** in State B (nanotubes) have shown that an annealing process can improve the molecular ordering in the assemblies and the tubes can be converted to the nanosheets (similar to State A), suggesting that State A is a more thermodynamically favourable phase. CD cooling experiment of State B (10% THF in water, $5\times10^{-5}$ M) at the rate of 2 °C/min monitored at 415 nm, showed a sudden appearance of the bisignated CD signal below 22 °C, characteristic of excitonically coupled chromophores (Figure 3.1.9.a). The development of a bisignated CD signal with annealing is corroborated by the appearance of a vibrionic shoulder at 440 nm in the absorption spectrum similar to that of State A (Figure 3.1.9.c). However, at higher temperatures (80 $^{o}$C), the assembly does not dissociate into monomers, as the monomeric absorption and fluorescence changes are not revived at high temperature, but goes to yet another CD silent weakly aggregated state, which on slow cooling leads to the formation of nanosheets.

The phase transitions could be also monitored by DLS studies, as they have distinct hydrodynamic radii. Interestingly, the hydrodynamic diameter of (***S***)**-OPV-ch** increased from 68 to 120 nm, with much broader distribution, upon annealing (Figure 3.1.9.b). Accordingly, the microscopic analyses of the thermodynamically stable phases revealed the presence of only nanosheets, suggesting the opening up of nanotubes upon annealing (Figure 3.1.9.d). This clearly explains that there are two means to achieve this thermodynamically favoured phase. Higher percentages of water directly leads to the formation of nanosheets while at lower aqueous percentages, an annealing process is required to attain it. The phase transition from sheets to tubes can be explained by the fact that with higher percentages of THF the assembly is a folded tube, probably an

attempt by the assembly to reduce the inter-facial energy. However, as the dielectric constant of the mixture increases (with increase in water percentage) the dipolar interactions of TEG chains decrease hence resulting in the opening of the structures forming sheets.

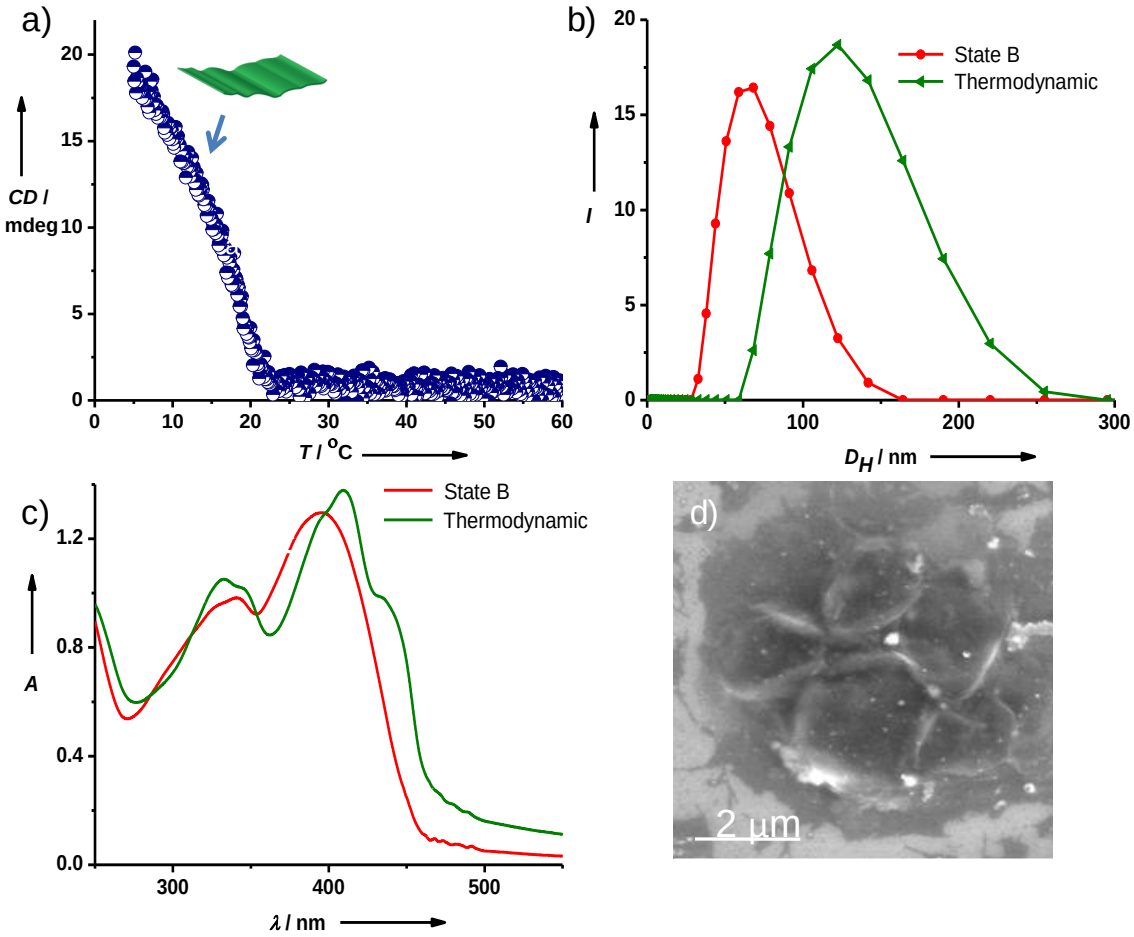


*Figure 3.1.9. Annealing induced phase transition in **(S)-OPV-ch** ($c=5\times10^{-5}$ M) self-assembly, in 10% THF/water solvent mixture: a) Temperature dependent cooling curve by monitoring the CD intensity at 415 nm (-dT/dt = 2 °C/min); b) DLS spectra of the assembly before (State B) and after (thermodynamic) annealing; c) Absorption changes on annealing a solution containing the self-assembled aggregates; d) Morphology changes to sheets in **OPV-ach** in State B (20% THF in water) upon annealing.*

Furthermore, we have investigated the effects of annealing on the thermodynamically stable sheets. DLS studies showed marginal changes in size, indicating the high strength of the synergistic π-π interactions of the OPV segments and

the hydrophobic interactions associated with amphiphilic interactions that render the self-assembled sheets high stability. Temperature dependent chiroptical and UV studies suggested that these nanosheets transform to a less-ordered phase from an excitonically coupled, ordered molecular organization in a highly cooperative fashion (Figure 3.1.10.d). The spectroscopic signatures of the excitonically coupled state, namely, the CD signal or the vibrionic shoulder in the absorption spectrum disappears with increasing temperatures (Figure 3.1.10.b, c). However, only marginal changes in the aggregate size were observed in temperature dependent DLS reiterating that this transition involves only molecular rearrangement ruled out any possibilities of melting of assemblies or rolling-up of the sheets (Figure 3.1.10.a).

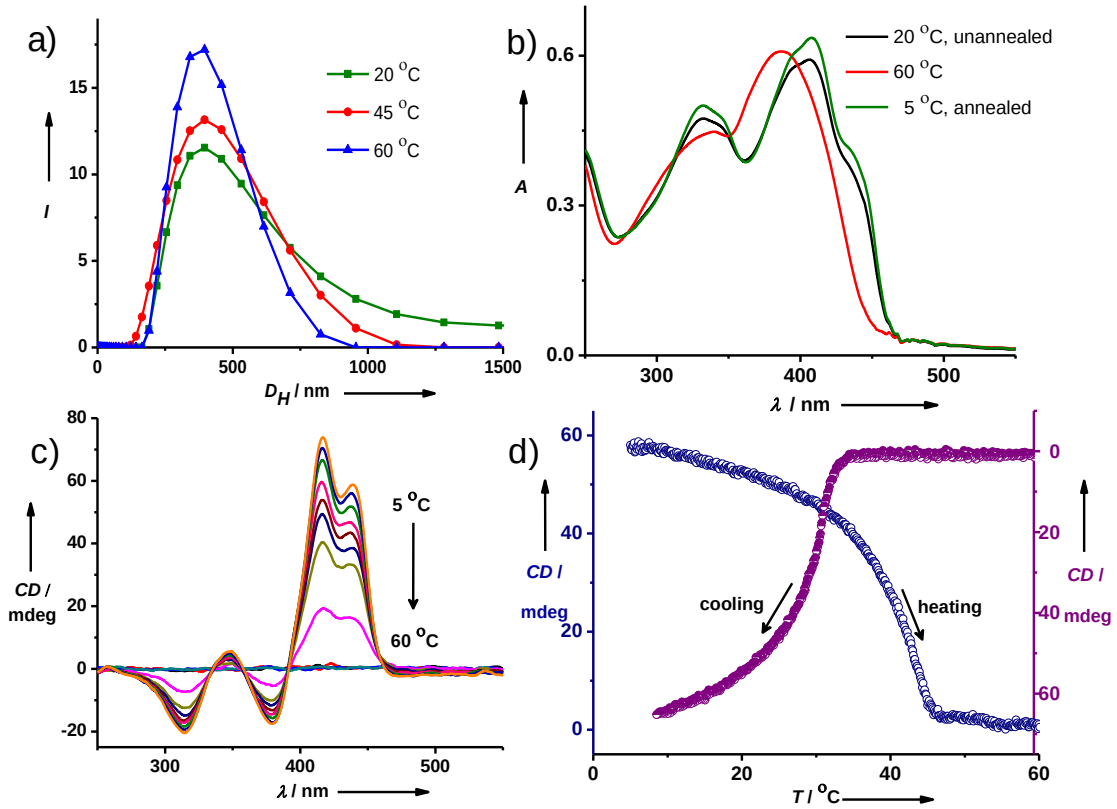


*Figure 3.1.10. Temperature dependent phase transition in the (**S**)-**OPV-ch** sheets (5 × $10^{-5}$ M, 2.5% THF in water): a) Changes in the aggregate size, monitored through DLS; b) Absorption changes (2.5% THF in water, c = 2.5 × $10^{-5}$ M solution); c) Temperature dependent CD spectra while heating; d) Heating and cooling curves (dT/dt = ±2 °C/min) of the sheets by monitoring the CD signal at 415 nm, demonstrating the cooperative phase transition.*

Since molecular organization plays a crucial role in the performance of devices; we probed the factors which influence this transition temperature ($T_t$) in the OPV sheets. The $T_t$ was higher at higher concentrations (Figure 3.1.11.a). Moreover, $T_t$ for **OPV-ach** assembly is found to be higher compared to (***S***)**-OPV-ch** at the same concentration suggesting that the chiral side chain leads to a comparably weaker packing than the achiral side chain (Figure 3.1.11.b).

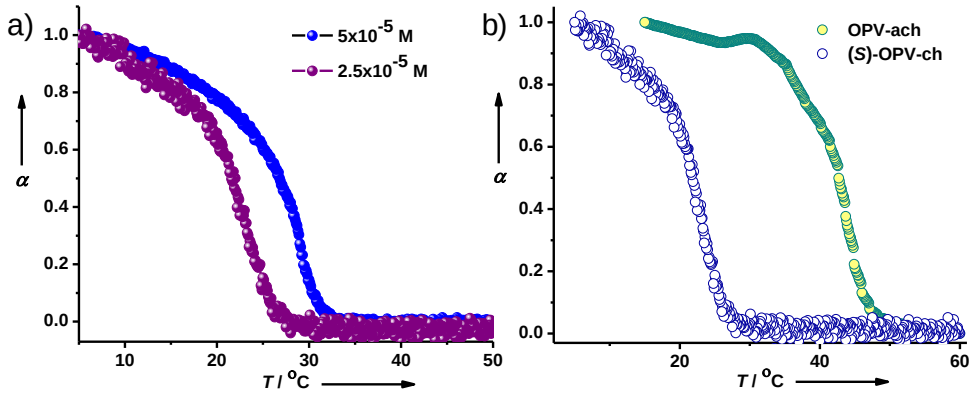


*Figure 3.1.11. Dependence of $T_t$ on: a) concentration of the solution (CD cooling curves of* ***(S)-OPV-ch*** *monitored at 415 nm) and b) nature of the amphiphile; cooling curves of 2.5 × $10^{-5}$ M solutions of* ***OPV-ach*** *monitored at 451 nm in the absorption spectrum and* ***(S)-OPV-ch*** *monitored at 415 nm in the CD spectrum (α is the fraction of the molecules which are excitonically coupled). The less cooperative nature of the* ***OPV-ach*** *cooling curve could be due to the monitoring the absorption changes, which is not as accurate as probing the CD changes in* ***(S)-OPV-ch****, because of the wavelength shifts in the band.*

## 3.1.4. OFET Device Characteristics

Detailed studies of organic field-effect transistor (OFET) devices based on the self-assembled OPV structures as the transport layer were carried out. In general, all the OPV systems including the tubes and the sheets exhibited *p*-type transport behaviour. The supramolecular active layer was introduced directly from the solution phase on the dielectric layer forming top-contact, bottom-gated FET structures. High Mobility value ($\mu_{FET}$) of $0.8\times10^{-2}$ $cm^2V^{-1}s^{-1}$ was obtained for **OPV-ach** sheets with an average hole mobility (averaged over 10 devices) of $5\times10^{-3}$ $cm^2V^{-1}$ $s^{-1}$ and current modulation on/off

ratio ≈ $10^3$ (Figure 3.1.12.a, b). On the other hand, sheets fabricated from (***S***)**-OPV-ch** also exhibited mobility of $7.5\times10^{-3}$ $cm^2V^{-1}s^{-1}$, suggesting that branched side chains do not influence the molecular organization to a great extent due to the strong hydrophobic interactions. Remarkably, these mobility values of the OPV sheets are three orders of magnitude greater than reported for assemblies of OPVs and higher than many other chromophoric systems on a FET device.[12] Moreover, the mobility achieved is only marginally lower than the highest value obtained for vacuum deposited OPV films.[6c] It is also noteworthy that FET mobilities of self-assembled chromophoric systems are lower, as expected, than the mobility values obtained from non-contact mode conductivity techniques.[5a]

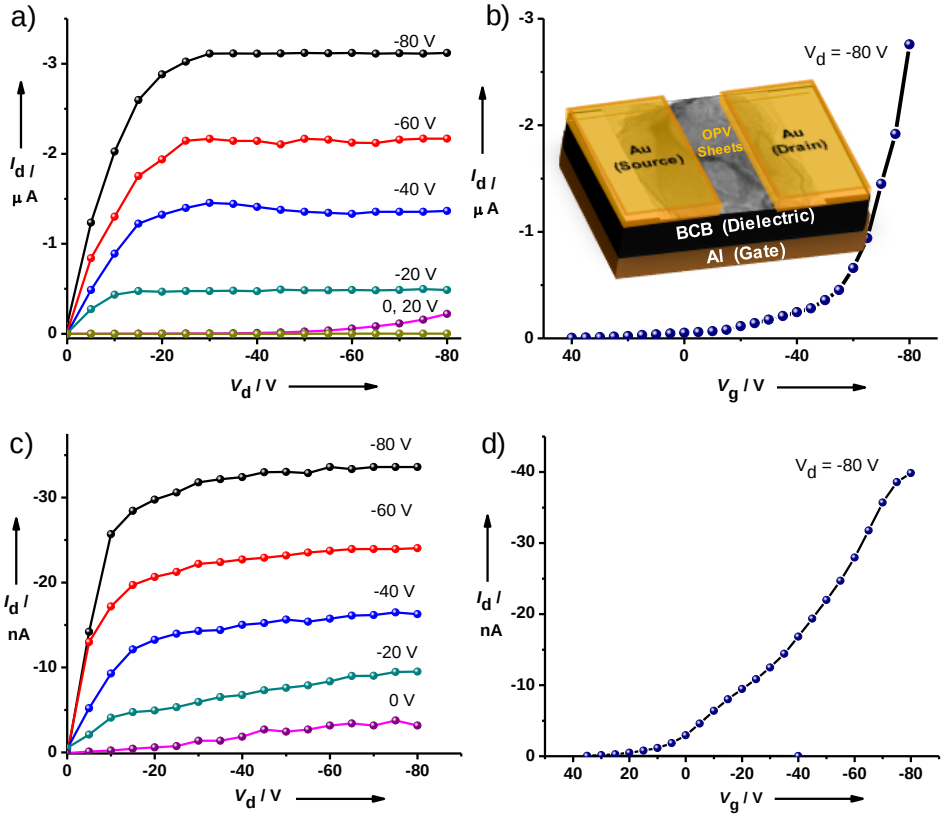


*Figure 3.1.12. a) and b) Typical output and transconductance curves for* ***OPV-ach*** *sheets in top contact bottom gate FET with L (channel length) ~ 20 µm, W (channel width) ~ 1 mm and C (capacitance per unit area of the gate insulator layer) ~ 4 nF/cm$^2$ (Inset of b) shows the schematics of the device structure with OPV sheets as active layer); c) and d) Typical output and transconductance curves for* ***OPV-ach*** *nanotubes in top contact bottom gate FET with L ~ 20 µm,W ~ 1 mm and C ~ 4 nF/cm$^2$.*

Interestingly, transistors fabricated from the rolled-tubes of **OPV-ach** showed much lower mobilities ($\mu_{FET}$ =1.03×10$^{-4}$ cm$^2$V$^{-1}$s$^{-1}$) (Figure 3.1.12.c, d).[16] This trend can be explained on the basis of both macroscopic and microscopic factors. Molecular organization resulting in the form of sheets is expected to have a better coverage in terms of occupying the entire area between the drain (D)–source (S) electrodes and ensuring a complete translation of gate voltage ($V_g$) to surface charges at the interfaces, while in case of a random assortment of tubes, the coverage is dependent on the packing fraction and is expectedly less dense. In case of tubes, the gate bias potential $V_g$ does not get completely translated into interface charges, thereby reducing the estimated mobility. In case of an extended two-dimensional microtube percolation network, the relationship between the percolation threshold ($N_c$) and tube length (L) takes the form, L $(\pi N_c)^{1/2}$ = 4.2.[20] Applying this condition for the present case where the tubes have length ≈ 1 μm, a percolation threshold of ≈ 5 μm$^{-2}$ is obtained. Since the film deposition was carried out by multiple drop-casting procedures from concentrated solutions, it was ensured that we were above the percolation threshold for 1D transport. The density of OPV tubes in our device is ≈ 10 μm$^{-2}$. Mobility at a microscopic level then is a representative figure of merit of the electrical characteristics of individual tube and sheet. Mobility arrived from FET measurements can be used as an estimate of molecular packing upon assuming optimized filling. Comparison of charges induced on the sheet and tubes with C (capacitance per unit area of the gate insulator layer) ≈ 4 nF/cm$^2$ and $V_g$ = -80 V gives an upper limit of the doping level (≈ 10$^9$ for rolled tubes and ≈ 10$^{11}$ for sheets). From a microscopic perspective, the sheet formation involves growth along the π-stacking direction and uniform lamellar packing is obtained with slipped sheets at the dielectric-semiconductor interface. Higher degree of charge-carrier delocalization is expected in the 2-D sheet than the 1-D tube structures, along with a higher tolerance for defects in the 2D systems compared to 1D systems.[21] The enhanced electrical transport processes of the OPV-sheets can be attributed to a combination of these factors. In general however, higher mobility in these nanostructures can be due to the existence of strong π– π interactions, by virtue of the amphiphilic design, along the charge transport direction coupled with a higher degree of order.

## 3.1.5. Conclusions

In conclusion, we have shown the unprecedented self-assembly of OPV amphiphiles into highly ordered sheets, with strong synergistic π-stacking and hydrophobic interactions. Furthermore, phase transitions of tubular scrolls into sheets, formed by solvent compositions or annealing effects have been probed carefully using spectroscopic, microscopic and light scattering techniques. FET devices have been fabricated by direct solution processing of these supramolecular assemblies, with different mobility values for the tubes ($1.03 \times 10^{-4} cm^2V^{-1}s^{-1}$) and self-assembled sheets ($8 \times 10^{-3} cm^2V^{-1}s^{-1}$, thermodynamic phase). More importantly, the mobility obtained for the OPV sheets ($8 \times 10^{-3} cm^2V^{-1}s^{-1}$) is one of the highest values reported for the self-assembled nanostructures of chromophores on a FET device structure. We envisage that the amphiphilic molecular design would be the key to obtaining self-assembled morphologies of higher structural order and hence better supramolecular device characteristics.

## 3.1.6. Experimental Section

### 3.1.6.1. General Methods

**Atomic Force Microscopy (AFM)**: AFM measurements were performed on a Veecodi Innova SPM operating in tapping mode regime. Micro-fabricated silicon cantilever tips doped with phosphorus and with a frequency between 235 and 278 kHz and a spring constant of 20-40 $Nm^{-1}$ were used. The samples were prepared by drop casting a solution of **OPV-ach** on a glass substrate and dried under high vacuum at room temperature.

**Field Emission Scanning Electron Microscopy (FE-SEM)**: FE-SEM measurements were performed on a NOVA NANO SEM 600 (FEI) by drop casting the solutions on glass substrate followed by drying under high vacuum at room temperature and was operated with an accelerating voltage of 30 kV.

**Transmission Electron Microscopy (TEM)**: TEM measurements were performed on a JEOL, JEM 3010 operated at 300 kV. Samples were prepared by placing a drop of the solution on carbon coated copper grids followed by drying at room temperature. The

images were recorded with an operating voltage 300 kV. In order to get a better contrast, the samples were stained with uranyl acetate (1 wt% in water) before the measurements.

**Confocal Microscopy**: Confocal Microscopy imaging was done at room temperature using a Zeiss LSM 510 META laser scanning confocal microscope. The microscope objective of 63X (NA 1.4) and 20X (NA 0.5) were employed. Samples were prepared by sealing the solution between two glass plates.

**Optical Measurements**: Electronic absorption spectra were recorded on a Perkin Elmer Lambda 900 UV-Vis-NIR Spectrometer and emission spectra were recorded on Perkin Elmer LS 55 Luminescence Spectrometer. UV-Vis and emission spectra were recorded in 10 mm path length cuvettes. Fluorescence spectra of solutions were recorded by exciting the **OPV-ach** and (***S***)**-OPV-ch** at 380 nm and 310 nm respectively. Circular Dichroism (CD) spectra and temperature dependent UV-Vis spectra were recorded on a Jasco J-815 spectropolarimeter where the sensitivity, time constant and scan rate were chosen appropriately. The temperature dependent measurements were performed with a CDF-426S/15 Peltier-type temperature controller with a temperature range of 263-383 K and adjustable temperature slope.

**NMR Measurements**: NMR spectra were obtained with a Bruker AVANCE 400 (400 MHz) Fourier transform NMR spectrometer with chemical shifts reported in parts per million (ppm) with respect to TMS.

**Dynamic light scattering Experiments (DLS)**: The measurements were carried out using a NanoZS (Malvern UK) employing a 532 nm laser at a back scattering angle of $173^{o}$. The samples were measured in a 10 mm glass cuvette.

**XRD Measurements**: Wide-angle XRD patterns of drop casted films of the solutions of the amphiphiles were recorded in a Bruker D8 Discover (40 kV, 30Ma) instrument using Cu $K_{\alpha}$ radiation ($2\theta = 5^{o}–60^{o}$). Small angle XRD patterns were recorded in Siefert XRD instrument using Co source ($\theta = 0.9^{o}–60^{o}$).

**Matrix-assisted laser desorption ionization time-of-flight (MALDI-TOF)**: MALDI-TOF spectra were obtained on a Brukerultraflex 2 MALDI-TOF mass spectrometer with α-cyano-4-hydroxycinnamic acid matrix.

**Field Effect Mobility Measurements:** Field effect mobility measurements were performed on top contact bottom gate transistor structures. The fabrication of the field effect transistor (FET) involved coating of Al electrode ($10^{-6}$ mbar, 40 nm thick) by physical vapour deposition on standard RCA treated cleaned glass substrates. This was followed by coating of the dielectric layer of hydroxyl free divinyl tetramethylsiloxane bis (benzocyclobutene) at 800 rpm for 1 min. and annealed in glove box atmosphere at 290 $^{o}$C. The effective capacitance per unit area (C) of the dielectric films measured using Keithley 4200 semiconductor parameter analyser was obtained to be ~ 4 nF/cm$^2$ for films of thickness 0.5-0.6 μm. The surface of the dielectric is further treated with hexamethyldisilazane in liquid by spin coating at 1500 rpm for 30 seconds and annealing at 110 $^{o}$C for 2 hrs in $N_2$ atmosphere. This was followed by solution casting the thin film of the OPV molecule in appropriate THF and water compositions to obtain films of thickness ~ 150-200 nm. The source-drain Au electrode were also vapor deposited ($10^{-6}$ mbar, 40 nm thick). The active layers were coated at different concentrations to to distinctly follow the morphological changes with the transport measurements. The electrical characterization of the FETs were done using a standard set up of Keithley 2400 Source meters and a high impedance electrometer (Keithley 6514). The measurements were also cross checked with Keithley 2400 semiconductor parameter analyser. The mobility values reported are the median value obtained from the measurements performed on 10-15 devices in each case which are representative of the general trends in these molecules.

### 3.1.6.2. Synthetic Methods

The starting materials used for synthesizing various compounds were obtained from commercial suppliers. The moisture sensitive reactions were performed under an atmosphere of argon. DMF was dried by distillation under vacuum and dried on 3 Å molecular sieves activated at 180 $^{\circ}$C. Analytical thin layer chromatography was carried out on Merck silica gel 60. Column chromatography was carried out on silica gel (100-

200 mesh). Freshly distilled solvents were used for column chromatography. Size exclusion chromatography was done on sephadex polystyrene biobeads S-X3 with chloroform as the eluent.

Proton chemical shifts are reported in ppm downfield from TMS (Tetramethylsilane) using the resonance of the deuterated solvent as internal standard. Splitting patterns are designated as s, singlet; d, doublet; bs, broad singlet; m, multiplet; t, triplet; q, quartet; dd, double doublet; ddd, double double doublet; quin, quintet and br, broad.

### 3.1.6.2.1 Synthetic Schemes

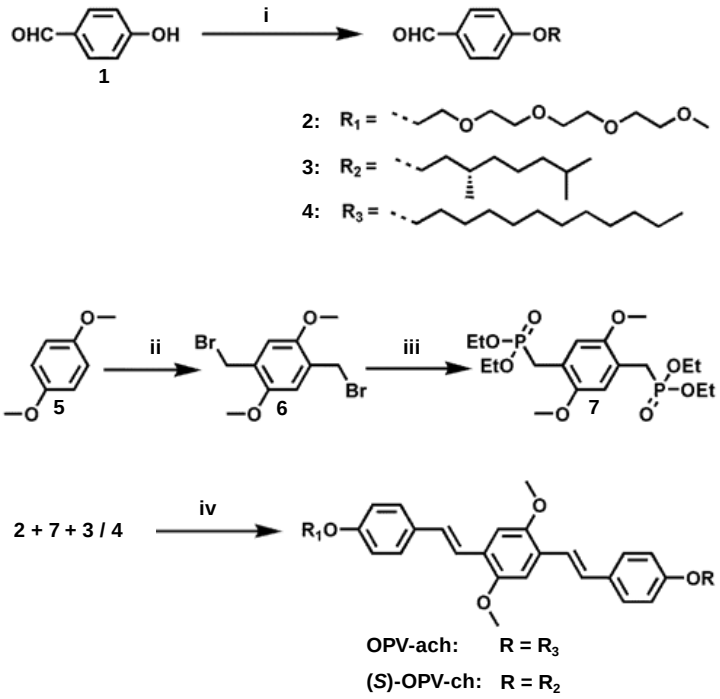


*Scheme 3.1.1. Synthetic pathway for* ***OPV-ach*** *and* ***(S)-OPV-ch****: i) $(C_2H_4O)_4OTs$ / $C_{10}H_{21}OTs$ / $C_{12}H_{25}Br$, 18-crown-6, $K_2CO_3$, acetone, 24 hrs (reflux), Ar atmosphere, ii) HCHO, HBr, $CH_3COOH$, 60 $^oC$-70 $^oC$, 2 hrs, iii) $P(OEt)_3$, 150 $^oC$, 4 hrs, iv) Potassium t-butoxide, dry DMF, rt, 3 hrs, Ar atmosphere.*

### 3.1.6.2.2. Synthetic Procedures

Compounds **2-4**, **6** and **7** were synthesized according to known literature procedures.[15, 11c] The OPV amphiphiles (**OPV-ach** and (***S***)**-OPV-ch**) were synthesized

through a statistical Wittig-Horner reaction between the bisphosphonate (**7**) and the respective aldehydes. Compound **7** (0.26 g, 0.64 mmoles) was taken in dry DMF (7 mL) under nitrogen atmosphere and stirred at room temperature till it dissolved completely. Potassium *t*-butoxide (0.23 g, 2.05 mmoles) was then transferred under inert conditions and the reaction mixture was stirred for 10 minutes until it turned dark, indicating the formation of anions. The aldehydes (0.64 mmol each) were weighed separately, dissolved in dry DMF (5 mL) and were added to the reaction mixture drop wise. The reaction mixture was allowed to stir under Ar atmosphere for additional 3 hours. After the completion of the reaction, an extraction was done with water / diisopropyl ether. The organic layer was collected, dried over $Na_2SO_4$ and was concentrated on a rotary evaporator. The crude mixture of **OPV-ach** and (***S***)**-OPV-ch** was purified by silica gel column chromatography and neutral alumina column chromatography (chloroform: methanol) respectively and size exclusion chromatography ($CHCl_3$, S-X3) to get **OPV-ach** and (***S***)**-OPV-ch** as yellow solids with the yields of 14.9% and 7.2%, respectively. The amphiphiles were obtained along with the bolaamphiphiles and the respective dialkyl substituted derivatives in the statistical reactions performed.

**OPV-ach:** $^1$H NMR (400 MHz, $CDCl_3$, $Me_4Si$): δ (ppm) = 7.47 (d, *J* = 8.8 Hz, 4H, ArH), 7.34 (d, *J* = 16.4 Hz, 2H, vinylic H), 7.33 (d, *J* = 16.4 Hz, 2H, vinylic H), 7.10 (s, 2H, ArH), 7.06 (d, *J* = 16.4 Hz, 2H, vinylic H), 7.05 (d, *J* = 16.4 Hz, 2H, vinylic H), 6.91 (d, *J* = 8.8 Hz, 2H, ArH), 6.88 (d, *J* = 8.8 Hz, 4H, ArH), 4.16 (t, *J* = 5.2 Hz, 2H, $OCH_2$,), 3.98 (t, *J* = 5.2 Hz, 2H, $OCH_2$,), 3.91 (s, 6H, Ar $OCH_3$), 3.73 (m, 2H), 3.67 (m, 8H), 3.54 (m, 2H), 3.38 (s, 3H, TEG $OCH_3$), 1.78 (m, 2H), 1.5-1.2 (m, 20H); $^{13}$C NMR (100 MHz, $CDCl_3$): δ (ppm) = 158.9, 158.6, 151.6, 151.5, 132.1, 130.7, 128.6, 128.5, 127.9, 126.8, 126.7, 121.4, 121.2, 114.9, 114.9, 109.2, 109.2, 72.1, 71.0, 70.8, 70.7, 69.9, 68.2, 67.6, 59.2, 56.6,29.8-29.7, 29.6-29.5, 26.2, 22.8, 14.3; MALDI-TOF-MS (ESI) *m/z*: calcd for $C_{45}H_{64}O_8$: 732.4601 $[M]^+$, found: 732.56; HRMS (ESI) *m/z*: calcd for $C_{45}H_{64}O_8$: 755.4601 $[M+Na]^+$, found: 755.4499.

(***S***)**-OPV-ch**: $^1$H NMR (400 MHz, $CDCl_3$, $Me_4Si$): δ (ppm) = 7.47 (d, *J* = 8.4 Hz, 4H, ArH), 7.34 (d, *J* = 16.4 Hz, 2H, vinylic H), 7.34 (d, *J* = 16.4 Hz, 2H, vinylic H), 7.11 (s, 2H, ArH), 7.06 (d, *J* = 16.4 Hz, 2H, vinylic H), 7.06 ( d, *J* = 16.4 Hz, 2H, vinylic H), 6.91 (d, *J* = 8.8 Hz, 2H, ArH), 6.89 (d, *J* = 8.8 Hz, 4H, ArH), 4.15 (t, *J* = 5.2 Hz, 2H,

$OCH_2$), 4.02 (m, 2H, $OCH_2$), 3.91(s, 6H, ArOMe H), 3.74 (m, 2H), 3.67 (m, 8H), 3.54 (m, 2H), 3.38 (s, 3H, TEG $OCH_3$), 1.78 (m, 2H), 1.9-0.8 (alkyl H,19H); $^{13}$C NMR (100 MHz, $CDCl_3$): δ = 151.5, 130.7, 128.6, 128.4, 127.9, 126.6, 121.4, 121.2, 114.9, 114.8, 109.2, 109.1, 72.1, 71.0, 70.8, 70.7, 69.9, 67.7, 66.6, 59.2, 56.6, 39.4,37.4, 36.4, 30.1, 28.1, 24.8, 22.8, 22.7,19.8; MALDI-TOF-MS (ESI) *m/z*: calcd for $C_{43}H_{60}O_8$: 704.4288 $[M]^+$, found: 704.39; HRMS (ESI) *m/z*: calcd for $C_{43}H_{60}O_8$: 727.4288 $[M+Na]^+$, found: 727.4186.

## 3.1.7. References


[1] a) F. Würthner, *Angew. Chem. Int. Ed.* **2001**, *40*, 1037; b) F. J. M. Hoeben, P. Jonkheijm, E. W. Meijer, A. P. H. J. Schenning, *Chem. Rev*. **2005**, *105*, 1491 c) A. P. H. J. Schenning, E. W. Meijer, *Chem. Commun*. **2005**, 3245; d) A. C. Grimsdale, K. Müllen, *Angew. Chem. Int. Ed.* **2005**, *44*, 5592.

[2] J. Roncali, *Chem. Rev.* **1992**, *92*, 711.

[3] a) R. E. Martin, F. Diederich, *Angew. Chem. Int. Ed.* **1999**, *38*, 1350; b) J. M. Tour, *Chem. Rev.* **1996**, *96*, 537; c) *Electronic Materials: The Oligomer Approach* (Eds.: K. Müllen, G.Wegner), WILEY-VCH, Weinheim, **1997**.

[4] a) T. Aida, E. W. Meijer, S. I. Stupp, *Science* **2012**, *335*, 813; b) S. S. Babu, S. Prasanthkumar, A. Ajayaghosh, *Angew. Chem. Int. Ed.* **2012**, *51*, 1766; c) A. Ajayaghosh, S. J. George, A. P. H. J. Schenning, *Top. Curr. Chem.* **2005**, *258*, 83; d) F. Würthner, *Chem. Commun.* **2004**, 1564; e) B. – K. An, J. *Gierschner*, S. Y. Park, *Acc. Chem. Res*. **2012**, *45*, 544.

[5] a) A. Saeki, Y. Koizumi, T. Aida, S. Seki, *Acc. Chem. Res.* **2012**, *45*, 1193; b) M. Hasegawa, M. Iyoda, *Chem. Soc. Rev*. **2010**, *39*, 2420; c) T. Lei, J. Pei, *J. Mater. Chem*. **2012**, *22*, 785.

[6] a) C. D. Dimitrakopoulos, P. R. L. Malenfant, *Adv. Mater*. **2002**, *14*, 99; b) P. T. Herwig, K. Müllen, *Adv. Mater*. **1999**, *11*, 480; c) T. Yasuda, M. Saito, H. Nakamura, T. Tsutsui, *Appl. Phys. Lett*. **2006**, *89*, 182108.

[7] a) Y. Yamamoto, T. Fukushima, Y. Suna, N. Ishii, A. Saeki, S. Seki, S. Tagawa, M. Taniguchi, T. Kawai, T. Aida, *Science* **2006**, *314*, 1661; b) H. J. Kim, T. Kim, M. Lee, *Acc. Chem. Res*. **2011**, *44*, 72; c) H. Shao, J. Seifert, N. C. Romano, M. Gao, J. J. Helmus, C. P. Jaroniec, D. A. Modarelli, J. R. Parquette, *Angew. Chem.*

*Int. Ed*. **2010**, *49*, 7688; d) C. Wang, Z. Wang, X. Zhang, *Acc. Chem. Res*. **2012**, *45*, 608; e) M. Kumar, S. J. George, *Chem. Eur. J.* **2011**, *17*, 11102; f) K. V. Rao, K. Jayaramulu, T. K. Maji, S. J. George, *Angew. Chem. Int. Ed.* **2010**, *49*, 4218.

[8] a) F. J. M. Hoeben, I. O. Shklyarevskiy, M. J. Pouderoijen, H. Engelkamp, A. P. H. J. Schenning, P. C. M. Christianen, J. C. Maan, E.W. Meijer, *Angew. Chem. Int. Ed.* **2006**, *45*, 1232; b) X. Zhang, Z. Chen, F. Würthner, *J. Am. Chem. Soc*. **2007**, *129*, 4886; c) K. V. Rao, S. J. George, *Org. Lett.* **2010**, *12*, 2656; d) L. C. Palmer, S. I. Stupp, *Acc. Chem. Res*. **2008**, *41*, 1674.

[9] a) W. J. Oldham, Jr., R. J. Lachicotte, G. C. Bazan, *J. Am. Chem. Soc.* **1998,** *120*, 2987; b) T. Goodson III**,** W. Li, A. Gharavi, L. Yu, *Adv. Mater*. **1997**, *9*, 639.

[10] a) J. H. Burroughes, D. D. C. Bradley, A. R. Brown, R. N. Masks, K. M. Mackay, R. H. Friend, P. L. Burns, A. B. Holmes, *Nature* **1990**, *347*, 539; b) M. Granstroöm, K. Petritsch, A. C. Arias, A. Lux, M. R. Andersson, R. H. Friend, *Nature* **1998**, *395*, 257; c) A. Kraft, A. C. Grimsdale, A. B. Holmes, *Angew. Chem. Int. Ed.* **1998**, *37*, 402.

[11] a) A. Ajayaghosh, V. K. Praveen, *Acc. Chem. Res*. **2007**, *40*, 644; b) D. G. Rodríguez, A. P. H. J. Schenning, *Chem. Mater.* **2011**, *23*, 310; c) A. Ajayaghosh, S. J. George, *J. Am. Chem. Soc.* **2001,** *123*, 5148; d) A. P. H. J. Schenning, P. Jonkheijm, E. Peeters, E. W. Meijer, *J. Am. Chem. Soc.* **2001**, *123*, 409; e) G. N. Tew, M. U. Pralle, S. I. Stupp, *Angew. Chem. Int. Ed.* **2000**, *39*, 516.

[12] a) P. Jonkheijm, N. Stutzmann, Z. Chen, D. M. de Leeuw, E. W. Meijer, A. P. H. J. Schenning, F. Würthner, *J. Am. Chem. Soc.* **2006**, *128*, 9535; b) M. Durkut, M. Mas–Torrent, P. Hadley, P. Jonkheijm, A. P. H. J. Schenning, E. W. Meijer, S. George, A. Ajayaghosh, *J. Chem Phys.* **2006**, *124*, 154704; c) Y. Yamamoto, G. Zhang, W. Jin, T. Fukushima, N. Ishii, A. Saeki, S. Seki, S. Tagawa, T. Minari, K. Tsukagoshi, T. Aida, *Proc. Nat. Acad. Sci.* **2009**, *106*, 21051.

[13] a) S. Xiao, M. Myers, Q. Miao, S. Sanaur, K. Pang, M. L. Steigerwald, C. Nuckolls, *Angew. Chem. Int. Ed*. **2005**, *44*, 7390; b) J. W. Chung, H. Yang, B. Singh, H. Moon, B. –K. An, S. Y. Lee, S. Y. Park, *J. Mater. Chem*. **2009**, *19*, 5920.

[14] For self-assembled sheets from π-conjugated systems see; a) E. Lee, J. K. Kim, M. Lee, *Angew. Chem. Int. Ed.* **2009**, *48*, 3657; b) J. Yin, Y. Zhou, T. Lei, J. Pei,

*Angew. Chem. Int. Ed*. **2011**, *50*, 6320; c) K. Liu, C. Wang, Z. Li, X. Zhang, *Angew. Chem. Int. Ed.* **2011**, *50*, 4952; d) G. Fernández, F. García, F. Aparicio, E. Matesanz, L. Sánchez, *Chem. Commun*. **2009**, 7155.

[15] Hulvat, M. F. Sofos, K. Tajima, S. I. Stupp, *J. Am. Chem. Soc.* **2005**, *127*, 366.

[16] Twisted tubular phase has been isolated as the kinetic intermediate in self-assembled hexabenzocoronenes: T. Yamamoto, T. Fukushima, A. Kosaka, W. Jin, Y. Yamamoto, N. Ishii, T. Aida, *Angew. Chem. Int. Ed*. **2008**, *47*, 1672.

[17] Y. Chen, B. Zhu, F. Zhang, Y. Han, Z. Bao, *Angew. Chem. Int. Ed.* **2008**, *47*, 6015.

[18**]** L. Radzihovsky, J. Toner, *Phys. Rev. Lett*. **1995**, *75*, 4752.

[19] L. Hu, D. S. Hecht, G. Gruner, *Nano Lett.* **2004**, *4*, 2513.

[20] H. Sirringhaus, P. J. Brown, R. H. Friend, M. M. Nielsen, K. Bechgaard, B. M. W. L.-Voss, A. J. H. Spiering, R. A. J. Janssen, E. W. Meijer, P. Herwig, D. M. de Leeuw , *Nature* **1999**, *401*, 685.

# Chapter-3.2.

## Self-Assembly of *n*-Type Naphthalene Diimide Amphiphiles: Aligned Fibers with High Mobility


## *Abstract*

*This Chapter deals with the effect of an amphiphilic design on the electronic properties of n-type naphthalene diimide core. The previous Chapter dealt with high hole mobility values achieved for self-assembled p-type OPV amphiphiles on Organic Field Effect Transistor (OFET) devices. In an attempt to generalize the concept of better chromophoric ordering achieved by synergistic π-π interactions and hydrophobic interactions in rich aqueous solvent compositions, leading to higher mobility value, we hereby present the detailed self-assembly and device fabrication studies of n-type naphthalene diimide (NDI). NDI aromatic cores, being small in size, generally show weak aromatic interactions. On the other hand, an amphiphilic design has been shown to improve the interchromophoric interactions by reinforcing π-π stacking and hydrophobic effects, leading to stronger self-assembly. The self-assembly of NDI amphiphile has been investigated in detail in Tetrahydrofuran/ Water solvent compositions by various spectroscopic and microscopic techniques.* ***NDI-Amph*** *has been observed to form fluorescent J-aggregates with intense luminescence on self-assembly that organize to form aligned nanofibers at higher percentages of water, which were then fabricated on an OFET device as the electroactive layer. Electron mobilities as high as* $8.5\times10^{-3} cm^2V^{-1}s^{-1}$ *were obtained with an average mobility of* $7.9\times10^{-3} cm^2V^{-1}s^{-1}$*, over 10 devices. These investigations, therefore, unambiguously prove that an amphiphilic design does improve the chromophoric ordering in the self-assembled state, which is reflected in the device properties.*


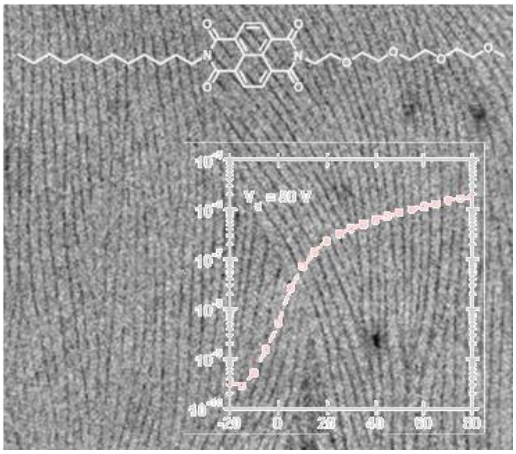

Manuscript based on this work is under preparation.

## 3.2.1. Introduction

Self-assembly of π-conjugated molecules[1] is rapidly gaining attention as a means of constructing functional nanostructures in the field of supramolecular materials,[2] biomedical engineering[3] and organic electronics.[4] Organic Field Effect Transistors and organic solar cells are replacing their inorganic counterparts as they prove to be more cost-effective and have advantages such as solution processability and ease of functionalization for wavelength tunability. In this regard, one-dimensional nanostructures are highly desirable due to the long channel lengths provided over extended arrays of electroactive chromophores.[5] Nanostructures built from self-assembled organic molecules generally show an ordering over lengths of 10-100 nm. However, if they are aligned on the substrate, the ordering exists over micrometer scales, which would drastically improve the device performance.

*n*-type rylene diimides,[6] particularly perylene bisimides have been sought for as a replacement for the active layer in organic electronics. However, functionalized perylene bimides, being highly hydrophobic molecules, face solubility problems. The smaller counterparts, naphthalene diimides are attractive in the aspects of easy functionalization and high solubility.[7] Functionalized naphthalene diimide (NDI) self-assemblies have been studied in solvents ranging from methylcyclohexane to aqueous systems. Various nanostructures have been constructed from the self-assembly of naphthalene diimides, such as tubes, tapes, ribbons and helices.[8] However, NDI aromatic cores are small and to create ordered assemblies, the interactions need to be reinforced. Parquette and co-workers have utilized peptidic self-assembly,[9] which has strong hydrogen bonds to create less dynamic assemblies with high association constants (Figure 3.2.1.a-c). Matile and co-workers have also employed NDIs to create synthetic ion channels,[10] and reinforced the NDI arrays by H-bonding interactions from the bay substituted groups (Figure 3.2.1.d-e).

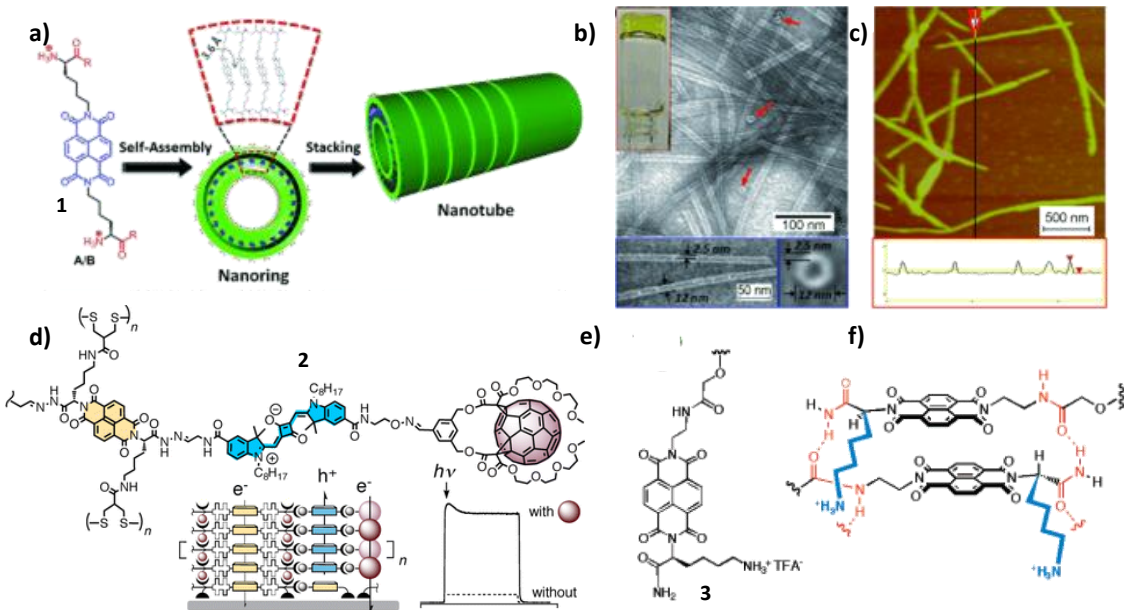


*Figure 3.2.1. Self-assembly of NDIs strengthened with assisted H-bonds: a) NDI-peptidic bolaamphiphiles that form rigid nanotubes upon self-assembly (The blue sections of* ***1*** *undergo hydrophobic π–π stacking interactions, and the red sections electrostatic interactions); b) TEM (250 μM; carbon-coated copper grid); 2% (w/w) uranyl acetate as negative stain (Blue insets: Two nanotubes and one nanoring); c) Tapping mode AFM image with the height profile of the nanotube at the bottom. Inset of b) shows a picture of gel formed by the peptidic NDI bola-amphiphile (****1****) upon self-assembly in an inverted vial; d) schematic of synthetic ion channels created by arrays of self-assembled NDI (****2****) by Matile and coworkers (the inset shows the schematic of photocurrent generated with and without fullerene); e) NDI molecule (****3****) used in the ion channel; f) H-bonded assisted NDI self-assembly of* ***3*** *(Figures a-c reproduced with permission from reference 9a and d-f reproduced with permissions from reference 10).*

Heirarchial self-assemblies of NDI amphiphiles have been demonstrated to form ordered nanostructures and exhibit interesting properties such as reversible vapochromism and aggregate to aggregate transformation (Figure 3.2.2),[11] but their electronic properties in the amphiphilic design have not been investigated so far. In an attempt to prove the role of an amphiphillic design to improve the molecular ordering, reflecting in their enhanced electronic properties, in this Chapter we study **NDI-Amph** on a device structure. **NDI-Amph** self-assembles to form aligned nanofibers which are several micrometers long in THF/water compositions and has strong π-stacking and

hydrophobic interactions. Top contact bottom gate transistor structures constructed from drop-casted solutions of **NDI-Amph** as the electroactive layer show *n*-type behaviour with electron mobility as high as $8.5\times10^{-3}cm^2V^{-1}s^{-1}$ and with an average mobility of $7.9\times10^{-3}cm^2V^{-1}s^{-1}$. Detailed investigations into the self-assembly characteristics and device fabrication have been discussed in this Chapter.

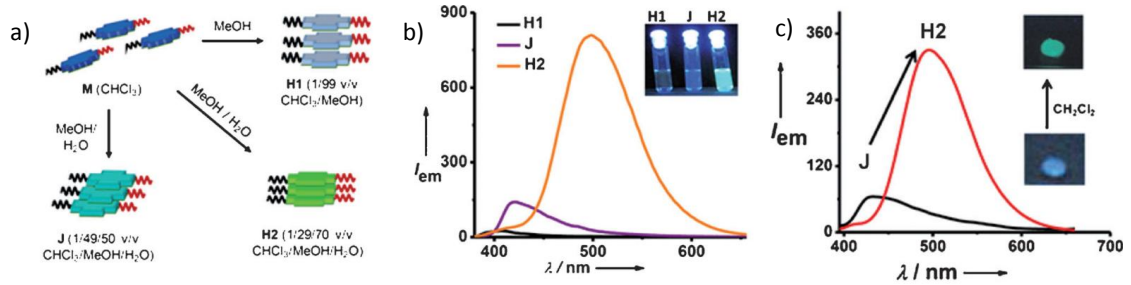


*Figure 3.2.2. Dynamic self-assembly of **NDI-Amph** demonstrated by George and coworkers: a) Schematics of different aggregates with various solvent compositions; b) steady state emission spectra ($\lambda_{ex}$ = 350 nm) of the various states; c) vapochromism in **NDI-Amph** leading to dynamic aggregate transformation (a-c reproduced with permission from reference 11).*

## 3.2.2. Design Strategy

The naphthalene diimide amphiphile (**NDI-Amph**) has a *n*-type naphthalene diimide core flanked by bay substituted hydrophobic dodecyl chain on one side and hydrophilic monomethyl tetraethyleneglycol side chain on the other side (Figure 3.2.3). The molecule was synthesized by a statistical condensation reaction of 1,4,5,8-naphthalenetetracarboxylic dianhydride with amine functionalized monomethoxy tetraethylene glycol and dodecylamine, with equimolar mixtures of all three reactants. The dodecyl amine and 1,4,5,8-naphthalenetetracarboxylic dianhydride were purchased from commercial sources while monomethoxy tetraethylene glycol amine was synthesized over four steps,[12] according to literature procedures. The corresponding bola-amphiphilic (ditertraethyleneglycol) and didodecyl substituted derivatives were obtained as by-products. The molecule was completely characterized by $^1H$ NMR, $^{13}C$ NMR, and high resolution mass spectrometry (HRMS) (See section 3.2.6. for detailed characterization). Substitution at the imide position rendered solubility to **NDI-Amph** in most organic solvents, like THF, $CHCl_3$ and toluene.

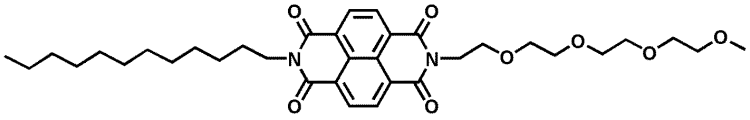

**NDI-Amph**

*Figure 3.2.3. Molecular structure of NDI amphiphile*.

The amphiphilic design is expected to increase interchromophoric interactions between the small NDI cores by enhanced π-stacking and hydrophobic interactions, leading to stable assemblies in polar solvents.

## 3.2.3. Self-Assembly of NDI Amphiphiles

The NDI amphiphile was studied in varying compositions of water/THF. Incremental percentages of water in THF led to self-assembly of **NDI-Amph**, which was characterized through various spectroscopic techniques like UV-Vis and fluorescence spectroscopy, light scattering techniques and microscopic investigations.

### 3.2.3.1. Photophysical Characterization

**NDI-Amph** remains in the monomeric state in $CHCl_3$ and THF, as characterized by sharp absorption features, with maxima at 357 nm and 378 nm, with the band at higher wavelength having higher absorbance (Figure 3.2.4.a). As the percentage of water is increased, broadening of absorption features, reversal of relative intensity of the two bands along with red shift and scattering occurs, indicative of self-assembly. Solvent compositions of water/THF, 70/30, (v/v) lead to bathochromic shifts with absorption maxima at 368 nm and 386 nm, with huge scattering, indicative of the presence of self-assembled nanostructures in solution.

Photoluminescence spectra of **NDI-Amph** in various solvent compositions, obtained on excitation at 350 nm showed an increase in fluorescence on aggregation (Figure 3.2.4b). The molecularly dissolved state was weakly fluorescent, with a maximum at 407 nm. However, increasing percentages of water in THF (> Water/THF, 67/33(v/v)), resulted in a huge increase in fluorescence (~ six times increase in the photoluminescence intensity) with a bathochromic shift of 18 nm, leading to shift of the final emission maxima to 425 nm.

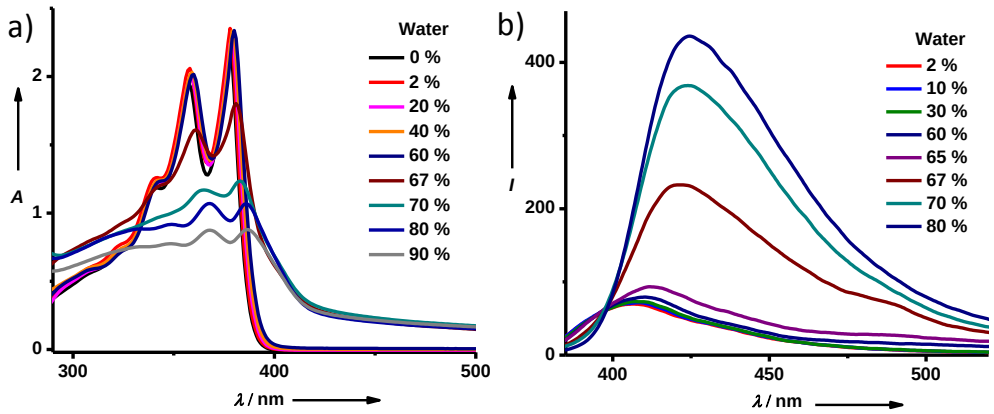


*Figure 3.2.4. Spectroscopic characterization of* ***NDI-Amph*** *self-assembly in incremental percentages of water in THF: a) Absorption spectra showing bathochromic shift and scattering on aggregation; b) Fluorescence spectra ($\lambda_{ex}$ =350 nm) with red-shifted enhanced emission on self-assembly (c=$10^{-4}$ M).*

Luminescent aggregates can result either from J-aggregation of NDIs or from formation of excimers. Excimers are long-lived species and are reported to have an emission maximum of 500 nm in case of **NDI-Amph**,[11] while the former can be proved by selective excitation of the aggregate band (if any) and by lifetime studies, where the aggregate species would have a lifetime comparable to the monomeric species.

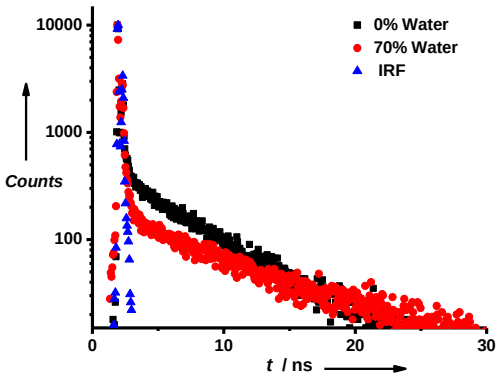


*Figure 3.2.5. The fluorescence lifetime decay profiles of* ***NDI-Amph*** *in the monomeric state (THF) and in the J-aggregated state (water/THF, 70/30, (v/v)), ($\lambda_{ex}$=375 nm) while monitoring the emission at 420 nm, c = 1x$10^{-4}$ M (IRF=Instrument Response Function).*

Fluorescence lifetime measurements carried out on the monomeric species in THF and the aggregated state (water/THF, 70/30, (v/v)) clearly ruled out the presence of excimers (Figure 3.2.5). The lifetime of the monomer was found to be 0.26 ns (95% contribution), while that of the aggregated state was determined to be 0.29 ns (97.6% contribution). This proves that the emissive aggregates are of J-type and there is no excimeric contribution.

### 3.2.3.2. Morphology of NDI-Amph

The morphology of J-aggregates of **NDI-Amph** was investigated through various microscopic techniques, like Transmission Electron Microscopy (TEM) and confocal microscopy, as the aggregates could be visualized easily by virtue of their strong fluorescence. The samples for TEM imaging were prepared by drop-casting a self-assembled solution on copper grid, which was then stained with 1 wt% uranyl acetate in water (negative staining agent) in order to get better contrast. The samples were dried under high vacuum and then imaged.

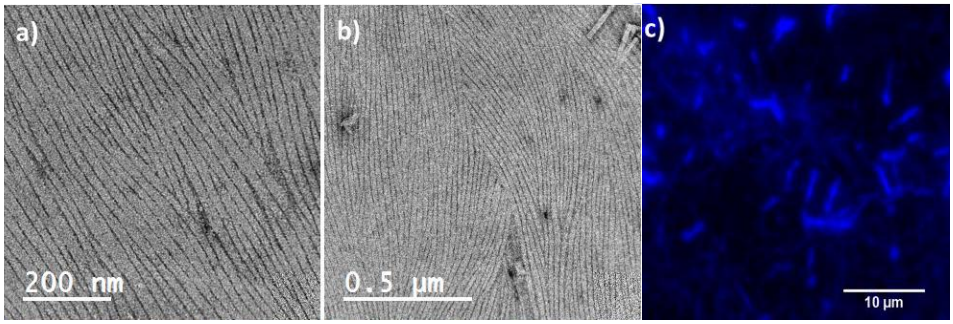


*Figure 3.2.6. Aligned nanofibers formed upon self-assembly of **NDI-Amph** in water/THF, 60/40(v/v), c=$10^{-4}$ M: a), b) TEM images of samples stained with uranyl acetate; c) Confocal image of a self-assembled solution sealed between glass slides; viewed on excitation with 400 nm laser, showing floating 1-D structures in solution.*

Transmission electron microscopy (TEM) imaging of the self-assembled **NDI-Amph** (Water/ THF, 60/40 (v/v)), c = $10^{-4}$ M) showed the formation of nanofibers with an average width of 20 nm and few micrometers long (Figure 3.2.6.a, b). Interestingly, these nanofibers were observed to have high ordering as evident from the observation of aligned self-assembled architectures. To rule out any artifacts resulting from drying effects on substrate, we carried out confocal microscopy investigations, which

unambiguously proved the existence of the fibers in solution. Confocal microscopy measurements, carried out on the solution sealed between glass slides, revealed the presence of free-floating fibers (Figure 3.2.6.c).

## 3.2.4. OFET Device Characteristics

A step ahead, we sought for the construction of an OFET device based on the aligned fibers of **NDI-Amph** as the electroactive layer. The **NDI-Amph** nanofibers exhibited *n*-type transport behaviour. The supramolecular active layer was introduced directly from the solution phase on the dielectric layer forming top-contact, bottom-gated FET structures. Electron mobility ($\mu_{FET}$) of $8.5\times10^{-3}cm^2V^{-1}s^{-1}$ was obtained for **NDI-Amph** fibers with an average mobility of $7.9\times10^{-3}cm^2V^{-1}s^{-1}$ (obtained from a set of 10 devices) and current modulation on/off ratio ≈ $10^3$ (Figure 3.2.7.a, b). These values are comparable to NDIs reported in thin film states,[13] reiterating the reinforced self-assembly by strong amphiphilic interactions.

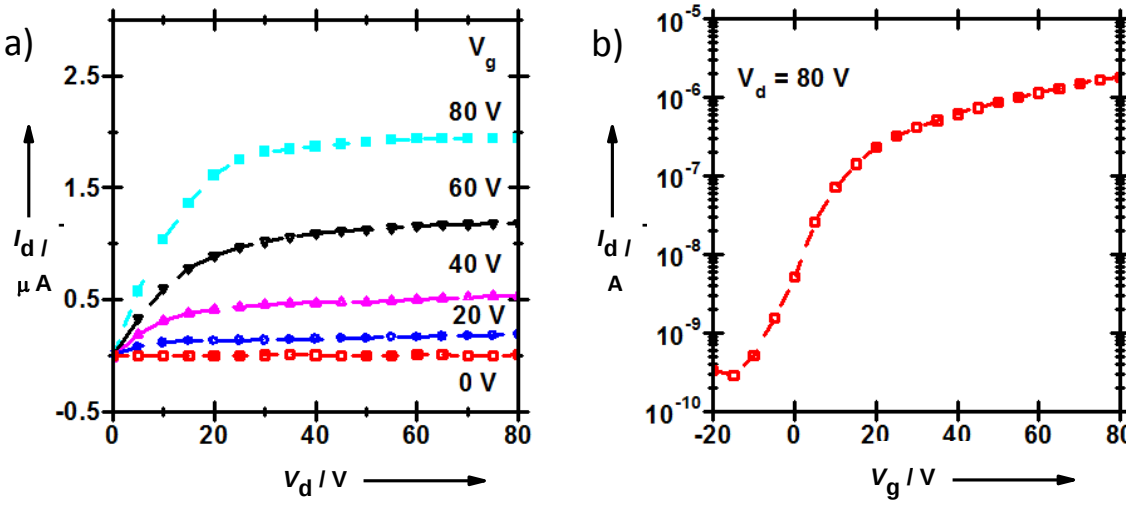


*Figure 3.2.7. OFET device characterization of device made with **NDI-Amph** as the electroactive layer: a) output, and b) transconductance curves in top contact bottom gate FET.*

## 3.2.5. Conclusions

We have thus demonstrated the role of an amphiphilic design in creating higher order structures from naphthalene diimides, by reinforcing the self-assembly by π-stacking interactions and hydrophobicity. The self-assembly was characterized carefully using spectroscopic and microscopic tools. Spectroscopic investigations ascertained the presence of luminescent J-aggregates, which have been unprecedentedly observed in NDI self-assemblies. Aligned nanofibers confirmed through microscopic investigations have been fabricated on OFET device structure that shows high mobility by virtue of an amphiphillic design.

## 3.2.6. Experimental Section

### 3.2.6.1.General Methods

**Transmission Electron Microscopy** (**TEM**): TEM measurements were performed on a JEOL, JEM 3010 operated at 300 kV. Samples were prepared by placing a drop of the solution on carbon coated copper grids followed by drying at room temperature. The images were recorded with an operating voltage 300 kV. In order to get a better contrast, the samples were stained with uranyl acetate (1 wt% in water) before the measurements.

**Confocal Microscopy**: Confocal microscopy imaging was done at room temperature using a Zeiss LSM 510 META laser scanning confocal microscope. The microscope objective of 63X (NA 1.4) and 20X (NA 0.5) were employed. Samples were prepared by sealing the solution between two glass plates.

**Optical Measurements**: Electronic absorption spectra were recorded on a Perkin Elmer Lambda 900 UV-Vis-NIR Spectrometer and emission spectra were recorded on Perkin Elmer Ls 55 Luminescence Spectrometer. UV-Vis and emission spectra were recorded in 10 mm path length cuvettes.

**NMR Measurements**: NMR spectra were obtained with a Bruker AVANCE 400 (400 MHz) Fourier transform NMR spectrometer with chemical shifts reported in parts per million (ppm) with respect to TMS.

**Matrix-assisted laser desorption ionization time-of-flight** (**MALDI-TOF**): MALDI-TOF spectra were obtained on a Brukerultraflex 2 MALDI-TOF mass spectrometer with α-cyano-4-hydroxycinnamic acid matrix.

**Field Effect Mobility Measurements**: Field effect mobility measurements were performed on top contact bottom gate transistor structures.

**Single Photon Counting Spectrometer**: Fluorescence decay was recorded in a time-correlated single-photoncounting spectrometer of Horiba-Jobin Yvon with 350-450 nm picosecond Ti-saphhire laser.

### 3.2.6.2. Synthetic Methods

The starting materials used for synthesizing various compounds were obtained from commercial suppliers. The moisture sensitive reactions were performed under an atmosphere of argon. DMF was dried by distillation under vacuum and dried on 3 Å molecular sieves activated at 180 $^{\circ}$C. Analytical thin layer chromatography was carried out on Merck silica gel 60. Column chromatography was carried out on silica gel (100-200 mesh). Freshly distilled solvents were used for column chromatography. Size exclusion chromatography was done on sephadex polystyrene biobeads S-X3 with chloroform as the eluent.

Proton chemical shifts are reported in ppm downfield from TMS (Tetramethylsilane) using the resonance of the deuterated solvent as internal standard. Splitting patterns are designated as s, singlet; d, doublet; bs, broad singlet; m, multiplet; t, triplet; q, quartet; dd, double doublet; ddd, double double doublet; quin, quintet and br, broad.

### 3.2.6.2.1. Synthetic Schemes

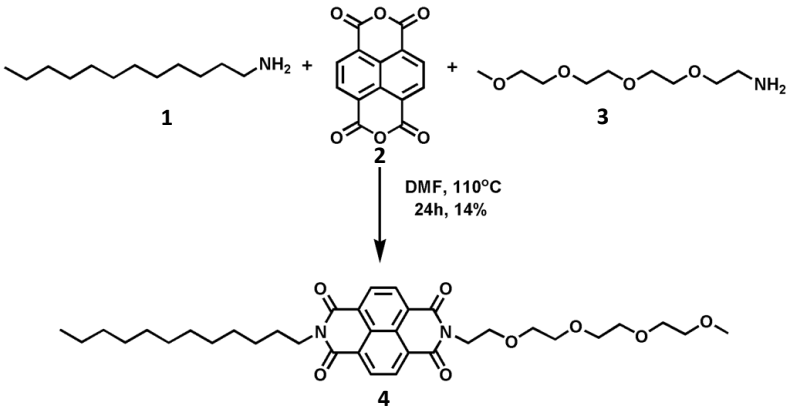


*Scheme 3.2.1. Synthetic Route to **NDI-Amph**.*

### 3.2.6.2.2. Synthetic Procedures

**NDI-Amph**: 0.97 g (3.645 mmol) of 1,4,5,8 naphthalenetetracarboxylicdianhydride (**2**), 0.91 g (4.37 mmol) of monomethoxytetraethylene-glycolamine (**3**) and 0.81 g (4.37 mmoles) of dodecylamine (**1**) were taken in 25 ml DMF and heated at 110 $^{o}$C for 24 h. Upon cooling the reaction mixture DMF was removed under vacuum. The reaction mixture was extracted with $CHCl_3$ / water. Organic layer was dried with anhydrous $Na_2SO_4$ and the solvent was removed under vacuum. Silica gel column chromatography (100-200 mesh, eluent 5-10 % MeOH in $CHCl_3$) gave **NDI-Amph** (0.32 g, 14 % yield) along with Bolaamphiphilic product (0.43 g, 18% yield) and the di-dodecyl derivative.

$^{1}$H NMR (400 MHz, $CDCl_3$, $Me_4Si$): δ (ppm) :8.75 (s, 4H, ArH), 4.45 (t, *J* =6 Hz, 2H, N-$CH_2$ of tetraethyleneglycol {TEG}), 4.18 (t, *J* =7.6 Hz, 4H, N-$CH_2$ of dodecyl), 3.84 (t, *J* =5.6 Hz, 2H, N-$CH_2CH_2$ of TEG), 3.70-3.49 (m, 12H, $CH_2$ of TEG), 3.35 (s, 3H, O-$CH_3$); 1.77-1.25 (m, 20H, $CH_2$ of dodecyl), 0.87 (t, *J* =7 Hz, $CH_3$ of dodecyl); $^{13}$C NMR (100 MHz, $CDCl_3$): δ (ppm): 163.05, 162.95, 131.13, 131.05, 126.93, 126.88, 126.85, 126.71,72.07, S370.76, 70.71, 70.63, 70.29, 67.95, 59.14, 41.16, 39.75, 32.05, 29.77, 29.76, 29.73, 29.66, 29.47, 28.23, 27.24, 22.82, 14.24 ; ESI- MS m/z: 647.55 $[M+Na]^+$, HRMS (ESI) *m/z*: calcd for $C_{35}H_{48}N_2O_8$: 624.3411; found: 625.3490 $[M+H]^+$.

## 3.2.7. References


[1] a) T. Aida, E. W. Meijer, S. I. Stupp, *Science* **2012**, *335*, 813; b) S. S. Babu, S. Prasanthkumar, A. Ajayaghosh, *Angew. Chem. Int. Ed.* **2012**, *51*, 1766; c) A. Ajayaghosh, S. J. George, A. P. H. J. Schenning, *Top. Curr. Chem.* **2005**, *258*, 83; d) F. Würthner, *Chem. Commun.* **2004**, 1564; e) B. – K. An, J. *Gierschner*, S. Y. Park, *Acc. Chem. Res*. **2012**, *45*, 544.

[2] a) R. P. Sijbesma, F. H. Beijer, L. Brunsveld, B. J. B. Folmer, J. H. K. K. Hirschberg, R. F. M. Lange, J. K. L. Lowe, E. W. Meijer, *Science* **1997**, *278* ,160; b) P. G. de Gennes, *J. Chem. Phys*. **1971**, *55*, 572.

[3] J. D. Hartgerink, E. Beniash, S. I. Stupp, *Science* **2001**, *294*, 1684; b) J. D. Hartgerink, E. Beniash, S. I. Stupp, *Proc. Natl. Acad. Sci. U.S.A.* **2002**, *99*, 5133.

[4] a) *Electronic Materials: The Oligomer Approach* (Eds.: K. Müllen, G.Wegner), WILEY-VCH, Weinheim, **1997**; b) b) A. Saeki, Y. Koizumi, T. Aida, S. Seki, *Acc. Chem. Res.* **2012**, *45*, 1193; c) M. Hasegawa, M. Iyoda, *Chem. Soc. Rev*. **2010**, *39*, 2420; c) T. Lei, J. Pei, *J. Mater. Chem*. **2012**, *22*, 785.

[5] a) F. Würthner, *Angew. Chem. Int. Ed.* **2001**, *40*, 1037; b) F. J. M. Hoeben, P. Jonkheijm, E. W. Meijer, A. P. H. J. Schenning, *Chem. Rev*. **2005**, *105*, 1491; c) A. P. H. J. Schenning, E. W. Meijer, *Chem. Commun*. **2005**, 3245; d) A. C. Grimsdale, K. Müllen, *Angew. Chem. Int. Ed.* **2005**, *44*, 5592.

[6] X. Zhan, A. Facchetti, S. Barlow, T. J. Marks, M. A. Ratner, M. R. Wasielewski, S. R. Marder, *Adv. Mater*. **2011**, *23*, 268.

[7] a) L. Zang, Y. Che, J. S. Moore, *Acc. Chem. Res.* **2008**, *41*, 1596; b) S. V. Bhosale, C. H. Jani, S. J. Langford, *Chem. Soc. Rev.* **2008**, *37*, 331.

[8] H. Shao, M. Gao , S. H. Kim , C. P. Jaroniec, J. R. Parquette, *Chem. Eur. J.* **2011**, *17*, 12882.

[9] a) H. Shao, J. Seifert, N. C. Romano, M. Gao, J. J. Helmus, C. P. Jaroniec, D. A. Modarelli, J. R. Parquette, *Angew. Chem. Int. Ed.* **2010**, *49*, 7598; b) H. Shao, T.

Nguyen, N. C. Romano, D. A. Modarelli, J. R. Parquette, *J. Am. Chem. Soc.* **2009**, *131*, 16374.

[10] a) P. Talukdar, G. Bollot, J. Mareda, N. Sakai, Stefan Matile, *J. Am. Chem. Soc*. **2005**, *127*, 6528; b) G. Sforazzini, E. Orentas, A. Bolag, N. Sakai, Stefan Matile, *J. Am. Chem. Soc*. **2013**, *135*, 12082.

[11] M. Kumar, S. J. George, *Chem. Eur. J.* **2011**, *17*, 11102.

[12] R. Voicu, R. Boukherroub, V. Bartzoka, T. Ward, J. T. C. Wojtyk, D. D. M. Wayner, *Langmuir* **2004**, *20*, 11713.

[13] N. B. Kolhe, R. N. Devi, S. P. Senanayak, B. Jancy, K. S. Narayan, S. K. Asha, *J. Mater. Chem.*, **2012**, *22*, 15235.

# Chapter-4

# $C_3$-Symmetric Naphthalene Diimides: Structural Control over Molecular Organization in the Bulk and Self-Assembled States

# Chapter-4

## $C_3$-Symmetric Naphthalene Diimides: Structural Control over Molecular Organization in the Bulk and Self-Assembled States


## *Abstract*

*Tunability of molecular organization by appropriate functionalization of chromophores to obtain desired functions from soft-structures is regarded as one of the assets of self-assembly of π-conjugated chromophores. Control over morphology and organization has been attained in the recent past at the molecular level by synthetic modifications and at the self-assembled stage by post-synthetic non-covalent modifications, such as adding a complementary moiety. In this chapter, detailed investigations of $C_3$-symmetric NDIs are presented, whereby control over molecular organization in the bulk and self-assembled states have been attained through a subtle modification of the spacer connecting the 1,3,5 Benzenetricarboxamide (BTA) core to the Naphthalene diimide chromophores. We have synthesized two molecules,* ***$C_3$-EDA-NDI*** *(with a flexible ethylenediamine spacer) and* ***$C_3$-ben-NDI*** *(with a rigid benzene spacer) and carried out detailed spectroscopic and chiroptical probing in the self-assembled state and calorimetric and phase charaterizations in the bulk state, to firmly establish a structure-property relationship. While* ***$C_3$-EDA-NDI*** *self-organizes into thermotropic liquid crystalline hexagonal arrays,* ***$C_3$-ben-NDI*** *has lamellar packing in the bulk state. On the other hand, despite having multiple chiral handles,* ***$C_3$-EDA-NDI*** *does not show supramolecular chirality in the solution phase while* ***$C_3$-ben-NDI****, by virtue of the rigid aromatic spacer, is efficient in translating the chirality from the periphery to the core, thus giving rise to chiral assemblies with excitonically coupled chromophores. These studies present one of the rarest examples in literature where remarkable differences in the bulk and self-assembled characteristics have been observed in the same multichromophoric system with a very slight modification of spacer.*


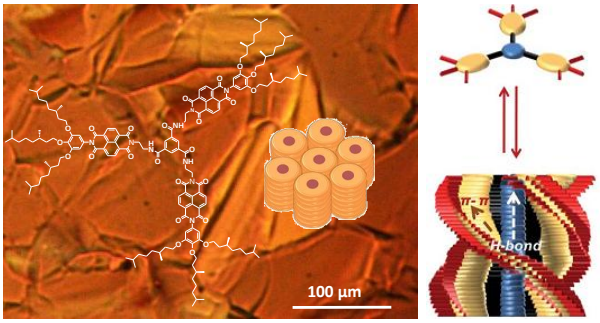


Manuscripts based on this work: B. Narayan, C. Kulkarni, S. J. George, *J. Mater. Chem. C* **2013**, *1*, 626; B. Narayan, K. Swamynathan, S. Kumar, S. J. George (under preparation).

## 4.1. Introduction

Self-assembly of organic π-conjugated systems has emerged as an attractive bottom-up strategy for the design of functional nano-structures, where the optoelectronic properties can be tuned effectively by controlling the molecular organization.[1] Programmed self-assembly, through autonomous interplay of synergistic non-covalent interactions, like π-stacking aromatic interactions, hydrogen-bonds, hydrophobic and van der waals interactions have resulted in the formation of desired morphology for functional applications.[2] In this regard, one-dimensional (1-D) organization of electroactive materials is highly desired for applications in electronic devices through homogeneous, solution-state fabrication of the self-assembled layer. 1,3,5 benzenetricarboxamide (BTA) motif has been extensively used for the design of dynamic, 1-D supramolecular assemblies via directional, three-fold H-bonding interactions.[3] Various *p*-type chromophores have been attached to the BTA core in the past for better understanding of mechanistic aspects governing the self-assembly processes and for materialistic perpectives.

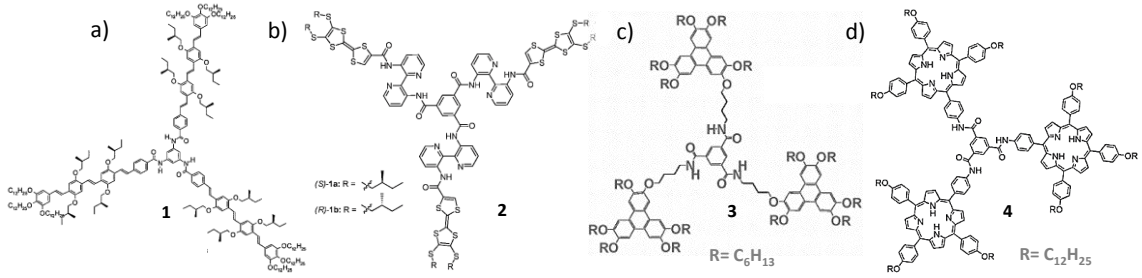


*Figure 4.1. Various BTA based $C_3$-symmetric multichromophoric systems: a) $C_3$-symmetric Oligo(p-phenylenevinylene) (**1**); b) BTA with tetrathiafulvalene units (**2**); c) $C_3$-symmetric triphenylene (**3**) and d) $C_3$-symmetric porphyrin (**4**)..*

A few notable examples are BTA functionalized oligo(*p*-phenylenevinylene),[4] and tetrathiafulvalene[5] that have given insights into the chiral expressions of the self-assembly (Figure 4.1.a, b). On the other hand, BTA functionalized to triphenylenes (Figure 4.1.c)[6] are liquid crystalline, while BTA based porphyrin discs,[7] have been used for creating patterned surfaces used for aligning liquid crystalline materials (Figure 4.1.d). Alkyl functionalized BTA self-assemblies have also resulted in

columnar liquid crystalline mesophases[8] exhibiting remnant polarization in the bulk phase[9] and functional supramolecular polymers in solution.[10]

The cooperative mechanism of self-assembly rendered by virtue of triple helical H-bonded core[11] has resulted in supramolecular self-assembled materials with longer stack lengths. However, the long range order achieved through self-assembly is of the order of 10 to 100 nm. Localized ordering of π-conjugated chromophores also leads to the formation of multidomains in bulk materials. It is always desirable to extend the interchromophoric interactions to 2-D or 3-D ordered materials to improve the fundamental properties of organic semiconductors like exciton diffusion length, electron transport and charge carrier mobility, which is possible in crystalline phase, where the ordering is achieved in micrometre scale dimensions.[12] Achieving a control over ordering of organic chromophores at all length scales ranging from molecules to devices, is thus, a challenge that needs to be addressed.

Liquid crystallinity, also known as the fifth state of matter, besides, solids, liquids, gases, and plasmas, confers long range orientational order comparable to crystalline material and structure tunability comparable to supramolecular assemblies. The localized nanometre scale ordering is extended to macroscopic scale by the monolithic structure of liquid crystalline materials. Since, their discovery in 1977, by S. Chandrasekhar and coworkers, discotics have gained importance as one of the very well-studied class of mesogens.[13] Columnar discotic mesogens[14] well-known in literature are mainly designed from discotic cores (Figure 4.2.a), such as hexa-*peri* hexabenzocoronenes,[15] hat-shaped cyclotriveratrylenes,[16] porphyrins,[17] phthalocyanines,[18] and substituted perylene bisimides, in both oligomeric and when embedded on a polymeric backbone investigated by Thelakkat and coworkers.[19] BTA discs have also emerged as one of the versatile scaffolds for creation of liquid crystalline materials, and have been extensively characterized in recent years.[4]

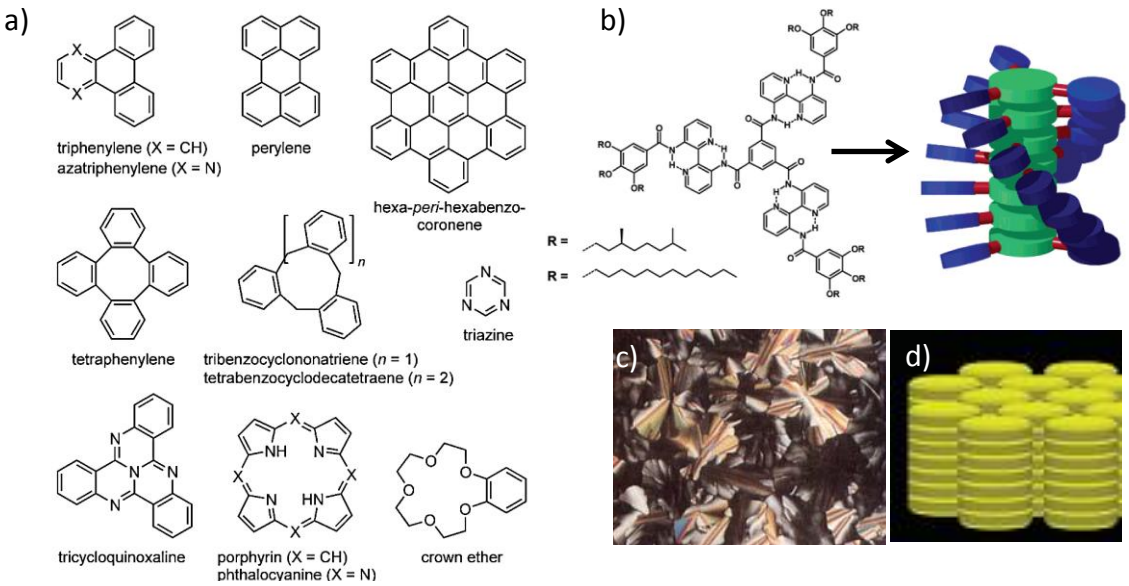


*Figure 4.2. a) Organic π-conjugated cores generally employed for discotic liquid crystals (adapted with permission from ref 14); b) Bipyridine appended big disc of BTA and its schematic organization to form ordered triple helical stacks; c) liquid crystalline texture of the big BTA disc as visualized through Polarized Optical Microscopy (POM), characteristic of $Col_h$ phase; d) Schematic representation of 2-D hexagonal columnar lattices in liquid crystalline BTAs (b, c, d reproduced with permission from reference 8d, 8a and 3a, respectively).*

Columnar assemblies possessing mesoscopic order have been shown to exhibit ferroelectric or antiferroelectric properties, depending on their spatial orientation as in the case of bowl shaped molecules, and have been efficiently employed in organic photovoltaics.[20] The charge carrier mobilities of discotic liquid crystalline HBCs have been investigated by Warman, Müllen and co-workers by non-contact conductivity techniques, such as Pulse Radiolysis-Time Resolved Microwave Conductivity (PR-TRMC), and found to be 0.13 $cm^2V^{-1}s^{-1}$ in the $Col_h$ phase.[21] The effect of substituents on these discotic cores with respect to electronic properties has also been thouroughly investigated. With these results and the observation from few other groups working on the electronic properties of ordered mesophasic discotics, $col_h$ was believed to be one of the best organizations to achieve high charge-carrier mobilities. Recent investigations by the research groups of Yagai and Thelakkat independently have shown the improvement of electon-mobility and charge carrying capacities in lamellar ordering

compared to hexagonal phase in the case of supramolecularly engineered perylene bisimides and covalently functionalized perylene bisimide (PBI) polymers and oligomers in the liquid crystalline phase respectively (Figure 4.3.a, b).[22] While 2-D hexagonal columnar lattices channelize charge-carriers along the stacks, lamellar ordering operates in a 3-D space and thereby, extends the orientational order to the next dimension. Moreover, annealing effects in liquid crystalline PBIs have improved the charge carrier mobility to double the value ($7\times10^{-3}$cm $^2V^{-1}s^{-1}$).[22b] Therefore, lamello-columnar and lamellar ordering are recently believed to be the best organization for superior electronic properties.

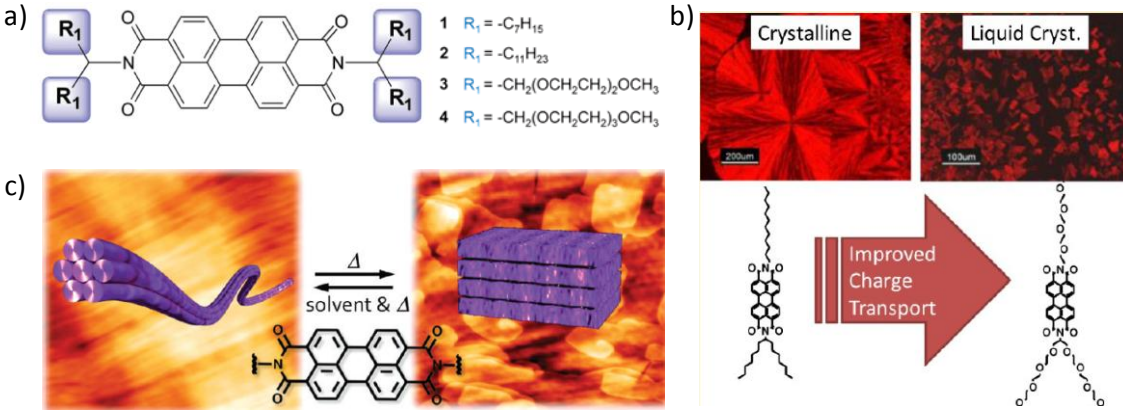


*Figure 4.3. Various studies done on perylene bisimides showing superior electronic properties of lamellar organization compared to hexagonal packing: a) liquid crystalline perylene bisimides obtained by swallow tail substitution of the chromophoric core with various alkyl and alkoxy chains; b) improved charge transport of $col_h$ phase of liquid crystalline perylene bisimide over crystalline perylene bisimide on annealing; c) transformation of hexagonal to lamellar phase having superior electron mobility values than the $col_h$ phase, which can be reversibly attained by heating along with exposure to solvent vapours (Figures a, b, and c reproduced with permissions from reference 22).*

In this chapter, we discuss the results of novel $C_3$-symmetric Naphthalene diimides, with the *n*-type chromophores attached to the BTA core with a slight variation of spacer. While the molecule with the flexible aliphatic spacer (**$C_3$-EDA-NDI**) orients to form 2-D hexagonal columnar lattices, that are liquid crystalline in nature, the $C_3$-symmetric NDI with the rigid aromatic spacer (**$C_3$-ben-NDI**) turns out to

have lamellar ordering in the bulk state. Significant differences in the self-assembled state in solution were also observed by virtue of the nature of the spacer groups. While the molecular chirality was efficiently translated into the supramolecular level in **$C_3$-ben-NDI**, the floppy spacer in **$C_3$-EDA-NDI** was unable to transfer the chirality from the nine peripheral chiral handles to the Naphthalene diimide chromophores. Although various *p*-type chromophores have been attached to the BTA core in the recent past, BTAs bearing well-studied *n*-type chromophores such as arylene diimides remain synthetically challenging and are hitherto unknown.

## 4.2. Design Strategy

The $C_3$-symmetric NDIs consist of 1,3,5 Benzenetricarboxamide (BTA) core, to which three Naphthalene diimides are attached with flexible ethylenediamine (EDA) spacers in **$C_3$-EDA-NDI** and rigid benzene spacers in **$C_3$-ben-NDI** (Figure 4.4). The appended Naphthalene diimides are unsymmetric in nature and bear gallic wedges containing (*S*)-(-)-3,7-dimethyloctyloxy side chains at their periphery, to aid chiroptical probing of the self-assembled states. The syntheses of these molecules are discussed in detail in the synthetic methods section (4.6.2).The gallic wedge (**1**), mono Boc-protected *p*-phenylenediamine (**8**) and mono Boc-protected ethylenediamine (**3**) were synthesized following the literature procedures.[23] The unsymmetrical NDI derivatives for the respective $C_3$-symmetric NDIs were synthesized through statistical reactions of naphthalene tetracarboxylic dianhydride (**2**) with the amines **1** and **8** for **$C_3$-ben-NDI** and amines **1** and **3** for **$C_3$-EDA-NDI**. Deprotection of these unsymmetric NDIs yielded *p*-phenylenediamine substituted and ethylenediamine substituted unsymmetric NDIs respectively, which were then coupled with 1,3,5 benzenetricarbonyl chloride (**6**) to obtain the final $C_3$-symmetric Naphthalenediimdes. The final molecules were fully characterized with various analytical techniques like $^1$H NMR, $^{13}$C NMR, MALDI-TOF and High Resolution Mass Spectrometry (HRMS) (see section 4.6.2. for detailed synthetic procedures and characterization).

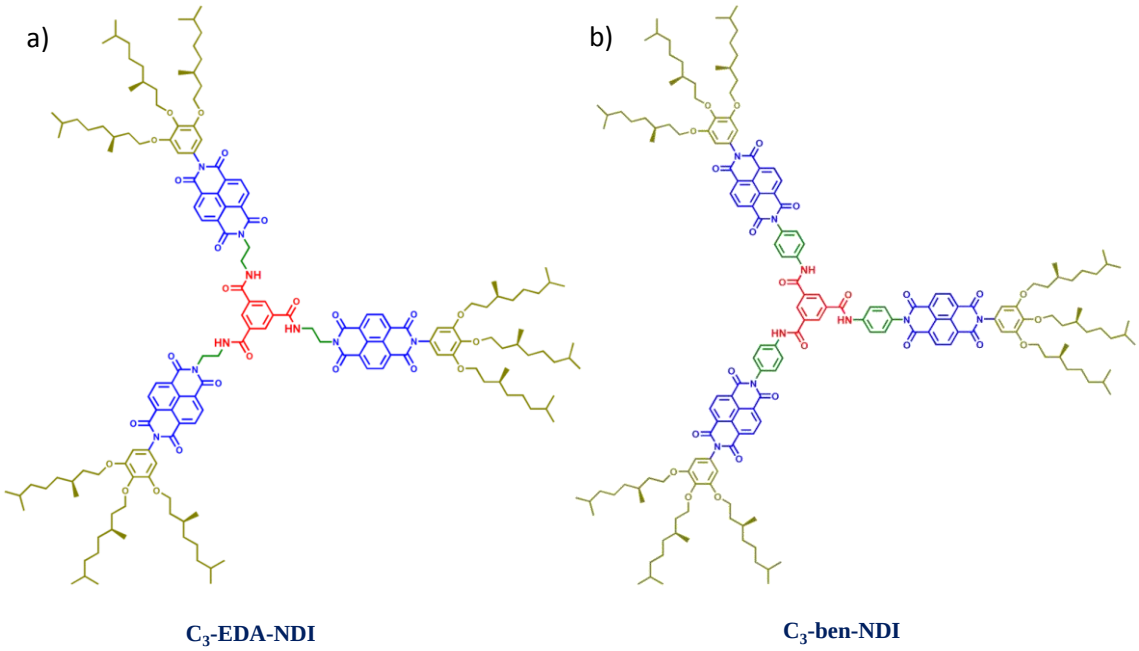


*Figure 4.4. Molecular structures of $C_3$-symmetric Naphthalene Diimides.*

## 4.3. Self-Assembly of $C_3$-Symmetric NDIs in Solution

The self-assembly of **$C_3$-ben-NDI** and **$C_3$-EDA-NDI** occurs in non-polar solvents like methylcyclohexane (MCH) and toluene through synergistic interplay of H-bonds and π-stacking interactions between the chromophores, while the monomeric state is prevalent in solvents of medium polarity like chloroform and 1,1,2,2 tetrachloroethane (TCE). Detailed investigations of the self-assembly process were done through various spectroscopic techniques like FT-IR, NMR, UV-Vis and circular dichroism (CD), light scattering techniques and various microscopic techniques like Field effect scanning electron microscopy (FE-SEM), Transmission Electron Microscopy (TEM) and Atomic Force Microscopy (AFM).

### 4.3.1. Investigation of Hydrogen Bonded Assemblies

The self-assembled state of $C_3$-symmetric NDIs is reinforced by multiple H-bonding by virtue of the BTA core, which is a well-known scaffold to render strong, stable assemblies by triple helical H-bonding in non-polar solvents due to the trisamide functionalities. This property makes the BTA core as an obvious choice in the

construction of 1-D nanowires through directional self-assembly and robust supramolecular materials due to the mechanical rigidity conferred to polymeric materials.[10]

The presence of H-bonding in $C_3$-symmetric NDI assemblies was investigated through $^1$H NMR and solution state FT-IR studies. Concentration dependent $^1$H NMR studies of **$C_3$-EDA-NDI** in $CDCl_3$ in concentrations ranging from $5x10^{-5}$ M to $7.5x10^{-3}$ M clearly showed a 0.49 ppm downfield shift in the chemical shift value of -NH protons with increasing concentrations, which indicates the presence of intermolecular H-bonds in the self-assembled stacks (Figure 4.5a). The presence of π-stacking interactions between NDI cores was also established through concentration dependent NMR. At lower concentrations, the four aromatic protons of NDI appear as a roof quartet which subsequently broadens to merge as a singlet at higher concentrations. This broadening is accompanied by a 0.12 ppm upfield shift in the given concentration range. The aromatic protons of the benzene 1,3,5 tricarboxamide core also experience an upfield shift of 0.16 ppm, suggesting the increasing electron density due to proximity of the molecules attained by the process of self-assembly. Subsequent shifts were also observed in the $–CH_2$ protons of the ethylenediamine spacer. However, neither the aromatic nor the aliphatic protons of the gallic wedge experienced any shift, possibly because it is not greatly affected during the process of H-bonding as it is distant from the trisamide moieties of the BTA core.

Furthermore, we have also employed the -NH shifts in $^1$H NMR as a tool to calculate the association constant which quantifies the strength of intermolecular H-bonding upon self-assembly. The association constant of **$C_3$-EDA-NDI** in $CDCl_3$ was calculated using the following expression (eq. 4.1):

$$\delta = \delta_m + (\delta_a - \delta_m)[1+ (1-\sqrt{8KC_t} + 1)/4KC_t], \text{ [24]} \quad \text{..... (eq. 4.1)}$$

Where $C_t$ is the total concentration, δ is the observed chemical shift, $\delta_a$ is the chemical shift in the self-assembled state, $\delta_m$ is the chemical shift of the monomer, and K is the association constant.

Substituting the values obtained from concentration dependent $^1$H NMR experiment, the association constant for H-bonded assemblies in **$C_3$-EDA-NDI** was determined to be $1.8 \times 10^3$ $M^{-1}$ which is high for this system in a solvent of medium

polarity like $CDCl_3$. The value of association constant may be even higher in non-polar solvents like MCH and toluene. However, similar concentration dependent $^1$H NMR studies could not be performed on **$C_3$-ben-NDI** as they remain H-bonded even in $CDCl_3$ at NMR concentrations. Thereby, no aromatic signals were visible when a $^1$H NMR was done on a solution of **$C_3$-ben-NDI** in $CDCl_3$. However, all aromatic signals appeared on addition of trifluoroacetic acid (TFA) which acts as H-bond acceptor and thus, breaks intermolecular H-bonds in the self-assembled stacks (Figure 4.5.b).

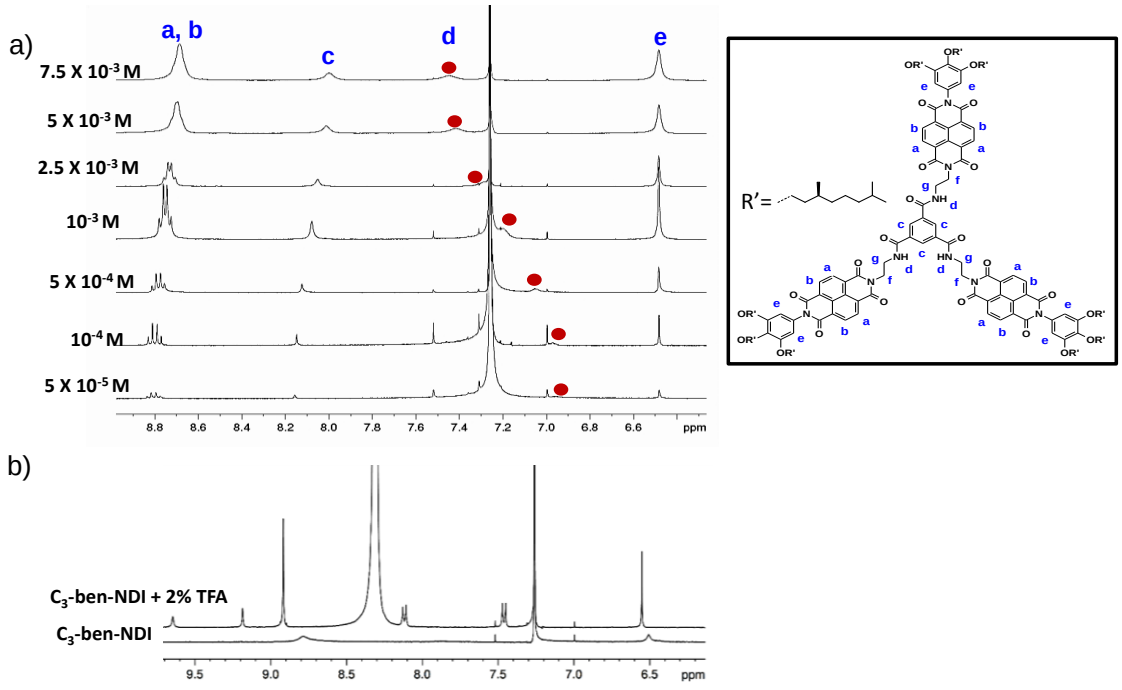


*Figure 4.5. $^1$H NMR investigations of H-bonding in $C_3$-NDI self-assembled systems: a) concentration dependent $^1$H NMR spectra of **$C_3$-EDA-NDI** ($CDCl_3$) stacked over each other, showing the shifts in the respective protons as marked in the molecular structure (inset) as a result of H-bonding (red dots are inserted in the spectra to guide the eye); b) $^1$H NMR spectra of **$C_3$-ben-NDI** ($CDCl_3$) showing the emergence of signals on addition of trifluoroacetic acid (TFA), which acts as a H-bond donor to break the intermolecular H-bonds.*

The spectroscopic evidence of the presence of H-bonds in self-assembled solutions of **$C_3$-ben-NDI** was obtained from solution state FT-IR studies (Figure 4.6). A $10^{-3}$ M solution of **$C_3$-ben-NDI** showed amide I band at 3303 $cm^{-1}$. Additionally, the C=O stretch appeared at 1675 $cm^{-1}$ which was at a much lower wavenumber as compared to

the C=O stretch for non H-bonded state in TCE (1710 $cm^{-1}$). Similar observations were made for solutions of **$C_3$-EDA-NDI**. While the -NH stretch vibrations could not be easily differentiated, there was a significant shift in the C=O stretch. A $10^{-3}$ M solution in TCE showed C=O stretch at 1731 $cm^{-1}$ whereas a MCH solution showed it at 1664 $cm^{-1}$.

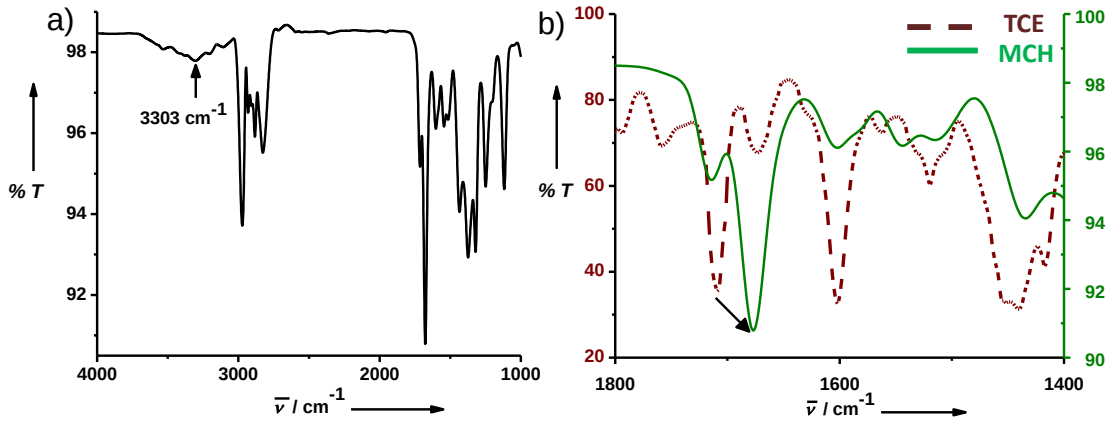


*Figure 4.6. FT-IR spectra of **$C_3$-ben-NDI** ($10^{-3}$ M) in solution phase as a proof of intermolecular hydrogen bonding: a) IR spectrum in MCH and b) Comparative solution state IR spectra in TCE and MCH showing the differences in the C=O stretch.*

## 4.3.2. Gelation Studies

The self-assembly of **$C_3$-ben-NDI** and **$C_3$-EDA-NDI** in non-polar solvents like methylcyclohexane and toluene were clearly evident through the formation of gels in these solvents at higher concentrations. The gels were made by suspending a weighed amount of the molecules in an increased percentage of nonpolar solvent like MCH and toluene in TCE which was then heated and subsequently sonicated to ensure homogeneous solvation and rigidification to form gels. The Critical Gelator concentrations (CGCs) obtained for these systems in the respective solvent systems are listed in table 4.1.

**$C_3$-ben-NDI** acts as a better gelator in nonpolar solvents than **$C_3$-EDA-NDI**, as concluded from the CGC value. This may be due to the rigid benzene spacer that leads to stronger H-bonding in the assemblies.

| Molecule | MCH/TCE, 90/10, (v/v) | Toluene/TCE, 90/10, (v/v) | Toluene |
|---|---|---|---|
| **$C_3$-EDA-NDI** | 3.8 mM | 3.6 mM | 3.5 mM |
| **$C_3$-ben-NDI** | 3.6 mM | 2.8 mM | 1.6 mM |

*Table 4.1. Critical Gelator Concentrations (CGCs) of **$C_3$-EDA-NDI** and **$C_3$-ben-NDI** in various solvent compositions.*

### 4.3.3. Photophysical Studies

To get insights into the self-assembly of $C_3$-symmetric NDIs in solution, detailed spectroscopic probing has been performed through UV-Vis and circular dichroism (CD) techniques in the solution phase. While **$C_3$-ben-NDI** ($c = 10^{-5}$ M) exists in a molecularly dissolved state in 100% TCE, as evident from the characteristic NDI absorption features and the absence of a CD signal, it self- assembles in non-polar solvents like MCH and toluene (Figure 4.7.a). This is evident from the changes in absorption spectra with increasing percentages of toluene in toluene–TCE solvent mixtures, which showed a gradual decrease in the absorbance of NDI at 358 and 378 nm, with concomitant increase in the blue-shifted absorption at 344 nm, characteristic of the H-aggregates of NDI chromophores. The self-assembly of chromophores is further marked by the appearance of a bisignated cotton effect with negative and positive maxima at 367 nm and 340 nm respectively (Figure 4.7.b). This indicates the presence of excitonically coupled helically ordered chromophores, with transfer of chirality from the peripheral side chains to the chromophore. Surprisingly, **$C_3$-EDA-NDI** forms CD silent assemblies, even in 100% MCH and toluene at high concentrations of $10^{-4}$ M, despite having nine chiral handles attached to the molecule, similar to **$C_3$-ben-NDI** to confer supramolecular chirality to the self-assembled stacks (Figure 4.7.d). We attribute this difference originating from the flexible ethylenediamine spacers which are not efficient in translating the chirality of the multiple side chains into ordered supramolecular helices in comparison with rigid benzene spacers in **$C_3$-ben-NDI**. However, the self-assembled state of **$C_3$-EDA-NDI** was ascertained from the changes in absorption spectral features, as a gradual decrease

in the absorption intensity occurred at 360 nm and 381 nm respectively, along with reversal of relative band ratios and broadening of absorption (Figure 4.7.c).

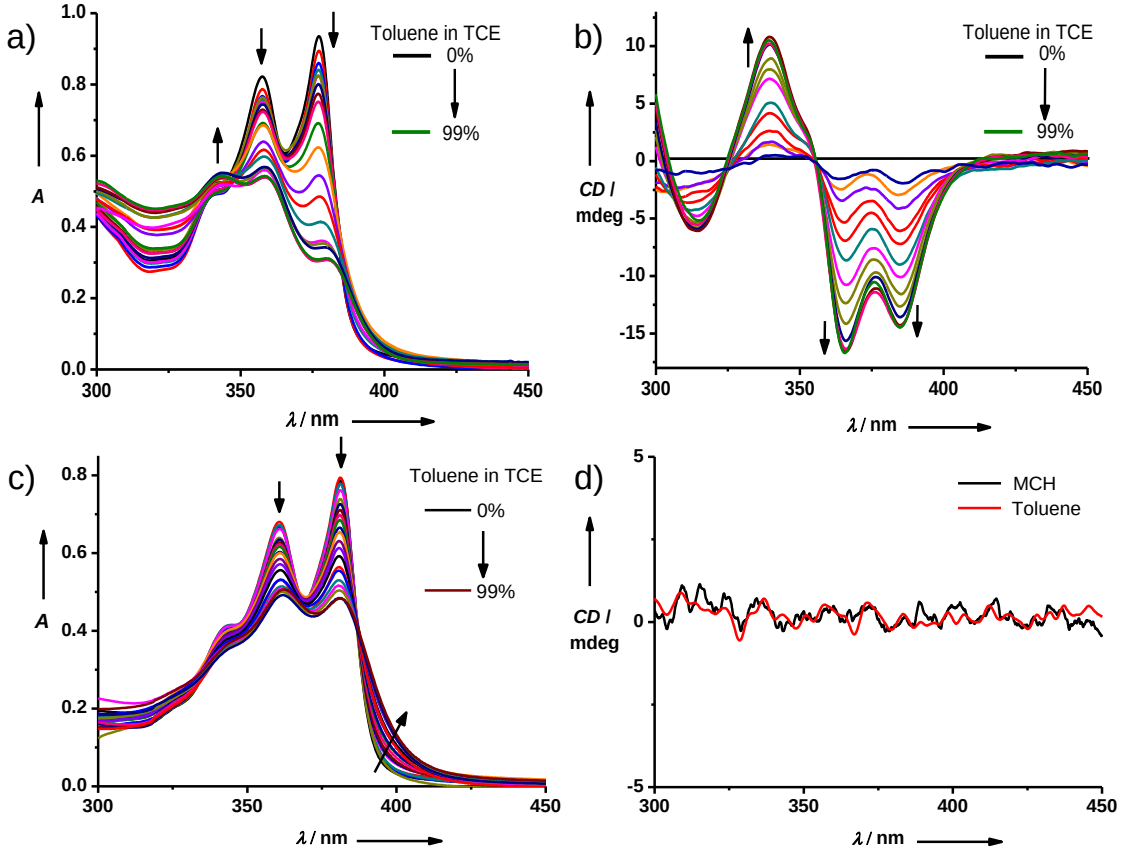


*Figure 4.7. Optical properties of $C_3$-NDI systems in toluene–TCE solvent mixtures illustrating the differences in the self-assembled features due to subtle change in the nature of spacer: a) absorption and b) CD spectra of* ***$C_3$-ben-NDI*** *($c=10^{-5}$ M); c) absorption spectra of* ***$C_3$-EDA-NDI*** *showing broadening of absorption features as a result of self-assembly ($c=10^{-5}$ M); d) CD silent self-assembled phase in* ***$C_3$-EDA-NDI*** *in MCH and toluene ($c=10^{-4}$ M).*

These molecules are weakly fluorescent in nature, even in the molecularly dissolved states, probably due to the photo-induced electron transfer from the electron rich gallic wedge to the NDI core.[25]

## 4.3.4. Morphology and Molecular Packing

To get insights into the morphology of the self-assembled nanostructures, detailed microscopic studies have been performed on $C_3$-NDI systems ($10^{-4}$ M) in a toluene/TCE, 90/10, (v /v) solvent mixture. Various microscopic techniques like Field effect Scanning electron microscopy (FE-SEM), Transmission Electron Microscopy (TEM) and Atomic Force Microscopy (AFM) were employed.

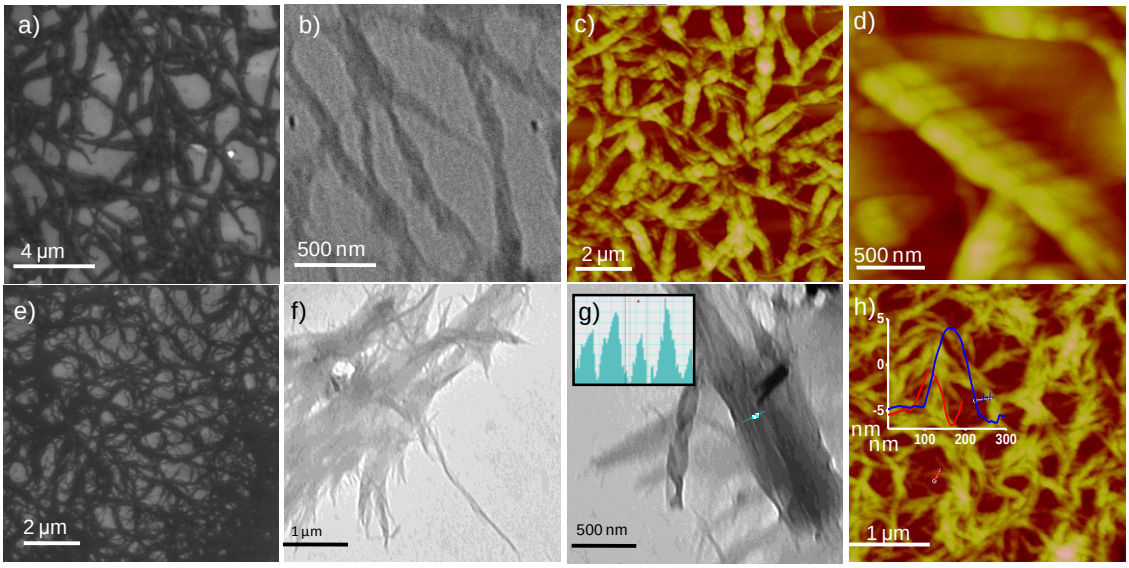


*Figure 4.8. Morphologies of $C_3$-symmetric NDIs (toluene/TCE, 90/10, (v /v), c=$10^{-4}$ M unless mentioned). a) FE-SEM; b) TEM (c = $5x10^{-5}$ M); c), d) tapping mode AFM images respectively of* ***$C_3$-ben-NDI*** *showing helically coiled, bundled fibers; e) FE-SEM; f), g) TEM ($5x10^{-5}$ M) that show majorly straight fibers and h) AFM (c = $5x10^{-5}$ M) respectively of* ***$C_3$-EDA-NDI.*** *The insets of TEM images and AFM images show molecular level dimensions from electron density analysis and height analysis respectively.*

FE-SEM of drop-casted self-assembled solutions on a glass substrate revealed the formation of fibrillar morphology (Figure 4.8.a). TEM of dilute ($5x10^{-5}$ M) drop-casts of **$C_3$-ben-NDI** showed the transfer of chirality at a hierarchial level (Figure 4.8.b). Several bundles of fibers having *M*-type helicity were seen uniformly throughout the sample. However, in the case of **$C_3$-EDA-NDI** the fiber bundles were majorly straight. An electron density analysis of these straight isolated fibers revealed

uniform periodicity of 4.6 nm which is again very close to the discotic diameter (Figure 4.8.f, g). AFM on the drop-casted solutions revealed bundles of fibers along with isolated ones. Left handed helices that were 5-6 µm long and 200 nm wide were observed throughout the sample in the case of **$C_3$-ben-NDI**, where the supramolecular chirality was expressed even in the morphological nanostructures (Figure 4.8.c, d). The average heights obtained from analysis of the tapping mode AFM images correlated well with the diameters of the discotic architectures. The heights were determined to be 5.2 nm in the case of **$C_3$-EDA- NDI** (Figure 4.8.h) and 5.1 nm in the case of **$C_3$-ben-NDI,** respectively. The calculated molecular diameters of these molecules were 5.6 nm and 5.5 nm, respectively.

To rule out the possibility of artifacts arising from drying effects of the solutions on glass substrate, Dynamic Light Scattering (DLS) studies were done. An average hydrodynamic radius of 5-6 µm was obtained through these studies which correlated well with the length of the aggregates obtained from microscopic measurements (Figure 4.9). This proved that the fibrous nano-structures were indeed formed in the solution state during the self-assembly process.

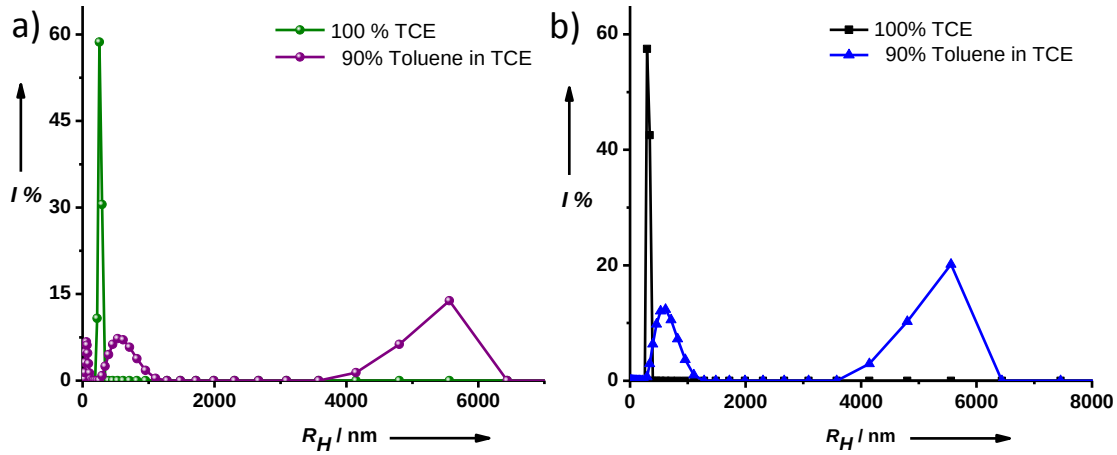


*Figure 4.9. Dynamic light scattering (DLS) studies of a) **$C_3$-ben-NDI** and b) **$C_3$-EDA-NDI** ($10^{-4}$ M) in TCE and toluene/TCE, 90/10, (v /v) solvent mixtures.*

The molecular packing in the self-assembled structures was investigated through low angle X-ray diffraction (XRD) studies. Uniform XRD films prepared on glass substrates by smearing the drop-casted gel samples showed the formation of lamellar structures in both the $C_3$-symmetric NDIs (Figure 4.10.a, b). The d-spacing

obtained in the low angle region in the case of **$C_3$-ben-NDI** was 4.4 nm which was less than the calculated molecular diameter (5.6 nm), suggesting tilting of the discs in the arrangement. A peak suggesting lamellar packing was observed at $2\theta = 5.1^{o}$ (d-spacing = 8.8 nm).

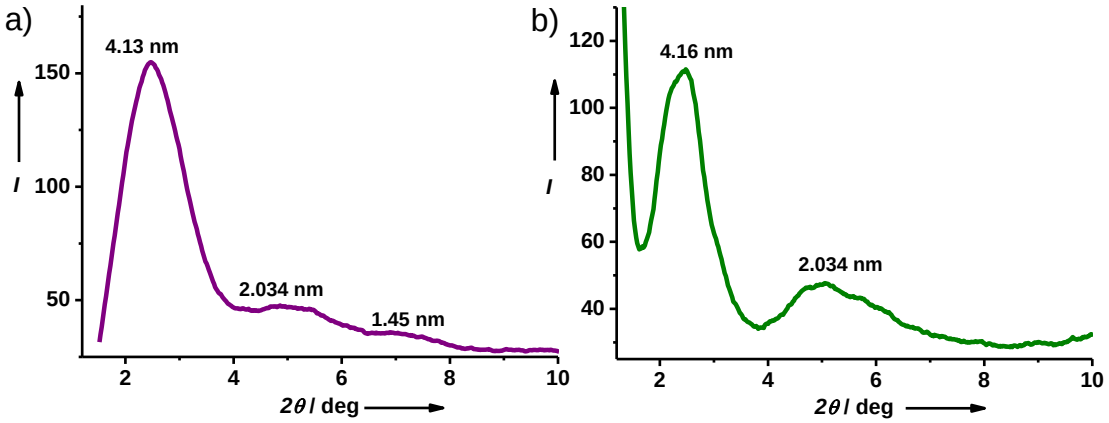


*Figure 4.10. Low angle XRD of gels of a) **$C_3$-EDA-NDI** and b) **$C_3$-ben-NDI** showing lamellar packing in the self-assembled state (glass substrate).*

## 4.3.5. Mechanistic Investigations

Mechanistic insights into the processes governing the self-assembly of monomers to supramolecular helices would enable us to rationalize the molecular features and intermolecular interactions that favor a particular path of self-assembly. Investigations of mechanisms in BTA based self-assembled systems have been extensively carried out by Meijer and coworkers, mainly through temperature dependent measurements.[26]

However, temperature dependent absorption and CD studies of $C_3$-NDI systems further showed that the disassembly could not occur even at 99 $^{o}$C, reiterating the stability of the assemblies due to strong intermolecular interactions arising from synergistic π-stacking and H-bonding (Figure 4.11.a). Therefore, probing the temperature induced spectroscopic changes was not suitable in the present systems, as a molecularly dissolved state could not be achieved. It has been recently shown that, not only temperature dependent measurements but also volume fraction of the solvent system, containing a good and a poor solvent used for self-assembly, can be used as a probe for mechanistic studies.[27] This approach was undertaken in the present studies to

understand the mechanism of self-assembly, resulting in a clear sigmoidal curve for **$C_3$-ben-NDI** when both the CD intensity at 365 nm and the optical density at 378 nm were plotted against the varying compositions of toluene in TCE, suggesting an isodesmic mechanism (Figure 4.11.b, c).

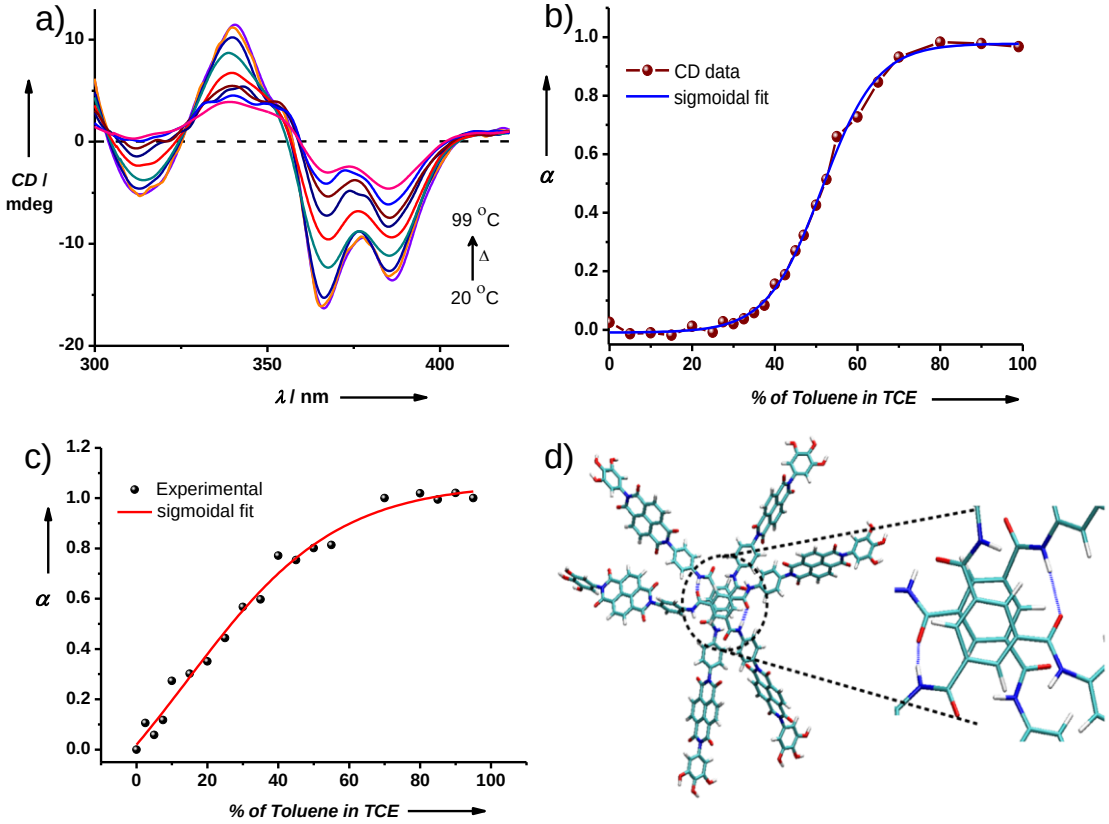


*Figure 4.11. Proof of isodesmic mechanism in **$C_3$-ben-NDI** and **$C_3$-EDA-NDI**: a) Temperature dependent CD spectra of **$C_3$-ben-NDI** in 80% toluene in TCE demonstrating rigid assemblies; b) plot of fraction of aggregation (α) versus the solvent composition obtained by plotting the CD intensity at 365 nm and corresponding fit to a sigmoidal function; c) plot of fraction of aggregation (α) versus the solvent composition obtained by plotting the absorbance at 400 nm and corresponding fit to a sigmoidal function showing isodesmic mechanism of self-assembly in **$C_3$-EDA-NDI**; d) The optimized geometry of the dimer of a **$C_3$-ben-NDI** analogue (alkoxy chains are replaced with hydroxy groups) calculated using the HF/6-31G level of theory.*

### 4.3.6. Theoretical Insights into Isodesmic Mechanism

Self-assembled systems based on BTA core are generally observed to follow cooperative mechanism of self-assembly.[3b] However, another BTA bearing OPV units is shown to follow an isodesmic mechanism of self-assembly.[4] The cooperativity in BTAs is explained through the presence of directional three-fold helical hydrogen bonding. To obtain more insights into the observed isodesmic mechanism of self-assembly in $C_3$-NDI systems, quantum chemical calculations were carried out at the HF/6-31G level of theory on **$C_3$-ben-NDI**. In order to reduce the computational cost, the peripheral alkoxy groups were replaced by hydroxy groups in the calculations. The dihedral angle between the benzene spacer and the central benzene ring in an optimized structure of monomer was found close to 20° (Figure 4.11.d). In the case of a dimer, this dihedral angle was found to vary from 30 to 48°, indicating the varied extent of rotations between the benzene core and the benzene spacer. Although, intermolecular hydrogen bonds were observed between the central amide groups in the dimer, all of them were not directed in the same direction. In fact, hydrogen bonds directed in the opposite direction were observed. This suggests that the presence of the benzene spacer along with the NDI moiety plays a key role in determining the conformation of the amide bonds. A previous report has also shown the effect of amide connectivity on the self-assembly of BTA.[28] The isodesmic mechanism of self-assembly observed in a **$C_3$-ben-NDI** system might be due to the lack of directional hydrogen bonds (as observed for the dimer in our calculations); this needs further study with more accurate theoretical methods.

## 4.4. Bulk State Investigations

The $C_3$-symmetric NDIs show remarkable differences in the bulk state organization due to the differences in the spacers connecting the NDI chromophore to the BTA core. Extensive characterization of the bulk state was carried out through calorimetric and microscopic techniques like Differential Scanning Calorimetry (DSC) and Polarizing Optical Microscopy (POM) that showed thermotropic phase transitions, which were then characterized through variable temperature XRD in the low angle region.

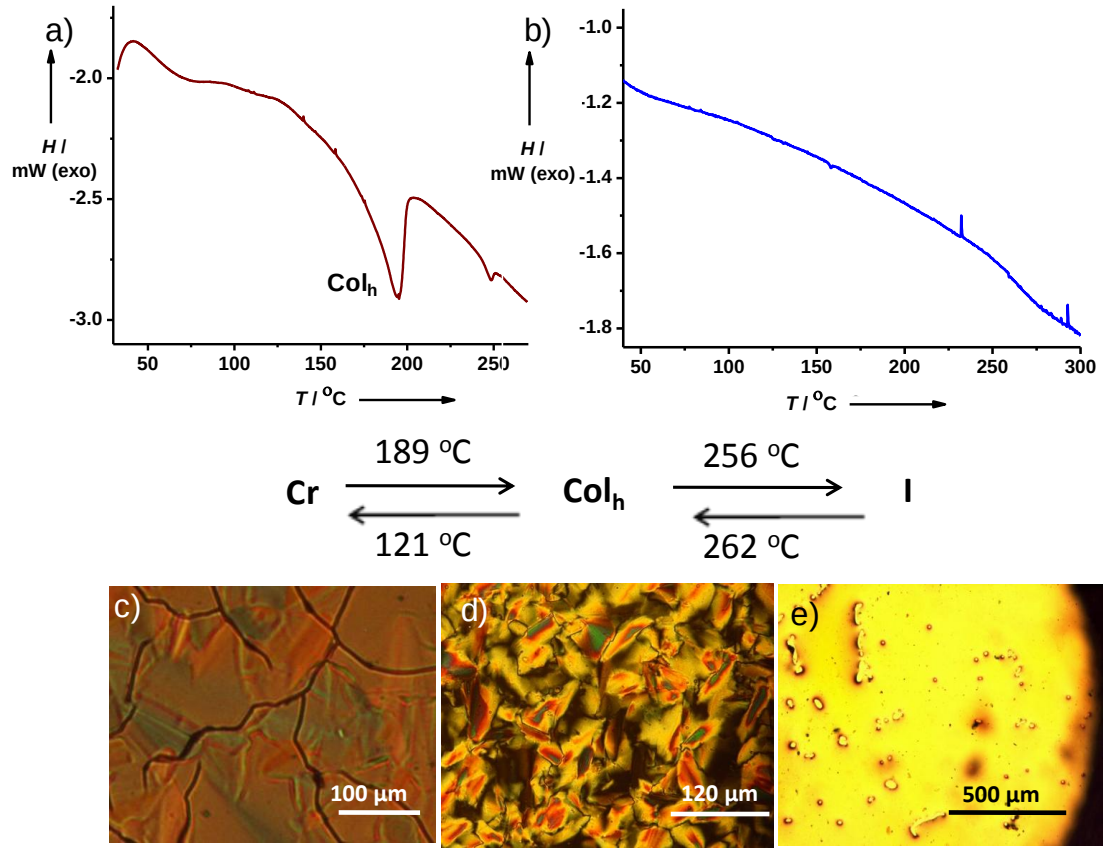


*Figure 4.12. Bulk state properties of $C_3$-NDIs: a) Differential scanning calorimetry (DSC) traces (dT/dt=5°C/min) of* ***$C_3$-EDA-NDI*** *showing endothermic transitions corresponding to liquid crystalline mesophase and melting respectively; b) DSC traces (dT/dt=5°C/min) of* ***$C_3$-ben-NDI*** *showing no significant endothermic transitions except a broad melting transition at 256 °C; c)-e) Polarizing optical microscope images of* ***$C_3$-EDA-NDI*** *showing crystalline to isotropic state with an intermediate liquid crystalline phase, with schematic arrow diagram of the phase transition on top of the images.*

DSC of a dried, powdered sample of **$C_3$-EDA-NDI** carried out over various cycles of heating and cooling with a temperature ramp of dT/dt=5 °C/min, revealed a thermotropic phase transition in a broad temperature range of 126 °C to 210 °C, followed by the transition to the isotropic melt at 256 °C (Figure 4.12.a). To ascertain the liquid crystalline nature of the phase transition, Polarized Optical Microscopy (POM) was carried out in which a dried, powdered sample of **$C_3$-EDA-NDI** was mounted on a coverslip and placed on a heating stage with a continuous flush of nitrogen and was viewed between cross polarizers. The heating and cooling rates were

maintained at 5 °C/min. The liquid crystalline (LC) phase was marked by the formation of a birefringent focal conical structure, which is identical to the texture of hexagonal columnar phase in observed for liquid crystalline discotic molecules (Figure 4.12.d).

To unambiguously assign the ordering adopted by **$C_3$-EDA-NDI** in the LC phase, detailed variable temperature low angle XRD measurements were carried out. The d-spacings obtained at 190 $^oC$ (LC temperature) were 3.9 nm, 2.2 nm and 1.8 nm which were in good correlation with relative d-spacing ratios of 1: 1/√3: 1/2 seen in hexagonal columnar ordering (Figure 4.13.a). The low angle peak at 3.9 nm corresponded to diameter of the molecular discotic in which the disks are tilted in the ordered structure.

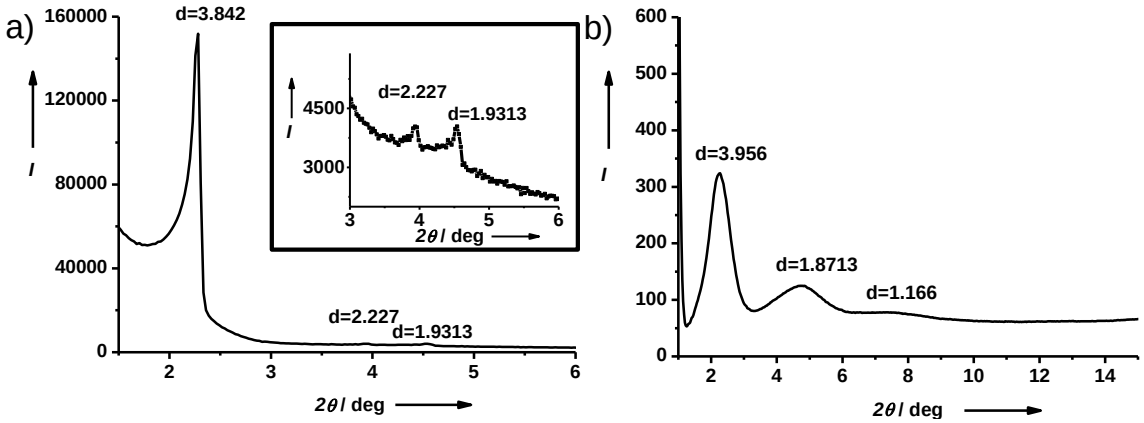


*Figure 4.13. Low angle XRD characterizations of the bulk states of $C_3$-NDI systems: a) XRD of **$C_3$-EDA-NDI** at 190 $^oC$ showing hexagonal columnar packing in the liquid crystalline phase, b) Low angle XRD of the bulk state of **$C_3$-ben-NDI** showing lamellar packing (the d values are in nm .*

However, **$C_3$-ben-NDI** did not show any phase transition on heating as the DSC curve revealed no endothermic transitions except a clear melting at 256 $^oC$ (Figure 4.12.b). Low angle XRD on the powder state of **$C_3$-ben-NDI**, surprisingly, showed that the molecules are arranged in a lamellar fashion which is very distinct from the results obtained in the case of **$C_3$-EDA-NDI** (Figure 4.13.b). The difference in the ordering of the bulk state is remarkable as two different organizations are obtained from two

molecules with essentially the same framework but a subtle difference in the nature of the spacer.

## 4.5. Conclusions

We have thus, presented here a case study of $C_3$-symmetric NDIs which possess remarkable differences in the organization in the bulk state and self-assembled characteristics by virtue of the nature of the spacer connecting the NDI chromophore to the BTA core. Detailed spectroscopic investigations through UV-Vis and CD have given insights into the supramolecular self-assemblies of these systems. The mechanism of self-assembly has also been probed through a solvent composition study, which has been further rationalized through quantum chemical calculations. Bulk state properties have been reported through detailed characterization through DSC, POM and XRD. As the two molecules have different modes of packing, we thus, expect a difference in the mobility values of the bulk state. Therefore, effect of molecular organization on the electronic property would be worth investigating.

## 4.6. Experimental Section

### 4.6.1. General Methods

**NMR Measurements**: NMR spectra were recorded with a Bruker AVANCE 400 (400 MHz) Fourier transform NMR spectrometer with chemical shifts reported in parts per million (ppm) with respect to TMS. Splitting patterns are designated as s, singlet; d, doublet; t, triplet; m, multiplet.

**FT-IR Measurements**: Solution state IR measurements were performed on a Perkin-Elmer Spectrum GX series with a resolution of 4 $cm^{-1}$. Caesium Fluoride cells with a spacer of 2 mm were used. The solutions for the IR measurements were prepared in Tetrachloroethane (TCE) and Methylcyclohexane (MCH) which were gently warmed and sonicated for making the solutions homogeneous and clear. Solid state Infrared spectra were recorded using a Bruker IFS 66 v/S spectrometer. The samples were prepared by using KBr pellets made by using KBr from local commercial suppliers.

**Optical Measurements**: Electronic absorption spectra were recorded on a Perkin Elmer Lambda 900 UV-Vis-NIR Spectrometer. Circular Dichroism (CD) spectra and temperature dependent UV-Vis spectra were recorded on a Jasco J-815 spectrometer where the sensitivity, time constant and scan rate were chosen appropriately. The temperature dependent measurements were performed with a CDF-426S/15 Peltier-type temperature controller with a temperature range of 263-383 K and adjustable temperature slope.

**Dynamic light scattering Experiments** (**DLS**): The measurements were carried out using a Nano ZS (Malvern UK) employing a 532 nm laser at a back scattering angle of $173^o$. The samples were measured in a 10 mm glass cuvette.

**Atomic Force Microscopy** (**AFM**): AFM measurements were performed on a Veeco diInnova SPM operating in tapping mode regime. Micro-fabricated silicon cantilever tips doped with phosphorus and with a frequency between 235 and 278 kHz and a spring constant of 20-40 $Nm^{-1}$ were used. The samples were prepared by drop-casting solutions of $C_3$-symmetric NDIs on glass substrates and dried under high vacuum at room temperature.

**Field Emission Scanning Electron Microscopy** (**FE-SEM**): FE-SEM measurements were performed on a NOVA NANO SEM 600 (FEI) by drop casting the solutions on glass substrate followed by drying under high vacuum at room temperature and was operated with an accelerating voltage of 5 kV.

**Transmission Electron Microscopy** (**TEM**): TEM measurements were performed on a JEOL, JEM 3010 operated at 300 kV. Samples were prepared by placing a drop of the solution on carbon coated copper grids followed by drying at room temperature. The images were recorded with an operating voltage of 300 kV. In order to get a better contrast, the samples were stained with uranyl acetate (1 wt% in water) before the measurements.

**XRD Measurements**: Small angle XRD patterns were recorded in Siefert XRD instrument using Cobalt (Co) source ($\theta = 0.4^o – 60^o$).

**Matrix-assisted laser desorption ionization time-of-flight** (**MALDI-TOF**): MALDI-TOF spectra were obtained on a Brukerdaltonics autoflex (ST- A2130) MALDI- TOF mass spectrometer with α-cyano-4-hydroxycinnamic acid matrix in reflector mode.

**Polarizing Optical Microscopy** (**POM**): The POM measurements were carried out on a Olympus BX-51 instrument. The sample was placed on a cover slip and put on a heating stage with continuous flow of nitrogen.

**Differential Scanning Calorimetry** (**DSC**): the DSC measurements were performed on Mettler-Toledo DSC-1 instrument. Three cycles (two heating and one cooling) were done to arrive at conclusions. The heating rate was maintained at 5 $^{o}$C/min

**Molecular Modelling Calculations**: Geometry optimizations were carried out at HF/6-31G level of theory using Gaussian- 09 suite of programs.[29] The molecules were visualized using Visual Molecular Dynamics.[30]

### 4.6.2. Synthetic Methods

The starting materials used for synthesizing various compounds were obtained from commercial suppliers. The moisture sensitive reactions were performed under an atmosphere of argon. DMF was dried by distillation under vacuum and dried on 3 Å molecular sieves activated at 180 $^{o}$C. Dry Dichloromethane (DCM) was prepared fresh by distilling DCM , pouring it on activated molecular sieves and keeping it undisturbed overnight. Analytical thin layer chromatography was carried out on Merck silica gel 60. Column chromatography was carried out on silica gel (100-200 mesh). Size exclusion chromatography was done on sephadex polystyrene biobeads S-X3 with chloroform as the eluent.

Proton chemical shifts are reported in ppm downfield from TMS (Tetramethylsilane) using the resonance of the deuterated solvent as internal standard. Splitting patterns are designated as s, singlet; d, doublet; bs, broad singlet; m, multiplet; t, triplet; q, quartet; dd, double doublet; ddd, double double doublet; quin, quintet and br, broad.

### 4.6.2.1. Synthetic Schemes

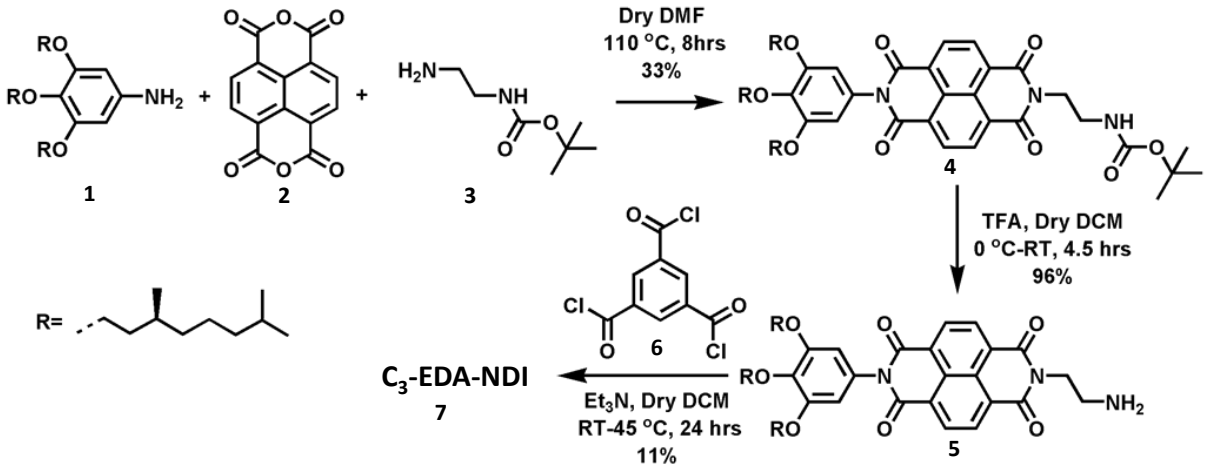


*Scheme 4.1. Synthetic scheme for* ***$C_3$-EDA-NDI****.*

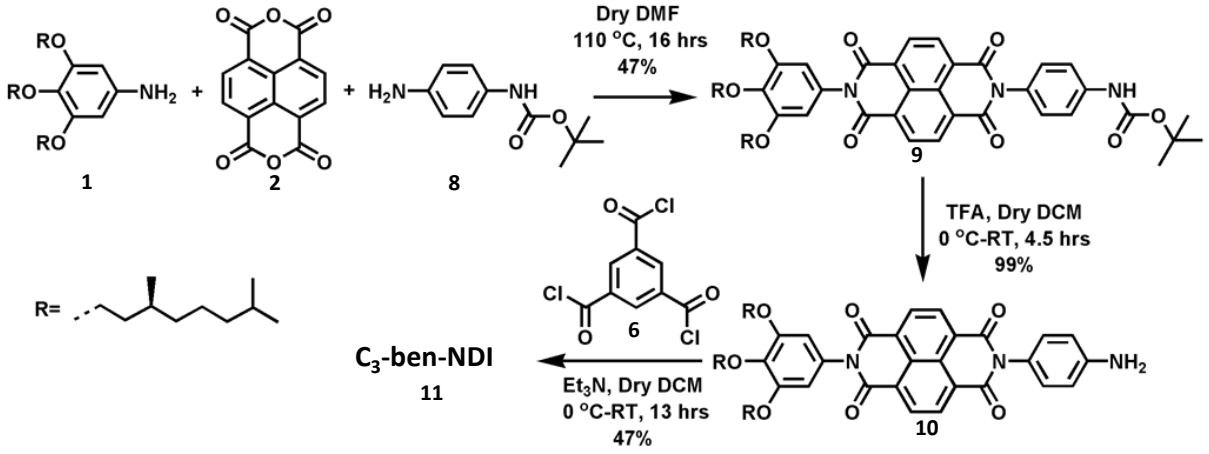


*Scheme 4.2. Synthetic route to* ***$C_3$-ben-NDI****.*

### 4.6.2.2. Synthetic Procedures

Compounds **1** and **3** were synthesized according to methods reported in literature.[23]

Unsymmetric Naphthalene diimide Derivative (**4**). 2.4 g (4.28 mmol) of **1** and 0.686 g (4.28 mmol) of **3** were mixed with 1, 4, 5, 8-Naphthalenetetracarboxylic dianhydride (**2**) (1.096 g, 4.09 mmoles) in 24 ml of dry DMF and was stirred under argon atmosphere at

110 °C for 16 hours. The unsymmetric diimide was obtained along with the symmetrical diimide derivatives. The completion of the reaction was checked by a TLC. DMF was evaporated on rotavapour under high vacuum and an extraction was done with $CHCl_3$/water solvent mixture. The organic layer was collected, dried on $Na_2SO_4$ and evaporated to get the mixture of the products of the statistical reaction. It was then purified using column chromatography (silica gel, 100-200 mesh, 2% methanol in chloroform) followed by size exclusion chromatography ($CHCl_3$, SX-3). Yield = 33% ; $^1$H NMR (400 MHz, $CDCl_3$): δ 8.81 (s, 4H, NDI ArH), 6.5 (s, 2H, ArH), 6.50 (s, 1H, -NH), 4.4 (t, 2H, EDA protons), 4.06- 3.99 (m, 6H, -$OCH_2$), 3.58 (t, 2H, EDA protons) 1.54 (s, 9H, -$C(CH_3)_3$), 1.9-0.8 (57H, alkyl H); LCMS (ESI): *m/z* calcd for $C_{57}H_{83}N_3O_9$: 953.61, found: 953.7 $[M]^+$

Unsymmetric Naphthalene diimide amine (**5**). 0.6 g (0.63 mmol) of **4** in 1.95 ml dry DCM was added drop wise to a mixture of Trifluoroacetic acid (TFA) (5.4 ml) and dry DCM (5 ml) and stirred at 0 °C under argon atmosphere. The ice bath was removed after 1.5 hours and the reaction mixture was allowed to stir at room temperature for an additional 3 hours. An extraction was done with 2 M NaOH/$CHCl_3$.The organic layer was dried on $Na_2SO_4$ and evaporated to get the deprotected product. Yield = 96%; $^1$H NMR (400 MHz, $CDCl_3$): δ 8.81 (s, 4H, NDI ArH), 6.50 (s, 2H, ArH), 4.33 (t, 2H, EDA protons), 4.05-3.97 (m, 6H, O-$CH_2$), 3.13 (t, 2H, EDA protons), 1.9-0.8 (57H, alkyl H); LCMS (ESI): *m/z* calcd for $C_{52}H_{75}N_3O_7$: 853.56, found: 895.7 $[M+K+3H]^+$.

**$C_3$-EDA-NDI** (**7**)**:** 0.4 g (0.14 mmol) of **6** was taken in 2 ml of dry DCM and stirred at 0 °C for 5 minutes under argon atmosphere. To this, a mixture of triethylamine (0.2 ml, 1.4 mmol) and the deprotected amine **5** (0.5 g, 0.6 mmol) in 13 ml of dry DCM was added drop wise. The resultant mixture was stirred on ice bath for 4 hours after which the stirring was continued for 27 hours. It was then refluxed for additional 1.5 hours to ensure the completion of the reaction. The reaction mixture was cooled to room temperature and was dried under vacuum. The unreacted amine **5** was removed by an ethyl acetate wash as the filtrate, while **$C_3$-EDA-NDI** was collected as the residue. The residue was further purified by a silica gel column chromatography (100-200 mesh, 2% methanol in chloroform) and size exclusion chromatography ($CHCl_3$, S-X3) to get the pure compound in 11% yield. The compound was obtained as a sticky solid after the

column chromatography, which on re-precipitation in methanol followed by drying in vacuum converted into a beige colour powder. $^1$H NMR (400 MHz, $CDCl_3$): δ 8.77 (q, 12H, NDI ArH), 8.1 (s, 3H, BTA core ArH), 7.15 (s, 3H, NH), 6.48 (s, 6H, ArH), 4.51 (t, 6H, EDA protons), 4.1-3.94 (m, 18H, -$OCH_2$), 3.86 (t, 6H, alkyl H), 1.9-1.14 (171H, alkyl H); $^{13}$C NMR (100 MHz, $CDCl_3$): δ 165.9 (3C, *1*), 163.6, 162.9 (6C, *17*), 153.9 (12C, *10*, *16*), 138.8 (3C, *18*), 134.4 (3C, *2*), 131.5 (3C, *17*), 131.4, 131.4 (3C, *3*), 129.5 (6C, *13*), 127.0, 126.8 (12C, *11*, *12*), 126.5 (12C, *5*, *6*, *8*, *9*), 71.9 (3C, *20*) , 67.6 (6C, *30*), 39.5 (3C, *21*), 39.4 (6C, *31*), 37.7 (3C, *23*), 37.6 (6C, *33*), 37.5 (3C, *24*), 36.5 (6C, *34*), 30.0 (3C, *23*), 29.9 (6C, *32*), 28.2, 28.1(9C, *26*, *36*), 24.9 (9C, *25*, *35*), 22.9 (3C, *29*), 22.8, 22.7 (6C, *38)*, 22.72, 19.8 (6C, *28*), 19.7(12C, *37*); MALDI-TOF MS: *m/z* calcd for $C_{165}H_{225}N_9O_{24}$: 2716.66, found: 2739.68 $[M+Na]^+$

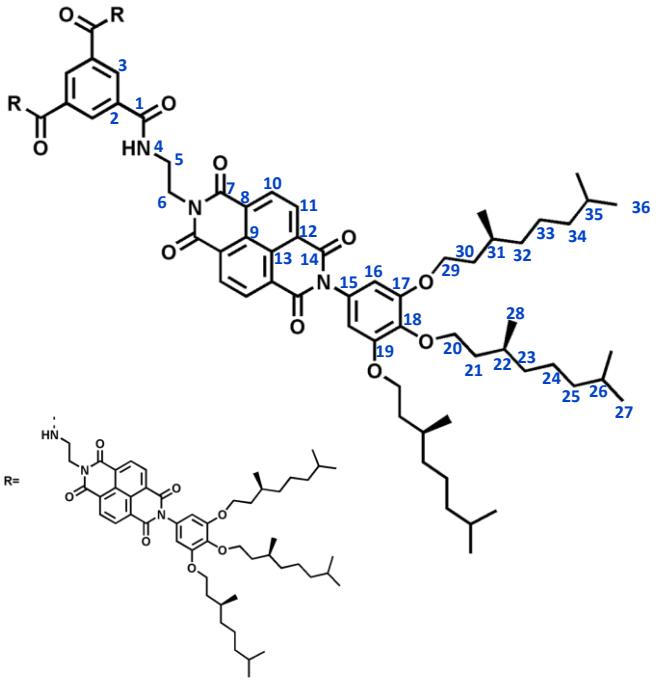

Unsymmetric Naphthalene diimide Derivative (**9**). 2.22 g (3.96 mmol) of **1** and 0.82 g (3.96 mmol) of **8** were mixed with 1, 4, 5, 8-Naphthalenetetracarboxylic dianhydride (**2**) (0.99 g, 3.69 mmoles) in 4 ml of dry DMF and was stirred under argon atmosphere at 110 °C for 16 hours. The unsymmetric diimide was obtained along with the symmetrical diimide derivatives. The hydrophobic symmetric digallic derivative was removed by washing with hexane, while **8** along with the symmetrical protected *p*-phenylenediamine derivative were collected as the precipitate. The mixture was then

subjected to a chloroform wash where the symmetrical di-Boc derivative precipitated and the desired compound **8** was collected in the filtrate. It was then dried under vacuum and purified using column chromatography (silica gel, 100- 200 mesh) in 2% methanol in chloroform followed by size exclusion chromatography ($CHCl_3$, SX-3). Yield = 47%; $^1$H NMR (400 MHz, $CDCl_3$): δ 8.84 (s, 4H, NDI ArH), 7.59 (d, *J* = 8.4 Hz, 2H, ArH), 7.26 (d, *J* = 8.4 Hz, 2H, ArH), 6.63 (s, 1H, -NH), 6.52 (s, 2H, ArH), 4.06- 3.99 (m, 6H, -$OCH_2$), 1.55 (s, 9H, -$C(CH_3)_3$), 1.9-0.8 (57H, alkyl H); $^{13}$C NMR (100 MHz, $CDCl_3$): δ 163.2, 153.9, 139.4, 138.8, 131.6, 129.6, 129.2, 129.1, 127.3, 127.2, 119.2, 106.9, 71.9, 67.6, 39.6, 39.4, 29.9, 28.5, 28.1, 24.9, 22.9, 22.8, 22.7, 19.8, 19.7; FT-IR (KBr): ν ($cm^{-1}$) = 3447, 3365 (Amide -NH stretch), 1675 (Amide –C=O stretch), 1524 (Amide (II) band); M.P. 240 °C-242 °C.

Unsymmetric Naphthalene diimide amine (**10**). 1.29 g (1.29 mmol) of **4** in 50 ml dry DCM was added drop wise to a mixture of Trifluoroacetic acid (TFA) (11.1 ml) and dry DCM (10 ml) and stirred at 0 °C under argon atmosphere. The ice bath was then removed after 1.5 hours and the reaction mixture was allowed stirring at room temperature for an additional 3 hours. An extraction was done with 2 M NaOH/$CHCl_3$ after which the organic layer was dried on $Na_2SO_4$ and evaporated to get the deprotected product. Yield = 99%; $^1$H NMR (400 MHz, $CDCl_3$): δ 8.83 (s, 4H, NDI ArH), 7.5 (d, *J* = 8.8 Hz, 2H, ArH), 6.84 (d, *J* = 8.8 Hz, 2H, ArH), 6.51 (s, 2H, ArH), 4.1-3.97 (m, 6H, O-$CH_2$), 1.9-0.8 (57H, alkyl H); $^{13}$C NMR (100 MHz, $CDCl_3$): δ 163.4 163.2, 153.9, 147.2, 138.7, 131.5, 129.2, 127.3, 127.2, 127.0, 115.8, 106.9, 71.9, 67.6, 45.9, 39.5, 39.3, 37.7, 37.5, 36.4, 30.0, 29.9, 29.8, 28.1, 24.9, 22.8, 22.7, 19.8, 19.7; HRMS (APCI): *m/z* calcd for $C_{56}H_{75}N_3O_7$: 906.5605, found: 906.5698 $[M]^+$; FT-IR (KBr): ν ($cm^{-1}$) = 3463, 3374 (-NH stretch); M.P. 172 °C-174 °C.

**$C_3$-ben-NDI** (**11**)**:** 0.08 g (0.3 mmol) of **6** was taken in 2 ml of dry DCM and stirred at 0 °C for 10 minutes under argon atmosphere. To this, a mixture of triethylamine (0.22 ml, 1.61 mmol) and the deprotected amine **9** (1.15 g, 1.28 mmol) in 5 ml of dry DCM was added drop wise. The resultant mixture was allowed to warm to room temperature and the stirring was continued for 11 hours after which it was refluxed for additional 2 hours to ensure the completion of the reaction. The reaction mixture was cooled to room temperature and was dried under vacuum. The unreacted amine **9** was removed by an

ethyl acetate wash as the filtrate, while **$C_3$-ben-NDI** was collected as the residue. The residue was further purified by a silica gel column chromatography (100-200 mesh, 2% methanol in chloroform, 1% TFA) and size exclusion chromatography ($CHCl_3$, SX-3) to get the pure compound in 47% yield. The compound was obtained as a sticky solid after the column chromatography, which on re-precipitation in methanol followed by drying in vacuum converted into a beige colour powder. $^1$H NMR (400 MHz, $CDCl_3$, 2% (v/v) TFA): δ 9.65 (s, 3H, NH), 9.19 (s, 3H, BTA core ArH), 8.92 (s, 12H, NDI ArH), 8.12 (d, *J* = 8.8 Hz, 6H, ArH), 7.46 (d, *J* = 8.8 Hz, 6H, ArH), 6.55 (s, 6H, ArH), 4.2-4.15 (m, 6H, -$OCH_2$), 4.0-3.99 (m, 12H, alkyl H), 1.9-1.14 (171H, alkyl H); $^{13}$C NMR (100 MHz, $CDCl_3$, 2% (v/v) TFA) : δ 165.9 (3C, *1*), 163.7, 163.6 (12C, *10*, *16*), 153.8 (6C, *19*), 138.0 (3C, *20*), 135.0 (3C, *2*) 132.2 (6C, *12*), 131.5 (3C, *17*), 131.1 (3C, *3*), 129.9, 127.3, 127.1 (18C, *11*, *14*, *15*), 129.5 (6C, *13*), 127.0 (6C, *4*, *7*), 122.2 (12C, *5*, *6*, *8*, *9*), 106.6 (6C, *18*), 73.3 (3C, *21*), 67.9 (6C, *30*), 39.5 (3C, *22*), 39.4 (6C, *31*), 37.6 (3C, *24*), 37.5 (6C, *33*), 37.0 (3C, *25*), 36.3 (6C, *34*), 30.0 (3C, *23*), 29.9 (6C, *32*), 28.1 (9C, *27*, *36*), 24.8 (9C, *26*, *35*), 22.8 (3C, *29*), 22.7 (6C, *38*), 19.7 (6C, *28*), 19.6 (12C, *37*); MALDI-TOF MS: m/z calcd for $C_{177}H_{225}N_9O_{24}$:2862.73, found: 2885.74 $[M+Na]^+$; HRMS (FAB): m/z calcd for $C_{177}H_{225}N_9O_{24}$: 2862.7316, found: 2880.6462 $[M+H_2O]^+$ ; FT-IR (KBr): ν ($cm^{-1}$) = 3361, 3482 (Amide -NH stretch), 1675 (Amide –C=O stretch), 1538 (Amide (II) band); M.P. 256 °C.

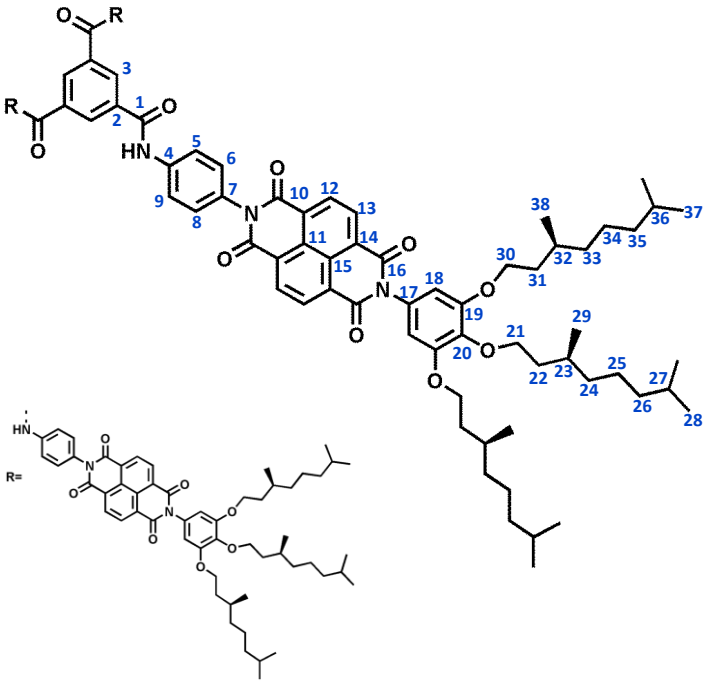

## 4.7. References


[1] a) T. Aida, E. W. Meijer, S. I. Stupp, *Science* **2012**, *335*, 813; b) S. S. Babu, S. Prasanthkumar, A. Ajayaghosh, *Angew. Chem. Int. Ed.* **2012**, *51*, 1766; c) F. Würthner, *Chem. Commun.* **2004**, 1564; d) F. J. M. Hoeben, P. Jonkheijm, E. W. Meijer, A. P. H. J. Schenning, *Chem. Rev*. **2005**, *105*, 1491.

[2] a) A. P. H. J. Schenning, E. W. Meijer, *Chem. Commun*. **2005**, *3245*; b) M. Hasegawa, M. Iyoda, *Chem. Soc. Rev.* **2010**, *39*, 2420; c) T. Lei, J. Pei, *J. Mater. Chem.* **2012**, *22*, 785; d) S. S. Babu, K. K. Kartha, A. Ajayaghosh, *J. Phys. Chem. Lett.* **2010**, *1*, 3413; e) D. B. Amabilino, J. Puigmarti-Luis, *Soft Matter* **2010**, *6*, 1605.

[3] a) S. Cantekin, T. F. A. de Greef, A. R. A. Palmans, *Chem. Soc. Rev*. **2012**, *41*, 6125; b) A. R. A. Palmans, E. W. Meijer, *Angew. Chem. Int. Ed*. **2007**, *46*, 8948.

[4] J. van Herrikhuyzen, P. Jonkheijm, A. P. H. J. Schenning, E. W. Meijer, *Org. Biomol. Chem.* **2006**, *4*, 1539.

[5] a) I. Danila, F. Pop, C. Escudero, L. N. Feldborg, J. Puigmarti-Luis, F. Riobe, N. Avarvari, D. B. Amabilino, *Chem. Commun*. **2012**, *48*, 4552; b) I. Danila, F. Riobe, F. Piron, J. Puigmarti-Luis, J. D. Wallis, M. Linares, H. Agren, D. Beljonne, D. B. Amabilino, N. Avarvari, *J. Am. Chem. Soc*. **2011**, *133*, 8344; c) I. Danila, F. Riobe, J. Puigmarti-Luis, A. Perez del Pino, J. D. Wallis, D. B. Amabilino, N. Avarvari, *J. Mater. Chem.* **2009**, *19*, 4495.

[6] I. Paraschiv, M. Giesbers, B. van Lagen, F. C. Grozema, R. D. Abellon, L. D. A. Siebbeles, A. T. M. Marcelis, H. Zuilhof, E. J. R. Sudhölter, *Chem. Mater.* **2006**, *18*, 968.

[7] a) R. van Hameren, P. Schön, A. M. van Buul, J. Hoogboom, S. V. Lazarenko, J. W. Gerritsen, H. Engelkamp, P. M. Christianen, H. A. Heus, J. C. Maan, T. Rasing, S. Speller, A. E. Rowan, J. A. A. W. Elemans R. J. M. Nolte, *Science* **2006**, *314*, 1433; b) N. Veling, R. van Hameren, A. M. van Buul, A. E. Rowan, R. J. M. Nolte J. A. A. W. Elemans, *Chem. Commun.* **2012**, *48*, 4371.

[8] a) A. R. A. Palmans, J. A. J. M. Vekemans, H. Fischer, R. A. Hikmet, E. W. Meijer, *Chem. Eur. J.* **1997**, *3*, 300; b) A. Timme, R. Kress, R. Q. Albuquerque,

H.-W. Schmidt, *Chem. Eur. J.* **2012**, *18*, 8329; c) K. Kreger, P. Wolfer, H. Audorff, L. Kador, N. S. Stutzmann, P. Smith, H.-W. Schmidt, *J. Am. Chem. Soc*. **2010**, *132*, 509; d) J. J. van Gorp, J. A. J. M. Vekemans, E. W. Meijer, *J. Am. Chem. Soc.* **2002**, *124*, 14759.

[9] a) C. F. C. Fitié , W. S. C. Roelofs, M. Kemerink, R. P. Sijbesma, *J. Am. Chem. Soc*. **2010**, *132*, 6892; b) C. F. C. Fitié, W. S. C. Roelofs, P. C. M. Magusin, M. Wübbenhorst, M. Kemerink, R. P. Sijbesma, *J. Phys. Chem. B*. **2012**, *116*, 3928.

[10] J. Roosma, T. Mes, P. Leclère, A. R. A. Palmans, E. W. Meijer, *J. Am. Chem. Soc*. **2008**, *130*, 1120.

[11] I. A. W. Filot, A. R. A. Palmans, P. A. J. Hilbers, R. A. van Santen, E. A. Pidko, T. F. A. de Greef, *J. Phys.Chem. B* **2010**, *114*, 13667.

[12] R. R. Lunt, J. B. Benziger, S. R. Forrest, *Adv. Mater.* **2010**, *22*, 1233.

[13] S. Chandrasekhar, B. K. Sadashiva, K. A. Suresh, *Pramana* **1977**, *9*, 471.

[14] A. Laschat, A. Baro, N. Steinke, F. Giesselmann, C. Hägele, G. Scalia, R. Judele, E. Kapatsina, S. Sauer, A. Schreivogel, M. Tosoni, *Angew. Chem. Int. Ed*. **2007**, *46*, 4832.

[15] a) P. Herwig, C. W. Kayser, K. Müllen, H. W. Spiess, *Adv. Mater*. **1996**, *8*, 510; b) A. J. Berresheim, M. Müller, K. Müllen, *Chem. Rev*. **1999**, *99*, 1747; c) M. D. Watson, A. Fechtenkötter, K. Müllen, *Chem. Rev*. **2001**, *101*, 1267; d) A. C. Grimsdale, J. Wu, K. Müllen, *Chem. Commun.* **2005**, 2197.

[16] a) V. Percec, C. G. Cho, C. Pugh, *J. Mater. Chem*. **1991**, *1*, 217; b) V. Percec, C. G. Cho, C. Pugh, *Macromolecules* **1991**, *24*, 3227; c) V. Percec, C. G. Cho, C. Pugh, D. Tomazos, *Macromolecules* **1992**, *25*, 1164.

[17] a) B. R. Patel, K. S. Suslick, *J. Am. Chem. Soc*. **1998**, *120*, 11802; b) A. Segade, M. Castella, F. Lopez-Calaborra, D. Velasco, *Chem. Mater.* **2005**, *17*, 5366.

[18] a) M. K. Engel, P. Bassoul, L. Bosio, H. Lehmann, M. Hanack, J. Simon, *Liq. Cryst*. **1993**, *15*, 709; b) J. Simon, C. Sirlin, *Pure Appl. Chem.* **1989**, *61*, 1625; c) H. Eichhorn, D. W. Bruce, D. Wöhrle, *Adv. Mater*. **1998**, *10*, 419.

[19] A. Wicklein, A. Lang, M. Muth, M. Thelakkat, *J. Am. Chem. Soc*. **2009**, *131*, 14442.

[20] a) H. Zimmermann, R. Poupko, Z. Luz, J. Billard, Z. *Natur-forsch. A* **1985**, *40*, 149; b) N. Spielberg, M. Sarkar, Z. Luz, R. Poupko, J. Billard, H. Zimmermann, *Liq. Cryst*. **1993**, *15*, 311.

[21] a) A. M. van de Craats, J. M. Warman, K. Müllen, Y. Geerts, J. D. Brand, *Adv. Mater*. **1998**, *10*, 36; b) A. M. van de Craats, J. M. Warman, A. Fechtenkötter, J. D. Brand, M. A. Harbison, K. Müllen, *Adv. Mater*. **1999**, *11*, 1469.

[22] a) M.-A. Muth, G. Gupta, A. Wicklein, M. C.-Orozco, T. T.-Albrecht, M. Thelakkat, *J. Phys. Chem. C*. **2014**, *118*, 92; b) S. Yagai, M. Usui, T. Seki, H. Murayama, Y. Kikkawa, S. Uemura, T. Karatsu, A. Kitamura, A. Asano, S. Seki, *J. Am. Chem. Soc*. **2012**, *134*, 7983.

[23] a) K. P. van den Hout, R. Martin-Rapun, J. Vekemans, E. W. Meijer, *Chem. Eur. J.* **2007**, *13*, 8111; b) J. K. Park, D. H. Lee, B. J. Song, J. B. Oh and H. K. Kim, *J. Pol. Sci.* **2006**, *44*, 1326.

[24] R.B. Martin, *Chem. Rev*. **1996**, *96*, 3043.

[25] For similar photo-electron transfer effects on perylenebisimides see: a) F. Würthner, C. Thalacker, S. Diele, C. Tschierske, *Chem. Eur. J.* **2001**, *7* , 2245; b) J. van Herrikhuyzen, A. Syamakumari, A. P. H. J. Schenning, E. W. Meijer, *J. Am. Chem. Soc.* **2004**, *126*, 10021.

[26] a) M. M. J. Smulders, A. P. H. J. Schenning, E. W. Meijer, *J. Am. Chem. Soc*. **2008**, *130*, 606; b) M. M. J. Smulders, M. M. L. Nieuwenhuizen, T. F. A. de Greef, P. van der Schoot, A. P. H. J. Schenning, E. W. Meijer, *Chem. Eur. J.* **2010**, *16* , 362; c) T. F. A. de Greef, M. M. J. Smulders, M. Wolffs, A. P. H. J. Schenning, R. P. Sijbesma, E. W. Meijer, *Chem. Rev*. **2009**, *109*, 5687.

[27] P. A. Korevaar, C. Schaefer, T. F. A. de Greef , E. W. Meijer, *J. Am. Chem. Soc.* **2012**, *134* , 13482.

[28] Y. Nakano, T. Hirose, P. J. M. Stals, E. W. Meijer, A. R. A. Palmans, *Chem. Sci*. **2012**, *3*,148.

[29] M. J. Frisch, G. W. Trucks, H. B. Schlegel, G. E. Scuseria, M. A. Robb, J. R. Cheeseman, G. Scalmani, V. Barone, B. Mennucci, G. A. Petersson, H. Nakatsuji, M. Caricato, X. Li, H. P. Hratchian, A. F. Izmaylov, J. Bloino, G. Zheng, J. L. Sonnenberg, M. Hada, M. Ehara, K. Toyota, R. Fukuda, J. Hasegawa, M. Ishida, T. Nakajima, Y. Honda, O. Kitao, N.Nakai, T. Vreven, J.

A. Montgomery, Jr. J. E. Peralta, F. Ogliaro, M. Bearpark, J. J. Heyd, E. Brothers, K. N. Kudin, V. N. Staroverov, T. Keith, R. Kobayashi, J. Normand, K. Raghavachari, A. Rendell, J. C. Burant, S. S. Iyengar, J. Tomasi, M. Cossi, N. Rega, J. M. Millam, M. Klene, J. E. Knox, J. B. Cross, V. Bakken, C. Adamo, J. Jaramillo, R. Gomperts, R. E. Stratmann, O. Yazyev, A. J. Austin, R. Cammi, C. Pomelli, J. W. Ochterski, R. L. Martin, K. Morokuma, V. G. Zakrzewski, G. A. Voth, P. Salvador, J. J. Dannenberg, S. Dapprich, A. D. Daniels, O. Farkas, J. B. Foresman, J. V. Ortiz, J. Cioslowski, D. J. Fox, Gaussian 09, Revision B.01, Gaussian, Inc, Wallingford CT, **2010**.

[30] W. Humphrey, A. Dalke, K. Schulten, *J. Mol. Graphics*, **1996**, *14*, 33.

# Chapter-5

## Amplification of Circularly Polarized Luminescence

# Chapter-5

## Chiroptical Amplification of Circularly Polarized Luminescence


### *Abstract*

*Circularly Polarized Luminescence (CPL) is rapidly gaining importance as an indispensable tool to probe the excited state properties of chiral molecular and supramolecular assemblies. Though lanthanides have high dissymmetry factors ($g_{lum}$) very close to the theoretically possible maximum $g_{lum}$ value (-2 to 2), solution processability, wavelength tunability and sensitization with a chiral organic dye still pose a challenge to employ lanthanides for practical purposes. Organic molecules, on the other hand, surpass these challenges, but have inherently low $g_{lum}$ values ($10^{-3}$ to $10^{-1}$). To increase the efficiency of small organic molecules in device applications, amplification of CPL is needed.*

*In this Chapter, we address this challenge by introducing the concept of 'sergeants and soldiers' in the excited state to amplify CPL. We have designed a CPL active molecule* ***$C_3$-Cyanostilbene*** *by incorporating cyanostilbene chromophore, which exhibits aggregation induced enhanced emission (AIEE) and chiral side chains in a $C_3$-symmetric design to create emissive, helical assemblies. The achiral analogue is also emissive but CPL inactive, as expected. Remarkable chiral amplification was observed upon incorporation of just 5% of chiral molecules in the achiral stacks. This chiral amplification was also reflected in the excited state, whereby, we observe the co-stacks to have $g_{lum}$ value same as that of the homochiral stacks.*


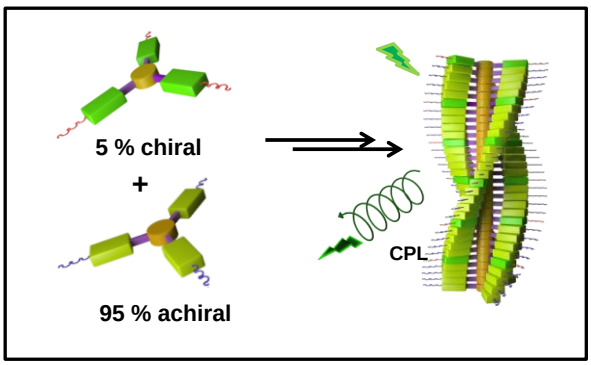


Manuscript based on this work: B. Narayan, G. Lakhwani, S. C. J. Meskers, S. J. George (under preparation).

## 5.1. Introduction

Circularly Polarized Luminescence (CPL) is the differential spontaneous emission of left or right circularly polarized light by chiral, luminescent molecules or assemblies.[1] It is the emission analogue of Circular Dichroism (CD) and elucidates the molecular configuration / conformation in the excited state, thus, acting as a supplementary technique to CD. The efficiency of CPL is measured by its luminescence anisotropic factor ($g_{lum}$), which is given by equation **5.1**.

$$g_{lum} = 2 (I_L - I_R) / (I_{L+} I_R) \qquad \text{.....(eq. 5.1.)}$$

in which $I_L$ and $I_R$ are the intensities of the left (L) and right (R) circularly polarized components of the emitted radiation.

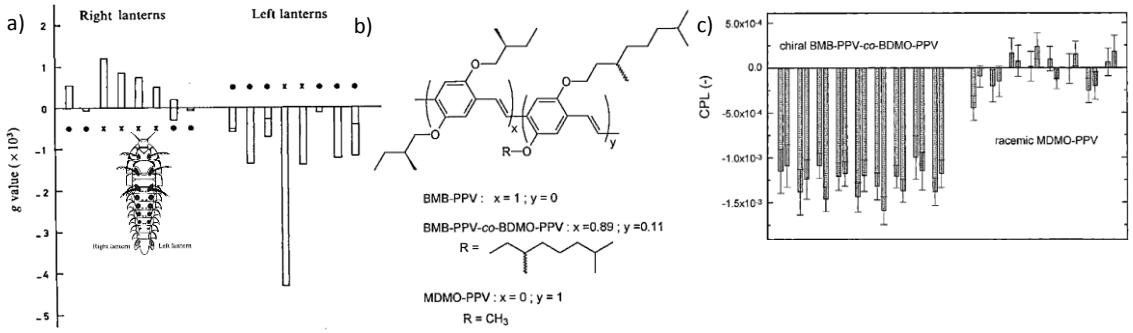


*Figure 5.1. Circularly Polarized Luminescence (CPL) obtained from bioluminescence and electroluminescence: a) g-values obtained from CPL measurements of firefly larvae lanterns of high emission intensity (inset: ventral view of a sketch of firefly larva); b) Molecular structures of poly{[2,5-bis[(S)-2-methylbutoxy]-phenylene]vinylene} (**BMB-PPV**) and its copolymeric derivative poly{[2,5-bis[(S)-2-methylbutoxy]-1,4-phenylene]vinylene}-co-{[2,5-bis[(3R,3S)-(3,7-dimethyloctyl)oxy]-1,4-phenylene]vinylene}(**BMB-PPV**-co-**BDMO-PPV**) and poly{[2-methoxy-5-[(3R,3S)-(3,7-dimethyloctyl)oxy]-1,4-phenylene]vinylene} (**MDMO-PPV**); c) Circularly Polarized Electroluminescence (CPEL) effect for nine independent polymer LEDs having an enantiomerically pure polymer layer (**BMB-PPV**-co-**BDMO-PPV**) and eight LEDs with a racemic layer (**MDMO-PPV**). Error bars indicate the standard error of the experimental result (Figures a and (b,c) reproduced with permissions from references 3 and 4 respectively).*

This concept has been explained in excellent reviews[2] and has also been observed in bioluminescence[3] from the lanterns of firefly larvae (Figure 5.1.a) and electroluminescence[4] (Figure 5.1.b, c) as well.

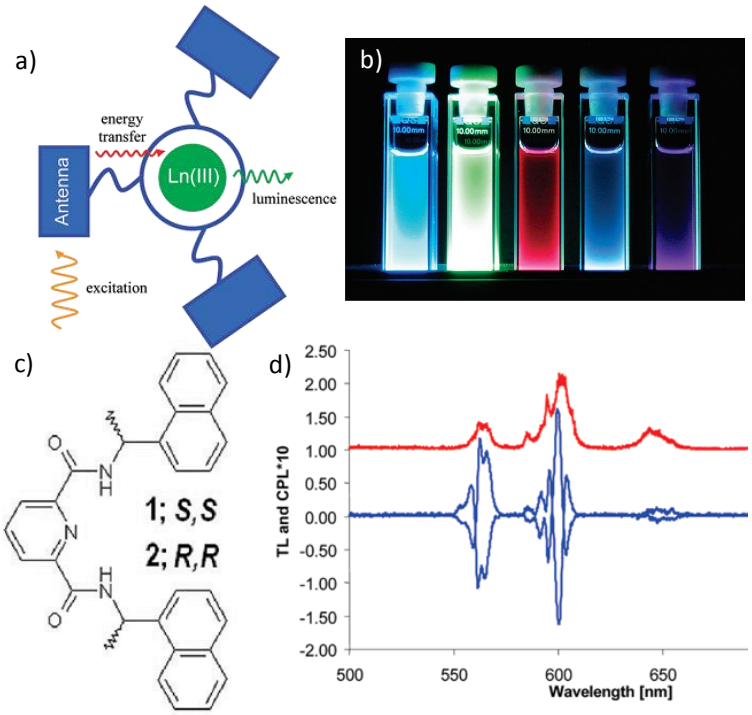


*Figure 5.2. Lanthanide emission and their CPL activity: a) Schematic representation of the antenna effect for Ln (III) sensitization using pendant chromophore ligand designs; b) Photographs of observed emission from Ln(III) cations sensitized by a 2-hydroxyisophthalamide ligand irradiated with a UV lamp ($\lambda_{ex}$ = 365 nm). From left to right, the solutions contain Tb(III), Eu(III), Dy(III), and Sm(III) complexes respectively; c) Molecular structures of chiral pyridyldiamide ligands **1** (S,S) and **2** (R,R); d) The luminescence emission spectra of the complex Sm(III) with **1** and **2** (in red) and the respective circular polarized emission spectra (in blue) the chiral emission from the Sm(III) ion (Figures a, b reproduced with permissions from reference 2b and c, d reproduced with permissions from reference 5f respectively).*

Lanthanides have been well-studied for CPL[5] as they have sharp absorption and emission features arising from the laporte-forbidden *f-f* transitions. However, these emissions are weak, and therefore direct excitation of the metals is inefficient unless the laser used for excitation is of very high power. Secondly, the wavelength of emission

cannot be easily tuned. Therefore, sensitization with an organic dye is necessary. In a process known as the 'Antenna Effect' the initial excitation occurs *via* the chromophore, which transfers energy to the Ln(III), populating the metal-centred excited state, which then emits (Figure 5.2.a-d). This drawback along with difficulties of solution processability limits the device applications of lanthanides.

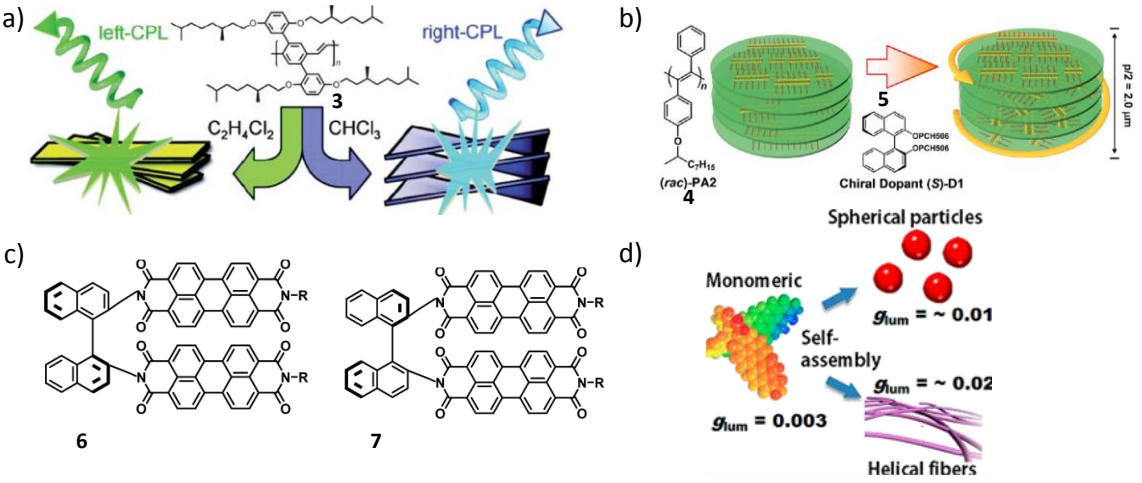


*Figure 5.3. Examples of Circulary Polarized Luminescence (CPL) studied in few polymeric and oligomeric systems: a) Schematic representation of right- and left-CPL obtained in different solvents originating from different organizations of chiral poly(p-phenylenevinylene) derivative* ***3****; b) liquid crystalline racemic polyacetylene derivative* ***4*** *and its organization to CPL active chiral nematic phase on doping with a binaphthyl derivative* ***5****; c) Molecular structures of binaphthyl based bischromophoric perylenebisimides* ***6*** *and* ***7****; d) Schematic representation of* ***6*** *and its self-assembly to form spherical particles and fibers, with the fibers having* $g_{lum}$ *value twice that of the particles (Figures a, b reproduced with permissions from references 4c and 7 respectively, c, d reproduced with permissions from reference 9).*

On the other hand, luminescent organic molecules or assemblies surpass this drawback with excellent quantum yields and wavelength tunability on functionalization. However, organic molecules have inherently low $g_{lum}$ values, as the CPL in organic molecules arises from the electric transition dipole moment (μ) allowed and magnetic dipole moment (m) forbidden transitions, while the opposite is true in the case of lanthanides.[6] The commonly observed $g_{lum}$ values in the case of organic molecules ranges from $10^{-3}$ to $10^{-1}$, while lanthanides have exhibited high $g_{lum}$ values

(0.1 to 1.5). Therefore, chiroptical amplification of CPL in organic molecules is needed to make CPL applicable for practical purposes.

CPL of organic chromophores has been studied both in polymeric and oligomeric systems. Investigations of CPL have been carried out in polymers like polythiophene, poly(*p*-phenylenevinylene) (PPV) (Figure 5.3.a) and polyacetylene derivatives. Enhancement of CPL in organic systems has been achieved in the recent past by chiral doping in liquid crystalline polyacetylene derivatives, resulting in chiral nematic phases with $g_{lum}$ of the order of $10^{-1}$ M (Figure 5.3.b).[7] Induction of chirality by using chiral solvents have also resulted in gigantic amplification of CPL.[8] Recent attempts by Kawai and co-workers have been successful in enhancing the CPL in the film state by tuning the morphology from spherical particles to fibers,[9] resulting in a two fold increase of $g_{lum}$ in solution processed thin film states (Figure 5.3.c, d). Most of these amplifications are achieved either in films or liquid-crystalline states. Amplification of CPL in solution state has been scarcely reported.

To address this challenge of amplification of CPL in organic assemblies, we have designed $C_3$-Cyanostilbenes appended with multiple chiral chains and chromophore with AIEE features,[10] which result in chiral, luminescent assemblies. We have also designed the achiral chromophore, which forms CPL inactive stacks. By co-assembling the chiral and achiral molecules by 'sergeants and soldiers' method, we have created homochiral stacks with 5% chiral and 95% achiral molecules which are CPL active. This strategy paves a new way to design functional molecules and extract CPL even from achiral molecules that are luminescent in the self-assembled state.

## 5.2. Design Strategy

The basic requirement to obtain CPL from a self-assembled state is to have chiral, luminescent assemblies. This is a serious limitation as most of the organic chromophores are fluorescent in the monomeric state but undergo quenching on aggregation (ACQ). However, there are a few exceptional chromophores that are weakly fluorescent in the monomeric state but form highly luminescent assemblies, due to a phenomenon called AIEE, whereby, the chromophores undergo restriction of rotation and result in highly emissive assemblies.[11] We have rationally employed

cyanostilbene (CSB) chromophores, which are well-studied for their AIEE properties,[11a] to obtain fluorescent assemblies and functionalized it with (S)-3,7-dimethyl-octyl side chain to provide an overall helicity to the self-assembled state. Furthermore, the design incorporates $C_3$-symmetric 1,3,5 benzenetricarboxamide (BTA) core[12] in the molecule which would lead to the formation of well-defined one-dimensional assemblies through triple hydrogen bonding by virtue of the trisamide moiety and render it a co-operative mechanism of self-assembly, which would play a crucial role in determining the extent of chiral amplification. Apart from the chiral molecule, we have also designed the achiral analogue in which the chiral side chains have been replaced with octyl chains (Figure 5.4). Both the molecules, **$C_3$-CSB-ch** and **$C_3$-CSB-ach** have similar designs to facilitate co-assembly and creation of supramolecular helical co-stacks for chiroptical amplification of CPL.

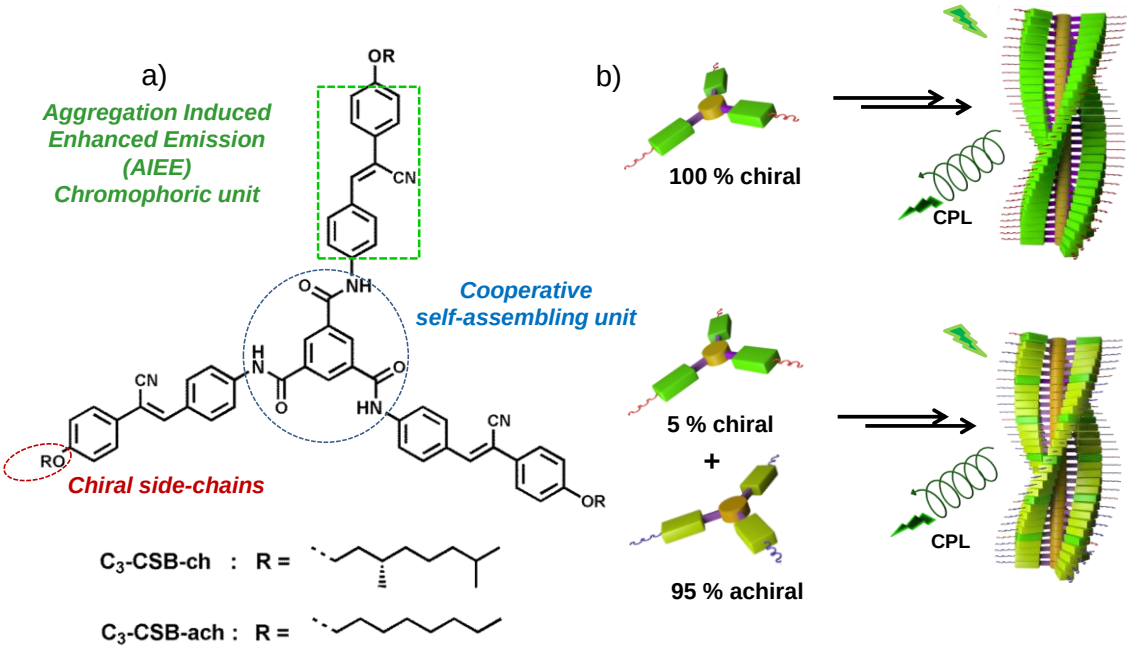


*Figure 5.4.a) Molecular Structures of $C_3$-Cyanostilbenes: **$C_3$-CSB-ach** and **$C_3$-CSB-ch** clearly illustrating the rationale behind the molecular design for a CPL active self-assembling molecule; b) Schematic illustration of the chiroptical amplification concept of CPL.*

The syntheses of **$C_3$-CSB-ch** and **$C_3$-CSB-ach** were accomplished through the coupling of 1,3,5 benzenetricarbonyl chloride with the amine functionalized

cyanostilbenes **5b** and **5a** respectively. The cyanostilbene amines were obtained through multistep syntheses which involved alkylation of *p*-hydroxyphenylacetonitrile, followed by the respective Knoevenagel condensations with *p*-nitrobenzaldehyde to give the chiral and achiral nitro cyanostilbenes which were then reduced by $SnCl_4$ to yield the respective amino cyanostilbenes having 'Z' configuration around the double bond. The final molecules have been synthesized in good yields and characterized through $^1H$ NMR, $^{13}C$ NMR and High Resolution Mass Spectromery (HRMS) (refer to section 5.8.2. for detailed synthetic protocols and characterization).

## 5.3. Self-Assembly of $C_3$-Cyanostilbenes

The self-assembly of $C_3$-Cyanostilbenes was investigated through detailed spectroscopic and microscopic techniques. The photophysical studies were carried out in solvent mixtures of methylcyclohexane (MCH) and 1,1,2,2 Tetrachloroethane (TCE). While the molecules existed in the monomeric state in solvents of medium polarity like chloroform and TCE, they formed highly fluorescent assemblies in non-polar solvents like MCH and toluene.

### 5.3.1. Spectroscopic Characterization of the Assemblies

The process of self-assembly could be probed by significant changes in the absorption and photoluminescence profiles of these molecules. While the monomeric form of **$C_3$-CSB-ach** (in TCE) has an absorption maximum of 363 nm, a vibrionic shoulder at 417 nm gradually evolves in increasing percentages of MCH in MCH/TCE solvent mixtures. This transition is marked by the presence of an isosbestic point at 393 nm (data not shown). Remarkable changes were observed in the fluorescence spectra in which the emission enhanced significantly due to the process of AIEE. Similar changes were observed in the spectroscopic features of **$C_3$-CSB-ch** upon self-assembly (Figure 5.5.a, b). Circular Dichroism (CD) could be employed to study the self-assembled state in the case of **$C_3$-CSB-ch**. The monomeric state of **$C_3$-CSB-ch** was characterized by an absorption maximum at 362 nm with no excitonic coupling between the chromophores as evident from the absence of a CD signal. The formation of the self-assembled state above 50% MCH in TCE was marked by the appearance of a vibrionic shoulder at 417 nm accompanied by a red shift in the absorption maximum by 2 nm (Figure 5.5.a).

Remarkably, a bisignated CD signal with positive maxima at 353 nm and 422 nm and minimum at 383 nm indicated the formation of helical supramolecular self-assembled state with efficient transfer of chirality from the peripheral side chains to the core and strong excitonic coupling between the cyanostilbene chromophores (Figure 5.5.d). The zero crossing of the CD signal exactly coincided with the absorption maximum. The self-assembly process was also followed through fluorescence spectroscopy. Whereas, the monomeric solution was weakly fluorescent with an emission maximum of 447 nm, the self-assembled state shows 13 times enhanced emission with maximum at 482 nm (Figure 5.5.b, c).

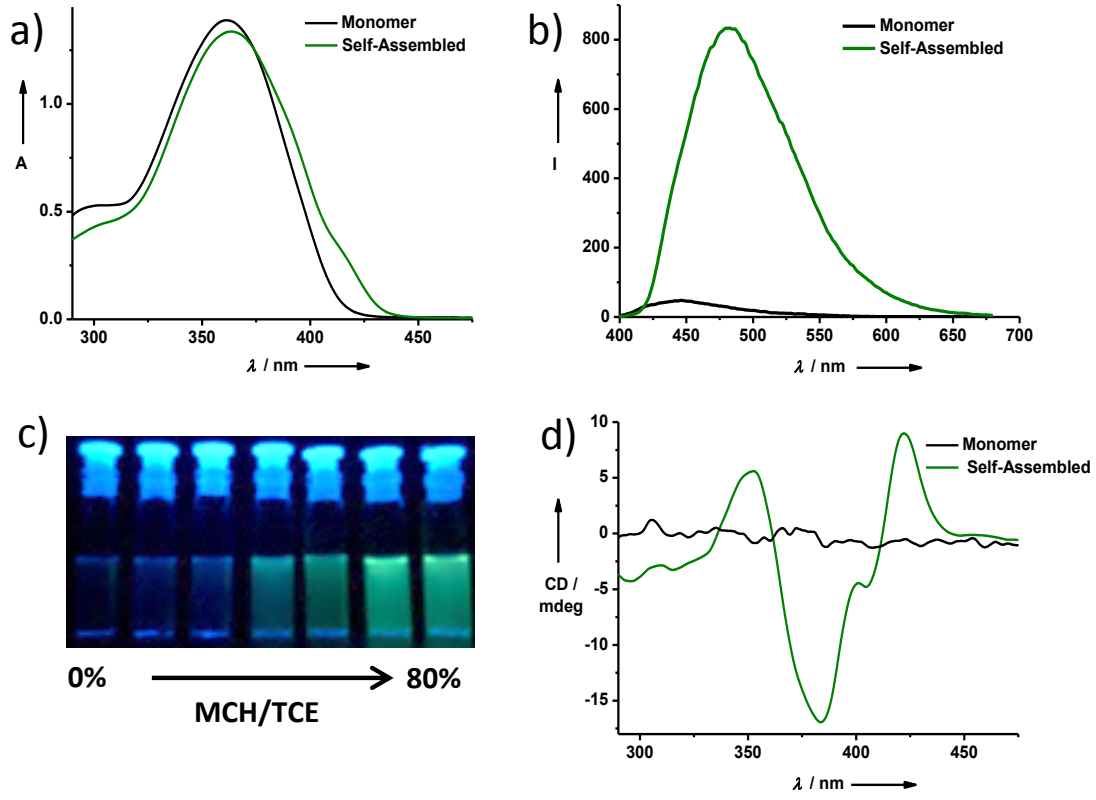


*Figure 5.5. Spectroscopic characterization of* ***$C_3$-CSB-ch*** *in the monomeric (TCE) and self-assembled (MCH/TCE, 60/40, (v/v)): a) Absorption spectra; b) Fluorescence spectra ($\lambda_{ex}$ = 350 nm) showing AIEE in the assemblies; c) Photograph of solutions of* ***$C_3$-CSB-ch*** *under UV 365 nm lamp in increasing percentages of MCH in solvent mixtures of MCH/TCE, clearly showing enhanced emission CD spectra indicative of excitonic coupling between the chromophores in the self-assembled state (c= $1.5x10^{-5}$ M).*

Emission spectrum obtained by selective excitation of the aggregate band of **$C_3$-CSB-ch** at 410 nm clearly indicated the formation of J-aggregates. The nature of the aggregates was further confirmed through time resolved fluorescence decay measurements. The lifetime in the self-assembled state has been measured by monitoring the decay at 490 nm upon excitation of the self-assembled samples with a laser of wavelength 380 nm. The lifetime of the aggregate was found to undergo a bi exponential decay (($\tau_1$ = 1.56 ns (33.02%), $\tau_2$ = 3.56 ns (66.98%)) where the major contribution was from the aggregate emission. The solution in the monomeric state was too weakly emissive to determine the lifetime and blended with the Instrument Response Function (IRF). Similar observations were made for **$C_3$-CSB-ach**, where the lifetime for the self-assembled state had major contribution from the assemblies ($\tau_1$ = 1.76 ns (23.37%), $\tau_2$ = 5.46 ns (76.63%)). Furthermore, the quantum yield of the self-assembled solution ($\varphi$ = 12%) was found to be an order of magnitude higher than the monomeric solution ($\varphi$ = 0.9%). These molecules also self-assemble in toluene/TCE mixtures with percentages of MCH above 40% to form fluorescent J-aggregates with AIEE (see section 5.6. for details).

| **$C_3$-CSB-ach** (TCE) | **$C_3$-CSB-ach** (MCH/TCE, 60/40, (v/v) | **$C_3$-CSB-ch** (TCE) | **$C_3$-CSB-ch** (MCH/TCE, 60/40, (v/v) |
|---|---|---|---|
| 0.007 | 0.16 | 0.009 | 0.12 |

*Table 5.1. Quantum yields of **$C_3$-CSB-ach** and **$C_3$-CSB-ch** ($c=1.5x10^{-5}$ M). The quantum yield measurements have been carried out using Quinine Sulfate dihydrate in 0.1 M $H_2SO_4$ as the standard.*

### 5.3.2. Morphological Investigations

Detailed microscopic investigations were carried out through Transmission Electron Microscopy (TEM) and confocal microscopy to probe the morphology adopted by these molecules in the self-assembled states. The samples for TEM were prepared by

drop-casting the self-assembled solution on a copper grid followed by staining with uranyl acetate (negative staining agent). The samples for confocal microscopy were ared by sealing the self-assembled solution between a glass slide and a cover slip and visualizing them upon excitation with a laser of 480 nm.

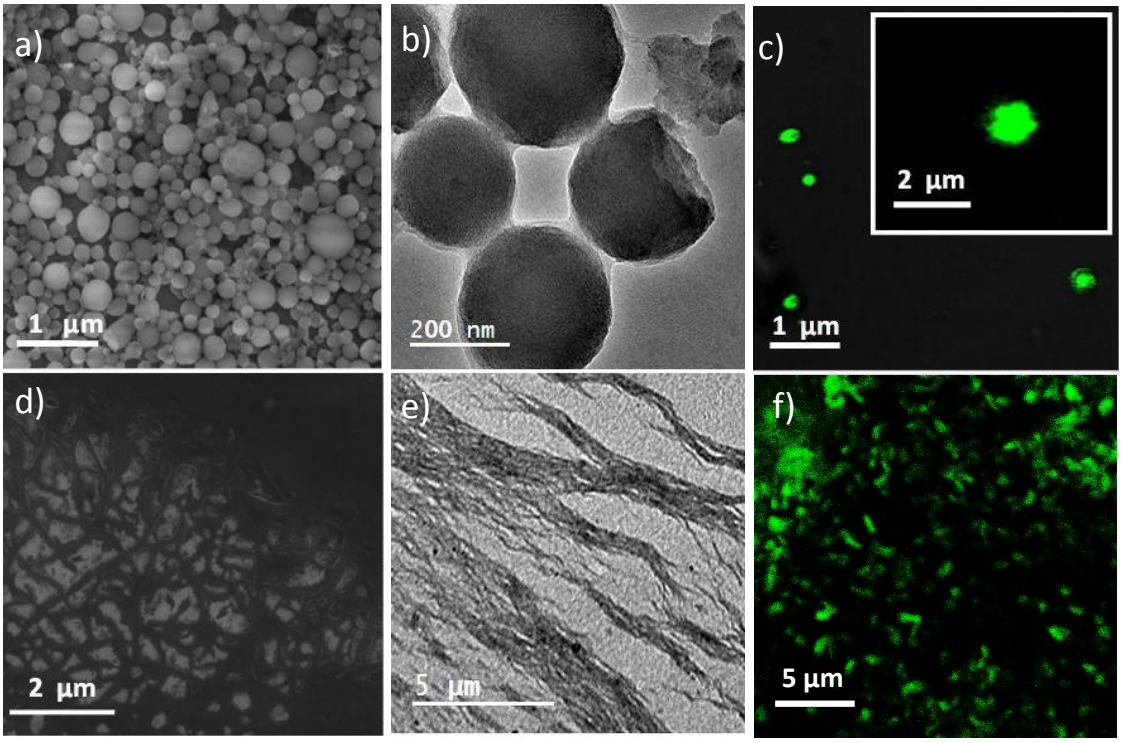


*Figure 5.6. Morphological studies of $C_3$-Cyanostilbenes: a), b) TEM images of **$C_3$-CSB-ch** showing the formation of spherical particles; c) is the confocal image obtained by exciting a self-assembled solution with a laser of 480 nm showing the presence of the nanostructures in solution; d), e) TEM images of bundles of fibres formed on self-assembling **$C_3$-CSB-ach** in MCH/TCE, 60/40, (v/v); f) Confocal image of **$C_3$-CSB-ach** that shows the existence of self-assembled fibres in solution, ruling out artifacts arising due to drying effects ($c=10^{-4}$ M for all microscopic investigations).*

**$C_3$-CSB-ach** forms bundles of fibers, probably due to the one-dimensional stacking induced through the triple H-bonding provided by BTA cores. Fibres of average lengths 5 µm and average widths of 100 nm were observed through TEM imaging (Figure 5.6.d, e). Confocal microscopy clearly proved the existence of the fibers in the self-assembled solution, thus ruling out artifacts arising due to drying effects on the copper grid (Figure 5.6.f). However, **$C_3$-CSB-ach** forms green fluorescent

effects on the copper grid (Figure 5.6.f). However, **$C_3$-CSB-ach** forms green fluorescent nanoparticles on self-assembly (Figure 5.6.a-c). A similar observation has been made in the case of enantioselective self-assembly of chiral cyanostilbene carboxylic acid and amine, whereby, nanospheres are produced if there is a possibility of a twist in the assembly, leading to reduced planarization than in nanofibers, where there is no twist. [13] The proposed hypothesis in this case is the difference in the surface bending energies. While the nanosphere has high surface bending energy, nanofibers have a comparatively low value of surface bending energy. Though we have not extensively studied the effect of various alkyl chains on the morphology of self-assembled $C_3$-Cyanostilbenes, a similar mechanism is possible, which is indicated from the low quantum yield of **$C_3$-CSB-ch** than **$C_3$-CSB-ach**. However, planarization is almost to the same extent in both the achiral and chiral derivatives, as the spectroscopic features of these derivatives are similar to each other.

### 5.3.3. Mechanistic Investigations

Insights into the mechanism of self-assembly of $C_3$-Cyanostilbenes were obtained by temperature dependent measurements. Self-assembled solutions of **$C_3$-CSB-ach**/ **$C_3$-CSB-ch** were heated to high temperatures (353.15 K), which led to dissociation of the assemblies. The solutions were cooled at a slow rate (-dT/dt = 1 K/min), experimental cooling curves obtained by monitoring 434 nm in the absorption spectrum of **$C_3$-CSB-ach/ $C_3$-CSB-ch** and 423 nm in the CD spectrum of **$C_3$-CSB-ch** were then fitted to well-accepted models of self-assembly developed by Meijer and co-workers[14] to get mechanistic insights.

A dilute solution of **$C_3$-CSB-ch** (15 µM) in MCH/TCE, 60/40, (v/v) disassembled into monomers on heating to 353.15 K which was characterized by the disappearance of the CD signal (Figure 5.7.a). This was accompanied by concomitant changes in the absorbance and fluorescence spectra. The vibrionic shoulder in the absorption spectrum disappeared and the fluorescence of the assemblies weakened. The bisignated CD signal gradually appears on cooling to 268.15 K at 1 K/min, which was observed by variable temperature CD spectra. The fraction of aggregates obtained by monitoring the process of self-assembly at 423 nm when plotted against temperature showed a non-sigmoidal behaviour and fitted well to the cooperative mechanism of self-

assembly, indicating the presence of a nucleation phase followed by a sudden elongation phase (Figure 5.7.b).

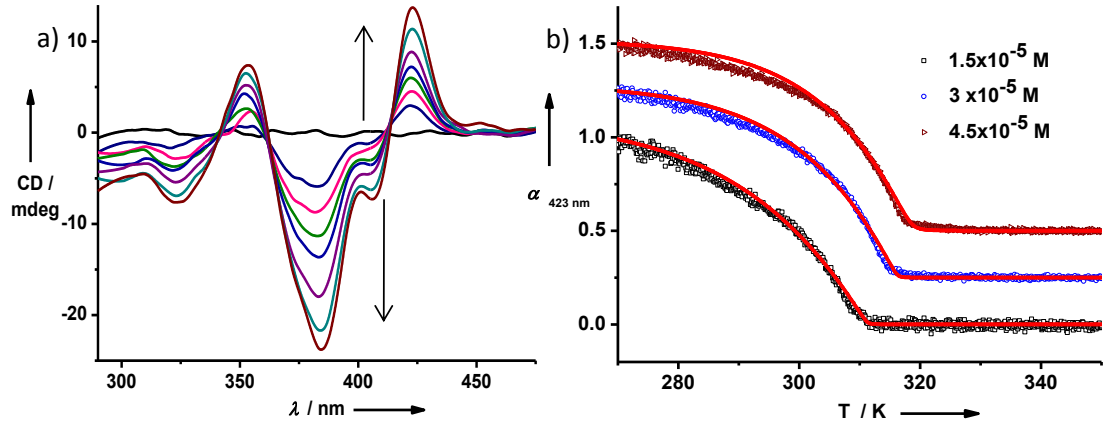


*Figure 5.7. Mechanistic investigations into self-assembled $C_3$-Cyanostilbenes in solution: a) Variable temperature CD spectra on cooling a dilute solution ($1.5x10^{-5}$ M) of **$C_3$-CSB-ch** from 353.15 K to 268.15 K with a temperature ramp of -dT/dt = 1 K/min showing the evolution of bisignated CD signal from excitonically coupled chromophores; b) Non-sigmoidal cooling curves obtained by monitoring 423 nm in the CD spectrum as dilute solutions ($1.5x10^{-5}$ M, $3x10^{-5}$ M, $4.5x10^{-5}$ M; solvent composition MCH/TCE, 60/40, (v/v) were cooled slowly from 353.15 K to 268.15 K with a temperature gradient of 1 K/min. The scatter plots represent the experimental data and the red solid lines are the co-operative fits.*

Monitoring the absorption changes at 434 nm and fluorescence changes at 482 nm also yielded highly cooperative curves (data not shown). The thermodynamic parameters derived from the cooperative fits are listed in Table 5.2. This behaviour may be attributed to the BTA core which is well-known to drive the self-assembly in a co-operative fashion by virtue of triple hydrogen bonding, as demonstrated unambiguously by Meijer and co-workers.[12]

Concentration dependent mechanistic investigations showed the elongation temperature ($T_e$) to occur at higher temperature for higher concentrations. The mechanism of self-assembly in **$C_3$-CSB-ach** was obtained by monitoring the absorption changes upon cooling dilute solutions at –dT/dt = 1 K/min, as the assemblies are not chiral. Notably, the elongation temperature ($T_e$) for **$C_3$-CSB-ach** was found to be

336.15 K at c=15 μM, while that of **$C_3$-CSB-ch** was much lower at 310.15 K at the same concentration, suggesting the role of the alkyl chains in the self-assembly processes. While the linear octyl chains gave rise to stronger achiral assemblies, the branched (S)-(-)-3,7-dimethyl-octyl chains in **$C_3$-CSB-ch** led to comparatively weaker assemblies, which may be attributed to slight disorder due to branching.

| Concentration (M) | $\Delta H°_e$ (kJ/mol) | $\Delta S°_e$ (kJ/mol.K) | $\Delta H°_{nuc}$ (kJ/mol) | $T_e$ (K) |
|---|---|---|---|---|
| $1.5x10^{-5}$ | -40.14±0.66 | -0.04±0.002 | -30.89±3.39 | 311.06±0.14 |
| $3x10^{-5}$ | -53.71±0.55 | -0.08±0.002 | -29.22±2.3 | 316.00±0.10 |
| $4.5x10^{-5}$ | -61.04±0.61 | -0.11±0.002 | -22.55±0.86 | 318.12±0.10 |

*Table 5.2. Thermodynamic parameters obtained from co-operative fits of cooling curves obtained by monitoring 423 nm in the CD spectra of **$C_3$-CSB-ch** at different concentrations in MCH/TCE, 60/40, (v/v).*

## 5.4. Chiral Amplification in $C_3$-Cyanostilbenes

In order to have chiroptical amplification of CPL, co-assembly of the chiral and achiral molecules with chiral induction is essential. In this direction, we performed 'sergeants and soldiers' experiment to investigate whether a minor percentage of the **$C_3$-CSB-ch** ('sergeant') drives the co-assembled stacks in a homochiral fashion.

In a typical experimental protocol, **$C_3$-CSB-ch** and **$C_3$-CSB-ach** were mixed in various percentages ranging from 0% to 100% of **$C_3$-CSB-ch** in TCE to make sub-stock solutions, which were further injected into TCE-MCH solvent mixtures, resulting in a total concentration of $1.5x10^{-5}$ M and a final composition of MCH/TCE, 60/40, (v/v). Each solution was heated to 353.15 K and then cooled down at 1 K/min to ensure that the co-assembled solutions are formed in thermodynamic fashion. The CD spectra of

the solutions thus obtained were recorded and a plot of g-value versus mole fraction of the sergeant was constructed by using the mathematical equation: g-value = CD / (A*32980) at a particular wavelength.

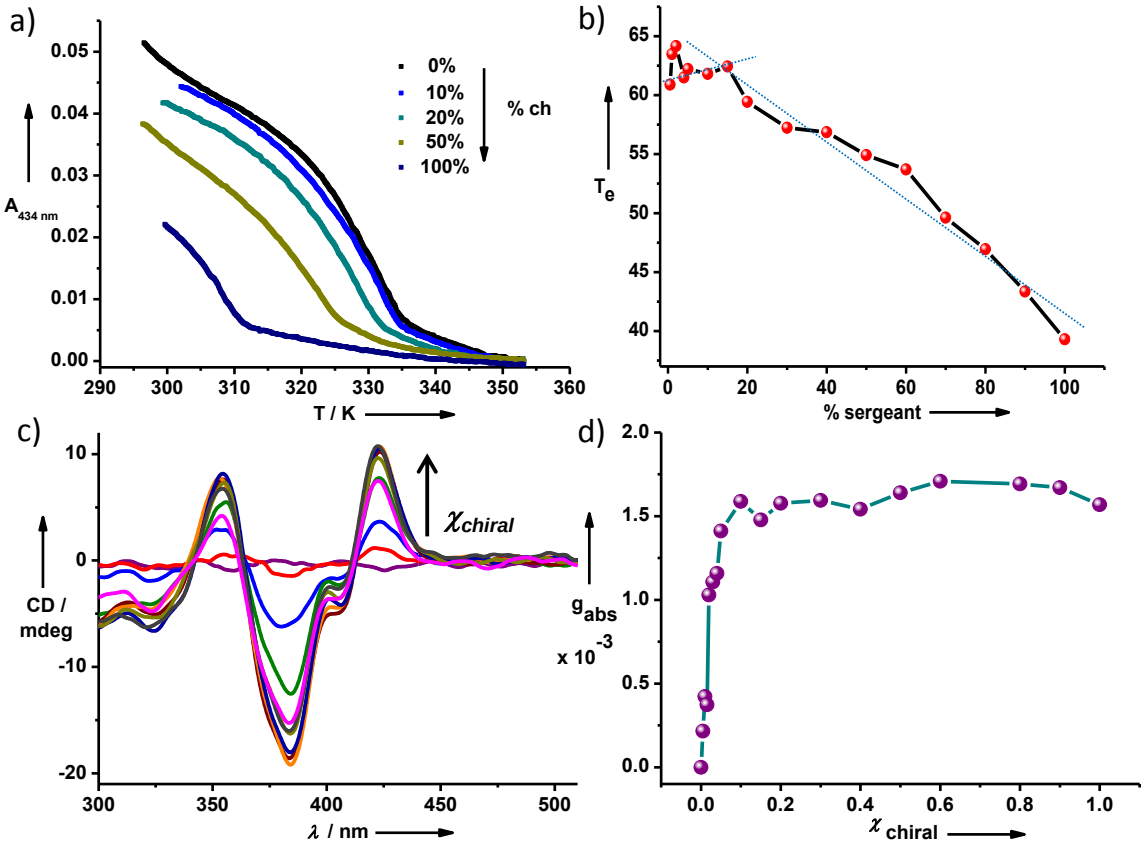


*Figure 5.8. Chiral amplification through co-assembly: a) Cooling curves of various percentage compositions of* ***$C_3$-CSB-ch*** *and* ***$C_3$-CSB-ach*** *obtained by monitoring absorption changes at 434 nm, as the co-assembled solutions were cooled from 353.15 K to 293.15 K, with a temperature ramp of –dT/dt = 1 K/min; b) Plot of elongation temperature ($T_e$) as obtained from cooling curves of co-assembled mixtures versus percentage of the chiral molecule (sergeant) in the respective compositions, indicating a non-linear trend, thus serving as a proof of co-assembly of* ***$C_3$-CSB-ch*** *and* ***$C_3$-CSB-ach****; c) CD spectra of increasing mole percentages of chiral in achiral. The co-assembly shows complete helical bias at 5% chiral, d) plot of g-value at 423 nm obtained from CD experiments versus percentage of chiral molecule that shows saturation at 5% sergeant, indicating remarkable chiral amplification.*

The cooling curves of the co-assembled solutions obtained by monitoring 434 nm in the absorption spectrum showed a non-sigmoidal behaviour, consistent with the co-operative mechanism of self-assembly of the individual components (Figure 5.8.a). A plot of $T_e$ versus % sergeant deviates from linearity, indicating co-assembly of **$C_3$-CSB-ch** and **$C_3$-CSB-ach** (Figure 5.8.b). CD spectra of the thermodynamic co-assembled solutions followed the bisignated pattern of **$C_3$-CSB-ch** with positive maxima at 353 nm and 422 nm and minimum at 383 nm (Figure 5.8.c).

The CD spectra along with the plot of g-value versus mole fraction of **$C_3$-CSB-ch** proved remarkable chiral amplification. The homochiral state was attained at $\chi_{chiral}$ = 0.05 which could be unambiguously concluded from the saturation of the g-value versus $\chi_{chiral}$ plot (Figure 5.8.d).

## 5.5. Chiroptical Amplification of CPL

To obtain amplification of CPL, we first looked into the CPL activity of self-assemblies of **$C_3$-CSB-ch**. Our design strategy of **$C_3$-CSB-ch** was successful in creating chiral, luminescent assemblies which are the basic requirements for obtaining CPL. Dilute self-assembled solutions ($c=1.5x10^{-5}$ M, MCH/TCE, 60/40, (v/v)) of $C_3$-Cyanostilbenes were tested for CPL activity. Remarkably, **$C_3$-CSB-ch** showed a $g_{lum}$ of 0.003, while **$C_3$-CSB-ach** was CPL inactive, due to the presence of racemic assemblies. However, **$C_3$-CSB-ch** was CPL inactive in the monomeric state in TCE and $CHCl_3$, proving the need for hierarchial chirality for CPL activity which is brought about by the process of self-assembly.

Next, we carried out the CPL measurements of the co-assembled solutions. The molecules **$C_3$-CSB-ch** and **$C_3$-CSB-ach** were again mixed in various percentage compositions in TCE and injected into a mixture of MCH/TCE to result in final solvent compositions of MCH/TCE, 60/40, (v/v) and total concentrations of $1.5x10^{-5}$ M. These solutions were heated to high temperature to disassemble the kinetic aggregates and cooled slowly to result in thermodynamic assemblies. The samples were excited at 430 nm. A plot of $g_{lum}$ versus mole fraction of **$C_3$-CSB-ch** was then constructed (Figure 5.9).

Remarkable amplification of CPL was observed in the co-assembled solutions. A co-assembled solution consisting of 5% **$C_3$-CSB-ch** showed a $g_{lum}$ of $3x10^{-3}$ in clear agreement with the chiral amplification experiment obtained from CD measurements (Figure 5.9.a, b). This proves that the ground state amplification of chirality as measured by CD also manifests itself in the excited state. Therefore, a molecular design where chirality and AIEE work in conjunction gives rise to CPL active molecules and moreover, systems which have chiral amplification and are CPL active are potential candidates for amplifying CPL (Figure 5.9.c).

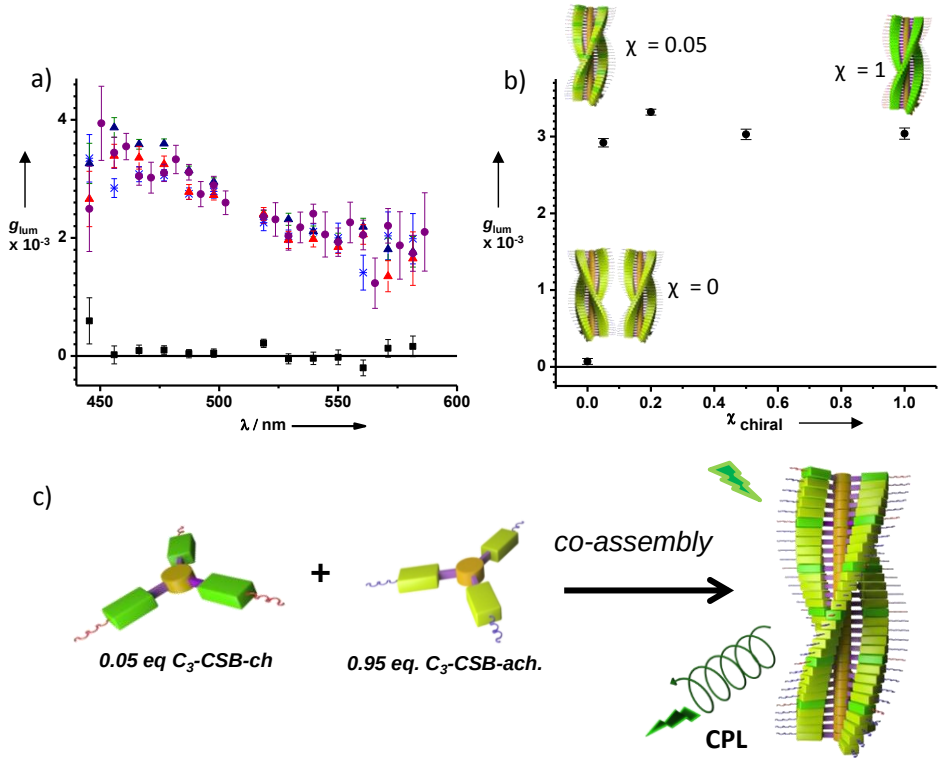


*Figure 5.9. Chiroptical amplification of CPL: a) CPL spectra of co-assembled samples of **$C_3$-CSB** systems with varying percentages of chiral in achiral (0%, 5%, 20%, 50%, 100% chiral co-assembled solutions are represented by black squares, blue asterix, blue triangles, red triangles, and purple circles respectively); b) CPL amplification represented by plots of $g_{lum}$ versus mole fraction of sergeant ($\chi_{chiral}$) showing saturation at 5% **$C_3$-CSB-ch**, well in agreement with the CD experiments; c) Schematics of co-assembly and CPL amplification showing the CPL active supramolecular stack with few chiral units.*

## 5.6. Co-assembly Studies in Toluene-TCE Mixtures

The molecules **$C_3$-CSB-ch** and **$C_3$-CSB-ach** self-assemble to form luminescent aggregates even in solvent mixtures of toluene/TCE. On chiroptical probing, **$C_3$-CSB-ch** was found to form chiral assemblies with a bisignated CD signal. However, the molecules do not co-assemble well and thereby, there was no amplification of CPL, despite having homochiral CPL assemblies of **$C_3$-CSB-ch** with a $g_{lum}$=0.002. This section discusses the importance of having chiral amplification in the ground state which can be exploited for chiroptical amplification of CPL in the excited state. The results presented in this section, therefore serve as blank experiments for the amplification of CPL and clearly point out the criteria for this phenomenon.

### 5.6.1. Spectroscopic Characterization

The $C_3$-Cyanostilbenes **$C_3$-CSB-ch** and **$C_3$-CSB-ach** were studied in varying solvent compositions of Toluene in TCE. A gradual transformation from monomeric to self-assembled state occurred with broadening of absorption spectra and appearance of a weak vibrionic shoulder at 408 nm (Figure 5.10.a). The emission enhanced almost by 18 times yielding green fluorescent assemblies (Figure 5.10.b). Chiroptical studies of 2 x $10^{-5}$ M **$C_3$-CSB-ch** in toluene/TCE, 40/60, (v/v) revealed the excitonic coupling of the chromophores in the self-assembled state, which was evident from the appearance of a bisignated CD signal with positive and negative maxima at 356 nm and 331 nm respectively. The zero crossing lay at 344 nm, which was close to the absorption maximum of the self-assembled state (Figure 5.10.c). However, the features of the CD signal was very different from that observed in TCE-MCH mixtures.

CPL measurements were carried out on the self-assembled state of **$C_3$-CSB-ch**. The samples were excited with a laser of 430 nm wavelength. These experiments revealed the existence of homochiral assemblies with $g_{lum}$=0.002 (Figure 5.10.d). This again validates our design strategy of creating helical stacks with fluorescence for the creation of CPL active assemblies.

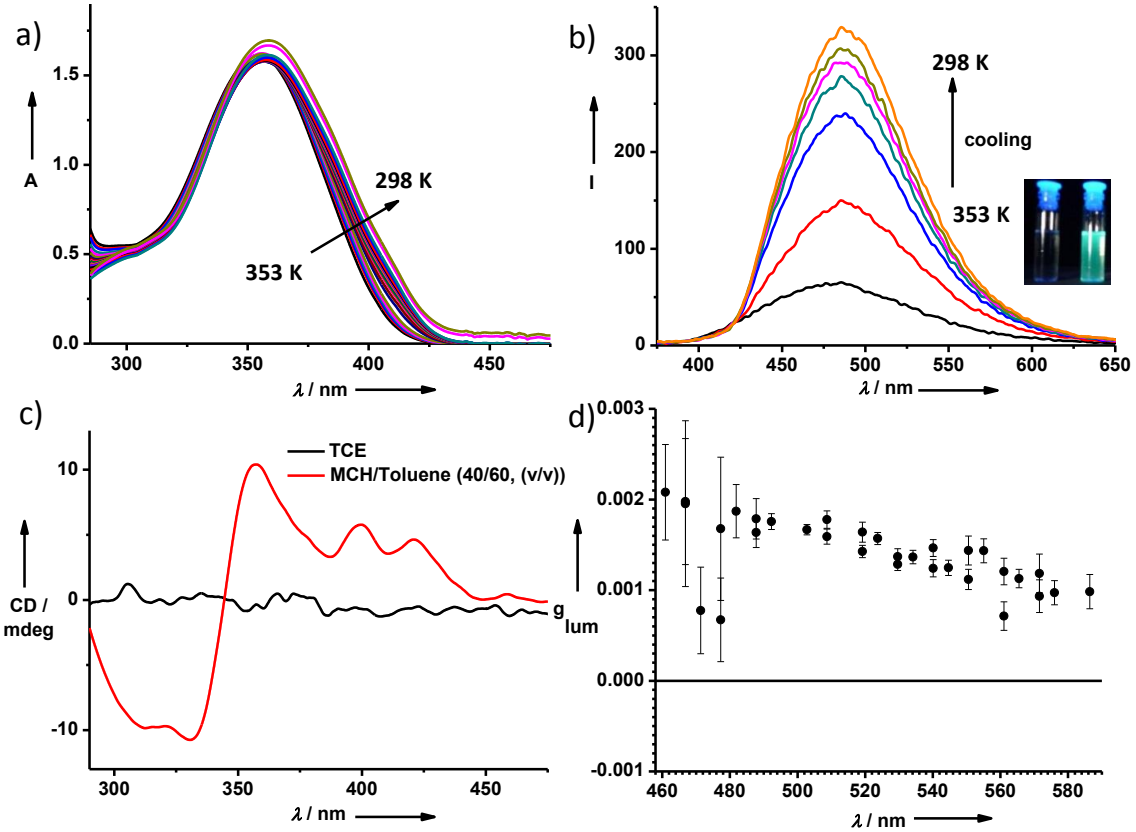


*Figure 5.10. Spectroscopic characterization of self-assemblies of* ***$C_3$-CSB-ch*** *in toluene/TCE, 40/60, (v/v): a) Variable temperature absorption spectra obtained on cooling a dilute solution of* ***$C_3$-CSB-ch*** *($2x10^{-5}$ M) at 1 K/min, showing the evolution of the vibrionic shoulder during the process of self-assembly; b) Temperature dependent fluorescence changes showing the enhanced luminescence as the assemblies are cooled down proving the presence of AIEE in these assemblies, the inset shows the photographs of a monomeric solution in TCE and self-assembled solution (toluene/TCE, 40/60, (v/v); c) CD spectra of dilute solutions of* ***$C_3$-CSB-ch*** *in TCE and toluene/TCE, 40/60, (v/v); d) CPL spectrum of the self-assembled state of* ***$C_3$-CSB-ch*** *($2x10^{-5}$ M, toluene/TCE, 40/60, (v/v), showing CPL active assemblies with $g_{lum}$=0.002.*

## 5.6.2. Mechanistic Investigations and Co-Assembly Studies

The mechanism of self-assembly in **$C_3$-CSB-ch** was investigated through temperature dependent measurements. Variable temperature spectra of dilute solutions ($5x10^{-5}$ M to $10^{-5}$ M) showed the disappearance of CD signal along with the disappearance of vibrionic shoulder in the absorption spectrum, indicating melting of

aggregates at higher temperature (353.15 K). The fluorescence of the assemblies weakened significantly on transformation from the self-assembled to the monomeric state. However, on cooling the solution to 298.15 K with a temperature slope –dT/dt = 1 K/min, the bisignated CD signal, vibrionic shoulder in the absorption spectrum and the fluorescence of the assemblies was regained. The mechanism was investigated by probing 354 nm in the CD spectrum. A non-sigmoidal curve was obtained that fitted well to the nucleation-elongation model, suggesting a cooperative mechanism of self-assembly (Figure 5.11.a). Similar experiments were carried out in the self-assembled state of **$C_3$-CSB-ach** (toluene/TCE, 40/60, (v/v)). Temperature dependent UV measurements indicated that the assemblies of **$C_3$-CSB-ach** never melted completely, even at 363.15 K. The vibrionic shoulder did not disappear completely as in the case of **$C_3$-CSB-ch**, and the $C_3$-Cyanostilbenes in MCH-TCE solvent compositions. However, on heating the co-assembled solutions at various percentages of **$C_3$-CSB-ch**, the assemblies melted, but the solutions became turbid on cooling and did not have similar features as before.

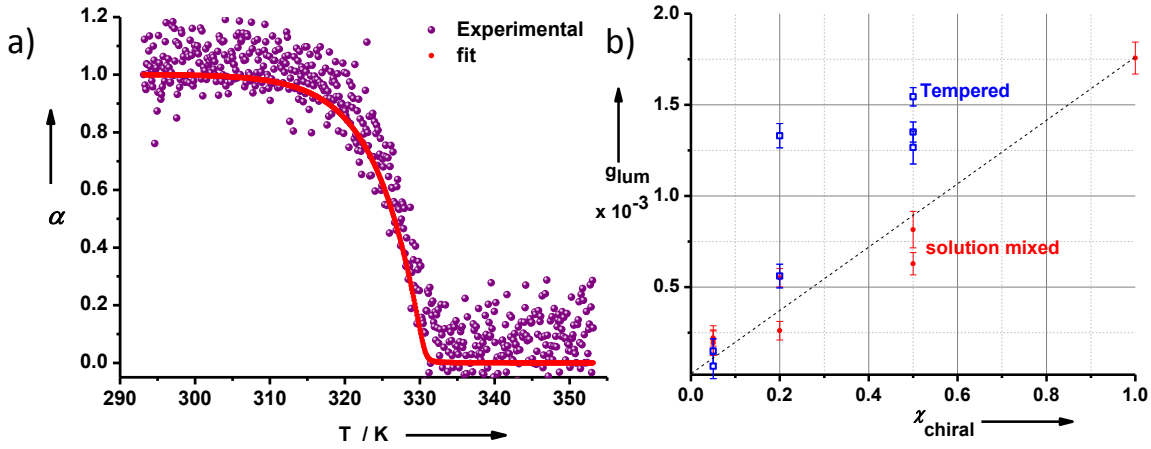


*Figure 5.11. a) Non-sigmoidal cooling curve with cooperative fit obtained by monitoring 315 nm in the CD spectrum as a dilute solution of **$C_3$-CSB-ch** ($2x10^{-5}$ M; solvent composition toluene/TCE, 40/60 (v/v) were cooled slowly from 353.15 K to 298.15 K with a temperature gradient of 1 K/min. The purple scatter plot represents the experimental data and the red line is the co-operative fit; b) CPL of co-assembled solutions of **$C_3$-CSB-ch** and **$C_3$-CSB-ach** showing a linear trend and no CPL amplification.*

Due to inefficient co-assembly, varying percentages of the two-component mixture showed a linear trend in the $g_{lum}$ in CPL measurements, suggesting no amplification (Figure 5.11.b). This experiment, thus, proves the need to have co-assembly and chiral amplification in the ground state to reflect in the chiroptical amplification in the excited state.

## 5.7. Conclusions

In conclusion, we have rationalized a design strategy of molecules which are CPL active by a combination of chirality and luminescence in the self-assembled state. Through a co-assembly of the chiral with the achiral molecules, we have been able to bias the racemic achiral assemblies in a homochiral fashion and extract CPL out of the co-assembled stacks. This is an unprecedented chiral amplification process through which a small percentage of a CPL active material can bring about chiroptical amplification of CPL. This opens a platform for various fluorescent supramolecular organic chiral assemblies to be applied in chiro-technological applications.

## 5.8. Experimental Section

### 5.8.1. General Methods

**NMR Measurements:** NMR spectra were recorded with a Bruker AVANCE 400 (400 MHz) Fourier transform NMR spectrometer with chemical shifts reported in parts per million (ppm) with respect to TMS. Splitting patterns are designated as s, singlet; d, doublet; t, triplet; m, multiplet.

**Optical Measurements:** Electronic absorption spectra were recorded on a Perkin Elmer Lambda 900 UV-Vis-NIR Spectrometer. Circular Dichroism (CD) spectra and temperature dependent UV-Vis spectra were recorded on a Jasco J-815 spectrometer where the sensitivity, time constant and scan rate were chosen appropriately. The temperature dependent measurements were performed with a CDF-426S/15 Peltier-type temperature controller with a temperature range of 263-383 K and adjustable temperature slope.

**Transmission Electron Microscopy (TEM):** TEM measurements were performed on a JEOL, JEM 3010 operated at 300 kV. Samples were prepared by placing a drop of the solution on carbon coated copper grids followed by drying at room temperature. The images were recorded with an operating voltage of 300 kV. In order to get a better contrast, the samples were stained with uranyl acetate (1 wt % in water) before the measurements.

**Confocal Microscopy:** Confocal microscopy measurements were carried out in LS-55 confocal instrument. The samples were excited with a laser of wavelength 480 nm.

**Curve Fittings**: Cooperative curve fittings were done with MATLAB software with the codes developed by H. M. M. ten Eikelder et al.[15]

### 5.8.2. Synthetic Methods

The starting materials used for synthesizing various compounds were obtained from commercial suppliers. The moisture sensitive reactions were performed under an atmosphere of argon. Photosensitive reactions were performed in amber coloured round bottomed flask and the purifications were done mostly in dark to avoid any isomerization. DMF was dried by distillation under vacuum and dried on 3 Å molecular sieves activated at 180 $^{\circ}$C. Analytical thin layer chromatography was carried out on Merck silica gel 60. Column chromatography was carried out on silica gel (100-200 mesh). Freshly distilled solvents were used for column chromatography. Size exclusion chromatography was done on sephadex polystyrene biobeads S-X3 with chloroform as the eluent.

Proton chemical shifts are reported in ppm downfield from TMS (Tetramethylsilane) using the resonance of the deuterated solvent as internal standard. Splitting patterns are designated as s, singlet; d, doublet; bs, broad singlet; m, multiplet; t, triplet; q, quartet; dd, double doublet; ddd, double double doublet; quin, quintet and br, broad.

## 5.8.2.1. Synthetic Schemes

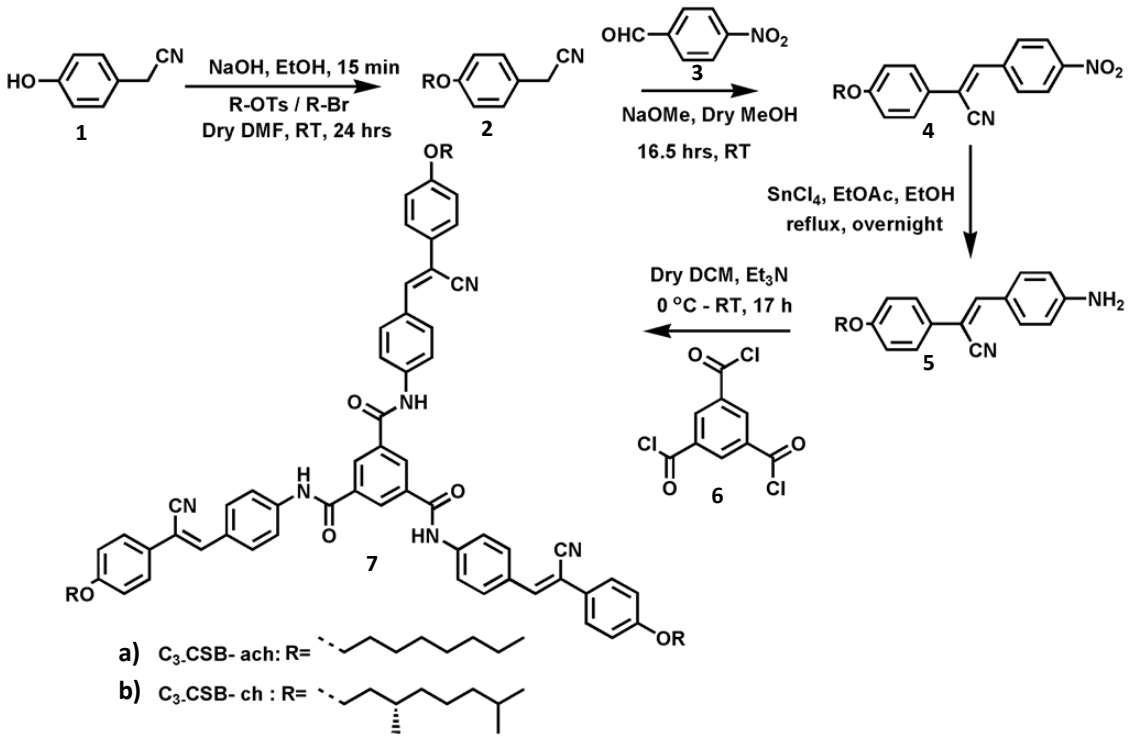


*Scheme 5.1. Synthetic scheme of $C_3$-Symmetric Cyanostilbenes*.

## 5.8.2.2. Synthetic Procedures

**2a** was synthesized according to a previously reported procedure.[16] The procedure was modified for **2b**.

*p*-alkoxyphenylacetonitrile (**2**): *p*-hydroxyphenylacetonitrile (4 g (30.1 mmol)) was added to a solution of sodium hydroxide (1.268 g, 31.7 mmol) in Ethanol (16.8 mL) and was stirred at room temperature for 15 min. The colourless solution turned dark yellow/brown due to the formation of phenoxide anions. Ethanol was removed completely under reduced pressure. Octyl bromide (5.81 g, 30.1 mmol) / (S)-3,7-dimethyl-octyl tosylate (9.4 g, 30.1mmol) in dry DMF were added drop wise under argon atmosphere to give the chiral and achiral substituted products respectively.

*p*-octylphenylacetonitrile (**2a**): Yield: 93%; $^1$H NMR (400 MHz, $CDCl_3$, δ): 7.22 (d, $J$ = 8.8 Hz, 2H, ArH), 6.85 (d, $J$ = 8.4 Hz, 2H, ArH), 4.00-3.98 (m, alkyl H, -$OCH_2$), 3.68 (s, 2H -$CH_2CN$), 1.85-0.82 (15 H, alkyl H).

*p*-citronellylphenylacetonitrile (**2b**): Yield: 90%; $^{1}$H NMR (400 MHz, $CDCl_3$, δ): 7.22 (d, *J* = 8.4 Hz, 2H, ArH), 6.89 (d, *J* = 8.8 Hz, 2H, ArH), 3.95 (t, 2H, alkyl H, -$OCH_2$), 3.68 (s, 2H -$CH_2CN$), 1.8-0.89 (19 H, alkyl H); $^{13}$C NMR (100 MHz, $CDCl_3$, δ): 160.0, 129.9, 129.1, 128.0, 121.6, 118.4, 115.2, 69.2, 66.5, 39.2, 37.4, 36.2, 29.9, 28.18, 24.8, 22.9, 192.7; GCMS (EI) *m/z*: $[M]^+$ calcd for $C_{18}H_{27}NO$: 273.2093; found, 273.15.

*p*-nitrocyanostilbene (**4**): **2** (5 g, 18.3 mmol) and *p*-nitrobenzaldehyde (2.76 g, 18.3 mmol) were added to a stirred solution of sodium methoxide (0.49 g, 9.15 mmol) in dry methanol (83.3 mL) and were stirred under an atmosphere of argon at room temperature for 16.5 hours. A lot of precipitates formed during the reaction. The completion of the reaction was monitored through TLC which showed the disappearance of the reactants. Methanol was completely removed and the reaction mixture was extracted with $CHCl_3$/ water solvent mixture. The organic layer was collected, dried over anhydrous $Na_2SO_4$ and concentrated to get the crude product of Knoevenagel condensation. The product was further purified through a column chromatography (eluent: 40% $CHCl_3$ in hexane). Though purification was done in dark, our further investigations proved that the compound was quite photostable and there was no Z to E isomerization.

*p*-nitro cyanostilbene–ach (**4a**): Yield: 80%; $^{1}$H NMR (400 MHz, $CDCl_3$, δ): 8.3 (d, *J* = 8.8 Hz, 2H, ArH), 8.0 (d, *J* = 8.4 Hz, 2H, ArH), 7.64 (d, *J* = 8.8 Hz, 2H, ArH), 7.46 (s, 1H, alkenyl H), 6.98 (d, *J* = 8.8 Hz, 2H, ArH), 4.01 (t, 2H, -$OCH_2$), 1.81-0.87 (15H, alkyl H); $^{13}$C NMR (100 MHz, $CDCl_3$, δ): 161.0, 159.0, 148.1, 140.2, 136.3, 129.8, 129.1, 127.8, 124.3, 121.6, 118.4, 115.3, 115.2, 113.1, 68.5, 68.3, 32.0, 31.0, 29.4, 29.3, 26.1, 22.9, 22.8, 14.2; LCMS (ESI) *m/z*: $[M+H]^+$ calcd for $C_{23}H_{26}N_2O_3$: 378.3; found, 378.3.

*p*-nitro cyanostilbene–ch (**4b**): Yield: 30%; $^{1}$H NMR (400 MHz, $CDCl_3$, δ): 8.3 (d, *J* = 8.8 Hz, 2H, ArH), 8.1 (d, *J* = 8.8 Hz, 2H, ArH), 7.64 (d, *J* = 9.2 Hz, 2H, ArH), 7.46 (s, 1H, alkenyl H), 6.98 (d, *J* = 8.8 Hz, 2H, ArH), 4.07-4.05 (m, 2H, -$OCH_2$), 1.85 (m, 1H, alkyl H), 1.83 (m, 1H, alkyl H), 1.36-0.87 (17H, alkyl H); $^{13}$C NMR (125 MHz, $CDCl_3$, δ): 161.0, 148.0, 140.2, 136.4, 129.8, 129.2, 127.8, 125.8, 124.3, 117.4, 115.7, 115.3, 115.2, 114.7, 66.8, 66.6, 39.4, 37.4, 36.2, 31.1, 30.0, 28.1, 26.1, 24.8, 22.9, 22.7, 19.8; HRMS (ESI) *m/z*: $[M+H]^+$ calcd for $C_{23}H_{31}N_2O_3$ , 407.2335; found, 407.2325.

*p*-amino cyanostilbene (**5**): **4** (4 g, 10.6 mmol) was taken along with $SnCl_2$ (20 g, 106 mmol) in a solvent mixture of ethyl acetate (150 mL) and ethanol (150 mL) in an amber coloured round bottomed flask. The reaction mixture was refluxed at 90 $^oC$ for 18 hours. The formation of the product was monitored through a TLC after a mini work up that showed the disappearance of the nitro derivative and the formation of ninhydrin active amine. The reaction mixture was cooled and extracted repeatedly with 2 N NaOH/ $CHCl_3$. The organic layer was collected, dried and concentrated under reduced pressure. The amine was further purified through a column chromatography (70% $CHCl_3$ in hexane on neutal alumina) followed by size exclusion chromatography (SX-3, $CHCl_3$) to get the chiral and achiral amine respectively.

*p*-amino cyanostilbene–ach (**5a**)**:** Yield: 80%; $^1H$ NMR (400 MHz, $CDCl_3$, δ): 7.74 (d, *J* = 8.8 Hz, 2H, ArH), 7.54 (d, *J* = 8.8 Hz, 2H, ArH), 7.28 (s, 1H, alkenyl H), 6.92 (d, *J* = 8.8 Hz, 2H, ArH), 6.70 (d, *J* = 8.4 Hz, 2H, ArH), 4.07-4.05 (m, 2H, -$OCH_2$), 1.85 (m, 1H, alkyl H), 1.83 (m, 1H, alkyl H), 1.36-0.87 (17H, alkyl H); $^{13}C$ NMR (100 MHz, $CDCl_3$, δ): 159.5, 148.7, 140.6, 131.2, 127.7, 127.0, 127.8, 124.5, 119.3, 115.0, 114.9, 106.2, 68.4, 31.9, 29.5, 29.4, 26.2, 22.8, 14.2; LCMS (ESI) *m/z*: $[M+H]^+$ calcd for $C_{23}H_{28}N_2O$: 349.2; found, 349.2.

*p*-amino cyanostilbene-ch (**5b**)**:** Yield: 51%; $^1H$ NMR (400 MHz, $CDCl_3$, δ): 7.74 (d, *J* = 8.8 Hz, 2H, ArH), 7.54 (d, *J* = 8.8 Hz, 2H, ArH), 7.28 (s, 1H, alkenyl H), 6.93 (d, *J* = 8.8 Hz, 2H, ArH), 8.1 (d, *J* = 8.8 Hz, 2H, ArH), 4.07-4.05 (m, 2H, -$OCH_2$), 1.85 (m, 1H, alkyl H), 1.83 (m, 1H, alkyl H), 1.36-0.87 (17H, alkyl H); $^{13}C$ NMR (100 MHz, $CDCl_3$, δ): 159.5, 148.7, 140.6, 131.8, 131.2, 130.3, 127.7, 126.9, 124.4, 119.3, 115.0, 114.8, 114.4, 106.1, 66.6, 39.4, 37.4, 36.3, 30.0, 28.1, 24.8, 22.8, 22.7, 19.8; HRMS (ESI) *m/z*: $[M+H]^+$ calcd for $C_{25}H_{32}N_2O$: 377.2593; found, 377.2576.

$C_3$-Cyanostilbene (**7**): 1,3,5 benzene tricarbonyl chloride (80 mg, 0.3 mmol) and dry DCM (4 mL) were taken in a two-necked 50 mL round bottomed flask and were stirred on an ice bath for 10 min. Amines **5a**/**5b** (441 mg) was dissolved in 20 mL dry DCM and was added dropwise to the reaction mixture. The contents were stirred on ice bath for 2 hours and then at room temperature overnight. The completion of the reaction was monitored through TLC and NMR. TLC showed the formation of an additional AIE

active compound accompanied by the disappearance of the limiting reagent. NMR done by adding 5% (v/v) of Trifluoroacetic acid showed the formation of the product. The reaction mixture was concentrated under reduced pressure and a filtration column was done on neutral alumina (1-2% TFA, 2-3% MeOH in chloroform). As the amine was completely soluble in ethyl acetate but the trisamide was not, a soxhlet extraction in ethyl acetate (117 $^{o}$C, 8 hours) was done to get the pure product in the thimble. The pure product was dried in vacuum oven overnight at 80 $^{o}$C to remove traces of ethyl acetate. The same procedure was followed to synthesize the chiral cyanostilbene derivative. Appearance: bright yellow fluffy solid, UV 365 active (yellowish fluorescent in solid state).

**$C_3$-CSB-ach** (**7a**): Yield: 43%; $^{1}$H NMR (400 MHz, $CDCl_3$, 2% TFA, ppm): δ= 9.55 (s, 3H); 9.11 (s, 3H); 7.93 (s , 12 H); 7.6 (d, *J*= 8.8 Hz, 6H); 7.50 (s, 3H); 6.99 (d, *J*= 8.8 Hz, 6H); 4.05 (m, 6H); 1.83- 0.87 (48 H, alkyl H; $^{13}$C NMR (100 MHz, $CDCl_3$, δ): 165.7, 140.6, 138.4, 134.9, 131.7, 131.1, 130.4, 127.5, 126.5, 121.5, 118.7, 115.9, 115.6, 113.1, 110.5, 110.2, 68.9, 32.0, 29.5, 29.4, 29.3, 26.1, 22.8, 14.2; HRMS (ESI) *m/z*: $[M+H]^+$ calcd for $C_{78}H_{84}N_6O_6$, 1200.6452; found, 1201.6546.

**$C_3$-CSB-ch** (**7b**): Yield: 56%; $^{1}$H NMR (400 MHz, $CDCl_3$, 2% TFA, ppm): δ= 9.56 (s, 3H); 9.13 (s, 3H); 7.94 (s , 12 H); 7.6 (d, *J*= 8.8 Hz, 6H); 7.52 (s, 3H); 7.0 (d, *J*= 8.8 Hz, 6H); 4.09 (m, 6H); 1.86- 0.85 (57 H, alkyl H; $^{13}$C NMR (100 MHz, $CDCl_3$, δ): 165.8, 140.5, 138.3, 134.9, 131.7, 131.1, 130.3, 127.5, 126.5, 121.6, 118.8, 115.9, 115.5, 113.1, 110.6, 110.3, 67.2, 39.4, 37.4, 36.2, 30.0, 28.2, 24.8, 22.8, 22.7, 19.7; HRMS (ESI) *m/z* : $[M+H]^+$ calcd for $C_{84}H_{96}N_6O_6$, 1200.6452; found, 1285.7568.

## 5.9. References


[1] Circular Dichroism: Principles and Applications, 2nd ed. (Eds.: N. Berova, K. Nakanishi, R. W. Woody), Wiley-VCH, New York, **2000**.

[2] a) J. P. Riehl, F. S**.** Richardson, *Chem. Rev*. **1986**, *86*, 1; b) E. G. Moore, A. P. S. Samuel, K. N. Raymond, *Acc. Chem. Res*. **2009**, *42*, 542; c) K. Watanabe, K. Suda, K. Akagi, *J. Mater. Chem. C* **2013**, *1*, 2797.

[3] H. Wynberg, E. W. Meijer, J. C. Hummelen, H. P. J. M. Dekkers, P. H. Schippers, A. D. Carlson, *Nature* **1980**, *286*, 641.

[4] a) E. Peeters, M. P. T. Christiaans, R. A. J. Janssen, H. F. M. Schoo, H. P. J. M. Dekkers, E. W. Meijer, *J. Am. Chem. Soc*. **1997**, *119*, 9909; b) S. M. Jeong, Y. Ohtsuka, N. Y. Ha, Y. Takanishi, K. Ishikawa, H. Takezoe, *App. Phys. Lett*. **2007**, *90*, 211106; ) A. Satrijo, S. C. J. Meskers, T. M. Swager, *J. Am. Chem. Soc*. **2006**, *128*, 9030.

[5] a) R. Carr, N. H. Evans, D. Parker, *Chem. Soc. Rev*. **2012**, *41*, 7673; b) J. C. G. Benzli, C. Piguet, *Chem. Soc. Rev*. **2005**, *34*, 1048; c) J. L. Lunkley, D. Shirotani, K. Yamanari, S. Kaizaki, G.Muller, *J. Am. Chem. Soc*. **2008**, *130*, 13814; d) J. A. Kitchen, D. E. Barry, L. Mercs, M. Albrecht, R. D. Peacock, T. Gunnlaugsson, *Angew. Chem. Int. Ed*. **2012**, *51*, 704; e) G. Bozoklu, C. Gateau, D. Imbert, J, Pécaut, K. Robeyns, Y. Filinchuk, F. Memon, G. Muller, Marinella Mazzanti, *J. Am. Chem. Soc*., **2012**, *134*, 8372; f) J. P. Leonard, P. Jensen, T. McCabe, J. E. O'Brien, R. D. Peacock, P. E. Kruger, T. Gunnlaugsson; *J. Am. Chem. Soc*. **2007**, *129*, 10986.

[6] F. Zinna, L. Di Bari, *Chirality* **2015**, *27*, 1.

[7] B. A. San Jose, S. Matsushita, K. Akagi, *J. Am. Chem. Soc*. **2012**, *134*, 19795.

[8] a) M. Fujiki, A. J. Jalilah, N. Suzuki, M. Taguchi, W. Zhang, M. M. Abdellatif, K. Nomura, *RSC Adv*. **2012**, *2*, 6663; b) M. Fujiki, Y. Kawagoe, Y. Nakano, A. Nakao, *Molecules* **2013**, *18*, 7035.

[9] J. Kumar, T. Nakashima, H. Tsumatori, T. Kawai, *J. Phys. Chem. Lett*. **2014**, *5*, 316.

[10] a) J. Liu, H. Su, L. Meng, Y. Zhao, C. Deng, J. C. Y. Ng, P. Lu, M. Faisal, J. W. Y. Lam, X. Huang, H. Wu, K. S. Wong, B. Z. Tang, *Chem. Sci*. **2012**, *3*, 2737; b) J. Mei, Y. Hong, J. W.Y. Lam, A. Qin, Y. Tang, B. Z. Tang, *Adv. Mater*. **2014**, *26*, 5429.

[11] a) B-K. An, J. Gierschner, S. Y. Park, *Acc. Chem. Res*. **2012**, *45*, 544; b) B-K. An, D.-S. Lee, J.-S. Lee, Y.-S. Park, H.-S. Song, S. Y. Park, *J. Am. Chem. Soc*. **2004**, *126*, 10232; c) B.-K. An, S. H. Gihm, J. W. Chung, C. R. Park, S.-K. Kwon, S. Y. Park, *J. Am. Chem. Soc.* **2009**, *131*, 3950; d) L. Zhua, Y. Zhao; *J. Mater. Chem. C* **2013**, *1*, 1059.

[12] a) S. Cantekin, T. F. A. de Greef, A. R. A. Palmans, *Chem. Soc. Rev*. **2012**, *41*, 6125; b) A. R. A. Palmans, E. W. Meijer, *Angew. Chem. Int. Ed*. **2007**, *46*, 8948; c)

M. M. J. Smulders, P. J. M. Stals, T. Mes, T. F. E. Paffen, A. P. H. J. Schenning, A. R. A. Palmans, E. W. Meijer, *J. Am. Chem. Soc*. **2010**, *132*, 620.

[13] D.-Mi Li, Y.-S. Zheng, *J. Org. Chem*. **2011**, *76*, 1100.

[14] M. M. J. Smulders, M. M. L. Nieuwenhuizen, T. F. A. de Greef, P. van der Schoot, A. P. H. J. Schenning, E. W. Meijer, *Chem. Eur. J.* **2010**, *16*, 362.

[15] H. M. M. ten Eikelder, A. J. Markvoort, T. F. A. de Greef, P. A. J. Hilbers, *J. Phys. Chem. B* **2012**, *116*, 5291.

[16] C.-Z. Dong, A. A. -Himidi, S. Plocki, D. Aoun, M. Touaibia, N. M. -Bel Habich, J. Huet, C. Redeuilh, J.-E. Ombetta, J.-J. Godfroid, F. Massicot, F. Heymans, *Bioorg. Med. Chem.* **2005**, *13*, 1989.

# Chapter-6

# Bischromophoric Cyanostilbenes: Luminescent, Enantiomeric Assemblies

# Chapter-6

## Bischromophoric Cyanostilbenes: Luminescent, Enantiomeric Assemblies


### *Abstract*

*Homochirality in nature has intrigued researchers for several years. Recognition of monomeric units of same chirality has been postulated as one of the prime causes of the prevalence of homochirality in nature. Understanding these processes in synthetic molecular systems is therefore, important. Moreover, chiral luminescent assemblies provide a platform to understand the excited state processes. In this Chapter, we present the self-assembly and luminescence properties of a novel class of Bischromophoric Cyanostilbenes. These enantiomeric molecules consist of trans-(1,2)-cyclohexanediamide core, which shows strong homochiral recognition and would undergo chirality driven self-sorting due to considerable chirality mismatch between the enantiomers. Cyanostilbenes have been chosen as the chromophores as these show aggregation induced enhanced emission (AIEE) phenomenon, contrary to conventional chromophores, which undergo quenching upon aggregation (ACQ). This property can be exploited in creating luminescent assemblies, which, in unison with chirality can make these assemblies potential candidates for emission of circularly polarized luminescence (CPL).*


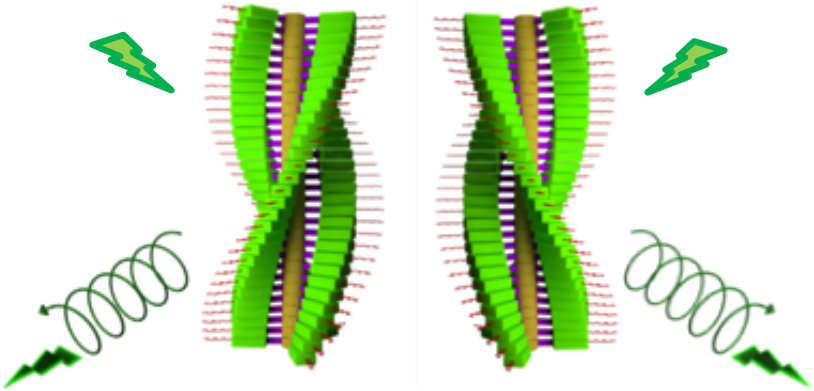

Manuscript based on this work: B. Narayan, S. J. George (under preparation).

## 6.1. Introduction

Homochirality in nature has been a subject of extensive research. Starting from the abundance of D-sugars and L-amino acids to evolved chiral pockets in enzymes for stereoselective reactions, there are many evidences for homochiral recognition in nature.[1] It is, therefore, important to study enantiomeric molecules and their self-assemblies.

The chiroptical properties of enantiomeric assemblies can be probed by Circular Dichroism (CD) in the ground state and by Circularly Polarized Luminescence (CPL) in the excited state. Circularly Polarized Luminescence (CPL) is the differential spontaneous emission of left or right circularly polarized light by chiral, luminescent molecules or assemblies.[2] It is the emission analogue of CD and elucidates the molecular configuration / conformation in the excited state, thus, acting as a supplementary technique to CD. The process of self-sorting can also be elucidated in the excited state by studying the CPL properties.

CPL is an interesting phenomenon for understanding the excitonic coupling between self-assembled chromophores in the excited state, as well as for chiro-technological applications, such as fluorescent tags, bar codes and for 3-D display.[3] A grave challenge for CPL in the self-assembled state is the need for the assemblies to be fluorescent. Conventionally, most of the chromophores are fluorescent in the molecularly dissolved state but undergo fluorescence quenching upon aggregation. Contrary to these chromophores, there is another class of organic molecules that are weakly luminescent in the molecularly dissolved state but display strong emission upon aggregation.[4] One of the well-studied chromophores in this regard is the cyanostilbene.[5] In solution state, they undergo intramolecular rotations, leading to solutions of low quantum yield. However, in the self-assembled state, due to 'Restriction of Intramolecular Rotation' (RIR), they demonstrate extensive planarization, leading to assemblies with enhanced emission (AIEE). This molecule has been well-studied by Park and co-workers and few other research groups in crystalline state,[6] as self-assembled luminescent nanowires[7] and for electronic purposes (Figure 6.1.a-d).[8]

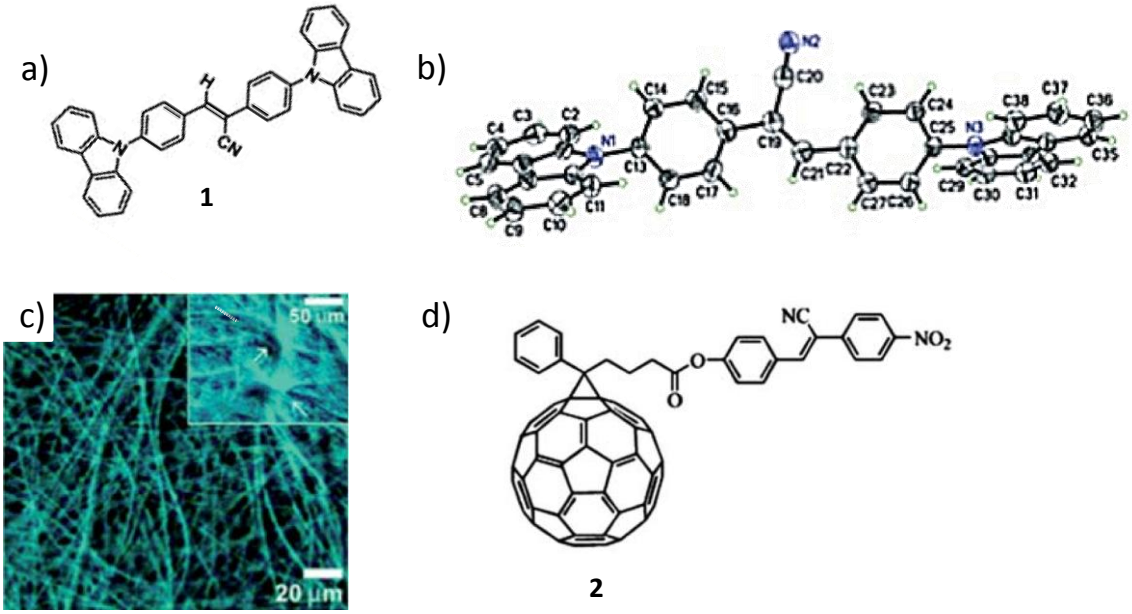


*Figure 6.1. Few examples of well-studied cyanostilbene derivatives: a) Carbazole containing cyanostilbene derivative **1** and b) its single crystal structure; c) fluorescent crystalline nanowires obtained from conjugated cyanostilbene derivatives; d) cyanostilbene modified acceptor used in bulk heterojunction solar cell (Figure a, b reproduced with permissions from reference 6, c from reference 7 and d from reference 8c).*

Various research groups have demonstrated elegant design strategies which would create self-assembled enantiomeric stacks.[9] For instance, Aida and co-workers have demonstrated the formation of homochiral assemblies in 'S-shaped diketopiperazine' moiety[10] and bowl-shaped molecules which were theoretically estimated to have an energy penalty of 2.3 kcal/mol for the formation of heterochiral dimers over the homochiral ones (Figure 6.2.a).[11] Similarly, Würthner and co-workers have designed atropoisomers where heterochiral dimer formation is a non-spontaneous process, with a Gibbs free energy of 14.5 $kJmol^{-1}$ (Figure 6.2.b).[12] Meijer and co-workers have observed homochiral polymerization in porphyrins[13] and in star shaped Oligo(*p*-phenylenevinylenes) [14] by virtue of multiple chiral side chains.

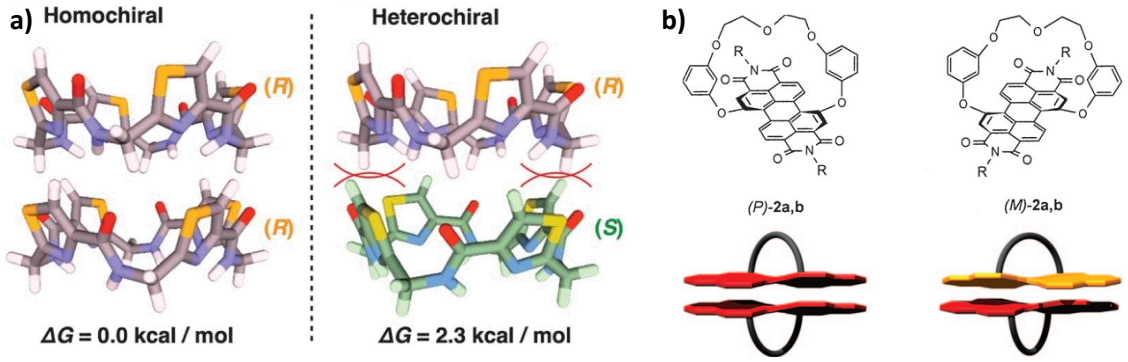


*Figure 6.2. Few design strategies for preferentially driving the homodimer formation over the heterodimer, by creating a strong chiral mismatch: a) Energy minimized structures of bowl-shaped macrocycles and the gibbs free energy (calculated) for the homodimer and heterodimer formation, suggesting the feasibility of homochiral polymerization; b) structures of Perylenebisimide based atropo-enantiomers and schematic representation of possible homo and heterodimers. (Figure a, b reproduced with permissions from reference 11 and 12 respectively).*

We aimed at synthesizing enantiomeric molecules for chiroptical functionality. This can be either achieved by attaching multiple chiral side chains or by employing chiral cores. As the former approach was synthetically challenging, we have chosen enantiomerically pure *trans*-1,2-bis(amido)cyclohexane with two stereogenic centres as the self-assembling chiral group in our molecular design. This moiety is derived from *trans*-1,2-cyclohexanediamine, which has been widely employed for the resolution of enantiomeric mixtures[15] and the corresponding rationally designed bischromophoric derivatives have been extensively used as model systems to study exciton chirality.[16] In a recent report, Kawai and co-workers have tethered Perylene bisimides to the trans-cyclohexane diamine[17] and binaphthyl cores[18] and observed opposite Circularly Polarized Luminescence (CPL) from dilute solutions and films of the resultant fluorescent assemblies. These molecules self-assemble in non-polar solvents and give rise to CPL due to the chiral, fluorescent assemblies. Moreover, they have observed an increase in the $g_{lum}$ value with change in morphology from spheres to fibres in the self-assembled state of binaphthyl tethered perylene bisimide by changing the solvent and concentration of the bischromophoric molecule.

We have designed enantiomeric Bischromophoric Cyanostilbenes (**RR-CSB** and **SS-CSB**), for luminescent chiral assemblies with an ability of homochiral recognition. This was done in order to make them potential candidates for CPL emission, which may enable us to understand the self-sorting processes in the excited state. However, the bigger goal of CPL investigations still needs to be addressed. This Chapter presents interesting results of chirality driven self-sorting in AIEE active luminescent assemblies, where the intramolecular and intermolecular interactions in the Bischromophoric Cyanostilbenes have been elucidated by chiroptical probing.

## 6.2. Design Strategy

The Bischromophoric Cyanostilbene molecules have been designed as potential candidates for enantiomeric Circularly Polarized Luminescence (CPL). The prime requisite for a CPL active assembly is chirality and luminescence. Conventional chromophores are emissive in molecularly dissolved state and exhibit quenched emission upon aggregation. We have therefore, chosen cyanostilbenes as the chromophore as they exhibit AIEE. The molecules (1R,2R)-(-)-Bischromophoric Cyanostilbene (**RR-CSB**) and (1S,2S)-(+)-Bischromophoric Cyanostilbene (**SS-CSB**) were synthesized through amidation reactions of the cyanostilbene acid with (1R,2R)-(-)-trans cyclohexanediamine and (1S,2S)-(+)-trans cyclohexanediamine respectively (Figure 6.3). The acid substituted cyanostilbene was synthesized through a Knoevenagel condensation between 4-formylbenzoic acid (**4**) and *p*-octyloxyphenylacetonitrile (**3**). The final molecules have been completely characterized by $^{1}$H NMR, $^{13}$C NMR and High Resolution Mass Spectrometry (HRMS) (Section 6.6).

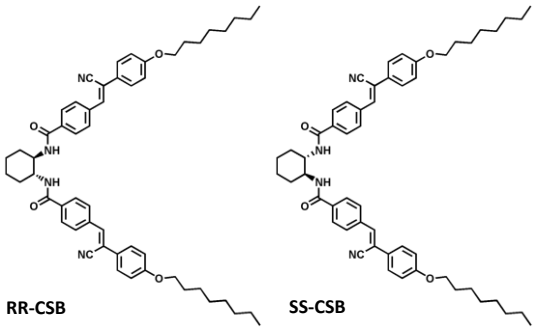


*Figure 6.3. Molecular structures of Bischromophoric Cyanostilbenes:* ***RR-CSB*** *and* ***SS-CSB****.*

## 6.3. Self-Assembly of Bischromophoric Cyanostilbenes in Solution

The self-assembly studies of the Bischromophoric Cyanostilbenes have been carried out in solvent compositions of Methylcyclohexane (MCH) in 1,1,2,2 tetrachloroethane (TCE). While these molecules exist in the monomeric state in TCE, they self-assemble in increasing percentages of MCH. Extensive characterization of the self-assembled state has been carried out through UV-Vis, Fluorescence and Circular Dichroism (CD) spectroscopy. Insights into the morphology adopted in the self-assembled state have been obtained through Transmission Electron Microscopy (TEM) and Confocal Microscopy. The details of all these investigations have been presented in this section.

### 6.3.1. Photophysical Characterization

Bischromophoric Cyanostilbene derivatives exist as monomers in TCE at room temperature and in MCH at high temperature as evident from the absorption spectra (Figure 6.4.a). While the monomeric state has an absorption maximum of 350 nm, the self-assembled state in MCH/TCE solvent mixture (99/1, (v/v)) is blue shifted with maximum at 337 nm, and has a strong vibrionic shoulder at 380 nm (Figure 6.4.c). Fluorescence spectra, interestingly, showed that both the monomeric and self-assembled states were luminescent (Figure 6.4.b, d). This, however, indicates that these enantiomers are different from well-studied cyanostilbene derivatives, which are non-fluorescent/weakly fluorescent in the molecularly dissolved state. The emission in the monomeric state may be resulting from the intramolecular interaction between the two cyanostilbene chromophores. Fluorescence spectrum of dilute solution ($2 \times 10^{-5}$ M), obtained upon excitation at 300 nm in both TCE and in MCH/TCE, 99/1, (v/v) were considerably emissive. However, on heating a self-assembled solution to 90 $^{o}$C, the intermolecular interactions weakened, resulting in lowering of emission intensity. Cooling a diassembled solution led to the revival of emission, thus, proving AIEE in the self-assembled state (Figure 6.4.d).

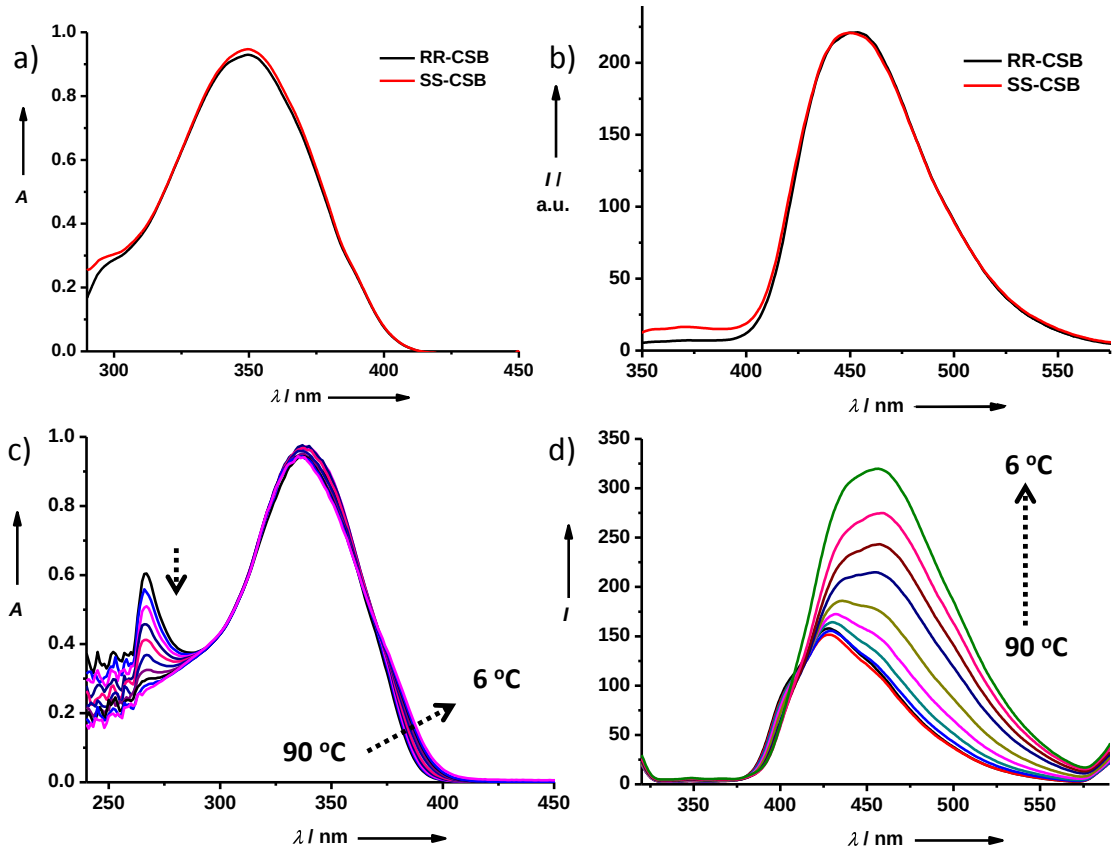


*Figure 6.4. Spectroscopic characterization (UV-Vis and Fluorescence) of **RR-CSB** and **SS-CSB** in TCE and (MCH/TCE, 99/1, (v/v)), c = 2x10$^{-5}$ M: a) Absorption spectra of Bischromophoric Cyanostilbene derivatives in TCE; b) Normalized Emission spectra of **SS-CSB** and **RR-CSB** obtained $\lambda_{exc}$ = 300 nm showing fluorescent monomeric state; c), d) Variable temperature absorption and emission spectra of a solution of **SS-CSB** showing appearance of vibrionic shoulder in the absorption and emission enhancement upon cooling from 90 $^{o}$C to 6 $^{o}$C.*

Valuable insights into the monomeric and self-assembled states were obtained from CD spectroscopy. Dilute solutions of **RR-/SS-CSB** in MCH/TCE (99/1, (v/v)) were annealed to ensure thermodynamic state of the assemblies, and their CD spectra was then recorded. Circular dichroism spectra of resulting solutions of **SS-CSB** and **RR-CSB** showed mirror image bisignated profile, typical of enantiomeric assemblies with helically organized chromophores (Figure 6.5.a, dashed lines). The bisignated CD signal in the self-assembled state showed maxima at 370 nm, 337 nm and 315 nm in the

cyanostilbene region, with zero-crossings close to the absorption maximum characteristic of exciton coupled NDI chromophores in a chiral environment.

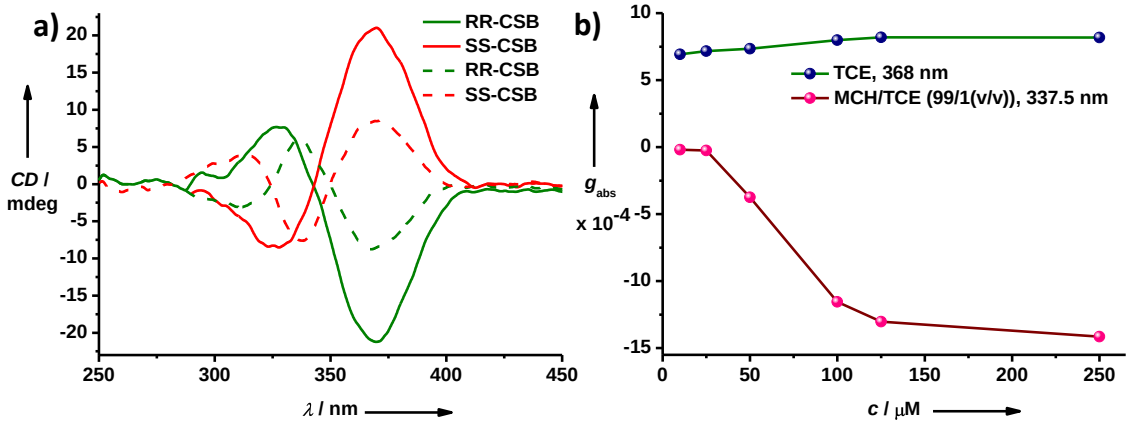


*Figure 6.5. a) CD spectra of **RR-/SS-CSB** in TCE (solid lines) and in (MCH/TCE, 99/1, (v/v)), (dashed lines), showing distinct CD profiles; b) concentration dependent g-value studies proving the CD in TCE arising from intramolecular and in (MCH/TCE, 99/1, (v/v)) arising from intermolecular interactions respectively.*

Interestingly, enantiomeric CSB monomers in TCE also showed bisignated mirror image CD spectra with maximum at 370 nm significantly different from that of the assemblies, thus indicating a different origin (Figure 6.5.a, solid lines). Heating the self-assembled solutions to 90 $^{o}$C also resulted in CD signal similar to that in TCE, hinting at intramolecular interactions (data not shown). Concentration dependent studies on the g-values further elucidated the difference in origin of CD signals in TCE and MCH. The g-values in TCE monitored at 368 nm remained constant at $7x10^{-4}$ for **SS-CSB** while there was a non-linear increase in the g-value ($-3x10^{-5}$ to $-1.4x10^{-3}$ on going from $10^{-5}$ M to $2.5x10^{-4}$ M) obtained at 337.5 nm in MCH, suggesting the intra and inter-monomeric interactions, respectively being the origin of different CD profiles (Figure 6.5.b).

## 6.3.2. Morphological Characterization

Insights into the morphology of the Bischromophoric Cyanostilbene assemblies were obtained through Transmission Electron Microscopy (TEM) and Confocal Microscopy. The TEM samples were prepared by drop-casting the dilute self-

assembled solution on a copper grid followed by staining with uranyl acetate. The samples were dried in high vacuum and then imaged.

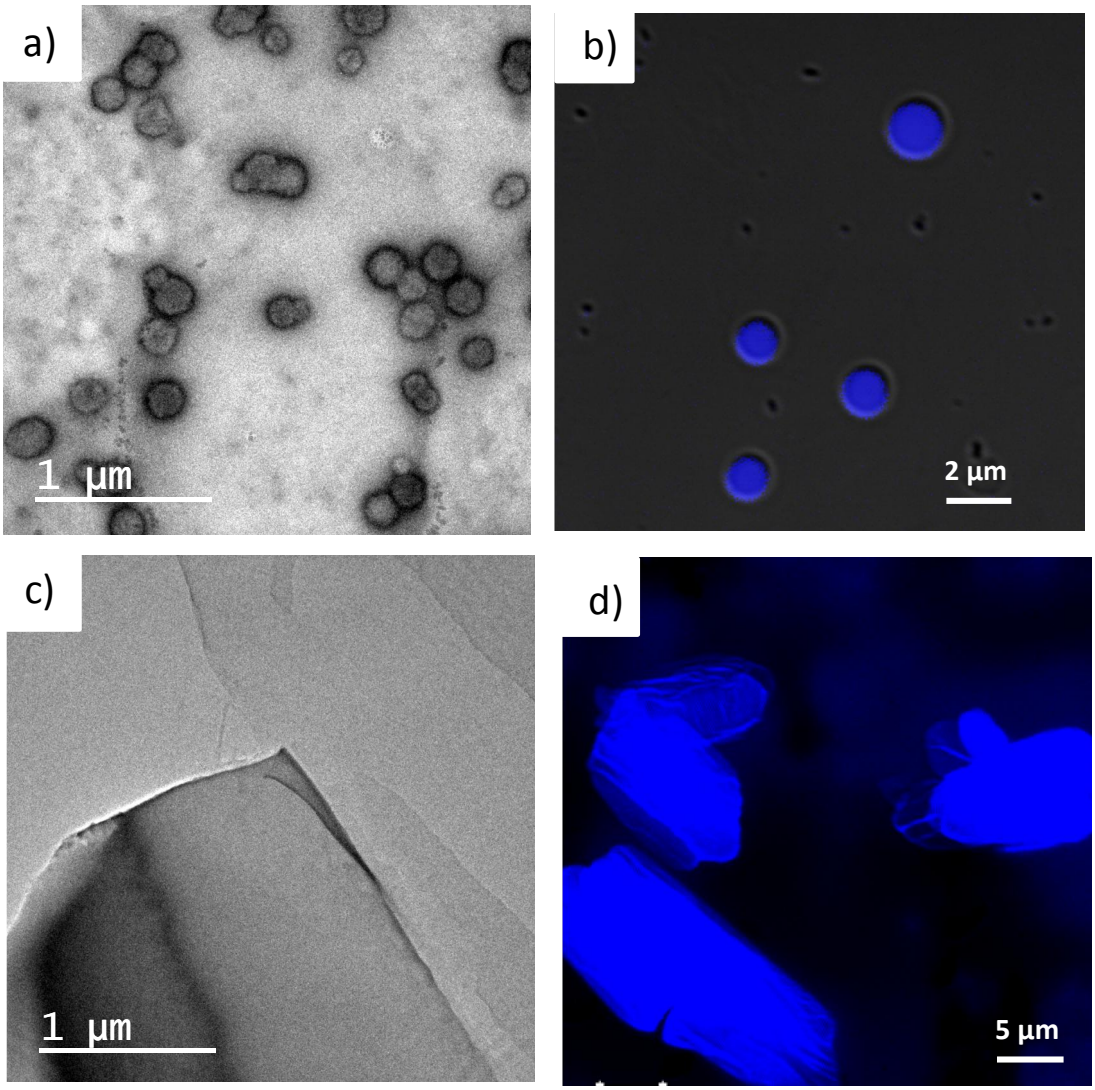


*Figure 6.6. Morphology of **RR-/SS-CSB** as determined by TEM and confocal imaging: a) TEM images of $2x10^{-5}$ M solution of **SS-CSB**, showing the formation of vesicles; b) confocal microscopy image showing vesicles in a dilute solution, thus confirming the presence of nanostructures in solution; c) TEM image of $10^{-3}$ M solution of **SS-CSB**, showing the formation of sheets; d) confocal microscopy image of **SS-CSB** ($10^{-3}$ M), confirming the presence of free-standing sheets in solution. Similar morphologies were obtained for **RR-CSB** at the same concentrations (data not shown).*

TEM imaging of a $2x10^{-5}$ M solution of **SS-CSB** in a solvent composition MCH/TCE (99/1, (v/v)) showed the presence of vesicles throughout the grid. The vesicles were of various diameters, ranging from 100 nm to 500 nm (Figure 6.6.a). The existence of nanostructures in solution was proved by confocal imaging. Samples were prepared by sealing the self-assembled solution between glass slides and viewing it upon excitation with a laser of 350 nm. Confocal microscopy images of a $2x10^{-5}$ M solution, showed the presence of spherical particles of an average diameter of 1000 nm, ruling out artifacts due to drying effects (Figure 6.6.b).

Interestingly, the morphology formed upon self-assembly of **SS-/RR-CSB** at high concentrations ($10^{-3}$ M) in solvent composition MCH/TCE (99/1, (v/v)) turned out to be sheets. These sheets were confirmed through TEM and confocal imaging, which unambiguously proved the existence of nanostructures in solution (Figure 6.6.c, d).

### 6.3.3. Homochiral Self-Assembly of Bischromophoric Cyanostilbenes

In order to understand the self-recognizing/self-discrimination behaviour of **RR-CSB**/**SS-CSB** enantiomers in self-assembled enantiomeric mixtures, temperature dependent supramolecular polymerization of bischromophoric mixtures with varying enantiomeric excess (ee) were carried out under thermodynamic conditions (MCH/TCE (99/1 (v/v)), c = $2x10^{-5}$ M) and the spectral characteristics of resulting assemblies were recorded at 25 °C. Absorption spectra of the self-assembled solution showed negligible changes, whereas the bisignated CD spectra showed a monotonic increase in their intensity with increase in ee (Figure 6.7.a, b). This is further evident from the plot of dissymmetry factor ($g_{CD}$) against ee which showed a linear change (Figure 6.7.c). This suggests that the assemblies constructed form the equimolar mixture of **SS-CSB** and **RR-CSB** (1:1 mixture) monomers are either self-recognition driven homochiral stacks (supramolecular conglomerates) or self-discrimination driven heterochiral stacks (supramolecular racemates).

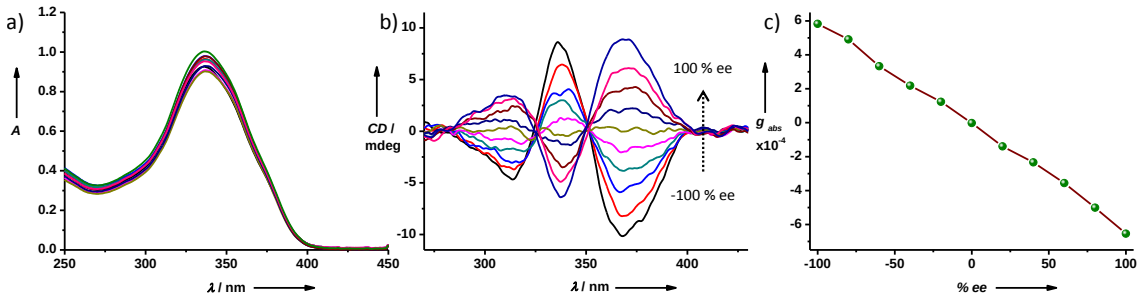


*Figure 6.7. Spectroscopic investigations of chirality driven self-sorting process in bischromophoric CSBs: a) Absorption spectra of thermodynamically cooled self-assembled solutions of various enantiomeric mixtures (-100% ee to 100% ee) showing negligible changes; b) respective CD spectra having a monotonic increment in the CD intensity with increasing ee; c) linear fit of g-value versus % enantiomeric excess (% ee) ruling out chiral amplification in mixed compositions, thus suggesting self-sorting.*

Similar observations were made in Chapter 2.1. in the case of homochiral supramolecular polymerization of RR-/SS-Naphthalenediimides, where the formation of supramolecular conglomerates could be ascertained through mechanistic investigations. We could resort to mechanistic investigations as the bischromophoric NDIs self-assembled in a cooperative fashion with a sharp elongation temperature ($T_e$) and the phenomenon of chirality driven self-sorting was demarcated by the intersection of $T_e$ of the equimolar mixture with the $T_e$ of the enantiopure sample at half the concentration. However, in this case, we could not employ mechanistic probes as the **SS-/RR-CSB**s do not follow a cooperative mechanism. But analogy drawn from our previous investigations along with theoretical insights (section 2.1.3.3.) has let us postulate a phenomenon of chirality driven self-sorting for enantiomeric mixtures of Bischromophoric Cyanostilbenes.

## 6.4. Conclusions

In conclusion, we have presented the synthesis and self-assembly of novel Biscromophoric Cyanostilbenes. Though synthetically challenging due to cis-trans isomerization of the double bond, we have been able to isolate the pure compounds in all trans conformation. The self-assembly studies provide insights into homochiral enantiomeric self-assembled states, due to the trans-(1,2)-bisamido chiral core. The

self-assembled state was highly luminescent, making these assemblies potential candidates for CPL emission.

## 6.5. Experimental Section

### 6.5.1. General Methods

**NMR Measurements**: NMR spectra were recorded with a Bruker AVANCE 400 (400 MHz) Fourier transform NMR spectrometer with chemical shifts reported in parts per million (ppm) with respect to TMS. Splitting patterns are designated as s, singlet; d, doublet; t, triplet; m, multiplet.

**Optical Measurements**: Electronic absorption spectra were recorded on a Perkin Elmer Lambda 900 UV-Vis-NIR Spectrometer. Temperature dependent UV measurements were done in Perkin Elmer Lambda 900 UV-Vis-NIR Spectrometer equipped with a temperature controller. Circular Dichroism (CD) spectra and temperature dependent CD spectra were recorded on a Jasco J-815 spectrometer where the sensitivity, time constant and scan rate were chosen appropriately. The temperature dependent measurements were performed with a CDF-426S/15 Peltier-type temperature controller with a temperature range of 263-383 K and adjustable temperature slope. Fluorescence measurements were carried out on a Perkin-Elmer LS-55 spectrometer equipped with a peltier.

**Transmission Electron Microscopy (TEM)**: TEM measurements were performed on a JEOL, JEM 3010 operated at 300 kV. Samples were prepared by placing a drop of the solution on carbon coated copper grids followed by drying at room temperature. The images were recorded with an operating voltage of 300 kV. In order to get a better contrast, the samples were stained with uranyl acetate (1 wt % in water) before the measurements.

**Confocal Microscopy**: Confocal Microscopy imaging was done at room temperature using a Zeiss LSM 510 META laser scanning confocal microscope. The microscope objective of 63X (NA 1.4) and 20X (NA 0.5) were employed. Samples were prepared by sealing the solution between two glass plates.

**High Resolution Mass Spectrometry (HRMS)**: HRMS spectra were obtained on a Agilent HRMS Spectrometer (Q-TOF).

## 6.5.1. Synthetic Methods

The starting materials used for synthesizing various compounds were obtained from commercial suppliers. The moisture sensitive reactions were performed under an atmosphere of nitrogen. N, N Dimethylformamide (DMF) was dried by distillation under vacuum and dried on 3 Å molecular sieves activated at 180 °C. Enantiomerically pure (1R,2R)-(-)-trans-1,2-cyclohexanediamine and (1S,2S)-(+)-trans-1,2-cyclohexanediamine were obtained from Aldrich and stored at 5 °C. Potassium Carbonate obtained from local suppliers was ground and dried at 180 °C before the alkylation reactions. Analytical thin layer chromatography was carried out on Merck silica gel 60. Column chromatography was carried out on silica gel (100-200 mesh). Size Exclusion Chromatography was performed on S-X1 biobeads, with chloroform as the solvent.

### 6.5.2.1. Synthetic Schemes

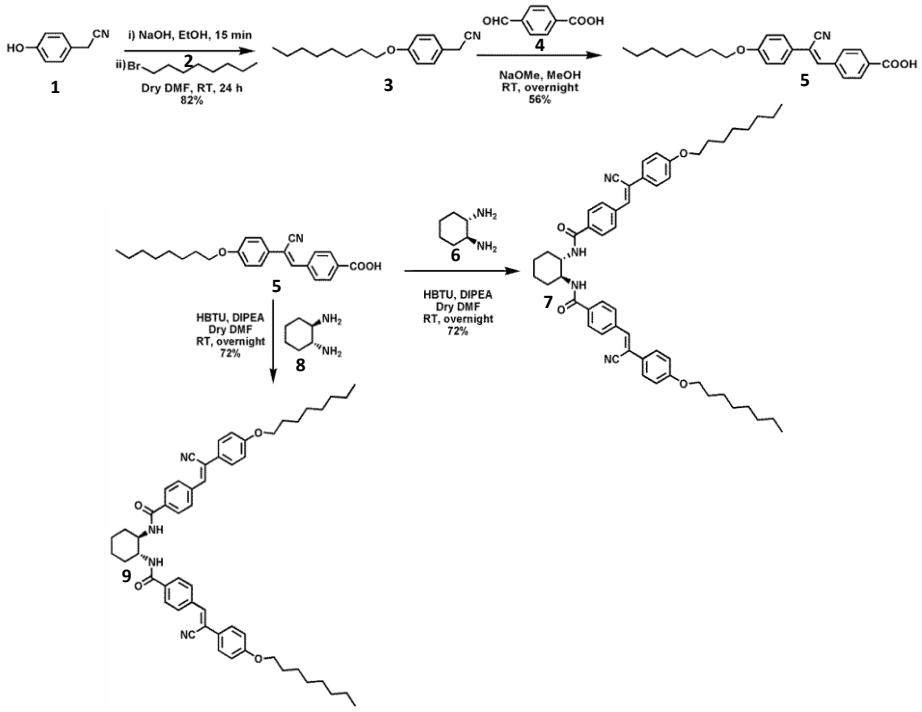


*Scheme 6.1. Synthetic route to Bischromophoric Cyanostilbenes.*

**6.5.2.2. Synthetic Procedures**

**3** was prepared according to a reported procedure.[19]

*p*-octyloxyphenylacetonitrile (**3**): *p*-hydroxyphenylacetonitrile (4 g, 30.1 mmol) was added to a solution of Sodium hydroxide (1.27 g, 31.7 mmol) in ethanol (16.8 mL) and was stirred at room temperature for 15 min. The colourless solution turned dark yellow/brown due to the formation of phenoxide anions. Ethanol was removed completely under reduced pressure. Octyl bromide (5.81 g, 30.1 mmol) in dry DMF was added drop wise under argon atmosphere and the reaction mixture was stirred in inert atmosphere for 24 h. The completion of the reaction was checked by monitoring a TLC that showed the complete disappearance of the starting material. The reaction mixture was then extracted with water/diisopropyl ether repeatedly. The organic layer was collected, dried on $Na_2SO_4$ and concentrated under reduced pressure. The alkylated derivative was purified by column chromatography (silica gel, 100-200 mesh, 70% $CHCl_3$ in hexane and polarity gradually increased to 2% MeOH in $CHCl_3$).

Yield: 82%; $^1$H NMR: (400 MHz, $CDCl_3$, ppm): δ= 7.22 (d, *J* = 8.8 Hz, 2H, ArH), 6.85 (d, *J* = 8.4 Hz, 2H, ArH), 4.00-3.98 (m, alkyl H, -$OCH_2$), 3.68 (s, 2H -$CH_2CN$), 1.85-0.82 (15 H, alkyl H).

Acid Substituted Cyanostilbene (**5**): In a 25ml 2-necked round bottomed flask containing magnetic stir bar sodium ethoxide (3 g, 12.2 mmol) and dry DMF (20 mL) were taken and stirred well at room temperature for 15 minutes. To that, **2** (900 mg, 12.2 mmol) taken with 28 mL of dry DMF and added dropwise to the reaction mixture. The reaction mixture was stirred well at room temperature overnight. Then the product was extracted with chloroform and water. The combined organic layers were dried with anhydrous sodium sulphate and the solvent was removed under reduced pressure to afford 59 % yield. $^1$H NMR (400 MHz, $CDCl_3$, ppm): δ= 8.1 (d, *J* =8.4 Hz, 2H); 7.94 (d, *J* =8.4 Hz, 2H); 7.63 (d, *J* =8.8 Hz, 2H); 7.46 (s, 1H); 6.9 (d, *J* =8.8 Hz, 2H); 4.01 (d, *J* =6.8 Hz, 1.84-1.29 (alkyl H, 15H); $^{13}$C NMR (100 MHz, $CDCl_3$, ppm, δ): 172, 160.7, 160.3, 139.6, 138.6, 131.1, 129.2, 127.7, 125.9, 116.1, 115.4, 113.3, 68.7, 31.9, 29.5, 29.4, 29.3, 26.1, 22.8, 14.2; LCMS (ESI) *m/z*: calcd for $C_{24}H_{27}NO_3$: 377.1991, found: 377.4 $[M]^+$.

**RR-CSB** (**9**) and **SS-CSB** (**7**): In a 25ml 2-necked round bottomed flask containing magnetic stir bar, **5** (500 mg, 1.3 mmol), diisopropylethylamine (0.21 g, 1.6 mmol), HBTU (0.44 g, 1.2 mmol) and dry DMF (5 mL) were taken and stirred well at room temperature for 15 minutes. To this **6** (0.06 g, 0.53 mmol) taken in dry DMF (4 mL) was added drop-wise and stirred well overnight in dark conditions at room temperature. The reaction mixture turns golden yellow. The completion of the reaction was checked by TLC and a $^{1}$H NMR performed on a miniscule amount that was worked up. The product was extracted with saturated solution of potassium carbonate, DCM and water. The combined organic layers were dried with anhydrous sodium sulphate and the solvent was removed under reduced pressure to afford 64 % yield. The resulting crude mixture was further purified by column chromatography (silica gel, 1-2 % MeOH in $CHCl_3$), followed by size-exclusion column chromatography (S-X3, $CHCl_3$).The purifications were performed in dark as the products were photosensitive and susceptible to cis-trans isomerization.

(**7**): Yield: $^{1}$H NMR (400 MHz, $CDCl_3$, ppm): δ = 7.73 (roof q, 8H); 7.51 ( d, J = 8.8 Hz, 4H); 7.32 (s, 2H); 7.21 (b, 2H, -NH), 6.87 (d, J = 8.8 Hz, 4H),; 3.96 (t, J = 6.4 Hz, 4H), 2.27-0.88 (alkyl H, 38H); $^{13}$C NMR (100 MHz, $CDCl_3$, ppm, δ): 167.7, 160.5, 138.4, 136.9, 135.2, 129.2, 127.7, 127.5, 126.4, 117.9, 115.1, 113.1, 68.4, 54.9, 32.4, 32.0, 29.5, 29.4, 29.3, 26.2, 25.1, 22.8, 14.2; HRMS (ESI) *m/z*: calcd for $C_{54}H_{64}N_4O_4$: 832.4928, found: 833.4973 $[M+H]^+$.

(**9**): Yield: 70%; $^{1}$H NMR (400 MHz, $CDCl_3$, ppm): δ = 7.73 (roof q, 8H); 7.51 ( d, J = 8.8 Hz, 4H); 7.32 (s, 2H); 7.21 (b, 2H, -NH), 6.87 (d, J = 8.8 Hz, 4H),; 3.96 (t, J = 6.4 Hz, 4H), 2.27-0.88 (alkyl H, 38H); $^{13}$C NMR (100 MHz, $CDCl_3$, ppm, δ): 167.7, 160.4, 138.4, 136.9, 135.2, 129.2, 127.7, 127.5, 126.4, 117.9, 115.1, 113.1, 68.4, 54.8, 32.4, 31.9, 29.5, 29.4, 29.3, 26.2, 25.1, 22.8, 14.2; HRMS (ESI) *m/z*: calcd for $C_{54}H_{64}N_4O_4$: 832.4928, found: 833.4969 $[M+H]^+$.

## 6.6. References

[1] a) B. Alberts, A. Johnson, J. Lewis, M. Raff, K. Roberts, P. Walter, *Molecular Biology of the Cell* 4th ed.; Garland Science: New York, **2002**; b) K.-E. Jaeger, T.

Eggert, *Curr. Opin. Biotechnol*. **2004**, *15*, 305; c) J. D. Watson, F. H. C. Crick, *Nature* **1953**, *171*, 737.

[2] Circular Dichroism: Principles and Applications, 2nd ed. (Eds.: N. Berova, K. Nakanishi, R. W. Woody), Wiley-VCH, New York, **2000**.

[3] a) J. P. Riehl, F. S**.** Richardson, *Chem. Rev*. **1986**, *86*, 1; b) E. G. Moore, A. P. S. Samuel, K. N. Raymond, *Acc. Chem. Res*. **2009**, *42*, 542; c) K. Watanabe, K. Suda, K. Akagi, *J. Mater. Chem. C* **2013**, *1*, 2797.

[4] a) J. Liu, H. Su, L. Meng, Y. Zhao, C. Deng, J. C. Y. Ng, P. Lu, M. Faisal, J. W. Y. Lam, X. Huang, H. Wu, K. Sing Wong, B. Z. Tang, *Chem. Sci*. **2012**, *3*, 2737; b) J. Mei, Y. Hong, J. W.Y. Lam, A. Qin, Y. Tang, B. Z. Tang, *Adv. Mater*. **2014**, *26*, 5429.

[5] B-K. An, J. Gierschner, S. Y. Park, *Acc. Chem. Res*. **2012**, *45*, 544.

[6] K. A. N. Upamali, L. A. Estrada, P. K. De, X. Cai, J. A. Krause, D. C. Neckers, *Langmuir* **2011**, *27*, 1573.

[7] a) B-K. An, D.-S. Lee, J.-S. Lee, Y.-S. Park, H.-S. Song, S. Y. Park, *J. Am. Chem. Soc*. **2004**, *126*, 10232; b) B.-K. An, S. H. Gihm, J. W. Chung, C. R. Park, S.-K. Kwon, S. Y. Park, *J. Am. Chem. Soc.* **2009**, *131*, 3950.

[8] a) J. H. Kim, Y. Jung, J. W. Chung, B.-K. An, S. Y. Park, *Small* **2009**, 5804; b) L. Zhua, Y. Zhao, *J. Mater. Chem. C* **2013**, *1*, 1059; c) J. A. Mikroyannidis, A. N. Kabanakis, S. S. Sharma, G. D. Sharma, *Adv. Funct. Mater*. **2011**, *21*, 746.

[9] a) M. M. Safont-Sempere, G. Fernández, F. Würthner, *Chem. Rev*. **2011**, *111*, 5784; b) J. M. Lehn, *Science* **2002**, *295*, 2400; d) L. Issacs, *Acc. Chem. Res*. **2014**, *47*, 2052; c) A. Saghatelian, Y. Yokobayashi, K. Soltani, M. R. Ghadiri, *Nature* **2001**, *409*, 797.

[10] Y. Ishida, T. Aida, *J. Am. Chem. Soc*. **2002**, *124*, 14017.

[11] K. Sato, Y. Itoh, T. Aida, *Chem. Sci.* **2014**, *5*, 136.

[12] M. M. Safont-Sempere, P. Osswald, K. Radacki, F. Würthner, *Chem. Eur. J.* **2010**, *16*, 7380.

[13] F. Helmich, M. M. J. Smulders, C. C. Lee, A. P. H. J. Schenning, E. W. Meijer, *J. Am. Chem. Soc.* **2011**, *133*, 12238.

[14] M. Wolffs, J. van Velthoven, X. Lou , R. A. A. Bovee, M. Pouderoijen, J. L. J. van Dongen, A.P. H. J. Schenning, E. W. Meijer, *Chem. Eur. J.* **2012**, *18*, 15057.

[15] a) D. E. Fuerst , E. N. Jacobsen, *J. Am. Chem. Soc*. **2005**, *127*, 8964; b) A. Berkessel, T. Günther, Q. Wang, J-M. Neudörfl, *Angew. Chem. Int. Ed*. **2013**, *52*, 8467; c) A. Berkessel, M. Brandenburg, E. Leitterstorf, J. Frey, J. Lex, M. Schä fer, *Adv. Synth. Catal*. **2007**, *349*, 2385; d) M. Kaik, J. Gajewy, J. Grajewski, J. Gawronski, *Chirality* **2008**, *20*, 301.

[16] a) J.-G. Dong, A. Wada, T. Takakuwa, K. Nakanishi, N. Berova, *J. Am. Chem. Soc*. **1997**, *119*, 12024; b) T. Nehira, C. A. Parish, S. Jockusch, N. J. Turro, K. Nakanishi, N. Berova, *J. Am. Chem. Soc*. **1999**, *121*, 8681; c) S. Boiadjiev, D. A. Lightner; *Chirality* **2005**, *17*, 316.

[17] a) J. Kumar, T. Nakashima, H. Tsumatori, M. Mori, M. Naito, T. Kawai, *Chem. Eur. J.* **2013**, *19*, 14090.

[18] a) J. Kumar, H. Tsumatori, J. Yuasa, T. Kawai, T. Nakashima, *Angew. Chem. Int. Ed.* **2015**, doi: 10.1002/anie.201500292; b) J. Kumar, T. Nakashima, H. Tsumatori, T. Kawai, *J. Phys. Chem. Lett*. **2014**, *5*, 316; c) T. Kawai, K. Kawamura, H. Tsumatori, M. Ishikawa, M. Naito, M. Fujiki, T. Nakashima, *ChemPhysChem* **2007**, *8*, 1465.

[19] C.-Z. Dong, A. A. -Himidi, S. Plocki, D. Aoun, M. Touaibia, N. M. -Bel Habich, J. Huet, C. Redeuilh, J.-E. Ombetta, J.-J. Godfroid, F. Massicot, F. Heymans, *Bioorg. Med. Chem.* **2005**, *13*, 1989.

# Curriculum Vitae

Bhawani Narayan was born on August 31st, 1986 in Jamshedpur, Jharkhand. She did her Bsc. (hons.) chemistry from Sri Sathya Sai University, Andhra Pradesh (2005-2008) and Masters in organic chemistry from Department of Chemistry, University of Pune (2008-2010). Thereafter she joined Jawaharlal Nehru Centre for Advanced Scientific Research in 2010 under the guidance of Prof. Subi J. George. Her research work at JNCASR focussed on development of various self-assembled chromophores for electronic and chiroptical functions.

# Appendices

# Appendices

## A1. General Methods

**1**. **NMR Measurements**: $^{1}H$ NMR spectra were recorded with a Bruker AVANCE 400 (400 MHz) Fourier transform NMR spectrometer with chemical shifts reported in parts per million (ppm) with respect to tetramethylsilane (TMS). $^{13}C$ NMR was recorded in the same instrument at 100 MHz. The number of scans for each sample was appropriately chosen. The NMR tubes used for experiments were purchased from NORELL. Common deuterated solvents such as chloroform-d, dimethyl sulfoxide-$d_6$, methanol-d, acetonitrile-$d_3$ purchased from Aldrich and Acros Organics were used. Trifluoroacetic acid (>99%), purchased from Sigma Aldrich was added to few NMR samples and has been mentioned in the thesis. Splitting patterns are designated as s, singlet; d, doublet; bs, broad singlet; m, multiplet; t, triplet; q, quartet; dd, double doublet; ddd, double double doublet; quin, quintet and br, broad.

**2**. **FT-IR Measurements**: Solution state IR measurements were performed on a Perkin-Elmer Spectrum GX series with a resolution of 4 $cm^{-1}$. Caesium Fluoride cells with a spacer of 2 mm were used. The solutions for the IR measurements were prepared in the respective solvent compositions which were gently warmed and sonicated for making the solutions homogeneous and clear. Solid state infrared spectra were recorded using a Bruker IFS 66 v/S spectrometer. The samples were prepared by using KBr pellets made by using KBr from local commercial suppliers. The KBr was dried at 150 $^{o}C$ before making the pellets for the measurements.

**3**. **Optical Measurements**: Electronic absorption spectra were recorded on a Perkin Elmer Lambda 900 UV-Vis-NIR Spectrometer. Temperature dependent UV measurements were done in Perkin Elmer Lambda 900 UV-Vis-NIR Spectrometer equipped with a temperature controller with a heating/ cooling rate of 1 K/min. Circular Dichroism (CD) spectra and temperature dependent CD spectra were recorded on a Jasco J-815 spectrometer where the sensitivity, time constant and scan rate were chosen appropriately. The temperature dependent measurements were performed with a CDF-426S/15 Peltier-type temperature controller with a temperature range of 263-383 K and adjustable temperature slope. For all the measurements, the concentration of the

sample, volume of sample and path length of the cuvette (10 mm, 5 mm, 2 mm and 1 mm) have been chosen appropriately. Necessary blanks with the same solvent composition and the chosen path length were recorded before the sample measurements. The solvents used for the optical measurements were of spectroscopic grade and were purchased from local commercial suppliers.

Fluorescence measurements were performed on Perkin Elmer LS 55 Luminescence Spectrometer. The path length and geometry (front face and normal geometry) were selected accordingly. Temperature dependent fluorescence measurements were performed by controlling the temperature with a peltier.

Circularly Polarized Luminescence spectra were measured on a customized setup that uses a photo-elastic modulator and a multichannel photon-counting detection system. The samples were excited at 430 nm. The solutions were tempered before the measurements. They were not purged before the CPL measurements.

**4**. **Lifetime Measurements**: Fluorescence decay was recorded in a time-correlated single-photoncounting spectrometer of Horiba-Jobin Yvon with 350-450 nm picosecond Ti-saphhire laser. The fits and residuals were performed by least square analysis.

**5**. **High Resolution Mass Spectrometry** (**HRMS**): High Resolution Mass Spectra (HRMS) were recorded on an Agilent 6538 Ultra High Definition (UHD) Accurate-Mass Q-TOF-LC/MS system using electrospray ionization (ESI) mode or Atmospheric Pressure Chemical Ionization (APCI) mode.

**6**. **Matrix-assisted laser desorption ionization time-of-flight (MALDI-TOF)**: MALDI-TOF masses reported in chapter 4 were performed on a Brukerdaltonics autoflex (ST-A2130) MALDI- TOF mass spectrometer with α-cyano-4-hydroxycinnamic acid matrix in reflector mode. The masses reported through MALDI-TOF in remaining chapters were obtained on a Brukerultraflex 2 MALDI-TOF mass spectrometer with α-cyano-4-hydroxycinnamic acid matrix.

**7**. **Liquid Chromatography Mass Spectrometry** (**LC-MS**): LC-MS experiments were performed on Shimadzu LC-MS system. The mode of ionization was electrospray ionization (ESI).

**8**. **Gas Chromatography Mass Spectrometry** (**GC-MS**): GC-MS was performed on a Shimadzu GC-MS instrument. The samples were ionized by chemical ionization method.

**9**. **Transmission Electron Microscopy** (**TEM**): TEM measurements were performed on a JEOL, JEM 3010 operated at 300 kV. Samples were prepared by placing a drop of the solution on carbon coated copper grids followed by drying at room temperature. The images were recorded with an operating voltage of 300 kV. In order to get a better contrast, the samples were stained with uranyl acetate (1 wt % in water) before the measurements.

**10**. **Atomic Force Microscopy (AFM)**: AFM measurements were performed on a Veecodi Innova SPM operating in tapping mode regime. Micro-fabricated silicon cantilever tips doped with phosphorus and with a frequency between 235 and 278 kHz and a spring constant of 20-40 $Nm^{-1}$ were used. The samples were prepared by drop casting the self-assembled solutions on glass substrates and dried under high vacuum at room temperature.

**11**. **Field Emission Scanning Electron Microscopy (FE-SEM)**: FE-SEM measurements were performed on a NOVA NANO SEM 600 (FEI) by drop casting the solutions on glass substrate followed by drying under high vacuum at room temperature and was operated with an accelerating voltage of 30 kV- 5kV.

**12**. **Confocal Microscopy**: Confocal Microscopy imaging was done at room temperature using a Zeiss LSM 510 META laser scanning confocal microscope. The microscope objective of 63X (NA 1.4) and 20X (NA 0.5) were employed. Samples were prepared by sealing the solution between a glass plates and a cover slip. The wavelengths for exciting the samples were chosen appropriately. The cross-sections of the morphologies in the confocal images may be wider than other microscopic techniques due to the resolution of the microscope.

**13**. **Dynamic light scattering Experiments (DLS)**: The measurements were carried out using a NanoZS (Malvern UK) employing a 532 nm laser at a back scattering angle of 173$^{o}$. The samples were measured in a 10 mm glass cuvette. Temperature dependent measurements of the hydrodynamic radius were performed on an inbuilt temperature controller in the DLS instrument.

**14**. **XRD Measurements**: Wide-angle XRD patterns of drop casted films of the self-assembled solutions on glass substrates were recorded in a Bruker D8 Discover (40 kV, 30 mA) instrument using Cu $K_{\alpha}$ radiation ($2\theta = 5^{o}–60^{o}$). Small angle XRD patterns were recorded in Siefert XRD instrument using Co source ($\theta = 0.9^{o}–60^{o}$).

XRD in the liquid crystalline state at high temperature were performed in a sealed capillary in SAXS mode. The source employed was Cu $K_{\alpha}$ radiation ($2\theta = 5^{o}–60^{o}$).

**15**. **Polarizing Optical Microscopy** (**POM**): The POM measurements were carried out on a Olympus BX-51 instrument. The sample was placed on a cover slip and put on a heating stage with continuous flow of nitrogen.

**16**. **Differential Scanning Calorimetry** (**DSC**): the DSC measurements were performed on Mettler-Toledo DSC-1 instrument. Three cycles (two heating and one cooling) were done to arrive at conclusions. The heating rate was maintained at 5 $^{o}$C/min.

**17**. **Field Effect Mobility Measurements:** Field effect mobility measurements were performed on top contact bottom gate transistor structures.

*Method for preparing FET devices as reported in chapter 3.1*: The fabrication of the field effect transistor (FET) involved coating of Al electrode ($10^{-6}$ mbar, 40 nm thick) by physical vapour deposition on standard RCA treated cleaned glass substrates. This was followed by coating of the dielectric layer of hydroxyl free divinyl tetramethylsiloxane bis (benzocyclobutene) at 800 rpm for 1 min. and annealed in glove box atmosphere at 290 $^{o}$C. The effective capacitance per unit area (C) of the dielectric films measured using Keithley 4200 semiconductor parameter analyser was obtained to be ~ 4 nF/cm$^{2}$ for films of thickness 0.5-0.6 μm. The surface of the dielectric is further treated with hexamethyldisilazane in liquid by spin coating at 1500 rpm for 30 seconds and annealing

at 110 $^{o}$C for 2 hrs in $N_2$ atmosphere. This was followed by solution casting the thin film of the OPV molecule in appropriate THF and water compositions to obtain films of thickness ~ 150-200 nm. The source-drain Au electrode were also vapor deposited ($10^{-6}$ mbar, 40 nm thick). The active layers were coated at different concentrations to distinctly follow the morphological changes with the transport measurements. The electrical characterization of the FETs were done using a standard set up of Keithley 2400 Source meters and a high impedance electrometer (Keithley 6514). The measurements were also cross checked with Keithley 2400 semiconductor parameter analyser. The mobility values reported are the median value obtained from the measurements performed on 10-15 devices in each case which are representative of the general trends in these molecules.

The electron mobilities reported in chapter 3.2. were also obtained from experiments performed on top contact bottom gate transistor structures.

The mobilities were reproducible over 10 devices.

**18**. **Theoretical calculations**:

*Theoretical calculations reported in chapter 2*: All the molecules have been modelled using DREIDING force field with Gasteiger charges as the partial charges. MD simulations were carried out using LAMMPS package. For initial relaxation, simulations were performed in gas-phase at 5 K in canonical ensemble (NVT). Further, these geometries were used as the input to determine the energies within a quantum chemical approach using Gaussian-09 at B3LYP/6-311+g(d,p) level of theory. Time-dependent density functional theory (TD-DFT) calculations were carried out at CAM-B3LYP at 6-31g(d) level of theory on the NDI-DAN CT pair to visualize the LUMO-HOMO diagram.

*Theoretical calculations reported in chapter 4*: Geometry optimizations were carried out at HF/6-31G level of theory using Gaussian- 09 suite of programs. The molecules were visualized using Visual Molecular Dynamics.

**19**. **Curve Fittings**: Cooperative curve fittings were done with MATLAB software with the codes developed by H. M. M. ten Eikelder et al. The fraction of aggregates ($\alpha$) have been obtained by normalizing the temperature dependent absorbance changes at a

particular wavelength from 0 to 1, as fraction of aggregates would be 0 at high temperature (monomeric state) and 1 at the maximum extent of aggregation.

## A2. Synthetic Methods

The starting materials used for synthesizing various compounds were obtained from commercial suppliers. The moisture sensitive reactions were performed under an atmosphere of nitrogen. N, N Dimethylformamide (DMF), acetone, acetonitrile, pyridine, triethylamine were dried by distillation under vacuum and dried on 3 Å molecular sieves activated at 180 $^{o}$C. Dry dichloromethane (DCM) and chloroform were obtained by pouring pre-distilled solvents 3 Å molecular sieves activated at 180 $^{o}$C. Mg granules were activated with 1 M HCl to remove MgO, washed repeatedly with water and acetone and were finally kept in oven at 200 $^{o}$C. Tetrahydrofuran (THF) was distilled over Na ribbons and benzoquinone and stored. Potassium Carbonate obtained from local suppliers was ground and dried at 180 $^{o}$C before the alkylation reactions. Analytical thin layer chromatography was carried out on Merck silica gel 60. Column chromatography was carried out on silica gel (100-200 mesh). Size Exclusion Chromatography was performed on S-X3 and S-X1 biobeads, with chloroform as the solvent.

The sources of reagents used and their purity are listed chapter wise below:

**Chapter 2**: (1R,2R)-(-)-1,2-Diaminocyclohexane, Sigma-Aldrich, 98%; (1S,2S)-(+)-1,2-Diaminocyclohexane, Sigma-Aldrich, 98%; 1,4,5,8 Naphthalenetetracarboxylic dianhydride, Sigma-Aldrich, > 98%; Dihexyl ketone, Sigma-Aldrich, 97%; 1-Bromohexane, Sigma-Aldrich, 98%; 1,5 Dihydroxynaphthalene, Sigma-Aldrich, 97%; β–alanine, Spectrochem, 98%; Di-tert-butyl dicarbonate, Spectrochem, 99.5%; Trifluoroacetic acid, Sigma-Aldrich, 99%; *n*-propanol, Spectrochem, 99%; N,N-Diisopropylethylamine (DIPEA), Spectrochem, 99%; HBTU, HIMEDIA, 99%; conc. HCl, SDFCl, 35-38%; Ethyl formate, SDFCl, 98%; *p*-toluenesulfonylchloride, Sigma-Aldrich, ≥ 98%; Ethyl-4-bromobutyrate, Spectrochem, 96%; ammonium acetate, SRL, 98%; sodium cyanoborohydride, Sigma-Aldrich, 95%.

**Chapter 3.1**: 4-hydroxy benzaldehyde, Spectrochem, 98%; tetraethyleneglycol, Sigma-Aldrich, 99%; S(-)-β-citronellol, Sigma-Aldrich, ≥ 99%; 1-bromododecane, Sigma-

Aldrich, 97%; *p*-toluenesulfonylchloride, Sigma-Aldrich, ≥ 98%; 1,4 dimethoxybenzene, Kemphasol, 98%; 18-crown-6, Sigma-Aldrich, ≥ 99%; paraformaldehyde, SDFCl, 96%; Hydrobromic acid, Spectrochem, (47% in water); triethylphosphite, Sigma-Aldrich, 98%; potassium-*t*-butoxide, Sigma-Aldrich, 95%.

**Chapter 3.2**: 1,4,5,8 Naphthalenetetracarboxylic dianhydride, Sigma-Aldrich, > 98%; sodium azide, SDFCl, > 99.5%; triphenylphosphine, Sigma-Aldrich, > 99% Dodecyl amine, MERCK, ≥ 98%; tetraethyleneglycol, Sigma-Aldrich, 99%; *p*-toluenesulfonylchloride, Sigma-Aldrich, ≥ 98%.

**Chapter 4**: Methyl 3,4,5 trihydroxybenzoate, Sigma-Aldrich, > 98%; S(-)-β-citronellol, Sigma-Aldrich, ≥ 99%; *p*-toluenesulfonylchloride, Sigma-Aldrich, ≥ 98%; potassium hydroxide, SDFCl, > 85%; oxalyl chloride, Sigma-Aldrich, ≥ 98%; tetrabutyl ammonium hydroxide, 40% in water; ethylenediamine, Spectrochem, 99%; 1,4,5,8 Naphthalenetetracarboxylic dianhydride, Sigma-Aldrich, > 98%; Trifluoroacetic acid, Sigma-Aldrich, 99%; 1,3,5 benzenetricarbonylchloride, Sigma-Aldrich, ≥ 98%; *p*-phenylenediamine, Sigma-Aldrich, 98%; triethylamine, SDFCl, 98%.

**Chapter 5**: *p*-hydroxyphenylacetonitrile, Sigma-Aldrich, 98%; sodium hydroxide, SDFCl, 98%; *p*-toluenesulfonylchloride, Sigma-Aldrich, ≥ 98%; 1-bromooctane,Spectrochem, 98%; *p*-nitrobenzaldehyde, Sigma-Aldrich, ≥ 98%; sodium methoxide, Spectrochem, 98%; tin (II) chloride, Sigma-Aldrich, 98%; 1,3,5 benzenetricarbonylchloride, Sigma-Aldrich, ≥ 98%.

**Chapter 6**: *p*-hydroxyphenylacetonitrile, Sigma-Aldrich, 98%; sodium hydroxide, SDFCl, 98%; 1-bromooctane,Spectrochem, 98%; 4-formyl benzoic acid, Sigma-Aldrich, ≥ 97%; sodium methoxide, Spectrochem, 98%; (1R,2R)-(-)-1,2-Diaminocyclohexane, Sigma-Aldrich, 98%; (1S,2S)-(+)-1,2-Diaminocyclohexane, Sigma-Aldrich, 98%; N,N-Diisopropylethylamine, Spectrochem, 99%; HBTU, HIMEDIA, 99%.